

**UNIVERSIDADE FEDERAL DE SANTA CATARINA
PROGRAMA DE PÓS-GRADUAÇÃO EM
ENGENHARIA MECÂNICA**

**MEASUREMENT AND PREDICTION OF SOUND ABSORPTION OF ROOM
SURFACES AND CONTENTS AT LOW FREQUENCIES**

**TESE SUBMETIDA À UNIVERSIDADE FEDERAL DE SANTA CATARINA PARA A
OBTENÇÃO DO GRAU DE DOUTOR EM
ENGENHARIA MECÂNICA**

GUSTAVO DA SILVA VIEIRA DE MELO

Florianópolis, Janeiro de 2002

AUTHOR'S BIOGRAPHY

Gustavo da Silva Vieira de Melo, born in Caruaru in the state of Pernambuco – Brazil, holds a BSc (1996) in Physics and has worked at ITEP (Instituto Tecnológico do Estado de Pernambuco) during six months in the same year. In 1997 he started his Post Graduate studies in the Mechanical Engineering Department of the Federal University of Santa Catarina (Brazil), in the area of Acoustics and Vibration, firstly at Master level, and then upgrading to PhD level in the following year, due to academic merit. His PhD has involved an eighteen-month joint programme with the Acoustics Research Unit (ARU) of The University of Liverpool (England). Professor Barry Gibbs (ARU) and Professor Samir Gerges (UFSC) constituted the joint supervision scheme. Melo has been always interested in Physics, with emphasis to the area of Acoustics.

**UNIVERSIDADE FEDERAL DE SANTA CATARINA
PROGRAMA DE PÓS-GRADUAÇÃO EM
ENGENHARIA MECÂNICA**

**MEASUREMENT AND PREDICTION OF SOUND ABSORPTION OF ROOM
SURFACES AND CONTENTS AT LOW FREQUENCIES**

GUSTAVO DA SILVA VIEIRA DE MELO

**Esta Tese foi julgada adequada para a obtenção do título de
DOUTOR EM ENGENHARIA
ESPECIALIDADE ENGENHARIA MECÂNICA
sendo aprovada em sua forma final.**

Prof. Samir N. Y. Gerges, Ph. D. – Orientador no Brasil

Prof. Barry M. Gibbs, Ph. D. – Orientador na Inglaterra

Prof. Júlio César Passos, Dr. – Coordenador do Curso

BANCA EXAMINADORA:

Prof. Arcanjo Lenzi, Ph. D. – Presidente (UFSC)

Prof. Sylvio R. Bistafa, Ph. D. – Relator (USP)

Prof. Eduardo B. Medeiros, Ph. D. (UFMG)

Prof. Marcelo K. Alves, Ph. D. (UFSC)

Profa. Elvira B. Viveiros, Dr. Eng. (UFSC)

**“É nosso dever aceitar a vida com alegria.
Mesmo sofrendo, é bom amar a vida.”
Joaquim Vieira de Melo**

A Patricia e Giovana, amores da minha vida.

ACKNOWLEDGEMENTS

First of all, I would like to thank God for giving me the opportunity, strength and health to accomplish this work. He also put by my side many important and supportive people that I shall thank below:

I express my gratitude to my family (specially my father Ivan, my mother Mercia and my sister Ivana), faithful supporters during all this long 'adventure'.

I could not forget to thank my friends from the LVA (Florianópolis) and the ARU (Liverpool) who not only taught me a lot about Acoustics, but also made my life pretty enjoyable. Special thanks here to 'Felipão' (Felipe Vergara), 'Cabelus' (Marcio Avelar), 'Companheiro-Xará' (Gustavo Dantas), 'Sir Newton' (Newton Soeiro), João Neto, Mauricy Souza and Fabiano Diesel from the LVA. Also, I will be always grateful to **Sophie Maluski**, Andy Moorhouse, Max de Salis, Ning Qi, Antony White, David Waddington, John Goodchild, and Anna Moncada from the ARU. I still remember when at the first chat with Professor Barry, he said to me that after my time in the ARU I would leave not simple colleagues, but actually good friends. He was definitely right.

There is also another person from the ARU to whom I will never be able to entirely thank for so much he has given to Pat, Giovana and me: Gary Seiffert (thank you so much Mate! You have no idea how deep your name is imprinted in our hearts).

Still from Liverpool, many thanks to Bob Birch, Fr. Jonh, Fr. Chris, Renato and Vânia (extraordinary Brazilian couple), special people who make me feel lucky to have them as friends.

My sincere gratefulness to singular Professors from UFSC who made me feel sure about what I have chosen to study: Prof. Acanjo Lenzi, Prof. Roberto Jordan, and Prof. Marcelo Alves.

Thanks to Coordenação de Aperfeiçoamento de Pessoal de Nível Superior (CAPES), who gave me all the financial support for my post-grad studies not only in Brazil, but also in England.

All my love and gratitude to Pat, who definitely changed my life, and for much better! I will be always indebted with you for giving me the greatest gifts I have ever received: your love and Giovana.

Last, but not least, I greatly thank two special Professors who have been fundamental to the accomplishment of this Thesis, each of them in his own particular way: Prof. Samir Gerges and Prof. Barry Gibbs. They have always encouraged me to go ahead, teaching me not only about Acoustics and technical aspects, but also aspects of life. Therefore, I shall think about them as brilliant Professors. More than that, I shall think of them as friends.

CONTENTS

LIST OF FIGURES.....	xii
LIST OF TABLES.....	xviii
GLOSSARY OF SYMBOLS.....	xix
RESUMO.....	xxi
ABSTRACT.....	xxii
1 INTRODUCTION.....	1
1.1 Motivation.....	1
1.2 Aims and objectives.....	2
1.3 Overview of the thesis.....	2
1.4 References.....	4
2 SOUND INSULATION AT LOW FREQUENCIES.....	5
2.1 Introduction.....	5
2.2 Infinite wall theory.....	5
2.3 Diffuse field assumption.....	7
2.4 Finite wall theory.....	10
2.5 Standard method.....	12
2.6 Summary.....	13
2.7 References.....	14
3 MODAL CHARACTERISTICS OF ROOMS AT LOW FREQUENCIES.....	15
3.1 Introduction.....	15
3.2 General wave theory.....	16
3.2.1 Basic equations.....	16
3.2.2 Linear Acoustics.....	20
3.2.3 Wave equation.....	20
3.2.4 Rectangular rooms.....	21
3.2.5 Eigenmodes and eigenfrequencies.....	22
3.2.6 Classification of normal modes.....	23
3.2.7 Modal density.....	23
3.2.8 Cut-off frequency and modal overlap factor.....	26

3.3 Models of sound fields in rooms.....	27
3.3.1 Analytical model.....	27
3.3.2 Numerical models.....	31
3.4 Summary.....	33
3.5 References.....	33
4 FINITE ELEMENT MODEL.....	37
4.1 Introduction.....	37
4.2 Applications in acoustics.....	37
4.3 Controlling parameters.....	38
4.4 Room-wall-room system.....	39
4.4.1 Acoustic field.....	39
4.4.2 Structural field.....	41
4.4.3 Acoustic-structural field.....	42
4.5 Model of test room.....	43
4.5.1 Assumptions.....	43
4.5.2 Sysnoise.....	44
4.6 Preliminary results.....	44
4.7 Summary.....	46
4.8 References.....	49
5 ROOM ABSORPTION.....	51
5.1 Introduction.....	51
5.2 Previous work.....	51
5.3 Air absorption.....	52
5.4 Absorption by porous surfaces.....	53
5.4.1 Theory.....	53
5.4.2 Locally reacting surfaces.....	54
5.4.3 Measurement methods.....	55
5.4.4 Parameter in FEM model.....	56
5.5 Modally reactive boundaries.....	57
5.6 Field measurements.....	59
5.7 Summary.....	61
5.8 References.....	61

6 REFERENCE TEST ROOM	65
6.1 Introduction.....	65
6.2 Measurement system.....	65
6.2.1 Maximum Length Sequences.....	66
6.2.2 Room details.....	67
6.2.3 Measurement instrumentation.....	69
6.3 Finite element model.....	73
6.4 Results.....	75
6.4.1 Preliminary comparison.....	75
6.4.2 Measurement and prediction of wall vibration.....	76
6.4.3 Adjusted model parameters.....	81
6.5 Summary.....	86
6.6 References.....	89
7 ROOM CONTENTS AS OBSTACLES	91
7.1 Introduction.....	91
7.2 Eigenfrequency shift.....	91
7.3 Standard unit and experimental set-up.....	93
7.4 Numerical model.....	96
7.5 Results.....	97
7.6 Summary.....	108
7.7 References.....	109
8 ROOM CONTENTS AS ABSORBERS	111
8.1 Introduction.....	111
8.2 Choice of sound absorption material.....	111
8.3 Impedance tube measurements.....	112
8.4 Absorbing floor area.....	116
8.5 Covered standard unit.....	120
8.5.1 Measurement.....	120
8.5.2 Prediction.....	120
8.6 Results.....	120
8.7 Summary.....	130

8.8 References.....	130
9 ROOM CONTENTS AS ‘SOFT’ ABSORBERS.....	132
9.1 Introduction.....	132
9.2 Effect of absorber thickness.....	132
9.3 Results.....	139
9.4 Summary.....	144
9.5 References.....	145
10 ROOM CONTENTS AS REAL FURNITURE.....	146
10.1 Introduction.....	146
10.2 Armchair.....	146
10.2.1 Measurements.....	146
10.2.2 Numerical model.....	151
10.3 Results.....	155
10.4 Summary.....	157
10.5 References.....	159
11 CONCLUDING REMARKS.....	160
11.1 Introduction.....	160
11.2 Conclusions.....	160
11.3 Topics for further research.....	164
APPENDIX – PUBLISHED PAPER.....	165

LIST OF FIGURES

Figure 2.1 – Sound transmission through an infinite thin wall.....	6
Figure 2.2 – Comparison between Mass Law (normal incidence), TL_m , and TL_{field}	9
Figure 2.3 – Sound transmission through a finite thin wall.....	11
Figure 3.1 – Sound pressure level in a corner of the small reverberant chamber of the ARU.....	16
Figure 3.2 – Finite volume of fluid, V , fixed in space.....	17
Figure 3.3 – Geometrical representation of the k -space.....	24
Figure 3.4 – Scheme used for the correct assessment of $N(f)$	25
Figure 3.5 – Experimental and analytical frequency response of a rectangular room of dimensions 5.78 m x 3.04 m x 4.24 m.....	31
Figure 4.1 – Room-Wall-Room system.....	39
Figure 4.2 – Percentile error between numerical and analytical eigenfrequencies for a room of dimensions 5.78 m x 3.04 m x 4.24 m.....	45
Figure 4.3 – Predicted room frequency response for the rectangular empty room model.....	46
Figure 4.4 – Spatial distribution of pressure amplitude for the first mode (1,0,0)...	47
Figure 4.5 – Spatial distribution of pressure amplitude for the fourth mode (0,1,0)	47
Figure 4.6 – Spatial distribution of pressure amplitude for the fifth mode (2,0,0)...	48
Figure 4.7 – Spatial distribution of pressure amplitude for the ninth mode (1,1,1).	48
Figure 5.1 – Measured and predicted frequency response of a 5.78 m x 4.89 m x 4.24 m room of plastered brick walls, and concrete floor and ceiling, according to Maluski and Gibbs (2001).....	60
Figure 5.2 – Measured and predicted frequency responses of a 4.24 m x 2.84 m x 2.40 m room with plasterboard and timber-frame walls, floor, and ceiling, according to Maluski and Gibbs (2001).....	60
Figure 6.1 – a) MLS of order 8 and b) its autocorrelation function according to Vorländer (1996).....	67
Figure 6.2 – Loudspeaker and microphone positions inside the investigated room, which has a change in angle at the door position.....	68
Figure 6.3 – Experimental set-up used in obtaining room frequency responses...	70
Figure 6.4 – Ratio of magnitudes of transfer functions for two microphones positioned at the lower corner of the investigated room.....	71

Figure 6.5 – Ratio of magnitudes for two measurements for the same microphone positioned inside the anechoic chamber of the ARU, with the 305 mm loudspeaker as the sound source.....	72
Figure 6.6 – Transfer function indicating the repeatability between two measurements for the same microphone positioned inside the anechoic chamber of the ARU, with the 457 mm loudspeaker as the sound source.....	72
Figure 6.7 – Comparison between measurement and preliminary prediction provided by the rectangular room model.....	74
Figure 6.8 – Isometric view of the refined finite element model of the test room...	74
Figure 6.9 – Predicted curves showing the differences between the results of improved room model and rectangular room model.....	75
Figure 6.10 – Preliminary comparison between measurement and prediction, for the improved room model with hard boundaries.....	76
Figure 6.11 – Experimental set-up for the investigation of wall vibration.....	77
Figure 6.12 – Vibratory response of test room wall.....	78
Figure 6.13 – Percentage error between theoretical and measured eigenfrequencies, as a function of the measured eigenfrequencies..	82
Figure 6.14 – Effect of increasing absorption coefficient on the room frequency response.....	83
Figure 6.15 – Level differences between measurement and prediction for hard wall, $\alpha = 2\%$, 5% , and 10%	84
Figure 6.16 – Curve of a polynomial expression simulating the loudspeaker roll-off at lower frequencies.....	85
Figure 6.17 – Prediction and measurement, after parameter adjustments.....	86
Figure 6.18 – Level differences between measurement and prediction for old model (Chapter 4) and new model with adjusted parameters.....	86
Figure 6.19 – Spatial distribution of pressure amplitude for the first mode (1,0,0).	87
Figure 6.20 – Spatial distribution of pressure amplitude for the fourth mode (0,1,0).....	87
Figure 6.21 – Spatial distribution of pressure amplitude for the fifth mode (2,0,0).	88
Figure 6.22 – Spatial distribution of pressure amplitude for the ninth mode (1,1,1).....	88
Figure 7.1 – Standard unit constructed of lightweight concrete blocks.....	93

Figure 7.2 – Standard unit also showing the detail of its internal construction.....	94
Figure 7.3 – Top view of the standard unit positions within the room. a) Central, b) centre wall, and c) corner position.....	95
Figure 7.4 – Effect of obstacle on room frequency response. Unit at central position.....	98
Figure 7.5 – Effect of obstacle on room frequency response. Unit at centre wall position.....	99
Figure 7.6 – Effect of obstacle on room frequency response. Unit at corner position.....	100
Figure 7.7 – Level difference between measured values and between predicted values. Unit at central position.....	101
Figure 7.8 – Level difference between measured values and between predicted values. Unit at centre wall position.....	102
Figure 7.9 – Level difference between measured values and between predicted values. Unit at corner position.....	102
Figure 7.10 – Effect of obstacle on room frequency response. Measurements shown in one-third octave bands.....	104
Figure 7.11 – Level difference between measured values and between predicted values. Results shown in one-third octave bands.....	105
Figure 7.12 – Spatial distribution of pressure amplitude for the first mode (1,0,0).	106
Figure 7.13 – Spatial distribution of pressure amplitude for the fourth mode (0,1,0).....	106
Figure 7.14 – Spatial distribution of pressure amplitude for the fifth mode (2,0,0).	107
Figure 7.15 – Spatial distribution of pressure amplitude for the ninth mode (1,1,1).....	107
Figure 8.1 – The selected sound absorbing material of thickness 150 mm.....	111
Figure 8.2 – Absorption coefficient for the selected foam extrapolated to low frequencies.....	114
Figure 8.3 – Absorption coefficient for the selected foam extrapolated to low frequencies.....	115
Figure 8.4 – Absorption coefficient, at a few discrete frequencies, as a function of the sound incidence angle.....	115
Figure 8.5 – Measurements of room frequency response for empty room, 29%, 49%, and 99% of the floor area covered with absorption.....	117

Figure 8.6 – Effect of covering the room floor with absorption material.....	117
Figure 8.7 – Effect of covering the room floor with absorption material showing the level difference between empty and 99% covered floor room responses.....	118
Figure 8.8 – Level difference between empty and 99% covered floor room responses. One-twelfth octave band results.....	118
Figure 8.9 – Measured and predicted frequency response of room with floor covered with 150 mm foam of absorption coefficient 50%.....	119
Figure 8.10 – Measured and predicted frequency response of room with standard unit in the corner position and covered with 150 mm absorption material.....	121
Figure 8.11 – Real and imaginary values of normal acoustic admittance obtained from the extrapolated absorption coefficients of Fig. 8.2.....	122
Figure 8.12 – Measured and predicted frequency response of room with floor covered with 150 mm absorption material. Measurement and prediction from refined room model.....	122
Figure 8.13 – Level differences between measurement and prediction of room with floor covered with 150 mm absorption material.....	123
Figure 8.14 – Measurements for empty room, hard box, and lined box at central floor position.....	123
Figure 8.15 – Results for the lined box in the central floor position indicating first axial (A), tangential (T) and oblique (O) modes.....	124
Figure 8.16 – Results for the lined box in the central floor position: comparison between measured and predicted level differences in 1/12 th octave bands.....	125
Figure 8.17 – Results for the lined box in the centre wall position indicating first axial (A), tangential (T) and oblique (O) modes.....	126
Figure 8.18 – Results for the lined box in the centre wall position: comparison between measured and predicted level differences in 1/12 th octave bands.....	126
Figure 8.19 – Results for the lined box in the corner position indicating first axial (A), tangential (T) and oblique (O) modes.....	127
Figure 8.20 – Results for the lined box in the corner position: comparison between measured and predicted level differences in 1/12 th octave	

bands.....	127
Figure 8.21 – Effect of obstacle on room frequency response. Measurements shown in one-third octave bands.....	128
Figure 8.22 – Level difference between measured values and between predicted values. Results shown in one-third octave bands.....	129
Figure 9.1 – Measured room frequency response for lined box case and soft box case. Results for central floor position.....	133
Figure 9.2 – Measured room frequency response for lined box case and soft box case. Results for centre wall position.....	133
Figure 9.3 – Measured room frequency response for lined box case and soft box case. Results for corner position.....	134
Figure 9.4 – Measured level differences between lined box FRFs and soft box FRFs in one-third octave bands.....	135
Figure 9.5 – Admittance as a function of frequency and material thickness.....	138
Figure 9.6 – Predicted room responses for smallest solid core case (Soft box-1), and largest solid core case (Soft box-3). Central room floor case....	139
Figure 9.7 – Level differences between measurement and prediction of room with soft unit in the centre of the room floor.....	140
Figure 9.8 – Comparison between measurement for the soft absorber and prediction for the ‘Soft box-2’ model. Central floor position results...	141
Figure 9.9 – Comparison between measurement for the soft absorber and prediction for the ‘Soft box-2’ model. Centre wall position results....	142
Figure 9.10 – Comparison between measurement for the soft absorber and prediction for the ‘Soft box-2’ model. Corner position results.....	142
Figure 9.11 – Effect of ‘soft absorber’ shown as level differences in one-third octave bands, taking the empty room results as a reference.....	143
Figure 10.1 – Armchair used in the real furniture investigations.....	147
Figure 10.2 – a) Comparison between frequency response measurements for empty room and room with the armchair at central floor position. b) Level difference between the two FRFs.....	148
Figure 10.3 – a) Comparison between frequency response measurements for empty room and room with the armchair at centre wall position. b) Level difference between the two FRFs.....	149
Figure 10.4 – a) Comparison between frequency response measurements for	

empty room and room with the armchair in the corner position. b)	
Level difference between the two FRFs.....	150
Figure 10.5 – Armchair at central floor position results.....	152
Figure 10.6 – Armchair at central floor position represented by the Chair-2 model	153
Figure 10.7 – Armchair at central floor position results. Comparison between measured and predicted level differences for the ‘Chair-2’ model....	154
Figure 10.8 – Level differences between measurement and prediction of room with armchair in the centre of the room floor.....	154
Figure 10.9 – Level differences between measurement and prediction of Chair-2 model at centre wall position.....	155
Figure 10.10 – Results for the armchair in the centre of the room floor.....	155
Figure 10.11 – Results for the armchair in the centre wall position.....	156
Figure 10.12 – Results for the armchair in the corner position.....	156
Figure 10.13 – Level difference between measured values and between predicted values. Results shown in one-third octave bands.....	158

LIST OF TABLES

Table 6.1 – Measured background noise level for the investigated room.....	68
Table 6.2 – Measured reverberation time for the investigated room.....	69
Table 6.3 – Equipment used in the experimental set-up shown in Fig. 6.3.....	70
Table 6.4 – Equipment used in the experimental set-up shown in Fig. 6.11.....	77
Table 6.5 – Identified wall modes.....	79
Table 6.6 – Wall material properties, according to Gibbs (1974).....	80
Table 6.7 – Theoretical eigenfrequencies (TE), numerical eigenfrequencies (NE), and percentage error (E) for the SSSS case.....	81
Table 6.8 – Theoretical eigenfrequencies (TE), numerical eigenfrequencies (NE), and percentage error (E) for the CCCC case.....	81
Table 7.1 – Comparison between values of reverberation time for the empty and furnished rooms, showing the standard unit unwanted sound absorption.....	94
Table 7.2 – Calculated absorption coefficient for the standard unit surface.....	95
Table 8.1 – Impedance tube results.....	113
Table 8.2 – Complex impedance and admittance results calculated from the values of Table 8.1.....	114
Table 9.1 – Values of admittance as a function of frequency and material thickness. Grey boxes indicate values obtained from measurements.....	137

GLOSSARY OF SYMBOLS

A_n	normal acoustic admittance
AE	analytical eigenfrequencies (Hz)
c_0	sound velocity in air (m/s)
c_l	longitudinal wave speed (m/s)
d	distance between the sample surface and the position of the first sound pressure level minimum
D	flexural rigidity
E	Young's modulus
f	frequency (Hz)
f_c	critical frequency (Hz)
f_{cc}	structural eigenfrequencies for a wall with clamped edges
f_{co}	coincidence frequency (Hz)
f_n	acoustic eigenfrequencies (Hz)
f_{ss}	structural eigenfrequencies for a simply supported wall
h	wall thickness (m)
k_0	incident wave number
k_b	bending wave number
m	mass per unit area of the wall (kg/m^2)
M	modal overlap factor
L_1	spatial averaged sound level in the source room (dB)
L_2	spatial averaged sound level in the receiving room (dB)
NE	numerical eigenfrequencies (Hz)
p_i	incident sound pressure (Pa)
p_r	reflected sound pressure (Pa)
p_t	transmitted sound pressure (Pa)
P_i	incoming sound power (W)
P_t	transmitted sound power (W)
P_n	acoustic eigenmodes
Q	scattering cross-section
r	distance between a radiating element on the wall and an observation point (m)
R	sound source strength

S	wall area (m ²)
S _s	total surface area (m ²)
t	time (s)
T	reverberation time (s)
TL	transmission loss (dB)
TL _m	transmission loss at random incidence (dB)
u	wall displacement (m)
v	wall surface velocity (m/s)
v _f	forced velocity of a thin wall (m/s)
V	room volume (m ³)
W	characteristic impedance
W _a	absorbed acoustic energy
W _i	incident acoustic energy
Z	acoustic impedance (rayl)
Z _h	acoustic impedance at thickness h
Z _{2h}	acoustic impedance at thickness 2h
Z _n	specific normal acoustic impedance
α	absorption coefficient
γ	propagation constant
Δ	phase angle
Δf	modal bandwidth
ζ	specific acoustic impedance
θ	sound incidence angle (rad)
λ ₀	wavelength of the incident sound (m)
ν	Poisson's ratio
ρ	wall density
ρ ₀	air density (kg/m ³)
σ	radiation efficiency
τ	transmission coefficient
Ψ	acoustic velocity potential
ω	angular frequency (rad/s)

RESUMO

Na área de transmissão sonora em edificações, uma recente ênfase tem sido dada ao estudo de freqüências audíveis, abaixo de 100 Hz. Isto se deve ao aumento do número de fontes de ruído de baixa freqüência, tais como uso de aparelhos domésticos de som ou TV com a capacidade de emitir sons graves cada vez mais potentes, etc. Existe uma preocupação especial com ruídos de baixa freqüência devido a sua eficiente propagação através do ar e eficácia reduzida de sua atenuação por parte de várias estruturas, como por exemplo, protetores auditivos e paredes entre residências. Contudo, em baixas freqüências, as abordagens teóricas mais utilizadas apresentam deficiências explicativas sobre a realidade estudada e precisam ser aprimoradas. Adicionalmente, observa-se que as normas referentes a isolamento sonoro não abrangem a região de freqüências abaixo de 100 Hz e nem mesmo a introdução do Anexo F da norma ISO 140/3 (1995) foi capaz de garantir um nível adequado de reprodutibilidade dos resultados. Nesse sentido, modelos de transmissão sonora entre salas que utilizam técnicas de EF têm demonstrado as características modais dos campos acústicos e vibratórios envolvidos no sistema sala-parede-sala, indicando a necessidade de modelos apropriados para a absorção sonora em baixas freqüências. Neste trabalho um novo modelo de EF foi utilizado para descrever as relações entre as características de absorção sonora das superfícies internas de uma sala e a resposta em freqüência desta sala, para o intervalo de freqüências de 20 Hz a 200 Hz. Inicialmente, o modelo numérico foi validado por comparação com resultados experimentais para uma pequena câmara reverberante vazia, denominada sala de referência. Adicionalmente, investigou-se o efeito da introdução de elementos de mobília no interior da sala, os quais foram abordados como obstáculos rígidos e macios, a fim de verificar possíveis modificações nas freqüências naturais e amortecimento seletivo dos modos do sistema. O efeito da localização de tais obstáculos também foi incluído nas investigações. Os resultados obtidos apresentaram um grau de concordância satisfatório entre valores medidos e simulados, permitindo a conclusão de que a absorção sonora não modifica significativamente as respostas em freqüência da sala em baixas freqüências.

ABSTRACT

Low frequency (below 100 Hz) sound transmission into and between dwellings is an increasing contribution to nuisance. This is due to a proliferation of hi-fi systems of high power and enhanced bass response, etc. There is a special concern about low frequency noise because of its efficient propagation in air, and the reduced ability of structures such as hearing protectors or separating walls to attenuate sound at these frequencies. It is at such low frequencies that existing theories of room acoustics and the relationships between sound level difference and sound reduction index are most tenuous. Current standards only deal with frequencies above 100 Hz, and despite the introduction of Annex F in ISO 140/3 (1995), for sound insulation measurements at low frequencies, there is still a poor repeatability between measurement results. A FE model of the sound transmission between dwellings has been developed which demonstrates the modal characteristics of the pressure and vibration fields of the rooms and separating wall, respectively. The work has highlighted the need for an appropriate model of sound absorption in small-furnished rooms at low frequencies. Therefore, in this thesis work, a new FE model is utilized to describe the relationship between the sound absorption characteristics of the internal surfaces of an enclosure, and its frequency response, for the frequency range below 200 Hz. Initially, a model of surface absorption appropriate for a modal description of contained sound fields at low frequencies is developed and an empty reference room is accurately modelled. In addition, the effect of inserting absorbent furniture is explored, in order to check for eigenmode shifts and selective damping of modes. The effect of furniture location is also investigated. Results indicate reasonable agreement between measurement and prediction allowing the conclusion that sound absorption has little effect on room frequency responses at low frequencies.

CHAPTER 1

INTRODUCTION

1.1 Motivation

One of the challenges in the area of Acoustics is to contribute to the development of knowledge necessary to the generation of conditions conducive to human comfort and activity. It is already known, for example, that prolonged exposure of people to high noise levels may give rise to stress and/or to hearing loss problems [Beranek (1971), Bies and Hansen (1996), Crocker (1997), Gerges (2000)]. Noise levels can be low and still constitute a nuisance. A definition of nuisance is the prevention of occupants' enjoyment of their own property. Acoustically, this enjoyment can take two simultaneous forms: the enjoyment of a quiet environment by a dweller and the enjoyment of loud music by a neighbour. This dual requisite requires that intervening walls and floors between dwellings should provide adequate sound insulation and impact isolation [Building Regulations of the U.K. Part E (2000)]. To help the Architect and Building Engineer comply with these standards, other standards exist containing recommended methods of measuring and rating the sound insulation of building elements, both in the laboratory and in the field [ISO 140 (1995)].

The standards apply to the frequency range 100-3150 Hz but a recent emphasis has been given to the study of the audible frequencies below 100 Hz. This is due to the increase in sources of low frequency noise, e.g., proliferation in hi-fi systems of high power and enhanced bass response, increased use of mechanical services and devices, and increasing traffic noise break-in. A review of the main low frequency noise sources can be found in the work of Berglund et al (1996). There is a special concern about low frequency noise because of its efficient propagation in air, and because of the reduced ability of structures such as hearing protectors or separating walls to attenuate sound at these frequencies [Mathys (1993), Berglund et al (1996)].

Unfortunately, it is at such low frequencies that existing theories of room acoustics and the relationships between sound level difference and sound reduction index are most tenuous. Current standards deal with frequencies above 100 Hz, and despite the introduction of Annex F in ISO 140/3 (1995), for sound insulation measurements at low frequencies, there is still a poor repeatability between

measurement results [Mathys (1993), Maluski and Bougdah (1997)]. The correction for receiver room absorption (and wall area), which relates the transmission loss of the separating wall to the sound level difference between the rooms, assumes a diffuse sound field condition. This assumption must be replaced with that which incorporates acoustic and vibration mode distributions. In a recent study by the Acoustic Research Unit (ARU) of the University of Liverpool, a Finite Element (FE) model has been developed to describe sound transmission between rooms at low frequencies [Maluski (1999)]. The model demonstrates that the modal characteristics of the pressure and vibration fields of the rooms and separating wall, respectively, strongly influence the sound level difference. The work has identified an important outstanding issue to be addressed, the need for an appropriate model of sound absorption in small furnished rooms at low frequencies, and the consideration of modally reactive absorption due to the vibration of the walls.

1.2 Objectives

The general objective of the thesis work was to characterise room absorption at low frequencies. In particular, the sound absorption at room surfaces and that due to room contents such as furniture was to be assessed with respect to their effect on steady-state sound level and therefore on sound level difference between rooms.

The specific objectives of the thesis work were to:

- Develop a model of surface absorption appropriate for a modal description of contained sound fields at low frequencies.
- Develop a model of contents absorption for the same modal description.
- Investigate experimentally, theoretically and numerically the effect of contents such as furniture on the frequency response of small rooms.

1.3 Overview of the thesis

The present work is contained in the broader area of sound transmission in buildings, and Chapter 2 states the general problem, introducing the basic theories on sound transmission through walls. Chapter 3 describes the resonant characteristics of rooms. The wave theory is presented as the most appropriate to

include the modal characteristics of rooms, and proposed investigation methods are considered.

Chapter 4 introduces the Finite Element Method (FEM), and its applications in the area of Acoustics. The basic theory is described, and preliminary numerical results are presented for an empty rectangular room. Chapter 5 describes the general theory of sound absorption, which is of main concern in this work. Locally and modally reactive assumptions are discussed and field measurements are presented and compared with FEM predictions.

Chapter 6 describes room frequency response measurements for an empty test room, which are to serve as a reference for the investigation of the effect of room contents on its frequency response. The measuring system characteristics are discussed, and the preliminary FE model developed in Chapter 4 is further implemented. Absorption is introduced in the numerical model, and the empty reference room is accurately modelled.

Chapter 7 introduces the investigation of the effect of room contents on the room frequency response. In this chapter, such contents are initially regarded as solid obstacles, and the investigation is performed by means of a 'standard unit' placed at different positions within the room. Eigenfrequency shifts, selective damping of modes and mode generation are analysed, using the empty room results of Chapter 6 as a reference. The room numerical model is modified to include the standard unit. Comparison between measurement and prediction is presented and discussed.

Chapter 8 advances in the investigation of room contents effect, commenced in Chapter 7, by considering the standard unit covered by a thick layer of a known sound absorbing material. A discussion is presented on the best possible way to include such a layer of absorption in the numerical model, and results are presented and fully analysed. Chapter 9 extends the investigation even further, by considering the standard unit entirely composed of absorbing foam, in total contrast with the solid obstacle described in Chapter 7. Once more modifications are applied to the numerical model to provide the best agreement with measurements, and the analyses performed in the previous chapters are employed again, in order to quantify the effect of introducing contents on the reference room frequency response.

The investigation is concluded in Chapter 10, by introducing a real element of furniture within the test room. The discussion of the results for the standard unit investigations, with the associated conclusions, dictates the best way to include the

considered element of furniture in the room model. Finally, Chapter 11 presents the overall work conclusions. Suggested topics for further research are also given in this final chapter.

1.4 References

BERGLUND, B., HASSMEN, P., SOAMES JOB, R. **Sources and effects of low-frequency noise**. Journal of the Acoustical Society of America, 99 (5), 2985-3002, 1996.

BERANEK, L. L. **Noise and vibration control**. McGraw Hill, New York, 1971.

BIES, D. A., HANSEN, C. H. **Engineering noise control: theory and practice**. E. and F. N. Spon, London, 1996.

CROCKER, M. J. **Handbook of acoustics**. John Wiley & Sons, New York, 1997.

Building Regulations of the UK Part E. **Resistance to the passage of sound**, 2000.

GERGES, S. **Ruído: fundamentos e controle**. Federal University of Santa Catarina U.P., Florianópolis, 2000.

ISO 140/3. **Measurement of sound insulation in buildings and of buildings elements - Part 3: Laboratory measurements of airborne sound insulation of buildings elements**. 1995.

MALUSKI, S. P. S., BOUGDAH, H. **Predicted and measured low frequency response of small rooms**. Journal of Building Acoustics, 4 (2), 73-85, 1997.

MALUSKI, S. P. S., **Low frequency sound insulation in dwellings**. Ph.D. Thesis, Sheffield Hallam University, Sheffield, 1999.

MATHYS, J. **Low-frequency noise and acoustical standards**. Applied Acoustics, 40, 185-199, 1993.

CHAPTER 2

SOUND INSULATION AT LOW FREQUENCIES

2.1 Introduction

It is recognised that low frequency (below 100 Hz) sound transmission into and between dwellings is an increasing contribution to nuisance. This is due to a proliferation of hi-fi systems of high power and enhanced bass response, increased use of domestic mechanical services and devices, and increasing traffic noise break-in [Berglund et al (1992), Mathys (1993), Maluski (1999), Melo et al (2001)]. However, in current standards for assessing sound insulation, the frequency range is normally limited to frequencies above 100 Hz [ISO 140/3 (1995), Maluski and Bougdah (1997), Kang (1999)]. For lower frequencies, measurements are not often performed since the sound fields in both source and receiving rooms are not sufficiently diffuse to meet the requirements of conventional standards. It also has been suggested that such measurements are only one facet of acoustic comfort at these frequencies [Mathys (1993)]. There is thus a recognised need for suitable methods to measure, evaluate and predict sound insulation below 100 Hz.

There are basically two mechanisms that inhibit the sound energy transmission between fluid spaces. In the first, sound energy is absorbed, particularly when passing through materials especially developed to efficiently convert acoustic energy into heat [Fahy (1985)]. Chapter 5 deals with this mechanism. In practice, it is the second mechanism that is used for sound insulation purposes. This involves the introduction of a change of impedance in the path of the sound, causing large reflection. The current chapter presents an overview of this second sound insulation mechanism.

2.2 Infinite wall theory

Consider a wall so large that effects, due to finite size, can be safely neglected. The wall is assumed thin, homogeneous, with no leaks, and with zero flexural rigidity (limp wall). The earliest model for sound transmission through a wall is as shown in Fig. 2.1 [Heckl (1981)]. An incident sound pressure field, p_i , impinges on a wall of

thickness h , at an angle θ between the incident wave vector and wall normal, and gives rise to a reflected and transmitted sound field p_r and p_t , respectively.

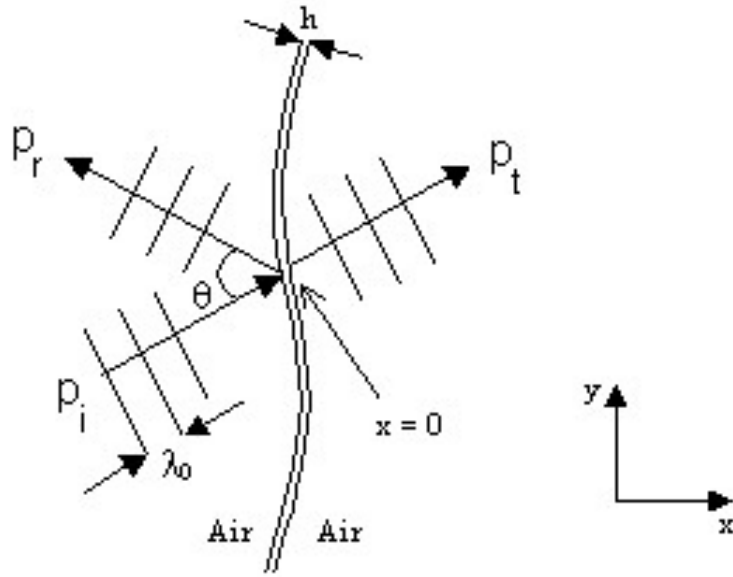


Figure 2.1 - Sound transmission through an infinite thin wall.

The angle is the same for the reflected and transmitted waves, since the medium is the same in both sides of the wall. Assuming harmonic pressure fields and omitting the factor $e^{i\omega t}$, the plane sound wave impinging on the wall is given by:

$$p_i(x, y) = A e^{-i(k_x x + k_y y)}, \quad (2.1)$$

where A is the sound pressure amplitude, and k_x and k_y are the components of the incident wave number k_0 in the x and y directions, respectively, where,

$$k_x = k_0 \cos \theta ; \quad k_y = k_0 \sin \theta ; \quad k_0 = \frac{2\pi}{\lambda_0} = \frac{\omega}{c_0}. \quad (2.2)$$

λ_0 is the wavelength of the incident sound. From equations (2.2) and (2.1):

$$p_i(x, y) = A e^{-i k_0 (x \cos \theta + y \sin \theta)}. \quad (2.3)$$

The corresponding expressions for the reflected and transmitted waves are

$$p_r(x, y) = B e^{i k_0 (x \cos \theta - y \sin \theta)} \quad (2.4)$$

$$p_t(x, y) = C e^{-i k_0 (x \cos \theta + y \sin \theta)}. \quad (2.5)$$

The continuity conditions for the sound pressure and particle velocity at the wall are

$$p_i(0, y) + p_r(0, y) - p_t(0, y) = \Delta P e^{-k_y y} \therefore A + B - C = \Delta P \quad (2.6)$$

$$\left\{ \begin{array}{l} v_i(0, y) + v_r(0, y) = v_t(0, y) \\ \rho_0 \frac{\partial v}{\partial t} = -\frac{\partial p}{\partial x} \end{array} \right. \therefore (A - B) \frac{\cos \theta}{\rho_0 c_0} = \frac{C \cos \theta}{\rho_0 c_0} = v_0, \quad (2.7)$$

where v_0 is the wall surface velocity and ΔP is the amplitude of the pressure difference that drives the wall. Newton's third law requires [Heckl (1981)]

$$\Delta P = i \omega m v_0, \quad (2.8)$$

where m is the mass per unit area of the wall. From equations (2.6) to (2.8):

$$\frac{C}{A} = \frac{1}{\left(1 + \frac{i \omega m \cos \theta}{\rho_0 c_0}\right)}. \quad (2.9)$$

The ratio of the transmitted and incident pressure amplitudes leads to the transmission coefficient for oblique incidence, $\tau(\theta)$, which is given by the ratio between the transmitted and incident sound intensities:

$$\tau(\theta) = \frac{I_t}{I_i} = \frac{\frac{|C|^2}{2 \rho_0 c_0}}{\frac{|A|^2}{2 \rho_0 c_0}} = \left| \frac{C}{A} \right|^2. \quad (2.10)$$

Finally, calculating the absolute value of equation (2.9) gives the transmission coefficient at oblique incidence [Heckl (1981), Gerges (1992)]:

$$\tau(\theta) = \frac{1}{1 + \left(\frac{\omega m \cos \theta}{2 \rho_0 c_0}\right)^2}. \quad (2.11)$$

2.3 Diffuse field assumption

In the calculation of the transmission coefficient, the classical (statistical) acoustics considers a sound field consisting of sound waves impinging on the wall from all directions with equal likelihood [Heckl (1981), Crocker (1997)]. This is the basic principle of a diffuse sound field, in which the incident waves are assumed to be uniformly distributed over all angles of incidence in such a way that each element of solid angle carries the same intensity towards the wall. Furthermore, it is assumed that the phases of the elementary waves are distributed at random, so that the

interference effects may be neglected and their energies can be simply added [Kuttruff (1981), ISO 140 (1995), Gerges (1992)].

Thus, in the computation of τ , it is necessary to average the latter for all possible angles θ . According to Heckl (1981) this is done by calculating the ratio of the transmitted sound power P_t to the incoming sound power P_i , giving:

$$\tau_m = \frac{P_t}{P_i} = 2 \int_0^{\pi/2} \tau(\theta) \cos \theta \sin \theta d\theta . \quad (2.12)$$

Introducing equation (2.11) into (2.12) and adopting $z = \cos(\theta)$, gives

$$\tau_m = 2 \int_0^1 \frac{z dz}{1 + \left(\frac{\omega m z}{2 \rho_0 c_0} \right)^2} . \quad (2.13)$$

Considering $R = (\omega m / 2 \rho_0 c_0)^2$ and using a new variable substitution, $u = 1 + R z^2$, gives

$$\tau_m = \frac{1}{R} \int_1^{1+R} \frac{du}{u} = \frac{1}{R} \ln(u) \Big|_1^{1+R} . \quad (2.14)$$

Performing the necessary calculations yields for the transmission coefficient for random incidence, τ_m :

$$\tau_m = \left(\frac{2 \rho_0 c_0}{\omega m} \right)^2 \ln \left[1 + \left(\frac{\omega m}{2 \rho_0 c_0} \right)^2 \right] . \quad (2.15)$$

From equation (2.15) an expression for the random incidence Transmission Loss TL_m is given by:

$$\begin{aligned} TL_m &= 10 \log \left(\frac{1}{\tau_m} \right) \therefore TL_m = 20 \log \left(\frac{\omega m}{2 \rho_0 c_0} \right) - 10 \log \left\{ \ln \left[1 + \left(\frac{\omega m}{2 \rho_0 c_0} \right)^2 \right] \right\} \therefore \\ \therefore TL_m &= 20 \log(m f) - 10 \log \left\{ \ln \left[1 + \left(\frac{\omega m}{2 \rho_0 c_0} \right)^2 \right] \right\} - 42.4 , \end{aligned} \quad (2.16)$$

where f is the frequency in Hz. Equation (2.16) is the so-called mass law formula (random incidence) and has been applied successfully in the normal frequency range [Heckl (1981)]. An approximate expression is given by [Reynolds (1981), Fahy (1985), Gerges (1992)]:

$$TL_{field} = 20 \log(m f) - 47.4 . \quad (2.17)$$

Equations (2.16) and (2.17) differ only by a small amount, as seen in Fig. 2.2.

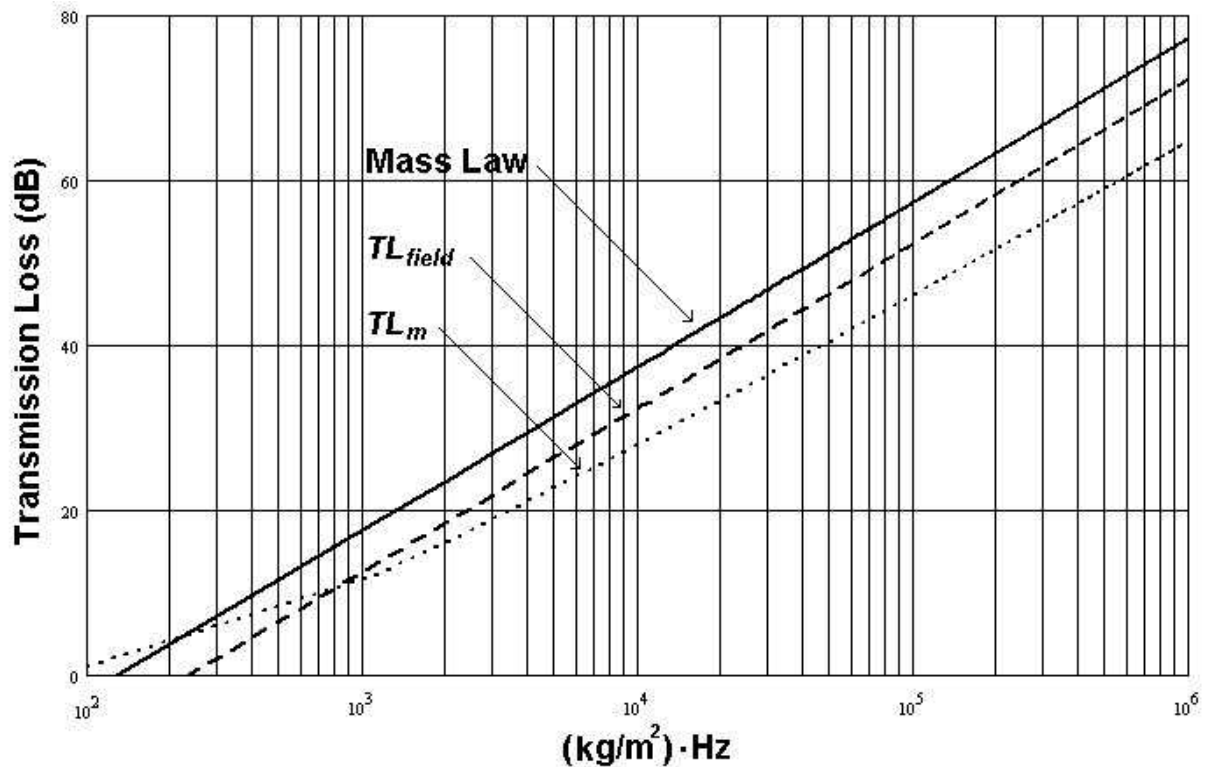


Figure 2.2 - Comparison between Mass Law (normal incidence), TL_m , and TL_{field} .

In order to introduce the flexural rigidity, D , in the sound transmission model, Kirchhoff's plate theory is used [Timoshenko and Young (1968, Heckl (1981))], giving for the flexural motion of a free thin wall:

$$D \left(\frac{\partial^4 v}{\partial y^4} + 2 \frac{\partial^4 v}{\partial y^2 \partial z^2} + \frac{\partial^4 v}{\partial z^4} \right) - \omega^2 m v = 0 , \quad (2.18)$$

where v is the wall velocity. The introduction of D in the model gives rise to a new phenomenon, the so-called coincidence effect, which occurs when the tangential component of the sound wave matches one of the free flexural waves of the wall. For a wall without damping, there will be total transmission when the vertical component of the incident wave number k_0 equals the free bending wave number on the wall, k_b , giving

$$k_b = k_0 \sin \theta , \quad (2.19)$$

where:

$$k_b = \sqrt[4]{\frac{\omega^2 m}{D}}. \quad (2.20)$$

Thus, the coincidence frequency, f_{co} , is given by [Heckl (1981), Fahy (1985), Gerges (1992)]

$$f_{co} = \frac{c_0^2}{1.8 h c_l \sin^2 \theta}, \quad (2.21)$$

where h is the wall thickness, and c_l is the longitudinal wave speed given by:

$$c_l = \sqrt{\frac{E}{\rho}}. \quad (2.22)$$

E is the Young's Modulus of the wall material and ρ is the wall density. From equation (2.21) it can be seen that the smallest coincidence frequency occurs for grazing incidence ($\theta = 0^\circ$). This frequency is called the critical frequency, f_c , which is given by:

$$f_c = \frac{c_0^2}{1.8 h c_l}. \quad (2.23)$$

Below f_c sound transmission occurs when the pressure fluctuation forces the wall to assume the same form of the acoustic field, such that the amplitude of the forced flexural wave does not depend on the wall damping. Such transmission is known as forced wall vibration, non-resonant wall response, or mass law, given by equation (2.16) [Heckl (1981), Fahy (1985), Maluski (1999), Gerges (1992)].

2.4 Finite wall theory

In calculating the sound transmission through a wall of finite size, as shown in Fig. 2.3, the radiation load [Heckl (1981)], which is a function of wall size, boundary conditions and mode shapes, is not included. This greatly simplifies the problem, but does not incur large errors since the additional mass due to the surrounding air is very small [Heckl (1981)]. Thus, the pressure driving the finite wall of Fig. 2.3 becomes twice the incoming pressure, and considering an incident wave as in equation (2.3), the forced velocity v_f of the thin wall is given by [Morse (1968), Heckl (1981), Kinsler et al (1982)]

$$v_f = \frac{2 A}{i \omega m'} e^{-i k_0 y \sin \theta}, \quad (2.24)$$

where m' is given by

$$m' = m \left[1 - \left(\frac{k_o \sin \theta}{k_b} \right)^4 \right]. \quad (2.25)$$

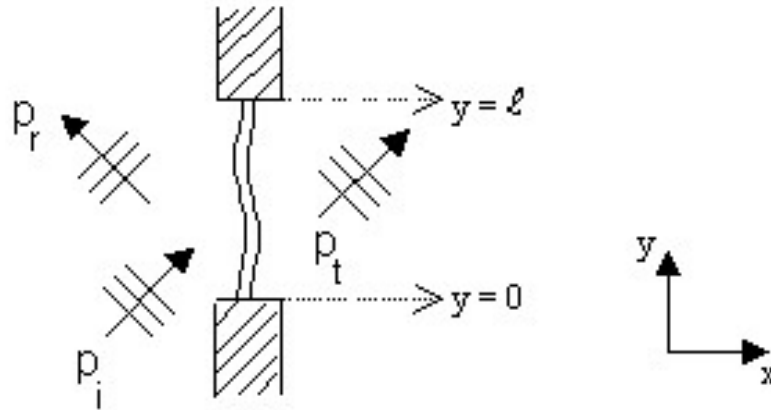


Figure 2.3 - Sound transmission through a finite thin wall.

Equation (2.24) does not satisfy the boundary conditions at $y = 0$ and $y = \ell$ and in order to do so, free waves, which are solutions of equation (2.18), must be introduced into equation (2.24) for the wall velocity

$$v = v_f + v_l = \frac{2A}{i\omega m'} e^{-ik_o y \sin \theta} + a_1 e^{-ik_b y} + a_2 e^{ik_b y} + a_3 e^{-k_b y} + a_4 e^{k_b y}, \quad (2.26)$$

where v_l is the velocity for the free wall motion. The constants a_i are determined from the boundary conditions:

$$\begin{cases} v(0) = v(\ell) = 0 \\ \left. \frac{\partial v}{\partial y} \right|_{y=0} = \left. \frac{\partial v}{\partial y} \right|_{y=\ell} = 0 \end{cases} \quad (2.27)$$

In the case where the wall is excited by a standing wave, the term representing the forced velocity in equation (2.26) must be replaced by

$$\frac{2A}{i\omega m'} (e^{-ik_o y \sin \theta} + e^{ik_o y \sin \theta}). \quad (2.28)$$

Thus, the transmitted sound may be obtained by the radiation of the wall considered as a baffled piston, having a velocity distribution as in equation (2.26). In this case, the Rayleigh's radiation formula yields:

$$p_t(x, y) = \frac{\omega \rho_o}{2} \int_0^l v(y) H_0^{(2)}(k_o r) dy, \quad (2.29)$$

where $H_0^{(2)}$ is the Hankel function [Gerges (1992)] and r is the distance between a radiating element on the wall, at $(0, y_o)$, and an observation point at (x, y) , i.e.,

$$r = \sqrt{x^2 + (y - y_o)^2}. \quad (2.30)$$

The full calculation of the transmitted power P_t from equation (2.29) is complicated. This problem is partially circumvented by treating the forced and free waves separately. However, the bending waves, due to forced and free motions, have different wavelengths, and therefore different radiation efficiencies, σ_f and σ_l , respectively [Heckl (1981)]. The transmitted power (neglecting the cross terms) becomes:

$$P_t = \frac{1}{2} S \rho_o c_o (v_f^2 \sigma_f + v_l^2 \sigma_l), \quad (2.31)$$

where S represents the wall area. The radiation efficiency, σ , gives an indication of how a sound source irradiates acoustic energy [Kinsler et al (1982), Gerges (1992)]. Additionally, Heckl (1981) considers as a reasonable approximation:

$$\begin{cases} \sigma_f \cong 1 \\ \sigma_l \cong \sigma_p, \end{cases} \quad (2.32)$$

where σ_p is the radiation efficiency for a point excitation [Maidanik (1962)].

From equations (2.26), (2.31) and (2.32), and assuming that the incident power P_i is given by

$$P_i = \frac{A^2 S}{4 \rho_o c_o}, \quad (2.33)$$

then the transmission loss may be obtained.

2.5 Standard method

The data describing sound insulation of solid building components are normally presented in terms of sound transmission loss (TL), also called sound reduction index (SRI). The assumptions inbuilt into the standard method of measurement [ISO 140/3 (1995)] is that damping effects are sufficiently described as a receiver room total absorption which relates the transmission loss, TL , to the resultant sound level

difference:

$$TL = L_1 - L_2 + 10 \log \left[\frac{S}{S_s \bar{\alpha}} \right], \quad (2.34)$$

where L_1 and L_2 are the spatial averaged sound levels in the source and receiving room, respectively, S is the area of the element under test, S_s is the total surface area and $\bar{\alpha}$ is the average sound absorption in the receiving room.

2.6 Summary

Increased consideration is being given to sound insulation at very low frequencies. Although unacceptable variations in inter-laboratory measurements have been intensively discussed since the 1950's, little has been done towards the development of a suitable measurement technique for frequencies below 100 Hz. The observed discrepancies are in part due to assumption of a diffuse field condition, which does not correspond to the modal characteristics encountered in rooms at low frequencies. This also influences the role of absorption in such sound fields.

The work reported in this thesis is a contribution towards a better understanding of the mechanisms of sound insulation at low frequencies by considering a modal approach to the analysis of sound fields in rooms. The work concentrates on the role of damping in the transmission of sound since there is not yet an agreed procedure for including room absorption (including furniture) in relating sound reduction index to the resultant sound level difference, below 100 Hz. The relationship is clearly understood above 100 Hz and is included in international standards, as described earlier. The question arises if similar relationships apply at low frequencies, or even if absorption needs to be included at all.

In order to investigate the absorbing effects of rooms and their contents, at low frequencies, the approach is to fully model and measure an empty test room and then to measure and predict the effects on room response of introducing contents, so as to be able to characterise them as obstructions and/or absorbers. The next chapter presents a general discussion of the wave theory used throughout this work to analyse the modal characteristics of rooms.

2.7 References

BERGLUND, B., HASSMEN, P., SOAMES JOB, R. **Sources and effects of low-**

- frequency noise.** Journal of the Acoustical Society of America, 99 (5), 2985-3002, 1996.
- CROCKER, M. J. **Handbook of acoustics.** John Wiley & Sons, New York, 1997.
- FAHY, F. **Sound and structural vibration: radiation, transmission and response.** Edition Academic Press, 1985.
- GERGES, S. **Ruído: fundamentos e controle.** Federal University of Santa Catarina U.P., Florianópolis, 1992.
- HECKL, M. *The tenth Sir Richard Fairey memorial lecture: sound transmission in buildings*, Journal of Sound and Vibration, 77 (2), 165-189, 1981.
- ISO 140/3. **Measurement of sound insulation in buildings and of buildings elements - Part 3: Laboratory measurements of airborne sound insulation of buildings elements.** 1995.
- KANG, J. **Measurement and prediction of airborne sound insulation at low frequencies in small rooms.** Personal correspondence, 1999.
- KINSLER, L. E., FREY, A. R., COPPENS A. B., SANDERS, J. V. **Fundamentals of acoustics.** Wiley, New York, 1982.
- KUTTRUFF, H. **Room acoustics.** Applied Science Publishers, 1981.
- MAIDANIK, G. **Response of ribbed panels to reverberant acoustic fields.** Journal of the Acoustical Society of America, 34, 809-826, 1962.
- MALUSKI, S. P. S., BOUGDAH, H. **Predicted and measured low frequency response of small rooms.** Journal of Building Acoustics, 4 (2), 73-85, 1997.
- MALUSKI, S. P. S. **Low frequency sound insulation in dwellings.** Ph.D. Thesis, Sheffield Hallam University, Sheffield, 1999.
- MALUSKI, S. P. S. Private Communication, 1999.
- MATHYS, J. **Low-frequency noise and acoustical standards.** Applied Acoustics, 40, 185-199, 1993.
- MELO, G. S. V., GIBBS, B. M., GERGES, S. N. Y. **A finite element model of sound absorption at low frequencies.** Proceedings of EURONOISE-2001, Patras, 2001.
- TIMOSHENKO, S., YOUNG, D. H. **Elements of strength of materials.** D. Van Nostrand Company, 1968.

CHAPTER 3

MODAL CHARACTERISTICS OF ROOMS AT LOW FREQUENCIES

3.1 Introduction

In Chapter 2, it was concluded that in order to achieve a full understanding of the acoustic properties of rooms at low frequencies, then classical acoustics, with diffuse sound field assumptions, should be replaced by a theory which accounts for acoustic and vibration mode distributions [Melo et al (2001)]. Diffuse sound field assumptions are generally used to describe sound pressure fields in rooms when there is a high modal density (number of modes per Hertz). While these assumptions are of some physical validity at medium and high frequencies, in the low frequency range room responses display a strong modal character [Gagliardini et al (1991)]. Large fluctuations in sound pressure, with respect to changes in both frequency and location, are observed. They are the result of the large spacing in frequency of the acoustic modes, where one mode can dominate the response in a particular frequency band [Maluski (1999)].

It is known that rooms such as concert halls, sound studios, lecture rooms, etc., display resonant characteristics. Knudsen (1932) reports the common observation that resonances are clearly perceptible in small hard-surfaced rooms. Also, many organists and choristers maintain that certain churches possess “sympathetic notes”, i.e., that these enclosures tend to reinforce certain tones [Knudsen (1932)]. According to Warnock and Vorländer (1993), rooms act like filters and, at low frequencies, only respond well at the resonances (see Fig. 3.1). Room frequency responses, measured in third-octave bands, may contain only one mode and it would be practically the same to measure only at that frequency, because for the other frequencies the room is ‘dead’ [Warnock and Vorländer (1993)].

This chapter presents an overview of the so-called wave theory of room acoustics [Kuttruff (1981)]. It can be argued that this theory, in its exact form, can only be applied to simple geometries, such as rectangular rooms, thus having immediate application to a very limited number of practical problems. However, as it will be shown in Chapter 4, the wave theory can be used in conjunction with

numerical methods, such as FEM, to describe enclosures of irregular shape, due to the presence of recesses, columns, wall irregularities, or even furniture.

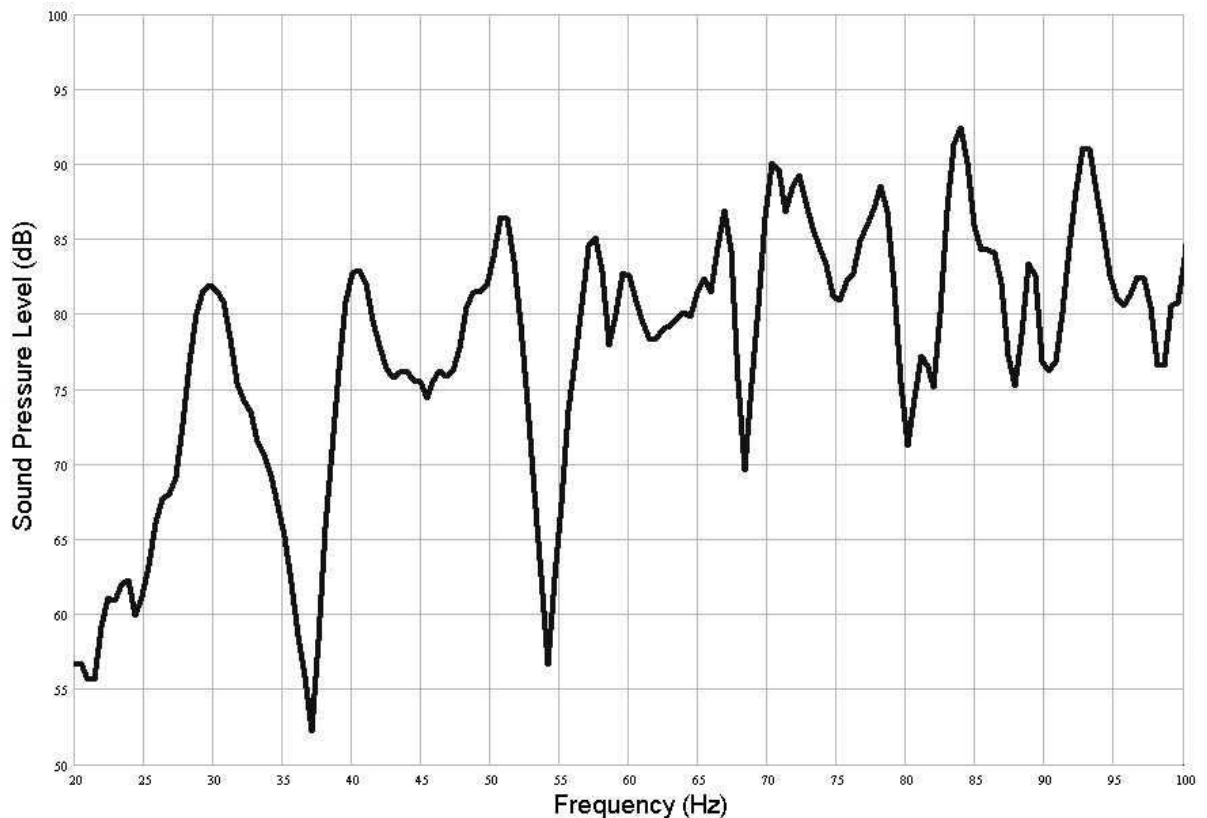


Figure 3.1 - Sound pressure level in a corner of the small reverberant chamber of the ARU (see Chapter 6).

3.2 General wave theory

The theory presented in the following sections allows the calculation of the sound pressure at any point within an enclosure, and takes into account important parameters which cannot be included in diffuse field based theories, such as source and receiver positions, shape and dimensions of the enclosure [Gagliardini et al (1991), Maluski (1999)].

3.2.1 Basic equations

The first of the fundamental equations of fluid dynamics (only non-viscous fluids will be considered here) is the continuity equation, which represents the conservation of mass [Arfken and Weber (1995)]. Consider a finite volume V , fixed in space, which has a surface S as its boundary, with a normal unit vector $\vec{n}(\vec{x})$, pointing in the

outward surface direction (see Fig. 3.2). Thus, at an arbitrary instant t , the total mass of fluid inside V is [Morse and Ingard (1968), Arken and Weber (1995), Lenzi (1998)]:

$$M = \int_V \rho(\vec{x}, t) dV. \quad (3.1)$$

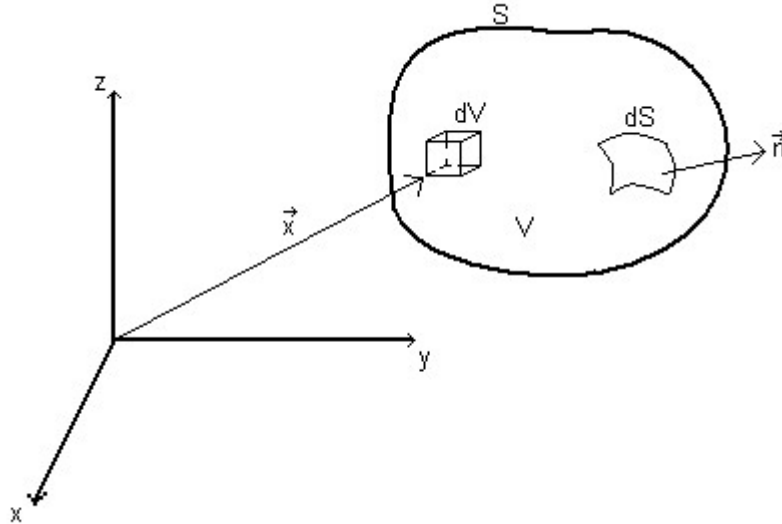


Figure 3.2 - Finite volume of fluid, V , fixed in space.

This mass may vary with time, and such variation can be described as:

$$\frac{d}{dt} \int_V \rho dV. \quad (3.2)$$

The rate must equal the rate of flow in, minus the rate of flow out of V . Thus, the conservation of mass requires:

$$\frac{d}{dt} \int_V \rho dV = \int_V \rho A(\vec{x}, t) dV - \int_S \rho \vec{v}(\vec{x}, t) \cdot \vec{n} dS, \quad (3.3)$$

where it is assumed that each volume unit has a velocity $\vec{v}(\vec{x}, t)$, and that at each point \vec{x} , inside V , the fluid mass increases at a rate $\rho A(\vec{x}, t)$, per unit volume. Thus, the first term in the right hand side of equation (3.3) represents the amount of fluid entering V , whereas the second term represents the amount of fluid leaving volume V throughout its boundaries. Since V is fixed in space, then:

$$\frac{d}{dt} \int_V \rho dV = \int_V \frac{\partial \rho}{\partial t} dV \quad (3.4)$$

From the Divergence Theorem [Morse and Ingard (1968), Cremer and Müller (1982), Arken and Weber (1995), Alves (1998)],

$$\int_S \rho \vec{v} \cdot \vec{n} dS = \int_V \vec{\nabla} \cdot (\rho \vec{v}) dV . \quad (3.5)$$

Thus,

$$\begin{aligned} \int_V \frac{\partial \rho}{\partial t} dV &= \int_V \rho A dV - \int_V \vec{\nabla} \cdot (\rho \vec{v}) dV \therefore \\ \therefore \int_V \left[\frac{\partial \rho}{\partial t} - \rho A + \vec{\nabla} \cdot (\rho \vec{v}) \right] dV &= 0 . \end{aligned} \quad (3.6)$$

As this result must apply to any arbitrary V , then the terms in the square brackets must be identically null at all points in the fluid. If there is no source inside V , such that $A = 0$, then the continuity equation is obtained in the form

$$\frac{\partial \rho}{\partial t} + \vec{\nabla} \cdot (\rho \vec{v}) = 0 . \quad (3.7)$$

The second fundamental equation of interest expresses conservation of momentum. Consider a volume element containing a fixed amount of mass, which moves with a velocity $\vec{v}(\vec{x}, t)$. This mass has a momentum given by

$$\vec{Q} = \int_V \rho \vec{v} dV . \quad (3.8)$$

The force associated with this momentum is

$$\begin{aligned} \vec{F} &= \frac{d\vec{Q}}{dt} = \int_V \frac{d}{dt} (\rho \vec{v}) dV \therefore \\ \therefore \vec{F} &= \int_V \rho \frac{d\vec{v}}{dt} dV . \end{aligned} \quad (3.9)$$

The force acting on the volume element is caused by normal and shear tensions on the element surfaces, and for unit volume:

$$\vec{f}_x = \vec{\nabla} \cdot (\sigma_x \hat{i} + \tau_{xy} \hat{j} + \tau_{xz} \hat{k}), \quad (3.10)$$

where $dF_x = f_x dV$; σ and τ represent normal and shear tensions, respectively, \hat{i} , \hat{j} and \hat{k} are unit vectors in the x , y and z directions, respectively, and similar expressions apply for f_y and f_z .

For a non-viscous (ideal) fluid the shear tensions vanish and the normal tensions equal the hydrostatic pressure, p [Lenzi (1998)]:

$$\sigma_x = \sigma_y = \sigma_z = -p. \quad (3.11)$$

Manipulation yields the equation of the equilibrium of forces:

$$\rho \frac{d\vec{v}}{dt} = -\vec{\nabla} p, \quad (3.12)$$

Since:

$$\frac{d\vec{v}}{dt} = \frac{\partial \vec{v}}{\partial t} + \frac{\partial \vec{v}}{\partial x} \frac{\partial x}{\partial t} + \frac{\partial \vec{v}}{\partial y} \frac{\partial y}{\partial t} + \frac{\partial \vec{v}}{\partial z} \frac{\partial z}{\partial t} \therefore \quad (3.13)$$

$$\therefore \frac{d\vec{v}}{dt} = \frac{\partial \vec{v}}{\partial t} + (\vec{v} \cdot \vec{\nabla}) \vec{v},$$

equation (3.12) can be rewritten as:

$$\rho \left[\frac{\partial \vec{v}}{\partial t} + (\vec{v} \cdot \vec{\nabla}) \vec{v} \right] + \vec{\nabla} p = \vec{0}, \quad (3.14)$$

which is known as Euler's equation [Morse and Ingard (1968), Temkin (1981), Lenzi (1998), Alves (1998)].

Finally, consider the equation of state, relating sound pressure and fluid density:

$$p \equiv p(\rho, s), \quad (3.15)$$

where s represents the entropy of the system. From equation (3.15):

$$dp = \left(\frac{\partial p}{\partial \rho} \right)_s d\rho + \left(\frac{\partial p}{\partial s} \right)_\rho ds. \quad (3.16)$$

It is assumed that the process is isentropic, i.e.:

$$\frac{ds}{dt} = 0 \therefore \quad (3.17)$$

$$\therefore \frac{dp}{dt} = \left(\frac{\partial p}{\partial \rho} \right)_s \frac{d\rho}{dt}.$$

As the term in brackets in equation (3.17) is a constant, then this expression may be rewritten as

$$\frac{dp}{dt} = c^2 \frac{d\rho}{dt}, \quad (3.18)$$

where c is the local propagating velocity of a perturbation in the fluid.

3.2.2 Linear acoustics

For the linear problem, it is possible to consider that the fluid dynamics results from small perturbations (p' , \vec{v}' , and ρ') in a uniform state represented by p_0 , \vec{v}_0 , and ρ_0 [Temkin (1981), Alves (1998)]. Thus, the fluid state, at any instant, may be represented by

$$\begin{aligned} p &= p_0 + p' \\ \vec{v} &= \vec{v}_0 + \vec{v}' \\ \rho &= \rho_0 + \rho' \end{aligned} \quad (3.19)$$

Substituting equation (3.19) into (3.7) and (3.14), and making use of (3.18) yields for the continuity equation

$$\frac{\partial p'}{\partial t} + \vec{v} \cdot \vec{\nabla} p' + \rho_0 c^2 \vec{\nabla} \cdot \vec{v} = 0, \quad (3.20)$$

and for Euler's equation

$$\rho_0 \left[\frac{\partial \vec{v}}{\partial t} + (\vec{v} \cdot \vec{\nabla}) \vec{v} \right] + \vec{\nabla} p' = 0. \quad (3.21)$$

Neglecting the terms involving products of acoustic parameters, and assuming c is approximately equal to c_0 (the velocity of sound in the non-perturbed fluid), then:

$$\frac{\partial p'}{\partial t} + \rho_0 c_0^2 \vec{\nabla} \cdot \vec{v} = 0 \quad (3.22-a)$$

$$\rho_0 \frac{\partial \vec{v}}{\partial t} + \vec{\nabla} p' = 0. \quad (3.22-b)$$

3.2.3 Wave equation

Differentiating equation (3.22-a) in relation to t and applying the divergent operator to equation (3.22-b) gives:

$$\frac{\partial^2 p'}{\partial t^2} + \rho_0 c_0^2 \frac{\partial}{\partial t} (\vec{\nabla} \cdot \vec{v}) = 0 \quad (3.23-a)$$

$$\rho_0 \frac{\partial}{\partial t} (\vec{\nabla} \cdot \vec{v}) + \nabla^2 p' = 0. \quad (3.23-b)$$

The first term in equation (3.23-b) appears in both expressions, and equation (3.23) now becomes [Knudsen (1932), Morse and Ingard (1968), Kuttruff (1981), Reynolds (1981), Cremer and Müller (1982)]:

$$\nabla^2 p' - \frac{1}{c_0^2} \frac{\partial^2 p'}{\partial t^2} = 0. \quad (3.24)$$

This is the so-called wave equation, which describes a pressure wave travelling in the fluid with velocity c_0 .

3.2.4 Rectangular rooms

The three-dimensional wave equation, for sound pressure, $p(x,y,z,t)$, is given by equation (3.24), where ∇^2 is the Laplacian operator [Reynolds (1981), Arken and Weber (1995)], t is time and c_0 is the sound velocity in air. Assuming harmonic sound signals, the sound pressure may be written

$$p(x, y, z, t) = P(x, y, z) \cdot e^{i \cdot \omega \cdot t}, \quad (3.25)$$

where ω is the angular frequency. Substituting equation (3.25) into (3.24) yields the three-dimensional Helmholtz equation for sound pressure

$$\nabla^2 P + k_0^2 P = 0, \quad (3.26)$$

where $k_0 = \omega/c_0$ is the wave number. This equation can be solved assuming separable functions, i.e.

$$P(x,y,z) = P(x) P(y) P(z). \quad (3.27)$$

Substituting this expression into the Helmholtz equation and separating the variables gives:

$$\frac{d^2 P(x)}{dx^2} + k_x^2 P(x) = 0, \quad (3.28)$$

with similar expressions for y and z , where:

$$k_x^2 + k_y^2 + k_z^2 = k_0^2. \quad (3.29)$$

Equation (3.28) has a general solution of the type (similar expressions apply for y and z)

$$P(x) = A_x \cos(k_x x) + B_x \sin(k_x x), \quad (3.30)$$

where A_x and B_x are constants. Furthermore, assuming a rectangular room with dimensions L_x , L_y , and L_z , and hard surfaces, the particle velocity at the walls is zero and the pressure is a maximum, i.e.

$$\vec{\nabla}P \cdot \vec{n} = 0, \quad (3.31)$$

where \vec{n} is the unit vector normal to the surface of the wall. Equation (3.31) is the boundary condition, upon which the sound field inside the room is strongly dependent [Bies and Hansen (1996), Crocker (1997)].

3.2.5 Eigenmodes and eigenfrequencies

The constants A_x, \dots, B_z from equation (3.30) are used to satisfy the boundary conditions prescribed by equation (3.31). The constant k_x must, therefore, assume one of the allowed values

$$k_x = \frac{n_x \pi}{L_x}, \quad (3.32)$$

where n_x is a non-negative integer. Using the previous results (together with the corresponding expressions for y and z) it is possible to obtain the general solution for the sound pressure inside the enclosure

$$P_n(x, y, z) = P_0 \cdot \cos\left(\frac{n_x \pi x}{L_x}\right) \cdot \cos\left(\frac{n_y \pi y}{L_y}\right) \cdot \cos\left(\frac{n_z \pi z}{L_z}\right), \quad (3.33)$$

where P_0 is a constant which can be interpreted as the maximum pressure amplitude [Maluski (1999)]. Furthermore, introducing the results for k_x , k_y and k_z into equation (3.29), and knowing that $\omega = 2 \pi f$, where f is the frequency in Hz, yields:

$$f_n = \frac{c_0}{2} \sqrt{\left(\frac{n_x}{L_x}\right)^2 + \left(\frac{n_y}{L_y}\right)^2 + \left(\frac{n_z}{L_z}\right)^2}. \quad (3.34)$$

Equations (3.33) and (3.34) specify, respectively, the shapes and natural frequencies of the acoustic modes that can exist in a rectangular room having dimensions L_x , L_y and L_z . Equation (3.33) represents a three-dimensional standing wave, and becomes complete with the factor $e^{j \omega t}$ describing the time dependence of the sound pressure. The collection of points at which the sound pressure is zero for

all times forms three equidistant planes (nodal planes), which are mutually orthogonal. However, for rooms of irregular shape the sets of points of vanishing sound pressure give birth to “nodal surfaces”, which are, generally, not planes [Kuttruff (1981)].

3.2.6 Classification of normal modes

If the cosine terms are expressed as exponentials, then equation (3.33) can be written as:

$$\underline{P}(x, y, z) = \underline{D} e^{i(\pm k_x x \pm k_y y \pm k_z z)}, \quad (3.35)$$

where \underline{D} is a constant. The underlining bar denotes complex quantities. Equation (3.35) indicates that there may be eight possible combinations of signs in the exponents, each of them representing (when multiplied by $e^{i\omega t}$) a plane travelling wave inside of a rectangular room [Gerges (2000), Kuttruff (1981), Cremer and Müller (1982)]. The standing waves described by equation (3.35) are classified in three categories:

- Axial modes: when two n 's are zero. These waves are made up of two travelling waves propagating parallel to one axis, and striking only two opposite walls;
- Tangential modes: when only one n is zero. In this case the standing wave is built up of four travelling waves, reflecting from four walls and moving parallel to the other two walls;
- Oblique modes: those for which none of the n 's are zero. These waves are made up of eight travelling waves, striking all the six room walls and moving in paths non-parallel to any of the room surfaces [Morse and Bolt (1944)].

3.2.7 Modal density

An expression for the modal density of a sound field in an enclosure can be obtained by considering the “ k -space”, where the wave numbers k_x , k_y , and k_z are interpreted as Cartesian coordinates (see Fig. 3.3). Then, each natural frequency is represented by discrete points [Morse and Bolt (1944), Kuttruff (1981)]. In turn, each of these points is determined by the intersection of three sets of equidistant, mutually

orthogonal planes, each of which cuts perpendicularly one of the axes at one of the allowed values of k_x , k_y , and k_z .

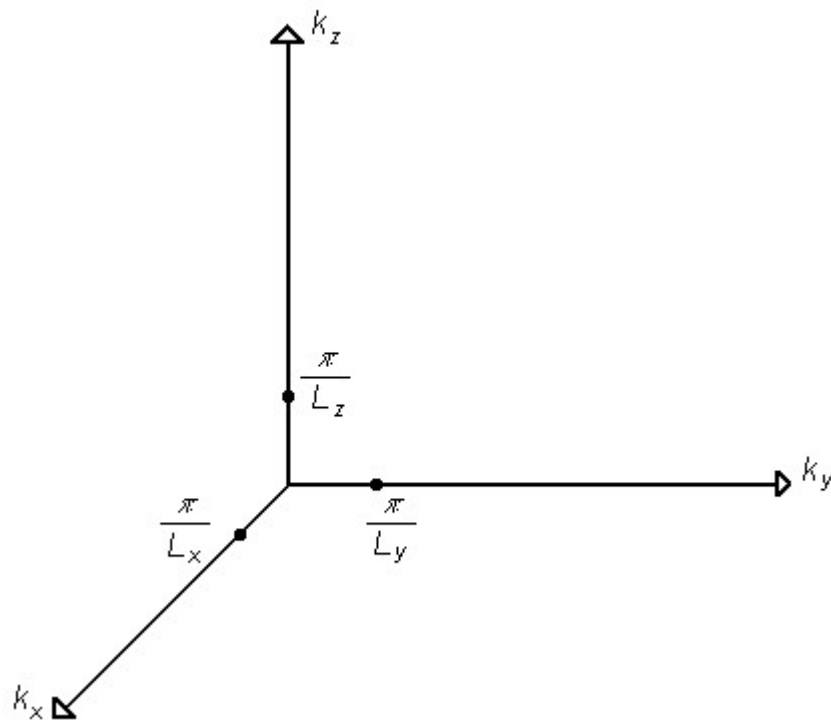


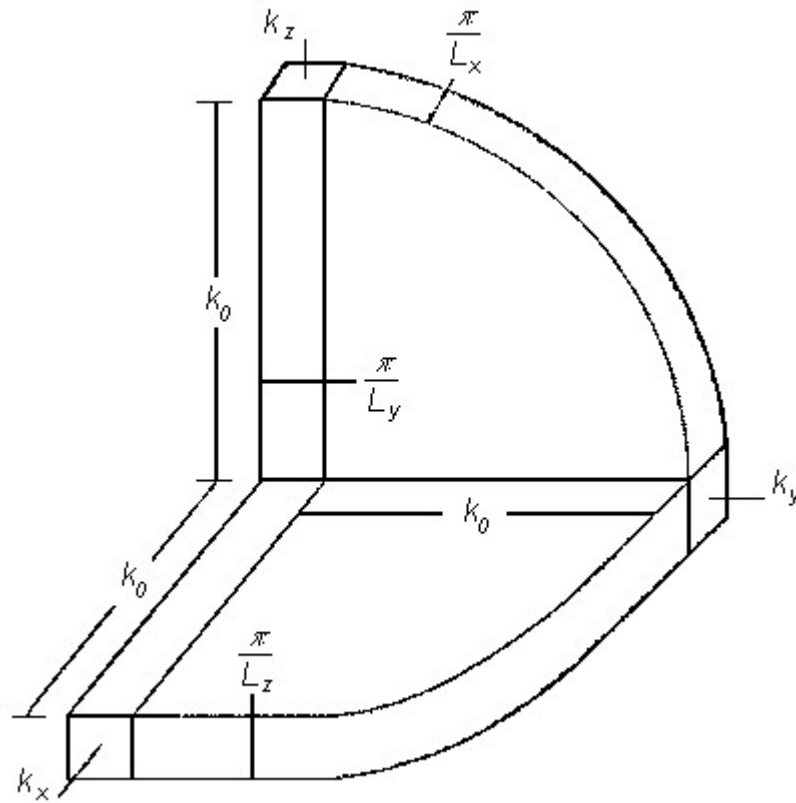
Figure 3.3 - Geometrical representation of the k -space.

Consequently, a rectangular lattice is formed in the first octant of the k -space, as negative eigenvalues are of no physical significance. With this geometrical representation, equation (3.29) may be seen as describing a spherical surface with radius k_0 [Kuttruff (1981), Cremer and Müller (1982)]. The volume enclosed by this sphere is thus $\frac{4}{3}\pi k_0^3$, where again, only one eighth of this volume is of interest. Two consecutive eigenfrequencies are spaced π/L_x , π/L_y , and π/L_z in the directions k_x , k_y , and k_z , respectively. Thus, the volume of a “unit cell” is given by:

$$\frac{\pi}{L_x} \frac{\pi}{L_y} \frac{\pi}{L_z} = \frac{\pi^3}{V}, \quad (3.36)$$

where V is the volume of the room.

Now let $N(f)$ be the number of modes from 0 Hz to an upper limit f , which is equivalent to the number of lattice points in the first octant of k -space, up to radius k_0 . To determine this quantity, one has to divide all the volume enclosed in the first octant, up to radius k_0 , by the volume of the unit cell, and in order to do this correctly it will be considered here the scheme shown in Fig. 3.4 [Lenzi (1998)].

Figure 3.4 - Scheme used for the correct assessment of $N(f)$.

Thus, using such scheme it is easier to see that the total volume occupied by the $N(f)$ modes is the summation of the following terms:

1. Volume, in the first octant, of sphere of radius k_0 :

$$V_1 = \frac{\pi k_0^3}{6}. \quad (3.37)$$

2. Volume of three fourths of discs (two of which are indicated in Fig. 3.4), having thickness $\pi/2L_x$, $\pi/2L_y$, and $\pi/2L_z$:

$$V_2 = \frac{\pi^2 k_0^2}{8} \left(\frac{1}{L_x} + \frac{1}{L_y} + \frac{1}{L_z} \right). \quad (3.38)$$

3. Volume of three rectangular columns of length k_0 , and having transversal sections $\pi^2/4L_x L_y$, $\pi^2/4L_x L_z$, and $\pi^2/4L_y L_z$:

$$V_3 = \frac{\pi^2 k_0}{4} \left(\frac{1}{L_x L_y} + \frac{1}{L_x L_z} + \frac{1}{L_y L_z} \right). \quad (3.39)$$

4. Volume of one eighth of the unit cell:

$$V_4 = \frac{\pi^3}{8V}. \quad (3.40)$$

In total, the number of modes, up to frequency f is:

$$N(f) = \frac{(V_1 + V_2 + V_3 + V_4)}{\pi^3/V} \therefore \quad (3.41)$$

$$\therefore N(f) = \frac{4\pi V}{3c_0^3} f^3 + \frac{\pi S}{4c_0^2} f^2 + \frac{L}{8c_0} f + \frac{1}{8},$$

where $S = 2(L_x L_y + L_x L_z + L_y L_z)$ and $L = 4(L_x + L_y + L_z)$. Finally, the number of modes per Hertz at the frequency f is given by:

$$n(f) = \frac{dN(f)}{df} \therefore \quad (3.42)$$

$$\therefore n(f) = \frac{4\pi V}{c_0^3} f^2 + \frac{\pi S}{2c_0^2} f + \frac{L}{8c_0}.$$

The three terms on the right hand side of equation (3.42) are respectively associated with oblique, tangential, and axial modes, described in Section 3.2.6.

3.2.8 Cut-off frequency and modal overlap factor

The sound field inside an enclosure can be assumed to be diffuse when the modal density becomes sufficiently large [Maluski (1999)]. This will happen above the so-called cut-off frequency, f_c , which depends on the limiting modal density assumed. Increasingly, reference is made to the modal overlap factor, M , given by [Schroeder (1969), Crocker (1997)]:

$$M = \frac{\sum \Delta f_i}{B}, \quad (3.43)$$

where Δf_i is the distance in Hertz between the -3 dB points (below the peak) on the response curve. B is the frequency band. Averaging the modal bandwidth over all modes in the frequency band B , gives [Cremer et al (1973)]:

$$\Delta f = \frac{2.2}{T}, \quad (3.44)$$

where T is the reverberation time. The modal overlap is a function of modal density and room loss factor since both contribute to a smoothing of the frequency response, and in more general terms may be defined as [Bies and Hansen (1996)]

$$M = \Delta f \cdot n(f). \quad (3.45)$$

The cut-off frequency is given by [Schroeder (1969), Crocker and Price (1975), Viveiros (1998), Maluski (1999)]

$$f_c = \sqrt{\frac{Mc_0^3 T}{8.8\pi V}}. \quad (3.46)$$

Generally, the sound field is assumed diffuse when the modal overlap factor is greater than or equal to 3 [Schroeder (1969), Bies and Hansen (1996)]. Above this, Crocker (1997) refers to the high-frequency range.

3.3 Models of sound fields in rooms

In the following sections different theoretical and numerical models of room frequency response are described with the intention of selecting the most appropriate for the proposed investigation.

3.3.1 Analytical model

An analytical model is described which allows the prediction of the transfer function between two points inside a rectangular enclosure. In order to obtain such an expression, the Helmholtz equation (3.26) is again considered, but this time to describe the sound pressure field inside a rectangular room. The room surfaces are assumed to be locally reacting, with acoustical properties determined by the surface impedance, Z , which in turn depends on the surface and the frequency, but not on the sound incidence angle [Kuttruff, (1981)]. Equation (3.31) assumes the form:

$$\vec{\nabla} P \cdot \vec{n} = \frac{\partial P}{\partial n} = -i\omega\rho_0 v_n, \quad (3.47)$$

where v_n is the normal component of the particle velocity at the wall surface [Morse and Ingard (1968), Cremer and Müller (1982), Gerges (2000)]. Using the concept of normal impedance, equation (3.47) becomes

$$Z \frac{\partial P}{\partial n} + i\omega\rho_0 P = 0, \quad (3.48)$$

and replacing Z by the specific impedance $\zeta = Z/\rho_0 c_0$ gives

$$\zeta \frac{\partial P}{\partial n} + ikP = 0. \quad (3.49)$$

The Helmholtz equation (3.26) yields non-zero solutions, fulfilling the boundary condition (3.49), only for discrete values of k , called eigenvalues and denoted by k_n [Kuttruff (1981)]. As in Section 3.2.5, each eigenvalue k_n is associated with an eigenfunction $P_n(r)$, where r denotes the position in space. If k has a fixed value in the boundary condition, which may be given by the driving frequency of a sound source, then it is possible to show that the eigenfunctions are mutually orthogonal [Cremer and Müller (1982), Kuttruff (1981), Gerges (2000)]:

$$\iiint_V P_n(r) P_m(r) dV = \begin{cases} K_n, & \text{if } n = m \\ 0, & \text{if } n \neq m \end{cases}, \quad (3.50)$$

where K_n is a constant and V is the room volume. If all the eigenvalues and eigenfunctions of a room are known, it is possible to obtain the steady state response to arbitrary sound sources. Assuming a sound source density function $a(r)$ with a driving (angular) frequency ω , the wave equation becomes (as when considering the term $A \neq 0$ in equation (3.6)):

$$\nabla^2 P + k^2 P = -i\omega\rho_0 a(r). \quad (3.51)$$

The sound source density function may be a complex function of sound sources, distributed throughout the room [Kuttruff (1981)]. Furthermore, since the eigenfunctions form a complete and orthogonal set of functions, $a(r)$ can be expanded in a series of P_n :

$$a(r) = \sum_n B_n P_n(r), \quad (3.52)$$

where the summation is extended over all possible values of n (i.e., n_x , n_y , and n_z), and B_n is a constant. For the sought solution $P(r, \omega)$ a similar expansion yields

$$P(r, \omega) = \sum_n C_n P_n(r), \quad (3.53)$$

and the solution can be determined once the coefficients C_n are calculated in terms of the coefficients B_n . Introducing both series into equation (3.51), and using $\nabla^2 P_n = -k_n^2 P_n$ gives:

$$C_n = i\omega\rho_0 \frac{B_n}{k^2 - k_n^2}. \quad (3.54)$$

Assume a point source at position r_0 , with a constant volume velocity A . The sound source density function may be expressed in terms of a Dirac delta function:

$$a(r) = A \delta(r - r_0). \quad (3.55)$$

This assumption allows a simple calculation of the coefficients B_n , which are then given by

$$B_n = \frac{1}{K_n} A P_n(r_0). \quad (3.56)$$

Substituting (3.56) into (3.54) and the result into (3.53) yields for the sound pressure inside a rectangular room excited by a point source:

$$P(r, \omega) = iA\omega\rho_0 \sum_n \frac{P_n(r)P_n(r_0)}{K_n(k^2 - k_n^2)}, \quad (3.57)$$

which is known as the Green's function of the room [Kuttruff (1981)]. If any portion of the room boundary has a complex value of impedance, the eigenvalues k_n will be also complex quantities [Morse and Ingard (1968)], i.e.

$$k_n = \frac{\omega_n}{c_0} + i \frac{\varpi_n}{c_0}, \quad (3.58)$$

and assuming $\varpi_n \ll \omega_n$, equation (3.57) becomes:

$$P(r, \omega) = iAc_0^2\omega\rho_0 \sum_n \frac{P_n(r)P_n(r_0)}{K_n(\omega^2 - \omega_n^2 - 2i\varpi_n\omega_n)}. \quad (3.59)$$

Equation 3.59 is the transfer function between the two points r and r_0 . The parameter ϖ_n is referred to as the modal damping constant [Kuttruff (1981)], which may be quantified in terms of the modal bandwidth, Δf . Writing equation (3.59) in a condensed form gives:

$$P(r, \omega) = \sum_n \frac{D_n}{\omega^2 - \omega_n^2 - 2i\varpi_n\omega_n}, \quad (3.60)$$

where D_n is a function not only of the source and receiver positions, but also of the frequency. The strong frequency dependence is indicated by the term $\omega^2 - \omega_n^2$ and it is possible to replace ω_n by ω in the last term of the denominator without any serious error. This allows a much simpler way of calculating the absolute value of the n^{th} term of equation (3.60) [Kuttruff (1981), Kropp and Pietrzyk (1999)]:

$$|P| = \frac{|D_n|}{\left[(\omega^2 - \omega_n^2)^2 + 4\omega^2 \varpi_n^2 \right]^{1/2}}. \quad (3.61)$$

The stationary sound pressure in a room, at a single exciting frequency, results from the combined effect of several resonance systems with angular resonance frequencies ω_n and damping constants ϖ_n , which lie mostly between 1 and 20 s⁻¹ [Kuttruff (1981)].

Summarising, the sound pressure is at resonance whenever $\omega = \omega_n$, and at the n^{th} resonance the n^{th} eigenvalue P_n predominates, having an amplitude inversely proportional to the imaginary part of k_n for that frequency [Morse and Ingard (1968)]. Based on equation (3.60), and using the software Matlab [Matlab Rev 5.1 (1997)] a computer routine was written in order to calculate a room frequency response for a rectangular room having the same overall dimensions as the small reverberant chamber of the Acoustics Research Unit (see Chapter 6). For such a room, the eigenvalues ω_n were calculated and the damping constants ϖ_n were obtained from the measured frequency response, using the half-power bandwidth method. The parameters D_n were assigned unit values, since sources and receivers were assumed to be in room corners. Fig. 3.5 presents a comparison between the analytical model and experimental results, which were primarily shown in Fig. 3.1.

The development of the analytical model was important as it gave insights into the modal characteristics of room resonances at low frequencies. However, it posed limitations to the proposed investigation. These arise mainly from the fact that this method can only deal with perfectly rectangular rooms and simple sound sources assumptions. Furthermore, it cannot deal with inhomogeneous surface absorption [Gagliardini et al (1991), Kihlman et al (1994), Kropp et al (1994), Maluski (1999)].

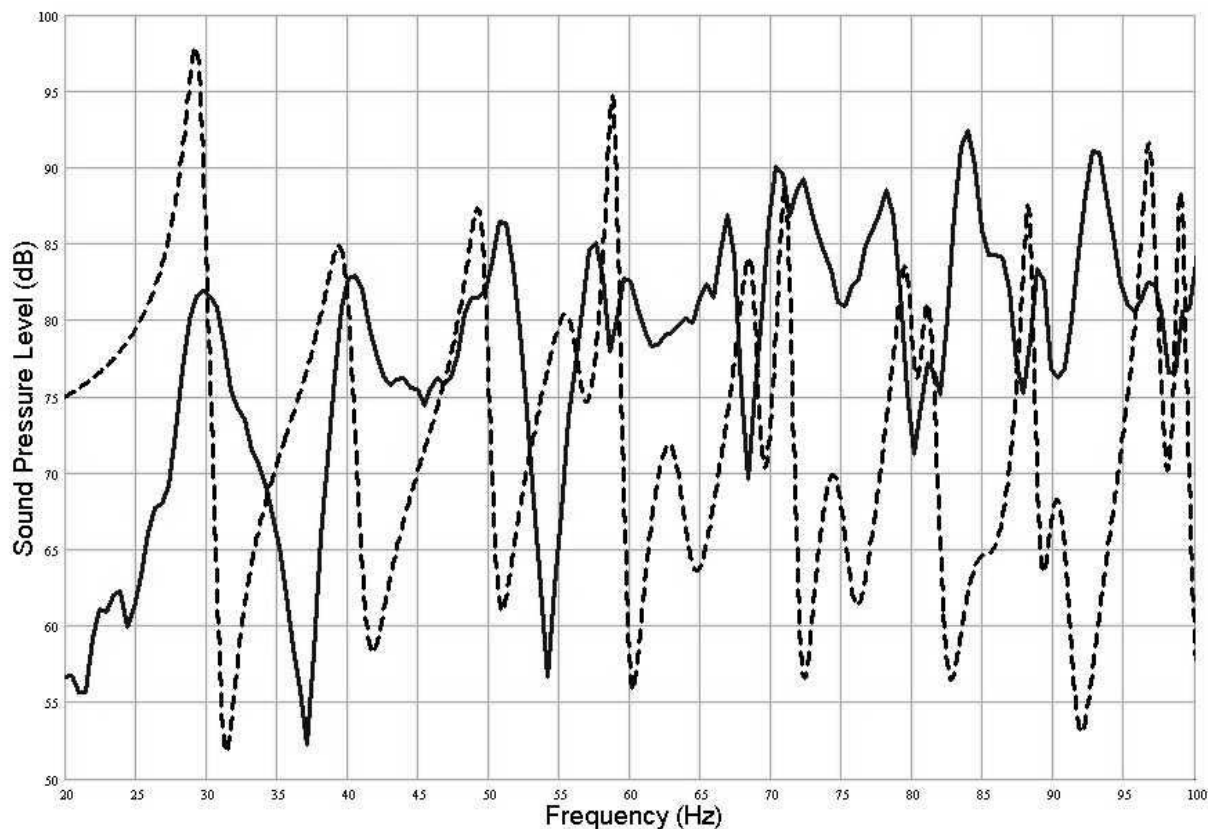


Figure 3.5 - Experimental (—) and analytical (---) frequency response of a rectangular room of dimensions 5.78 m x 3.04 m x 4.24 m.

The poor agreement between analytical and experimental results shown in Fig. 3.5 is principally due to the impossibility of such a model to account for even small irregularities in the room geometry, as was the case of the room measured (see Chapter 6). Also, it was difficult to correctly estimate the damping constants due to modal superposition. It was concluded that an analytical model would not be sufficiently flexible or accurate for the investigation proposed.

3.3.2 Numerical models

While separable coordinate systems are available for enclosures of simple geometries, it is necessary to resort to numerical methods, e.g., the Boundary Element Method (BEM) and the Finite Element Method (FEM) for enclosures of complex geometries [Bai (1992)]. In the 1960's the integral equations had important influence in the development of FEM (this method is discussed in greater detail in Chapter 4).

Later, a method was developed to model the system at its boundaries, allowing the prediction of radiation and scattering phenomena in infinite domains. Boundary Element Methods have been reported in the literature [Cops (1994), Atalla and Bernhard (1994), Crocker (1997), Maluski (1999)]. BEM is a numerical method for obtaining approximate solutions to boundary integral equations. The equations provide a well defined formulation of boundary-value problems in different branches of engineering, e.g., elasticity, plasticity, fracture mechanics, wave propagation, etc. [Tullberg (1983), Holmström (2001)].

Initially, boundary integral equations were considered to be a different type of analytical method, somewhat unrelated to other approximate methods such as the Finite Element Method [Holmström (2001)]. As with FEM, the interest for BEM has increased with the development of computer speed and power [Tullberg (1983), Brebbia (1984), Holmström (2001)]. In both methods the problem domain must be discretized into finite elements. However, while in FEM the entire domain has to be discretized, in BEM only the bounding surface of the domain is divided into elements. BEM consists basically of two different approaches: the indirect and the direct approach. For the direct approach, at least one closed boundary is required, and the physical variables (sound pressure and normal particle velocity for acoustic problems) can only be considered on one side of the surface. This approach can be used for internal or external problems, but not both. On the other hand, the indirect approach yields the variables discontinuities through the surface, dealing with interior and exterior problems simultaneously [Tullberg (1983), Brebbia (1984), Crocker (1997)]. Although BEM may seem particularly attractive, since dimensionality of the problem is reduced by the fact that only boundary meshes need to be constructed [Bai (1992)], it is recognized that its main applications are for exterior problems, as acoustic mode prediction is relatively poor [Pietrzyk and Pedersen (1996), Crocker (1997), Maluski (1999)]. Therefore, this method was not selected for the prediction of room frequency response.

FEM on the other hand can effectively solve interior acoustic problems, related to bounded geometries. So far, it has proved to be a valid analysis technique for acoustic problems with various dissipative boundary conditions. The strength of this method lies in its flexibility regarding room geometry, boundary conditions and forcing functions [Bernhard (1985), Ma and Hagiwara (1991), Smith and Bernhard (1992), Sysnoise Rev 5.1 (1993)]. FEM can take into account locally absorbing linings of

various thicknesses and therefore offered the possibility of considering room contents (furniture and other obstructions) as absorbers as well as non uniform distributions of surface absorption. For these reasons, this method was selected as the appropriate technique to predict room frequency responses, for comparison with measurements throughout this work.

3.4 Summary

Rooms display resonant features at low frequencies. Such modal character is exemplified by narrow band measurements of room response. It is the purpose of this work to fully model and measure the frequency response of an empty test room, and then to measure and predict the effects of introducing contents on this room response, so as to be able to characterize such contents as obstructions and/or absorbers.

Different investigation methods have been considered, including analytical and Boundary Element Methods. FEM was selected as the most appropriate approach for this study. It is better suited than BEM for the determination of natural frequencies and mode shape of cavities. It is able to deal with non-rectangular geometries (unlike analytical models) and dissipative boundary conditions. FEM is described in greater detail in the next chapter.

3.5 References

- ALVES, M. K. **Teoria Linear**. Lecture notes of the Post Graduate Course in Mechanical Engineering, Federal University of Santa Catarina, Florianópolis, 1998.
- ARFKEN, G. B., WEBER, H. J. **Mathematical methods for physicists**. Academic Press, San Diego, 1995.
- ATALLA, N., BERNHARD, R. J. **Review of numerical solutions for low frequency structural-acoustic problems**. Applied Acoustics, 43 (3), 271-294, 1994.
- BAI, M. R. **Study of acoustic resonance in enclosures using eigenanalysis based on boundary element methods**. Journal of the Acoustical Society of America, 91 (5), 2529-2538, 1992.
- BERNHARD, R. J. **Synthesis of acoustical shapes using the finite element**

- method.** Journal of Sound and Vibration, 98 (1), 55-65, 1985.
- BIES, D. A., HANSEN, C. H. **Engineering noise control: theory and practice.** E. and F. N. Spon, London, 1996.
- BREBBIA, C. A. **Boundary element techniques in computer-aided engineering.** Martin Nijho, Publisher, Dordrecht, 1984.
- COPS, A. **Progress in building acoustics.** Proceedings of Inter-Noise 94, 1, 23-42, Yokohama, 1994.
- CREMER, L., HECKL, M., UNGAR, E. E. **Structure-borne sound.** Springer-Verlag, New York, 1973.
- CREMER, L., MÜLLER, H. **Principles and applications of room acoustics.** Volume 2, Applied Science Publishers, London, 1982.
- CROCKER, M. J., PRICE, A. **Noise and noise control.** Vol. 1, CRC, Press, 1975.
- CROCKER, M. J. **Handbook of acoustics.** John Wiley & Sons, New York, 1997.
- GAGLIARDINI, L., ROLAND, J., GUYADER, J., L. **The use of a functional basis to calculate acoustic transmission between rooms.** Journal of Sound and Vibration, 145, 457-478, 1991.
- GERGES, S. **Ruído: fundamentos e controle.** Federal University of Santa Catarina U.P., Florianópolis, 2000.
- HOLMSTRÖM, F. **Structure-acoustic analysis using BEM/FEM; implementation in Matlab.** Master Dissertation, Structural Mechanics & Engineering Acoustics, Lund, 2001.
- KIHLMAN, T., KROPP, W., PIETRZYK, A. **Concept of reduction index at low frequencies.** Proceedings of Inter-Noise 94, 1, 1463-1468, Yokohama, 1994.
- KNUDSEN, V. O. **Resonance in small rooms.** Journal of the Acoustical Society of America, 4 (1), 20-37, 1932.
- KROPP, W., PIETRZYK, A., KIHLMAN, T. **On the meaning of sound reduction index at low frequencies.** Acta Acustica, 2, 379-392, 1994.
- KROPP, W., PIETRZYK, A. **Statistical analysis of the influence of the room dimensions on the sound insulation at low frequencies.** Report F-99-03, Department of Applied Acoustics, Gothenburg, 1999.

- KUTTRUFF, H. **Room acoustics**. Applied Science Publishers, 1981.
- LENZI, A. **Acústica avançada**. Lecture notes of the Post Graduation Course in Mechanical Engineering, Federal University of Santa Catarina, Florianópolis, 1998.
- Ma, Z. D., HAGIWARA, I. **Sensitivity analysis methods for coupled acoustic-structural system**. AIAA Journal, 29 (11), 1787-1801, 1991.
- MALUSKI, S. P. S. **Low frequency sound insulation in dwellings**. Ph.D. Thesis, Sheffield Hallam University, Sheffield, 1999.
- MATLAB REV 5.1. **User Manual**. The Math Works, Inc., 1997.
- MELO, G. S. V., GIBBS, B. M., GERGES, S. N. Y. **A finite element model of sound absorption at low frequencies**. Proceedings of EURONOISE-2001, Patras, 2001.
- MORSE, P. M., BOLT, R. H. **Sound waves in rooms**. Reviews of Modern Physics, 16 (2), 1944.
- MORSE, P. M., INGARD, K. U. **Theoretical acoustics**. McGraw Hill, New York, 1968.
- PIETRZYK, A., PEDERSEN, D. B. **Numerical simulation of laboratory sound insulation determination experiments**. Proceedings of Inter-Noise 96, 4, 1773-1778, Liverpool, 1996.
- REYNOLDS, D. **Engineering principles of acoustics**. Allyn and Bacon, 1981.
- SCHOEDER, M. R. **Effects of frequency and space averaging on the transmission response of multimode media**. Journal of the Acoustical Society of America, 46 (2), 277-283, 1969.
- SMITH, D. C., BERNHARD, R. J. **Computation of acoustic shape design sensitivity using a boundary element model**. ASME Journal of Vibration and Acoustics, 114, 127-132, 1992.
- TEMKIN, S. **Elements of acoustics**. John Wiley & Sons, New York, 1981.
- TULLBERG, O. **A study of the boundary element method**. Department of Structural Mechanics, Chalmers University of Technology, 1983.
- VIVEIROS, E. B. **Evaluation of the acoustical performance of Louvre by impulse response analysis**. Ph.D. Thesis, Federal University of Santa Catarina, Florianópolis, 1998.

WARNOCK, A., VORLÄNDER, M. **Inter-laboratory comparison of low frequency sound transmission – finite element studies**. Proceedings of Inter-Noise 93, 929-932, Leuven, 1993.

CHAPTER 4

FINITE ELEMENT MODEL

4.1 Introduction

The development of the digital computer in the 1950's allowed rapid developments in data handling and calculation. Of particular interest here has been the development of numerical calculation methodologies, such as the Finite Element Method (FEM), which is a numerical procedure for analysing continua. This method represents an automatic operation to construct a set of equations describing a static or dynamic system [Cook et al (1989), Fancello and Mendonça (1997), Crocker (1997)]. A model of the system is created and then modelled mathematically. From the mathematical equations created, it is possible to obtain an analytical or numerical solution (the latter occurring most of the time) [Zienkiewicz and Taylor (1971), Melo et al (2001)]. Although results are rarely exact, errors are reduced by processing more equations to achieve engineering accuracy at reasonable cost [Cook et al (1989)].

4.2 Applications in acoustics

According to Craggs and Stead (1976), the use of FEM in the area of Acoustics was first suggested by Gladwell (1965) for simple one and two-dimensional problems. Later, Mason (1967) worked on the development of extremely accurate rectangular parallelepiped elements having 32 degrees of freedom, although it was concluded that the size and shape of such elements restricted their application. Jennequin (1971) used a two-dimensional FE model to study the sound field inside the passenger section of a car. FEM continues to have applications in Acoustics, as recently reviewed by Crocker (1997), Astley (1998), and Maluski (1999).

Of particular interest here are the contributions in the area of room acoustics, including the study of the sound field inside irregular enclosures, damping effects, panel flexibility, and coupling between structural and acoustical subsystems [Craggs (1973), Craggs and Stead (1976), Petyt et al (1976), Geddes and Porter (1988), Easwaran and Craggs (1995), Augusztinovicz (1998)].

Maluski (1999) has employed FE modelling to study the sound insulation between dwellings at low frequencies. This model was validated by comparison with scale model measurements [Maluski and Bougdah (1997), Gibbs and Maluski (1998), Maluski (1999)], and the associated model of transmission between rooms demonstrated that the modal characteristics of the pressure and vibration fields of the rooms and separating wall, respectively, strongly influence the sound level difference. Maluski's work has identified important outstanding issues to be addressed, e.g., the need for an appropriate model of sound absorption in small-furnished rooms at low frequencies, and the consideration of modally reactive absorption due to the vibration of the walls [Maluski (1999)].

4.3 Controlling parameters

When working with FEM, the structure or continuum under study must be divided into elements, in a process called *discretization* [Zienkiewicz and Taylor (1971), Cook et al (1989)]. *Nodes* indicate where the elements are connected to one another, and each element has its properties formulated. In acoustic and structural analyses, the nodal variables are, in general, sound pressure and particle displacement, respectively. A fine discretization of the domain is likely to produce very accurate results, although this may involve long computation times, even when working with powerful computers. Thus, a compromise has to be established between accuracy and processing time, and since reliable predictions require, at least, 6 elements to properly represent the pressure field over the governing wavelength [Atalla and Bernhard (1994), Maluski and Bougdah (1997)], the *element size* is automatically determined by the upper frequency of interest [Astley (1998)].

In addition to element size, the accuracy of the results depends on the *element type*. A rectangular or approximately rectangular domain allows the use of cubic elements during the discretization process. 'Hex8' and 'Hex20' represent, for example, two types of cubic elements, having 8 and 20 nodes, respectively [Patran Rev 8.0 (1999), Maluski (1999)]. In the case of a room model, a greater number of nodes allows a more accurate prediction of the room eigenfrequencies [Crocker (1997)]. For this reason, the Hex20 element type was used in the FE models developed in this work.

4.4 Room-wall-room system

In order to estimate the sound transmission between two rooms, the sound pressure field in each of them, and the particle velocity field on the separating wall must be determined [Fahy (1985)]. Furthermore, it is necessary to know the effects of the sound source on the source room, the influence of the pressure field over the separating wall vibration field, and the response of the receiving room to this vibrating field [Craggs and Stead (1976), Gagliardini et al (1991), Maluski (1999)].

4.4.1 Acoustic field

Consider a Room-Wall-Room system as shown in Fig. 4.1.

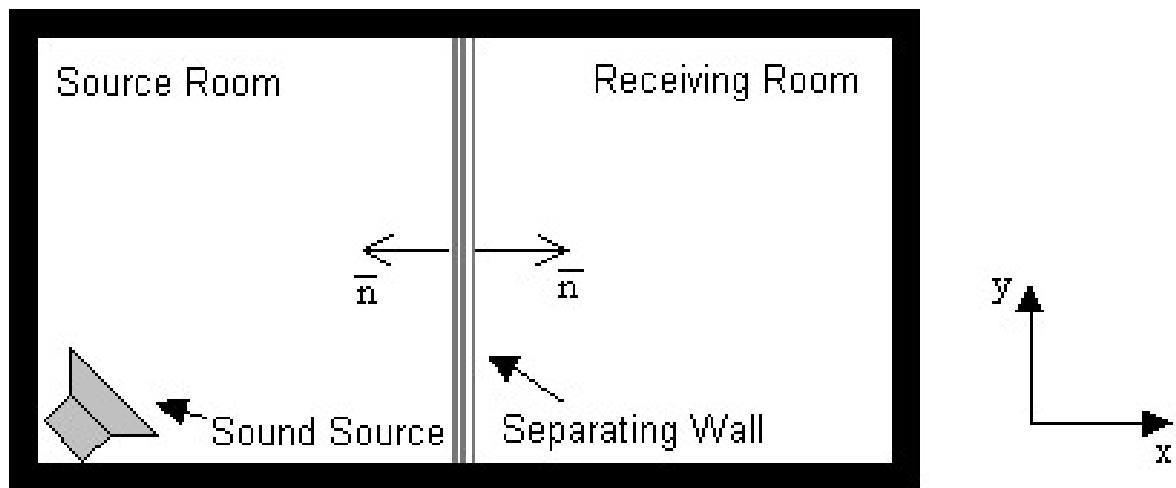


Figure 4.1 - Room-Wall-Room system.

Soon after the sound source is switched on, a steady state sound field within the rooms is achieved, allowing the assumption of a harmonic pressure field, p , of the type

$$p(x, y, z, t) = P(x, y, z) e^{i\omega t}, \quad (4.1)$$

where x , y , and z are the spatial coordinates, t is the time, P is the pressure amplitude, and ω is the angular frequency. The sound pressure field inside the source room is given by

$$\begin{cases} \nabla^2 P_1(x, y, z) + k_o^2 P_1(x, y, z) = R(x, y, z); & \text{in the room volume } V \\ \bar{\nabla} P_1 \cdot \bar{n} = -\omega^2 \rho_o u; & \text{on the separating wall} \\ \bar{\nabla} P_1 \cdot \bar{n} = 0; & \text{elsewhere,} \end{cases} \quad (4.2)$$

where $k_o = \omega / c_o$, R is the sound source term, \bar{n} is a unit vector normal to the separating wall, ρ_o is the air density, and u is the wall displacement in the x direction.

Applying the Galerkin method [Zienkiewicz and Taylor (1971)] to equation (4.2) yields

$$\int_V (\nabla^2 P_1 + k_o^2 P_1 - R) \hat{p} dV = 0, \quad (4.3)$$

where \hat{p} is an arbitrary function that must be null wherever the pressure P_1 is prescribed. Expanding equation (4.3) and knowing that

$$\bar{\nabla} \cdot (\bar{\nabla} P_1 \hat{p}) = \nabla^2 P_1 \hat{p} + \bar{\nabla} P_1 \cdot \bar{\nabla} \hat{p}, \quad (4.4)$$

then

$$\int_V \bar{\nabla} \cdot (\bar{\nabla} P_1 \hat{p}) dV - \int_V \bar{\nabla} P_1 \cdot \bar{\nabla} \hat{p} dV + \int_V k_o^2 P_1 \hat{p} dV - \int_V R \hat{p} dV = 0. \quad (4.5)$$

From the Divergence Theorem [Morse and Ingard (1968)], together with the last two expressions of equation (4.2) gives

$$-\int_S \omega^2 \rho_o u \hat{p} dS - \int_V \bar{\nabla} P_1 \cdot \bar{\nabla} \hat{p} dV + \int_V k_o^2 P_1 \hat{p} dV - \int_V R \hat{p} dV = 0. \quad (4.6)$$

This integral formulation has importance in that the set of functions P_1 satisfying equation (4.6) is wider than the set of solutions of equation (4.2) [Zienkiewicz and Taylor (1971)]. This equation may be discretized using the so-called Galerkin's approximation method [Cook et al (1989)]:

$$P_1 \cong p_{1i} N_{p_i}; \quad \hat{p} \cong p_j N_{p_j}; \quad u \cong u_i N_{u_i}, \quad (4.7)$$

where p_i and u_i are the approximated values of pressure and displacement, respectively, at the i^{th} node of the FE mesh, while N_{p_i} and N_{u_i} are the shape functions associated with this node [Sysnoise Rev 5.3 (1993)]. Similar definitions apply for index j . Substituting equation (4.7) into (4.6), and taking into account the following conventions:

$$\begin{aligned}
\int_S \rho_o N_{u_i} N_{p_j} dS &= Q_{ij}; \text{ coupling term} \\
\int_V \bar{\nabla} N_{p_i} \bullet \bar{\nabla} N_{p_j} dV &= K_{p_{ij}}; \text{ acoustic stiffness} \\
\frac{1}{c_o^2} \int_V N_{p_i} N_{p_j} dV &= M_{p_{ij}}; \text{ acoustic mass} \\
\int_V R N_{p_j} dV &= F_{p_j}; \text{ acoustic force,}
\end{aligned} \tag{4.8}$$

gives the following discretized equation for the source room:

$$-\omega^2 Q_{ij} u_i - K_{p_{ij}} p_{1i} + \omega^2 M_{p_{ij}} p_{1i} = F_{p_j}. \tag{4.9}$$

The same procedure applies for the receiving room, except that for this room the sound source term is null and the normal vector points to the opposite direction (see Fig. 4.1). The discretized equation for the receiving room is given by:

$$\omega^2 Q_{ij} u_i - K_{p_{ij}} p_{2i} + \omega^2 M_{p_{ij}} p_{2i} = 0. \tag{4.10}$$

4.4.2 Structural field

For the separating wall of Fig. 4.1, with height L_y , thickness h , and flexural rigidity D , the structural field is described by the following system of equations:

$$\begin{cases} D \nabla^4 u - \omega^2 \rho h u = (P_1 - P_2); & \text{on the wall surface} \\ u = 0 \text{ and } \bar{\nabla} u = 0; & \text{at } y = 0 \\ u = 0 \text{ and } \bar{\nabla} u = 0; & \text{at } y = L_y \end{cases} \tag{4.11}$$

$$D = \frac{E h^3}{12 (1 - \nu^2)},$$

where E is the Young's modulus, ν is the Poisson's ratio, and ρ is the volumetric density of the wall material. Following the same process as in Section 4.4.1:

$$\int_S (D \nabla^4 u - \omega^2 \rho h u - P_1 + P_2) \hat{u} dS = 0, \tag{4.12}$$

where \hat{u} is an arbitrary function that must be null wherever the displacement u and its gradient are prescribed. Expanding equation (4.12) it is possible to obtain:

$$\begin{aligned}
\int_S D \bar{\nabla} \bullet (\bar{\nabla} \nabla^2 u \hat{u}) dS - \int_S D \bar{\nabla} \bullet (\nabla^2 u \bar{\nabla} \hat{u}) dS + \int_S D \nabla^2 u \nabla^2 \hat{u} dS - \\
-\omega^2 \int_S \rho h u \hat{u} dS - \int_S P_1 \hat{u} dS + \int_S P_2 \hat{u} dS = 0.
\end{aligned} \tag{4.13}$$

From the Divergence theorem and the boundary conditions of equation (4.11) the integral equation follows:

$$\int_S D \nabla^2 u \nabla^2 \hat{u} dS - \omega^2 \int_S \rho h u \hat{u} dS - \int_S P_1 \hat{u} dS + \int_S P_2 \hat{u} dS = 0. \quad (4.14)$$

As in the previous section, in order to discretize equation (4.14), the following approximations must be used:

$$u \cong u_i N_{u_i}; \quad \hat{u} \cong u_j N_{u_j}; \quad P_1 \cong p_{1i} N_{p_i}; \quad P_2 \cong p_{2i} N_{p_i}. \quad (4.15)$$

Thus, substituting equation (4.15) into (4.14), and observing the conventions:

$$\begin{aligned} \int_S \rho N_{p_i} N_{u_j} dS &= Q_{ij}; \text{ coupling term} \\ \int_S D \nabla^2 N_{u_i} \nabla^2 N_{u_j} dS &= K_{u_{ij}}; \text{ structural stiffness} \\ \int_S \rho h N_{u_i} N_{u_j} dS &= M_{u_{ij}}; \text{ structural mass,} \end{aligned} \quad (4.16)$$

the discretized equation for the separating wall is obtained:

$$K_{u_{ij}} u_i - \omega^2 M_{u_{ij}} u_i - Q_{ij} (p_{1i} - p_{2i}) = 0. \quad (4.17)$$

4.4.3 Acoustic-structural field

Equations (4.9), (4.10) and (4.17) can be linked in one general matrix equation,

$$\begin{bmatrix} -\omega^2 Q_{ij} & (-K_{p_{ij}} + \omega^2 M_{p_{ij}}) & 0 \\ \omega^2 Q_{ij} & 0 & (-K_{p_{ij}} + \omega^2 M_{p_{ij}}) \\ (K_{u_{ij}} - \omega^2 M_{u_{ij}}) & -Q_{ij} & Q_{ij} \end{bmatrix} \begin{Bmatrix} u_i \\ p_{1i} \\ p_{2i} \end{Bmatrix} = \begin{Bmatrix} F_j \\ 0 \\ 0 \end{Bmatrix}. \quad (4.18)$$

Knowing the “acoustic force” term, F_j , and calculating the acoustic and structural matrices, it is possible to obtain the solution for the separating wall displacement, u , and the sound pressure fields in the source room, p_1 , and in the receiving room, p_2 . Consequently, the sound level difference between the two rooms may be obtained, allowing the determination of the sound transmission characteristics of the room-wall-room system.

4.5 Model of test room

As described in Section 2.5, the thesis work considers a room model that takes into account the modal characteristics of low frequency sound fields inside enclosures. The core of the work was to fully model and measure an empty test room (see Chapter 6), and then to measure and predict possible effects on room frequency response produced by introducing contents, so as to be able to characterise the room contents as obstructions and/or absorbers.

4.5.1 Assumptions

One of the specific objectives of this work was to contribute in the expansion of knowledge already acquired in the area of building acoustics for the frequency range from 100 Hz to 3150 Hz. The complementary work was to include frequencies below the standard range, but extending into it. Thus, the original idea was to investigate sound fields from 20 Hz to 400 Hz. However, preliminary predictions revealed that an excessively long processing time was required to obtain room responses up to 400 Hz (up to three days on Sun Workstations). Thus, it was decided to reduce the upper limiting frequency to 200 Hz, without loss of generality, since the core of the present study is related to the very low frequencies. Furthermore, due to the test room dimensions, the acoustic field inside the room starts to assume diffuse characteristics above 200 Hz (see Chapter 3). The frequency responses presented throughout this work were calculated up to 210 Hz, in order to take into account (at least partially) the higher mode contributions. Since reliable predictions require, at least, 6 elements to properly represent the pressure wave over the governing wavelength (see Section 4.3), and since the upper frequency of interest was 200 Hz, an element size of 0.28 m was selected.

In Chapter 6, a detailed model of the test room is presented. Here, a preliminary representation is discussed, which served as a basis for the improved model. It was not the intention of this work to develop a new FE computer program. Instead, a commercial software package [Sysnoise Rev 5.4 (1999)] was used. The software does not have a mesh builder, and another commercial package [Patran Rev. 8.0 (1999)] was used for this purpose.

To summarise, a mesh of 3375 Hex20 cubic elements of 0.28 m was used to model a rectangular room of dimensions 5.78 m x 3.04 m x 4.24 m, employing a

Patran format and imported to Sysnoise. Since this phase of the work constituted only a preliminary development of an empty room model, no forms of acoustic energy loss were included. An omni directional point source and two omni directional receivers were introduced into the room corners (see Fig. 6.2), in order to excite and measure all room modes inside the frequency range of interest.

4.5.2 Sysnoise

Sysnoise Rev 5.4 (1999) is a commercial software package that uses FEM and BEM to perform numerical calculations for acoustic and structural-acoustic systems. In Sysnoise, interior acoustic problems involving various boundary conditions, which are of particular interest here, may be effectively simulated using FEM. One limitation of Sysnoise is that it does not include a mesh builder, although full communication is allowed between this program and all of the main FEM commercial software packages. Other FEM based commercial packages, including Ansys and Patran, were available, however, unlike Sysnoise these programs are not optimised for acoustic problems. Also, the present work was part of a joint programme between the Federal University of Santa Catarina (UFSC), Brazil, and The University of Liverpool, England, and the software Sysnoise was already available to both research groups.

4.6 Preliminary results

In order to verify the accuracy of the rectangular empty room model, the room eigenfrequencies were obtained analytically, making it possible to compare the numerical and analytical results. According to equation (3.34) the eigenfrequencies of a rectangular enclosure are given by:

$$f_n = \frac{c_0}{2} \sqrt{\left(\frac{n_x}{L_x}\right)^2 + \left(\frac{n_y}{L_y}\right)^2 + \left(\frac{n_z}{L_z}\right)^2}. \quad (4.19)$$

To evaluate the inaccuracy due to the FE discretization, an error E was calculated [Melo et al (2001)]:

$$E = \frac{NE - AE}{AE} \cdot 100, \quad (4.20)$$

where NE and AE are the numerical eigenfrequency and analytical eigenfrequency, respectively. Fig. 4.2 shows that although the error is increasing with increased frequency, it is less than 0.05% for all the eigenfrequencies inside the frequency range of interest.

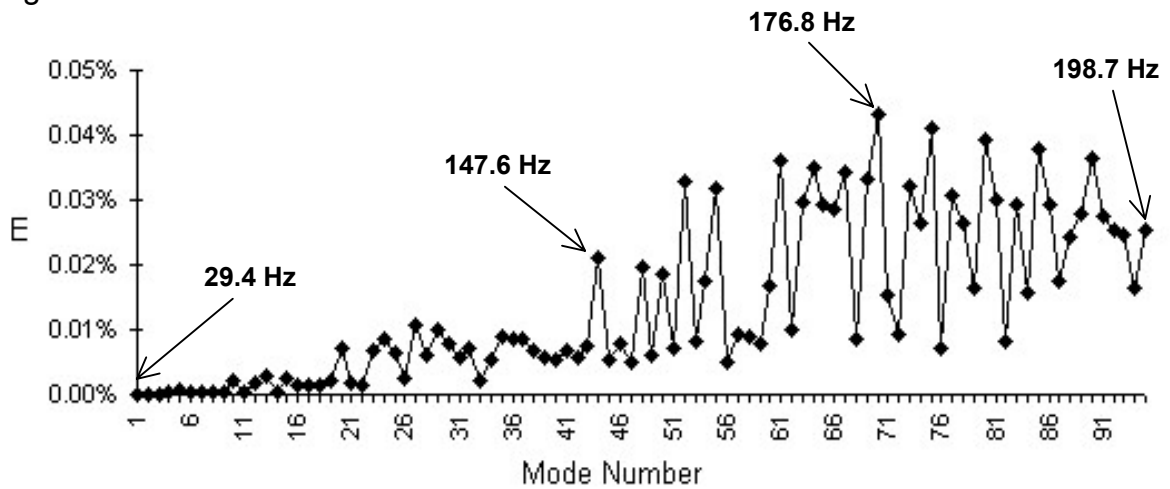


Figure 4.2 - Percentile error between numerical and analytical eigenfrequencies for a room of dimensions 5.78 m x 3.04 m x 4.24 m.

Fig. 4.3 shows a predicted room response, obtained for the empty rectangular room model. It is possible to observe the modal characteristics of the sound field at low frequencies. The first modes are well spaced, but the modal density increases rapidly with frequency, and the peaks observed close to the upper frequency limit are in reality formed by the overlapping of several modes. As stated in Section 4.5.1, this preliminary model did not include absorption, and this explains the sharp peaks and dips of the predicted curve. The peaks are finite, however, due to inherent limitations in the computer program. In a study by Maluski (2000), using similar software, it was demonstrated that the 'artificial' Q-values of the response peaks corresponded to a room with average absorption coefficient of 0.01 [Maluski and Gibbs (2000)].

Results also can be presented in the form of modal patterns at selected frequencies (for example, see Figs. 4.4 to 4.7, for pressure distributions at 29.4 Hz, 55.9 Hz, 58.8 Hz and 74.8 Hz, respectively). Spatial variation is indicated in the discussion of the effect of introducing obstacles into rooms (see Chapter 7, for instance). However, such effects are described primarily in terms of changes in signature of frequency response.

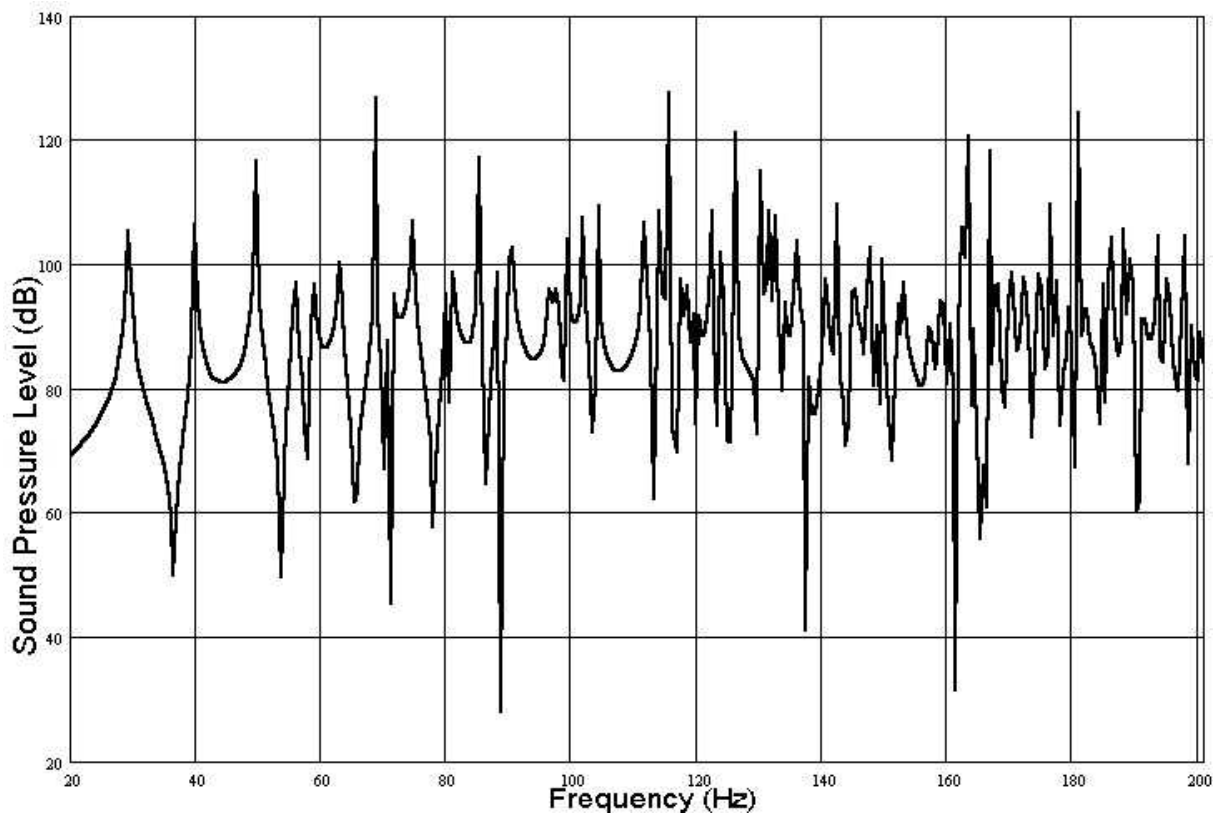


Figure 4.3 - Predicted room frequency response for the rectangular empty room model.

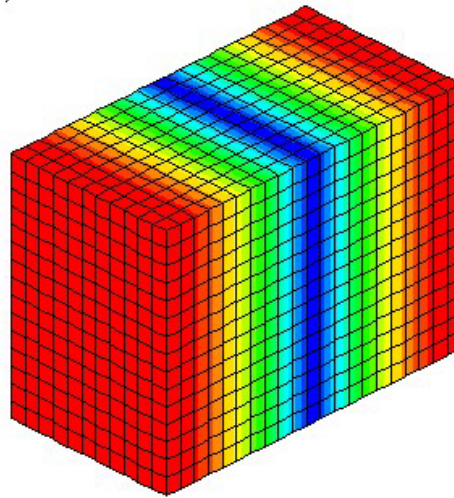
4.7 Summary

In Chapter 3 the modal characteristics of the acoustic field in rooms, at low frequencies, were discussed. This chapter introduced the basic principles of FEM, which was considered as the most appropriate approach to take into account modal characteristics. A preliminary model was developed for the empty rectangular test room. Although this model was to be further developed, as described in Chapter 6, to achieve the objectives set out in Section 2.5, it was possible to conclude that an accurate FEM model could be obtained without excessive computer time. The computed eigenfrequencies agreed with analytical values within 0.05% in the frequency range of interest, revealing the accuracy of this preliminary model and justifying the use of the chosen controlling parameters, as discussed in Section 4.5.1. So far, the developed room model has not included surface or content absorption. This topic is explored in Chapter 5.

SYSNOISE – COMPUTATIONAL VIBRO-ACOUSTICS

Rectangular Room, $\alpha=0\%$ and $c=340\text{m/s}$

Acoustic Modes at 29.412 Hz (Amplitude)



Acoustic Modes

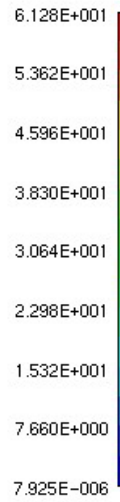
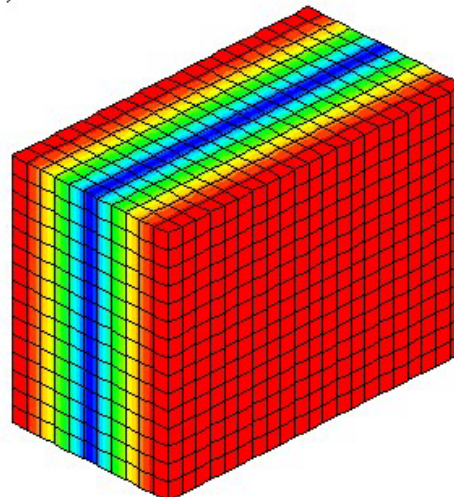


Figure 4.4 - Spatial distribution of pressure amplitude for the first mode (1,0,0).

SYSNOISE – COMPUTATIONAL VIBRO-ACOUSTICS

Rectangular Room, $\alpha=0\%$ and $c=340\text{m/s}$

Acoustic Modes at 55.921 Hz (Amplitude)



Acoustic Modes

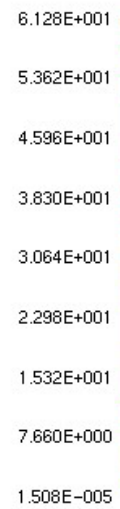


Figure 4.5 - Spatial distribution of pressure amplitude for the fourth mode (0,1,0).

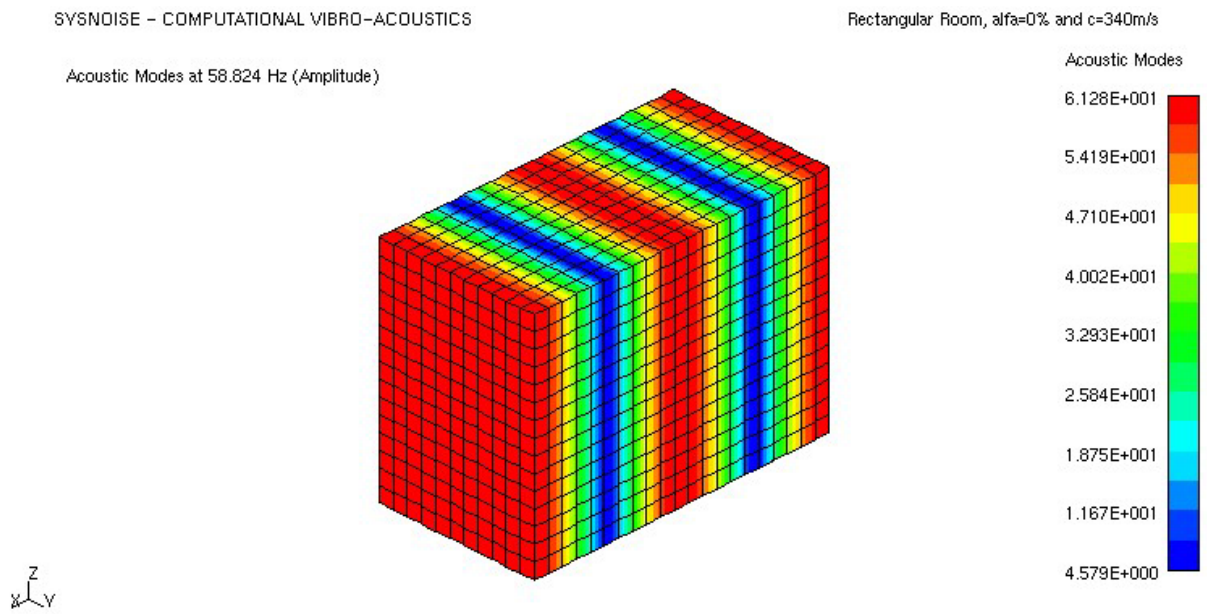


Figure 4.6 - Spatial distribution of pressure amplitude for the fifth mode (2,0,0).

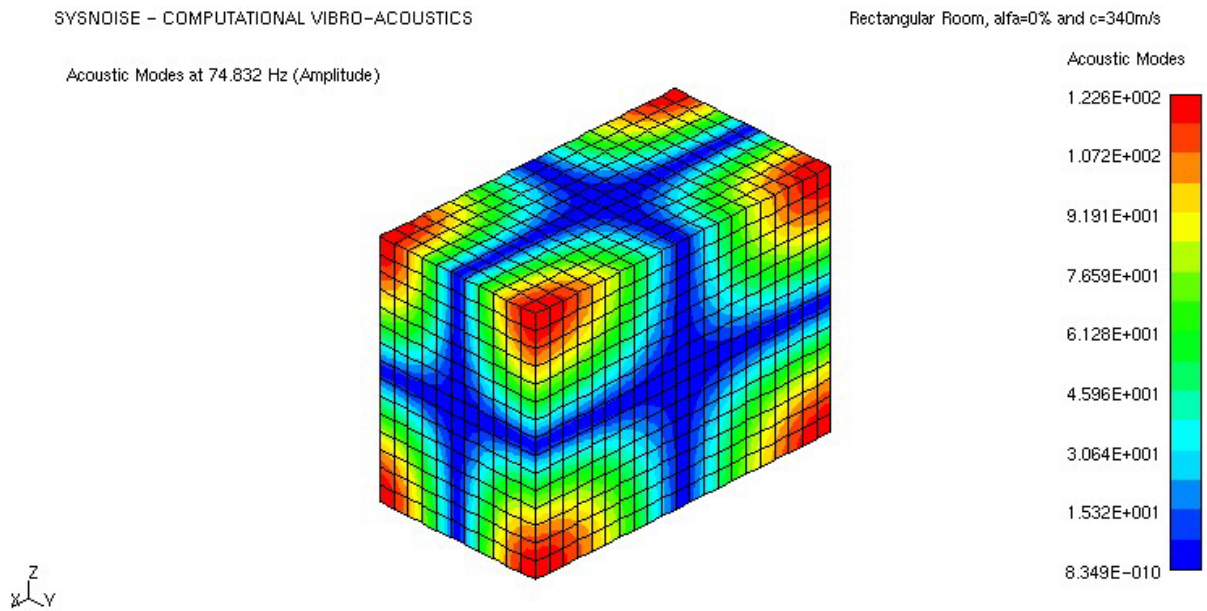


Figure 4.7 - Spatial distribution of pressure amplitude for the ninth mode (1,1,1).

4.8 References

ASTLEY, R. J. **Finite elements in acoustics**. Proceedings of Inter-Noise 98, New Zealand, 1998.

ATALLA, N., BERNHARD, R. J. **Review of numerical solutions for low frequency structural-acoustics problems**. Applied Acoustics, 43 (3), 271-294, 1994.

AUGUSZTINOVICZ, F. **State of the art of practical applications of numerical methods in vibro-acoustics**. FIA, 18° Encontro da SOBRAC, Congresso Iberoamericano de Acústica, 154-168, Florianópolis, 1998.

COOK, R.D., MALKUS, D. S., PLESHA, M., E. **Concepts and applications of finite element analysis**. John Wiley & Sons, New York, 1989.

CRAGGS, A. **An acoustic finite element approach for studying boundary flexibility and sound transmission between irregular rooms**. Journal of Sound and Vibration, 30 (3), 343-357, 1973.

CRAGGS, A., STEAD, G. **Sound transmission between enclosures - a study using plate and acoustic finite elements**. Acustica, 35 (2), 89-98, 1976.

CROCKER, M. J. **Handbook of acoustics**. John Wiley & Sons, New York, 1997.

EASWARAN, V., CRAGGS, A. **On further validation and use of the finite element method to room acoustics**. Journal of Sound and Vibration, 187 (2), 195-212, 1995.

FAHY, F. **Sound and structural vibration: radiation, transmission and response**. Edition Academic Press, 1985.

FANCELLO, E., MENDONÇA, P. **Introdução ao método dos elementos finitos**. Course Notes of the Mechanical Engineering Department of the Federal University of Santa Catarina, Florianópolis, 1997.

GAGLIARDINI, L., ROLAND, J., GUYADER, J., L. **The use of a functional basis to calculate acoustic transmission between rooms**. Journal of Sound and Vibration, 145, 457-478, 1991.

GEDDES, E. R., PORTER, J. C. C. **Finite element approximation for low frequency sound in a room with absorption**. Journal of the Acoustical Society of America, 83 (4), 1431-1435, 1988.

GLADWELL, G. M. L. **A finite element method for acoustics**. V International

Congress on Acoustics, Liege, 1965.

JENNEQUIN, G. **Is the computation of noise level inside a car feasible?** Proceedings of the Institute of Mechanical Engineers Symposium on Vibration and Noise in Motor Vehicles, London, 1972.

MALUSKI, S. P. S., BOUGDAH, H. **Predicted and measured low frequency response of small rooms.** Journal of Building Acoustics, 4 (2), 73-85, 1997.

MALUSKI, S. P. S. **Low frequency sound insulation in dwellings.** Ph.D. Thesis, Sheffield Hallam University, Sheffield, 1999.

MALUSKI, S. P. S., GIBBS, B. M. **Application of a finite-element model to low-frequency sound insulation in dwellings.** Journal of the Acoustical Society of America, 108 (4), 1741-1751, 2000.

MASON, V. **On the use of rectangular finite elements.** Institute of Sound and Vibration Report N° 161, University of Southampton, 1967.

MELO, G. S. V., GIBBS, B. M., GERGES, S. N. Y. **A finite element model of sound absorption at low frequencies.** Proceedings of Euronoise-2001, Patras, 2001.

MORSE, P. M., INGARD, K. U. **Theoretical acoustics.** McGraw Hill, New York, 1968.

PATRAN REV 8.0. **User Manual.** PDA Engineering, 1999.

PETYT, M., LEA, J., KOOPMAN, H. **A finite element method for determining the acoustic modes of irregular shaped cavities.** Journal of Sound and Vibration, 45 (4), 495-502, 1976.

SYSNOISE REV 5.4. **User Manual.** Numerical Integration Technologies, 1999.

ZIENKIEWICZ, O., TAYLOR, R. **The finite element method.** Mc Graw Hill, 1971.

CHAPTER 5

ROOM ABSORPTION

5.1 Introduction

In the present work, room absorption at low frequencies is examined in order to assess its influence on the general problem of sound insulation between adjacent rooms. The approach adopted was to input damping data into a validated FE model and adjusting this data until good agreement with measurement is obtained. Surface absorption was considered first, and then that due to room contents, with an emphasis on furniture. As a prelude to the study, a description is given of the fundamental processes of absorption in rooms.

5.2 Previous work

The use of sound absorbing materials remains one of the main forms of noise control in car and aircraft industries, as well as in enclosed spaces [Balvedi (1998)]. When sound waves propagate through the air and strike objects and boundary surfaces in enclosures, absorption takes place, both within the propagating medium and at the boundaries. In room acoustics, an understanding of the energy loss mechanisms is important in the determination of sound pressure levels resulting from sound sources within enclosures [Bies and Hansen (1996), Crocker (1997)]. The study of such mechanisms began at the end of the nineteenth century with the work of Rayleigh, who published on the absorption in porous materials [Rayleigh (1945)]. In 1900, after five years of research conducted in various halls at Harvard, Sabine developed an equation for the reverberation time, T in an enclosed space that remains a fundamental parameter to this day [Sabine (1900), Beranek (1992)]:

$$T = 0.163 \frac{V}{A}, \quad (5.1)$$

where T is the time taken for the sound field to decay 60 dB, V is the room volume, and A is the total sound absorption in the room at the frequency of measurement in square metres.

Biot (1956) developed the theory of Rayleigh on the propagation of elastic waves in porous materials, concluding that three waves (two dilatational and one rotational) may simultaneously exist in such materials depending on the ratio between the Young's modules of the porous material and of the fluid inside the material [Biot (1956)]. The dilatational waves are denoted as waves of the first and second kind. The waves of the first kind are true waves, i.e., the dispersion is practically negligible with a phase velocity increasing or decreasing with frequency depending on the mechanical parameters. The waves of the second kind are highly attenuated. They are in the nature of a diffusion process, and the propagation is closely analogous to heat conduction. The rotational wave comes from the fact that a rotation of the solid causes a partial rotational entrainment of the fluid through an inertia coupling [Biot (1956)].

Beranek (1971) described the thermodynamic phenomena related to porous materials and their physical properties. He also proposed one of the first mathematical models for the determination of the characteristic acoustic impedance [Beranek (1971)]. A more profound study on the theory of porous materials was undertaken by Ingard (1994), who divided the energy loss mechanisms into viscous and inertial, thermal and structural effects. Bolton (1997) discussed the different types of porous material (rigid, flexible and elastic), and the influence of their macroscopic properties on their acoustic behaviour [Bolton (1997), Balvedi (1998)].

The energy loss mechanisms that occur at the main surfaces within a room may take one of two forms, depending on their vibroacoustic properties, the frequency range, and the dimensions of the room [Bies and Hansen (1996), Crocker (1997)]. The first mechanism is related to locally reactive surfaces and the second to modally reactive surfaces. The present chapter deals with each of these mechanisms, their effective frequency range, the need to include them in the FE model and the possible ways to do so.

5.3 Air absorption

Sound waves are attenuated during propagation through air. The decrease in intensity is expressed in terms of the medium attenuation constant $m = 2\alpha$ (α is the air absorption coefficient) [Kuttruff (1979), Gerges (2000)]. Equation (5.1) now becomes [Bies and Hansen (1996), Gerges (2000)]:

$$T = 0.163 \frac{V}{A + 4mV}. \quad (5.2)$$

According to Gerges (2000), the effect of air absorption may be neglected up to 2 kHz. Crocker (1997), however, states that the small propagation loss is generally only important in very large rooms and at frequencies above about 500 Hz. The attenuation of sound waves by the air may represent a serious problem in scale model measurements [Kuttruff (1979)]. This is not the case of the present study, and as the upper frequency of interest here is 200 Hz, the effects related to air absorption may be safely neglected.

5.4 Absorption by porous surfaces

Porous materials may be thought of as being formed of two distinct parts: the solid phase relates to the structural part of the material, and the fluid phase relates to the fluid (air) inside the pores of the material. Due to their low density, they are not efficient for sound insulation purposes. However, porous materials are frequently used as sound absorbers, due to their ability to convert acoustic energy into heat [Biot (1956), Kuttruff (1979), Ingard (1994), Balvedi (1998)].

5.4.1 Theory

The absorption characteristics of a given material are determined by the absorption coefficient, α , which is defined as the ratio of the acoustic energy absorbed by the material, W_a , to the incident acoustic energy, W_i :

$$\alpha = \frac{W_a}{W_i}. \quad (5.3)$$

The values of α are always positive ($0 \leq \alpha \leq 1$), mainly depending on the frequency, sound incidence angle, assumed sound field (diffuse, plane waves, etc.), material density, thickness and internal structure [Beranek (1971), Kuttruff (1979), Gerges (2000)]. The original postulate that the absorption coefficient is a fundamental property of the material has now been discarded in favour of an impedance concept [Beranek (1940-a, 1940-b, 1942), Gibbs (1970)]. Of particular interest here is the specific acoustic impedance, Z , which is defined as the ratio of acoustic pressure to associated particle velocity [Kinsler and Frey (1982), Bies and Hansen (1996)]. This

parameter is important in describing the propagation of sound in free space and is continuous at junctions between media. It is also important in describing the reflection and transmission of sound at an absorptive lining in a duct or on the walls of a room. Beranek (1942) developed a method to measure the specific normal acoustic impedance of a material, Z_n , which involves the acoustic pressure at the material surface and the component of the particle velocity perpendicular to the material surface. Zwicker and Kosten (1947) have shown that the acoustic impedance of a rigidly backed material is given by

$$Z = W \coth(\gamma h), \quad (5.4)$$

where W is the characteristic impedance, γ is the propagation constant, and h is the material thickness. The propagation constant and the characteristic impedance are material constants that fully describe the acoustic properties of porous materials [Gibbs (1970), Balvedi (1998)].

5.4.2 Locally reacting surfaces

The concept of a locally reactive boundary is of importance as it serves to uncouple the cavity and wall modes and greatly simplifies the analysis [Morse (1939), Bies and Hansen (1996)]. The locally reactive surface is defined as one for which the response at each point of the surface is only dependent on the local sound pressure and independent of the response at any other part of the boundary, i.e., local reaction means that the response to an imposed force at a point is determined only by local properties of the surface at the point of application of the force [Pan and Bies (1988), Bies and Hansen (1996)]. Thus, assuming locally reactive surfaces and using the impedance tube method developed by Beranek, it is possible to obtain a relation between the normal absorption coefficient, α_n , and the specific normal acoustic impedance, Z_n , given by [Brüel and Kjær (1955 & 1979), Beranek (1971)]

$$Z_n = \frac{1 + \sqrt{1 - \alpha_n}}{1 - \sqrt{1 - \alpha_n}} \cdot \rho_0 c_0. \quad (5.5)$$

Paris (1928) related the sound absorption coefficient α , at a particular angle θ , to the normal impedance by the expression

$$\alpha(\theta) = 1 - \frac{\left| \left(\frac{Z_n}{\rho_0 c_0} \right) \cos \theta - 1 \right|^2}{\left| \left(\frac{Z_n}{\rho_0 c_0} \right) \cos \theta + 1 \right|^2} \quad (5.6)$$

Although the traditional description of sound fields in enclosures begins with the assumption that the walls are locally reactive, or effectively infinitely stiff, a complementary approach that the walls may be modally reactive at low frequencies must be considered, which gives importance to the coupling between structural and acoustic modes [Pan and Bies (1988), Bies and Hansen (1996)]. This is the subject of Section 5.5.

5.4.3 Measurement methods

The well established methods for obtaining the absorption coefficient of a material, as a function of frequency, either involve the use of a standing wave apparatus (or impedance tube) [Cremer and Müller (1982)] or a reverberant room [ISO 140/3 (1995)]. Recent approaches include the transfer function method that utilizes one or two microphones and a digital FFT analyser but it requires further development [Gerges (2000), Balvedi (1998)]. In the impedance tube method a tube has a loudspeaker in one end, while the other end is rigidly blocked [Cremer and Müller (1982, Gerges (2000))]. The sample of sound absorbing material is placed at the closed end. A sinusoidal signal generator feeds the loudspeaker in order to produce a standing wave, at a given frequency, inside the tube. A microphone probe measures the acoustic pressure along the tube. The probe also allows the measurement of the distance between the sample surface and the measuring position, by means of a graduated scale. Although simple and accurate, the impedance tube method is slow due to the need to measure at many discrete frequencies. Furthermore, only measurements of normal incidence absorption coefficient are possible [Seybert and Ross (1970), Beranek (1971), Cremer and Müller (1982), Balvedi (1998), Gerges (2000)].

The determination of the absorption coefficient in a reverberation room is performed by the analysis of the effect produced by the absorption material on the reverberation time, T , of the enclosure [ISO R354 (1985), Gerges (2000)]. A diffuse sound field is assumed, meaning that the sound energy is uniformly distributed within

the room. The principle of this technique consists in measuring T , without and with the absorption material placed on the room floor. Although it is possible to obtain the absorption coefficient for random incidence using this method, the observation of different values of α for the same material, when measured in different rooms, is not uncommon. This is due to a variation in the diffuse sound field characteristics observed for the different rooms [Bies and Hansen (1996)].

5.4.4 Parameter in FEM model

The mechanisms of acoustic energy loss can be included in a FEM model in various ways: by defining a complex sound velocity to represent the absorption of sound as it passes through the medium, by defining acoustic modal damping characteristics, by modelling the characteristics of bulk absorbent materials, or by adding complex impedance boundary conditions to the surfaces of the cavity. As discussed in Section 5.3, the absorption of sound as it passes through the air may be neglected, and the definition of a complex sound velocity becomes unnecessary. The assignment of an acoustic modal damping characteristic is viable only for the first few acoustic modes of the cavity, since these characteristics must be determined experimentally. This becomes difficult with increasing frequency, due to modal superposition. The modelling of bulk absorbent materials requires the use of a special finite element formulation [Sysnoise Rev 5.4 (1999)]. The properties of the absorbent material (effective density of the fluid inside the material, sound velocity inside the material, resistivity, porosity, and structural factor) must be determined experimentally, which may not represent a simple task [Balvedi, (1998)]. The most common way to approach the absorption mechanism in a FE model of a room is by adding complex impedance boundary conditions [Pan and Bies (1988)].

Absorbent linings on surfaces can be simulated in FEM by imposing complex normal impedance (or admittance) boundary conditions. In this case the material is considered as locally reactive, and only the normal component of acoustic particle velocity is relevant. An advantage of this approach is that the impedance characteristics of the absorbent material may be derived from the absorption coefficient.

5.5 Modally reactive boundaries

In the low frequency range, structural-acoustic modal coupling plays an important part in the absorption mechanism in an enclosure. Experiments regarding the interaction between the sound field and its boundaries have demonstrated that the walls of a reverberation chamber are modally reactive, in which case the sound absorption mechanism is associated with structural-acoustic mode coupling [Pan and Bies (1988 & 1990), Pan et al (1999)]. Consider a room with five rigid walls and one simply supported panel. The free vibration of the room-panel system may be characterised in terms of the sound field in the cavity, the panel displacement due to flexural vibration, and the exterior sound field due to the panel sound radiation [Pan and Bies (1990-a)]. Inside the cavity, the sound field may be described in terms of the acoustic velocity potential, Ψ , yielding

$$\nabla^2 \Psi - \frac{1}{c_0^2} \frac{\partial^2 \Psi}{\partial t^2} = 0. \quad (5.7)$$

The air particle velocity v and the sound pressure P are given, respectively, by

$$\begin{aligned} \vec{v} &= \vec{\nabla} \Psi \\ P &= -\rho_0 \frac{\partial \Psi}{\partial t}. \end{aligned} \quad (5.8)$$

The five non-vibrating walls are assumed to be locally reactive and the boundary condition for these walls is given by:

$$\vec{\nabla} \Psi \cdot \vec{n} = -\frac{\rho_0}{Z} \frac{\partial \Psi}{\partial t}, \quad (5.9)$$

where Z is the specific normal acoustic impedance of the surfaces. For the flexible panel the continuity of the particle velocity and the normal panel velocity yields

$$\vec{\nabla} \cdot \vec{n} = \frac{\partial w}{\partial t}, \quad (5.10)$$

where w is the panel normal displacement. The behaviour of the panel flexural motion, for a thin isotropic panel, is determined by [Heckl (1981), Fahy (1985), Pan and Bies (1990-a)]

$$\nabla^4 w \frac{Eh^3}{12(1-\mu^2)} + \rho h \frac{\partial^2 w}{\partial t^2} = \rho_0 \left(\frac{\partial \Psi_e}{\partial t} - \frac{\partial \Psi}{\partial t} \right), \quad (5.11)$$

where E , h , μ , ρ , are the Young's modulus, thickness, Poisson's ratio and density of the panel, respectively, and Ψ_e is the acoustic velocity potential on the outside surface of the panel, which is given by the Rayleigh integral for sound waves radiating from a baffled panel [Rayleigh (1896)]

$$\Psi_e = -\frac{1}{2\pi} \int_{A_M} \frac{\partial W}{\partial t} \frac{e^{-i\vec{k}\cdot\vec{r}}}{r} dA, \quad (5.12)$$

where A_M is the the modally reactive surface, \vec{k} is the wave number of the sound field, and r is the distance from the panel surface to the observation point. The harmonic term $e^{i\omega t}$ can be omitted. The differential equations (5.7) and (5.11) may be put in an integral form, which has the advantage of providing a convenient formulation for numerical approximations [Zienkiewicz and Taylor (1971), Pan and Bies (1990-a)]. This procedure requires a Green's function that satisfies the original partial differential equations having a Dirac delta function as a point source [Feshbach (1944)]. The constructed Green's function is a transfer function from the point source to the velocity potential at an observation point in the cavity, and may be obtained by normal mode expansion [Morse and Ingard (1968)] giving

$$G_R(\vec{r}, \vec{r}_0, \omega) = \sum_N \frac{\Phi_N(\vec{r}) \Phi_N(\vec{r}_0)}{\omega^2 - \omega_{R_N}^2}, \quad (5.13)$$

where \vec{r}_0 is the source point, ω_{R_N} is the N^{th} room eigenfrequency, and Φ_N is the N^{th} normal acoustic mode, which according to Section 3.25, for a rectangular room, is

$$\Phi_N = \cos\left(\frac{l\pi x}{L_x}\right) \cos\left(\frac{m\pi y}{L_y}\right) \cos\left(\frac{n\pi z}{L_z}\right). \quad (5.14)$$

Thus, the acoustic velocity potential in the cavity is determined by integrating the distributed velocity contribution on the boundaries [Pan and Bies (1990-a)]:

$$\Psi = - \int_{A_M+A_L} \vec{\nabla}\Psi \cdot \vec{n} G_R dA = i \frac{\omega}{c_0} \int_{A_L} \beta \Psi G_R dA - \int_{A_M} \frac{\partial W}{\partial t} G_R dA, \quad (5.15)$$

where A_L corresponds to the locally reactive surfaces and β is the specific normal acoustic admittance given by

$$\beta = \frac{\rho_0 c_0}{Z}. \quad (5.16)$$

For the simply supported panel, the Green's function is given by

$$G_P(\bar{x}, \bar{x}_0, \omega) = -\sum_M \frac{\varphi_M(\bar{x}) \varphi_M(\bar{x}_0)}{\omega^2 - \omega_{P_M}^2}, \quad (5.17)$$

where \bar{x} and \bar{x}_0 are the observation and source points on the panel surface, respectively, ω_{P_M} is the M^{th} panel eigenfrequency, and φ_M is the M^{th} normal structural mode given by

$$\varphi_M = \sin\left(\frac{u\pi x}{L_x}\right) \sin\left(\frac{v\pi y}{L_y}\right). \quad (5.18)$$

Thus, the normal displacement of the panel, resulting from the distributed sound pressure on the panel surface, is given by [Pan and Bies (1990-a)]

$$w = -j \frac{\rho_0 \omega}{\rho h} \int_{A_M} G_P(\Psi - \Psi_e) dA. \quad (5.19)$$

Finally, once Ψ and w are obtained, the fluid-structure interaction characteristics may be obtained [Dowell et al (1977), Pan and Bies (1990-a)]. The geometry of the cavity and the boundaries used in this analysis are very simple, but the method of modal coupling may be applied to more complex cases, since numerical methods (e.g. FEM) are available for finding the mode shapes of virtually any uncoupled enclosure and boundary structures [Pan and Bies (1990-a & b)].

5.6 Field measurements

In a study of the effects of construction material on room frequency responses at low frequencies, Maluski and Gibbs (2001) have obtained field measurement data for the sound fields in living rooms and bedrooms of dwellings with heavyweight masonry or lightweight cavity construction [Maluski and Gibbs (2000 and 2001)]. Using a large speaker placed in one corner, the acoustic fields were measured for the frequency range from 25 Hz to 205 Hz, at a single microphone position. Fig. 5.1 shows the measured room response of a 5.78 m x 4.89 m x 4.24 m room of plastered brick walls, and concrete floor and ceiling, whereas Fig. 5.2 shows the measured room response of a 4.24 m x 2.84 m x 2.40 m room with plasterboard and timber-frame walls, floor, and ceiling.

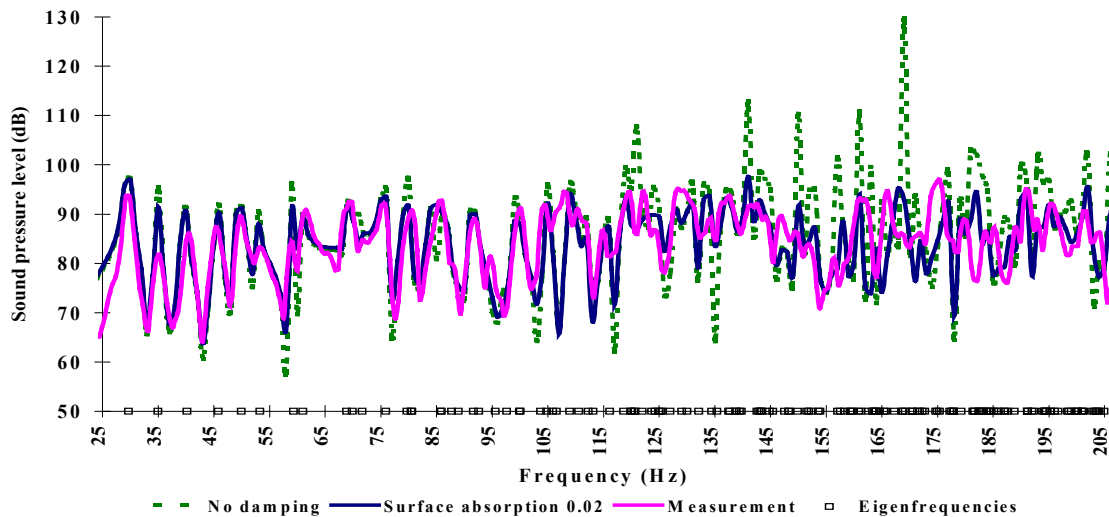


Figure 5.1 - Measured and predicted frequency response of a 5.78 m x 4.89 m x 4.24 m room of plastered brick walls, and concrete floor and ceiling, according to Maluski and Gibbs (2001).

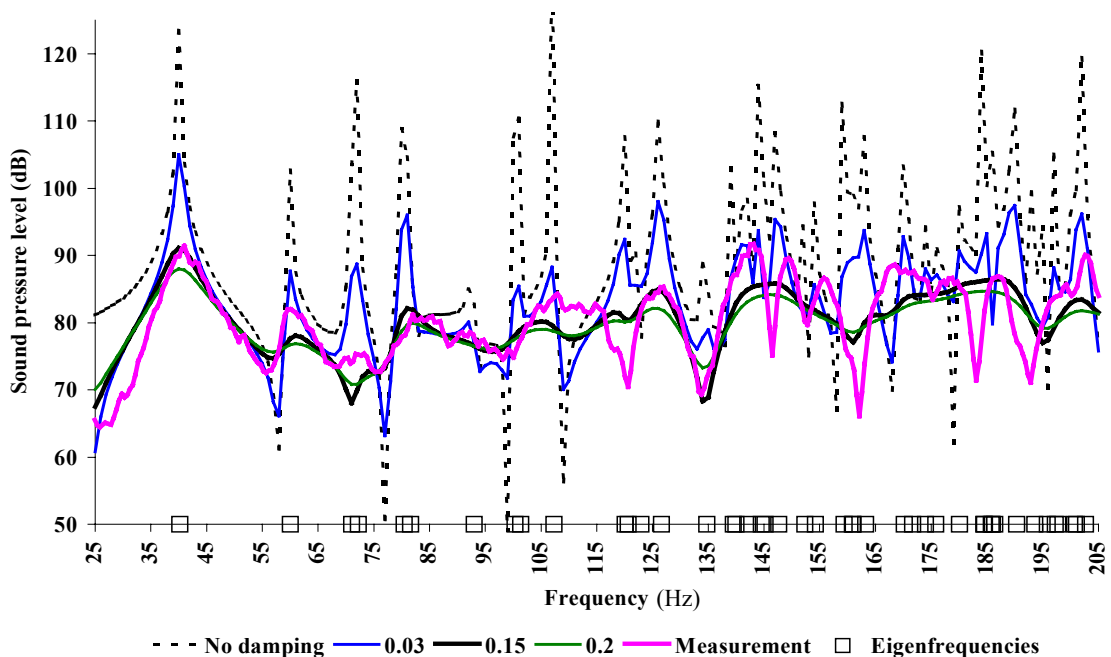


Figure 5.2 - Measured and predicted frequency responses of a 4.24 m x 2.84 m x 2.40 m room with plasterboard and timber-frame walls, floor, and ceiling, according to Maluski and Gibbs (2001).

FE models of the rooms were constructed for comparison with measurements and it was found that the material construction introduces a damping effect on the room sound field, which may be characterised by an equivalent, frequency invariant,

surface absorption coefficient. Below 100 Hz, the equivalent absorption coefficient of 2% reproduced the effect of the masonry and concrete construction (see Fig. 5.1), whereas it was found that an absorption coefficient of 15% provided the best agreement with measurement for the lightweight cavity construction (see Fig. 5.2).

5.7 Summary

The nature of the interaction between a sound field in an enclosure and its boundaries is fundamental in the study of room acoustics. In classical acoustics based on the diffuse sound field assumption, this interaction is described by the concept of the sound absorption coefficient, physically representing the characteristics of the sound energy exchange over the boundaries. Sabine's formula provides a relationship between the absorption coefficient and the reverberation time in a room. However, discrepancies between classical theory and measurements of low frequency sound fields in rooms, where diffusion cannot be assumed, indicate the need of a modal approach, taking into account the wave nature of sound within enclosures.

Traditionally, the sound wave behaviour inside a room is investigated with the introduction of the concept of normal specific acoustic impedance, where the boundaries are described as locally reacting surfaces. Field and laboratory measurements (see Section 5.7 and Chapter 6, respectively) have shown the local reaction assumption to be a good approximation, even for very low frequencies, where the incident sound waves set the walls into vibratory motion. In the next chapter, an empty test room is fully measured and modelled, which will serve as a basis for the investigation of the absorbing effects of rooms and their contents, at low frequencies.

5.8 References

BALVEDI, A. M. **Medição e simulação acústica de materiais porosos e sistemas multicamadas**. Master Dissertation, Federal University of Santa Catarina, Florianópolis, 1998.

BERANEK, L. L. **Precision measurement of acoustic impedance**. Journal of the Acoustical Society of America, 12, 3-13, 1940-a.

- BERANEK, L. L. **Acoustic impedance of commercial materials and the performance of rectangular rooms with one treated surface.** Journal of the Acoustical Society of America, 12, 14-23, 1940-b.
- BERANEK, L. L. **Acoustic impedance of porous materials.** Journal of the Acoustical Society of America, 13, 248-260, 1942.
- BERANEK, L. L. **Noise and vibration control.** McGraw Hill, New York, 1971.
- BERANEK, L. L. **Concert hall acoustics – 1992.** Journal of the Acoustical Society of America, 92 (1), 1-39, 1992.
- BIES, D. A., HANSEN, C. H. **Engineering noise control: theory and practice.** E. and F. N. Spon, London, 1996.
- BIOT, M. A. **Theory of propagation of elastic waves in a fluid-saturated porous solid. I – Low frequency range. II – High frequency range.** Journal of the Acoustical Society of America, 28, 169-191, 1956.
- BOLTON, J. S., KANG, Y. J. **Elastic porous materials for sound absorption and transmission control.** Society of Automotive Engineers, Inc., 1997.
- BRÜEL & KJAER. **Technical review.** Nº 1, 1955.
- BRÜEL & KJAER. **Standing wave apparatus type 4002.** 1979.
- CREMER, L., MÜLLER, H. **Principles and applications of room acoustics.** Volume 2, Applied Science Publishers, London, 1982.
- CROCKER, M. J. **Handbook of acoustics.** John Wiley & Sons, New York, 1997.
- DOWELL, E. H., GORMAN, G. F., SMITH, D. A. **Acoustoelasticity: general theory, acoustic natural modes and forced response to sinusoidal excitation, including comparisons with experiments.** Journal of Sound and Vibration, 52, 519-542, 1977.
- FAHY, F. **Sound and structural vibration: radiation, transmission and response.** Edition Academic Press, 1985.
- FESHBACH, H. **On the perturbation of boundary conditions.** Physics Review, 65, 307-318, 1944.
- GERGES, S. **Ruído: fundamentos e controle.** Federal University of Santa Catarina U.P., Florianópolis, 2000.

GIBBS, B. M. **The inter-relation between the distribution of absorbent material amongst the room surfaces and the distribution of sound energy and reverberation times within the room.** Master Thesis, University of Sheffield, Sheffield, 1970.

HECKL, M. **The tenth Sir Richard Fairey memorial lecture: sound transmission in buildings.** Journal of Sound and Vibration, 77 (2), 165-189, 1981.

INGARD, K. U. **Notes on sound absorption technology.** Noise Control Foundation, New York, 1994.

ISO R354. **Measurement of sound absorption in a reverberation room.** 1985.

ISO 140/3. **Measurement of sound insulation in buildings and of buildings elements - Part 3: Laboratory measurements of airborne sound insulation of buildings elements.** 1995.

KINSLER, L. E., FREY, A. R. **Fundamentals of acoustics.** Wiley, New York, 1982.

KUTTRUFF, H. **Room acoustics.** Applied Science Publishers, 1979.

MALUSKI, S. P. S., GIBBS, B. M. **Application of a finite-element model to low-frequency sound insulation in dwellings.** Journal of the Acoustical Society of America, 108 (4), 1741-1751, 2000.

MALUSKI, S. P. S., GIBBS, B. M. **Use of finite element method to investigate the effect of furniture, wall recess and construction materials on the sound field in dwellings at low frequencies.** Proceedings of the 17th International Congress on Acoustics, Rome, 2001.

MORSE, P. M. **Some aspects of the theory of room acoustics.** Journal of the Acoustical Society of America, 11, 56-66, 1939.

MORSE, P. M., INGARD, K. U. **Theoretical acoustics.** McGraw Hill, New York, 1968.

PAN, J., BIES, D. A. **An experimental investigation into the interaction between a sound field and its boundaries.** Journal of the Acoustical Society of America, 83 (4), 1436-1444, 1988.

PAN, J., BIES, D. A. **The effect of fluid-structural coupling on sound waves in an enclosure – theoretical part.** Journal of the Acoustical Society of America, 87 (2), 691-707, 1990-a.

PAN, J., BIES, D. A. **The effect of fluid-structural coupling on sound waves in an enclosure – experimental part.** Journal of the Acoustical Society of America, 87 (2), 708-717, 1990-b.

PAN, J., ELLIOTT, S. J., BAEK, K. H. **Analysis of low frequency acoustic response in a damped rectangular enclosure.** Journal of Sound and Vibration, 223 (4), 543-566, 1999.

PARIS, E.T. **On the coefficient of sound absorption measured by the reverberation method.** Philosophical Magazine, 5, 489, 1928.

RAYLEIGH, J. W. S. **The theory of sound.** Volume II, 1896, reprinted by Dover Publications, New York, 1945.

SABINE, W. C. **Collected papers on acoustics.** Harvard U.P., Cambridge, 1900, reprinted by Dover Publications, 1964.

SEYBERT, A. F., ROSS, D. F. **Experimental determination of acoustic properties using a two-microphone random-excitation technique.** Journal of the Acoustical Society of America, 61, 1362-1370, 1970.

SYSNOISE REV 5.4. **User Manual.** Numerical Integration Technologies, 1999.

ZIENKIEWICZ, O., TAYLOR, R. **The finite element method.** Mc Graw Hill, 1971.

ZWICKER, C., KOSTEN, C. W. **Sound absorbing materials.** Elsevier Publishing Co. Inc., 1947.

CHAPTER 6

REFERENCE TEST ROOM

6.1 Introduction

In this chapter, the methodology and instrumentation used in performing the experimental part of this work is described. In addition, the numerical model, preliminarily constructed in Chapter 4 for the empty test room, is further developed and described. The objective of this phase of the investigation was to obtain reliable room frequency response measurements for the empty room, which was to serve as a basis for numerical model validation, and as a reference for the investigation of furnished rooms (see Chapters 7 to 10).

6.2 Measurement system

The assessment of acoustical problems is often facilitated by the determination of gain factors between excitation sources and receiver location responses. The fundamental quantity of interest here is the frequency response function ('FRF', sometimes called the transfer function) between two points of interest. Thus, given an excitation source signal $x(t)$ and a simultaneously measured response signal $y(t)$, the frequency response function is given by the ratio of the cross-spectral density function, between source and receiver signals, and the auto-spectral density function of the source signal [Beauchamp and Yuen (1980), Bendat and Piersol (1986), Beranek (1988), Beranek and Vér (1992)]. The frequency response function is generally a complex-valued quantity, giving both gain and phase difference. However, in many applications, only the gain is of interest, as was the case most of the time in the present work.

Various methods may be used to obtain frequency response functions of rooms. Examples include, impulse methods [Vorländer (1996)], pure tone excitation [Chu (1984)], white noise [Maluski (1999)], etc. With impulsive excitation, the dynamic range (range of amplitudes within which a system can work without underload or overload) is low, due to the generally poor signal-to-noise (s/n) ratio associated with this technique [Vorländer (1996)]. With pure tone excitations, the measuring process

is very slow [Chu (1984 & 85), Maluski (1999)]. With white noise the spectral energy is continuously distributed over frequency bands, thus exciting all room modes. On the other hand, due to its random nature, white noise based measurements need to be averaged several times, which improves the s/n ratio, but also creates stochastic deviations [Chu (1984 & 85), Bjor and Winsvold (1994), Maluski (1999)]. These difficulties can be circumvented by use of recent methods of digital signal processing. Of particular importance is the Maximum Length Sequences (MLS) technique, due to its efficiency and also to the availability of portable PC-based equipment [Vorländer (1996), Gomes (1998), Sampaio (1998)].

6.2.1 Maximum Length Sequences

MLS is a specific type of correlation measuring technique that, in principle, can be used for measurement of FRFs of acoustic systems, provided they are linear and time-invariant (LTI) [Vorländer (1996)]. Most acoustic systems may be considered approximately as LTI systems. While linearity is an important prerequisite for application of Fourier methods, time invariance means that the acoustic properties of the system under investigation remain unchanged during the measurement interval.

MLS are periodic binary pseudo-stochastic signals with an autocorrelation function that approximates a Dirac pulse. They are generated by use of a shift register with feedback loops. Thus, with m denoting the order of the shift register, at most $L = 2^m - 1$ different combinations of 0's and 1's are possible; only the state with 0's in all elements is omitted, because then it will be impossible for a 1 to occur, and the shift register will remain frozen in this state [Vorländer (1996), Viveiros (1998)]. By introducing a clock frequency to the shift register, a periodic sequence of register states will be created. The sequence used as signal can be taken from any point in the register, and the important point is that with certain feedback loops the period of the repeated sequence has its maximum length L . Thus, the resulting signal is a "maximum length sequence" [Vorländer (1996)]. As an illustration, Fig. 6.1 presents one period of a maximum length sequence of order 8, over two periods of the autocorrelation function.

Using the MLS technique, a significant saving in time is obtained in comparison to other methods, due to the availability of fast correlation algorithms [Rife and

Vanderkooy (1989), Vorländer (1996), Viveiros (1998), Gomes (1998)]. Also, due to its deterministic nature, a MLS signal should give exactly repeatable results.

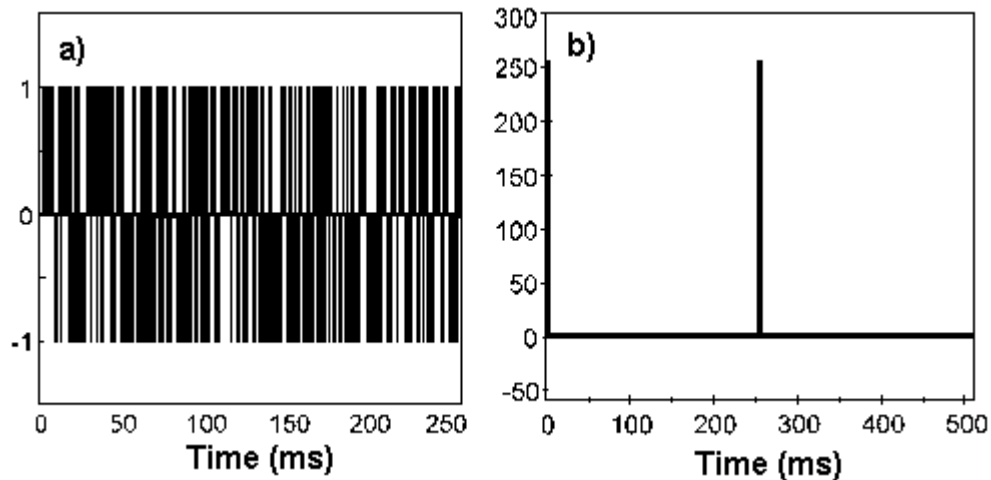


Figure 6.1 - a) MLS of order 8 and b) its autocorrelation function [Vorländer (1996)].

This allows the application of synchronous averaging, increasing the s/n ratio by 3 dB per doubling of the number of averages [Vorländer (1996)]. However, it should be remembered that the MLS technique is based on the theory of LTI systems, although weak non-linearities may be tolerated. Violations of this prerequisite are the subject of continuing research by others, and first studies indicate that errors may occur in outdoor measurements, or in measurements with extremely long averaging times and with unstable environmental conditions of temperature and static pressure [Rife and Vanderkooy (1989), Atkinson (1990), Mommertz and Müller (1995), Vorländer (1996)], none of which are the case in the present work.

6.2.2 Room details

In this work the reference room was one of the reverberant chambers of the Acoustics Research Unit (ARU) of the University of Liverpool. The main room dimensions are $L_x = 5.78$ m, $L_y = 3.04$ m, and $L_z = 4.24$ m. The room was not perfectly rectangular, having a small change in angle at the door position as indicated in Fig. 6.2. The room walls were of dense brick of thickness 122 mm with painted 15 mm fine grain plaster on the internal surface. The test aperture (3.5 m² in the centre of the wall opposite to the door wall), was filled with dense block work and skimmed with 10 mm of plaster, unpainted. The floor was a 100 mm thick reinforced concrete slab, cast on a resilient mat (for isolation from the building). The ceiling was of similar

construction as the floor. The door was of a heavy steel construction with compression seals.

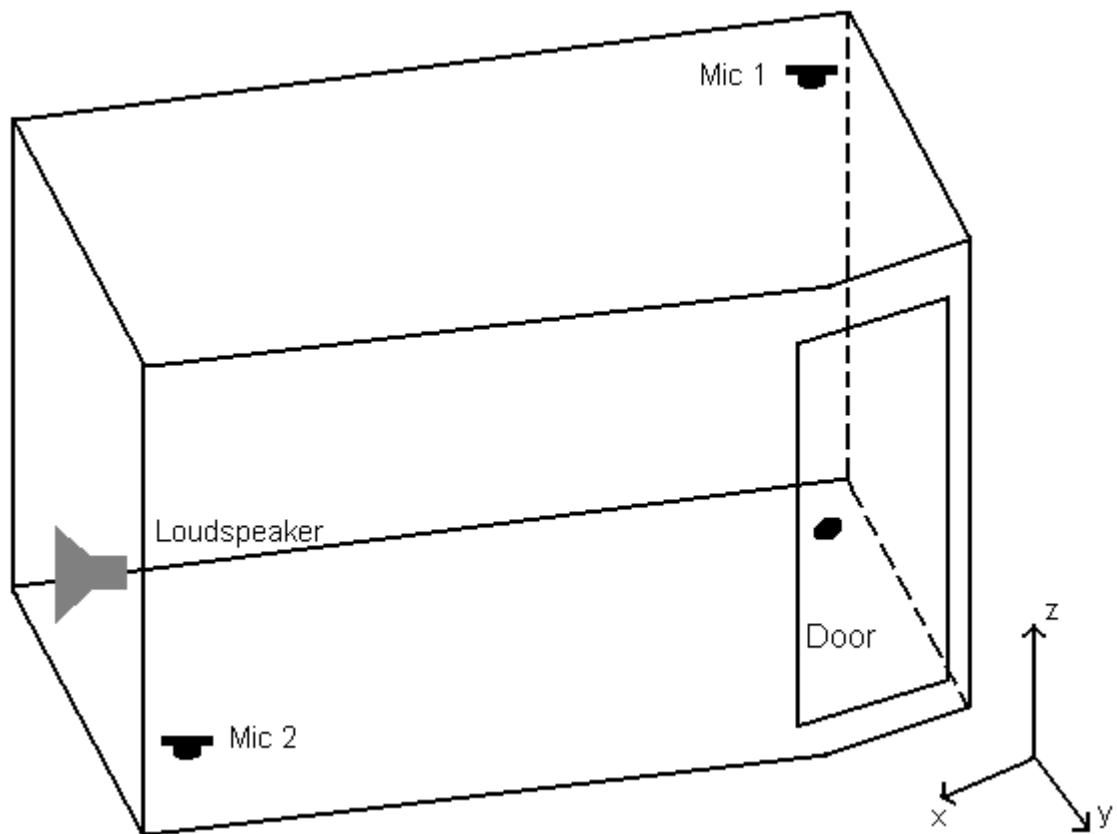


Figure 6.2 - Loudspeaker and microphone positions inside the investigated room, which has a change in angle at the door position.

Conventional measurements of background noise level and reverberation time were performed for the investigated room, and the figures obtained are listed in Tables 6.1 and 6.2. The background noise levels shown in Table 6.1 were sufficiently low to avoid signal masking even at frequencies as low as 25 Hz.

Table 6.1 - Measured background noise level for the investigated room.

Frequency Band (Hz)	Background Noise Level (dB)
31.5	49.5
63	40.0
125	35.0
250	25.0
500	15.0

The reverberation times measured (see Table 6.2) were short enough to avoid aliasing errors [Ewins (1984), Bendat and Piersol (1986)], when measuring room frequency responses with the maximum length sequences technique [Rife and Vanderkooy (1989), MLSSA (1994)].

Table 6.2 - Measured reverberation time for the investigated room.

Frequency Band (Hz)	Reverberation Time (s)
100	5.78
125	4.14
160	4.51
200	5.82
250	5.7
315	5.31
400	5.36
500	5.62

6.2.3 Measurement instrumentation

All measurements were carried out with a loudspeaker placed at one corner, and two microphones located at two other opposite corners (see Fig. 6.2). Two loudspeakers were tested prior to the experimental investigation: a 305 mm drive unit (single cone) in a ported cabinet of dimensions 300 mm x 380 mm x 550 mm, and a 457 mm drive unit (also single cone) in a ported cabinet 790 mm deep by 550 mm wide by 630 mm high. Both loudspeakers were 'base reflex', i.e., their ported cabinet had a path that allowed the out-of-phase motion of the loudspeaker to enhance the low frequency response. This allowed the excitation of all room modes in the frequency range of interest. Room frequency responses (sound pressure level versus frequency) were obtained using a MLS based system, and a schematic of the experimental set-up is shown in Fig. 6.3. Table 6.3 presents a list of the equipment employed.

The MLS based system was a Maximum Length Sequence System Analyser [MLSSA (1994)] installed on a PC, and was used to generate a burst stimulus of length 65535 as excitation signal. This signal was then amplified before exciting the

room by means of the loudspeaker. Although the frequency range of interest is from 20 Hz to 200 Hz, measurements frequency interval was typically 0 – 1 kHz.

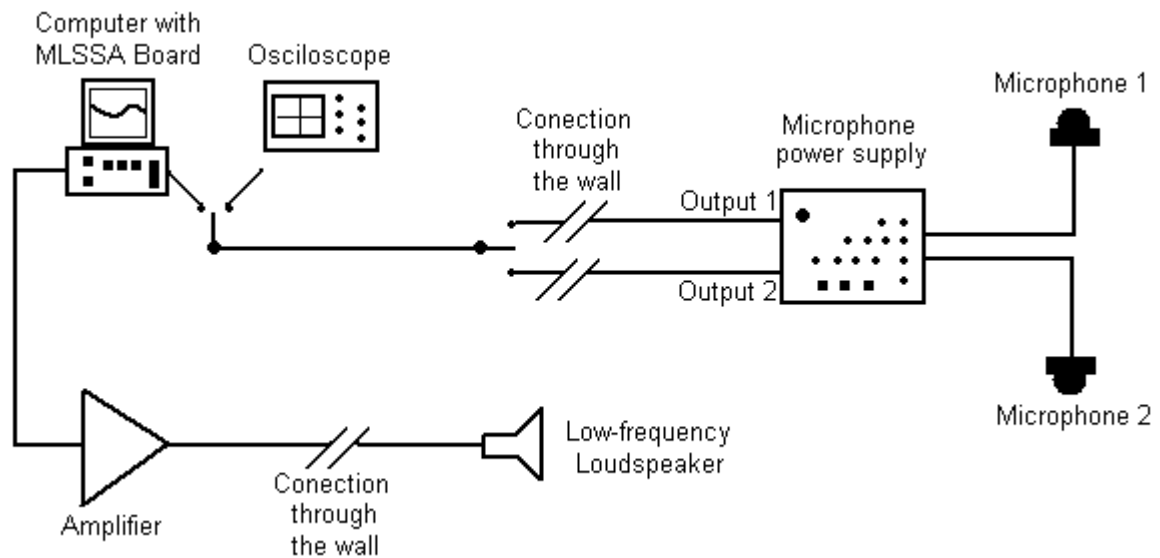


Figure 6.3 - Experimental set-up used in obtaining room frequency responses.

The sound pressure was sampled at a rate of 4 kHz, acquiring 65536 points, displayed as a time history. Using a Blackman-Harris window [MLSSA (1994)], an 8192 points FFT was used to obtain the room frequency response with spectral resolution of 0.49 Hz.

Table 6.3 - Equipment used in the experimental set-up shown in Fig. 6.3.

Device	Type
Amplifier	Quad 50 E
Loudspeaker	Yamaha SW 118 IV
Microphones	B&K 4165
Microphone Power Supply	B&K 5935

Prior to the room response measurements, a series of tests was performed, in order to verify the functioning of the equipment and its optimum configuration. In order to verify the equivalence of the output of the two matched microphones, the signals obtained at the same position inside the room were compared. Transfer functions were measured between each microphone and the loudspeaker. The transfer functions obtained were complex, but the results are presented as magnitudes. The ratio of the two transfer functions was then obtained. This ratio

should be a constant of 0 dB. The results show a reasonable flat spectrum at 0 dB within ± 1 dB to allow the assumption of reasonably equivalent microphones (see Fig. 6.4).

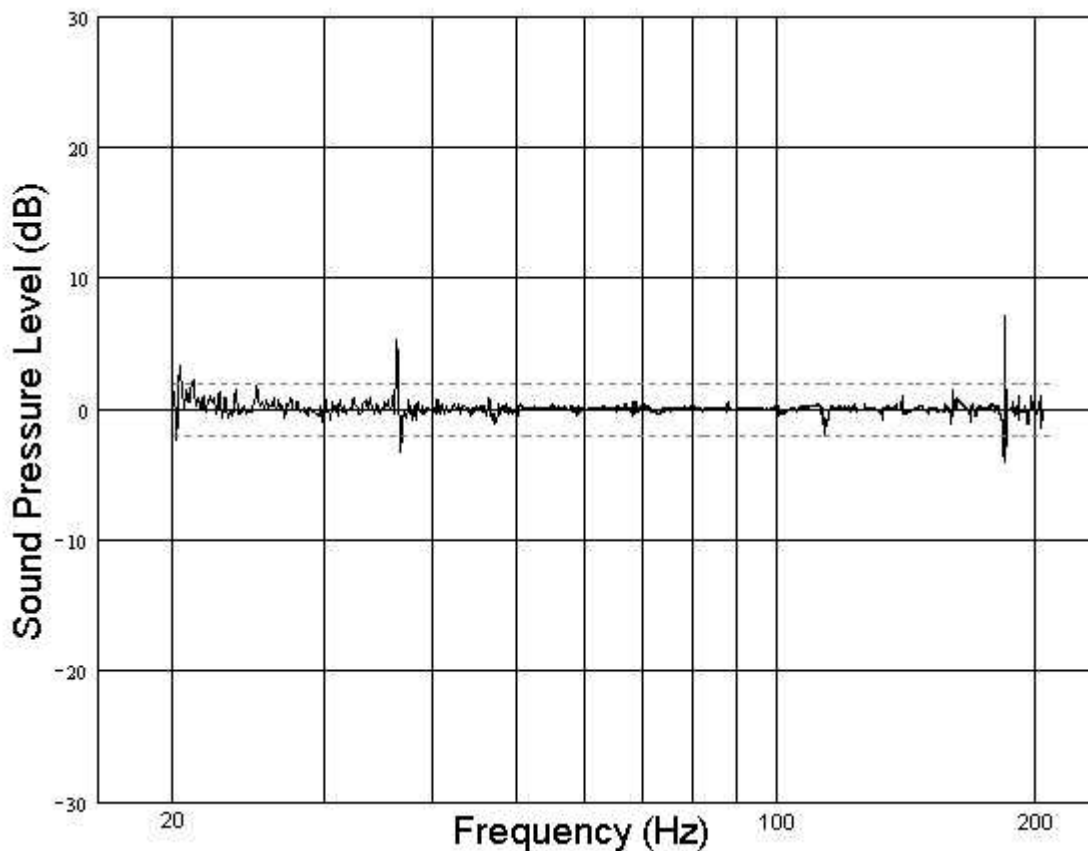


Figure 6.4 - Ratio of magnitudes of transfer functions for two microphones positioned at the lower corner of the investigated room.

The calibration measurements were repeated using a conventional Fourier Analyser, with white noise as excitation signal. A flat spectrum at 0 dB was obtained, though the results are not shown. Thus, it was concluded that the observed spikes at approximately 35 Hz and 190 Hz in Fig. 6.4 are simply due to the sensitivity of the MLS technique to system variations. The use of two fixed microphones allowed a much faster measurement procedure, with the additional advantage of guaranteeing exactly the same measuring positions between two consecutive experiments.

In order to quantify the repeatability provided by the measuring system, the transfer function between one microphone and the loudspeakers was measured in the anechoic chamber of the ARU. The experimental set-up was the same as described previously, but with a low-pass filter, which was included in the measuring chain to reject a persistent low frequency background noise and thereby increase the signal to noise ratio. Again, the repeatability was expressed as a ratio of repeated

results (see Figs. 6.5 and 6.6). The curve shown in Fig. 6.5 was obtained using the 305 mm loudspeaker with repeatability within ± 1 dB, above 50 Hz, and within ± 10 dB below 50 Hz.

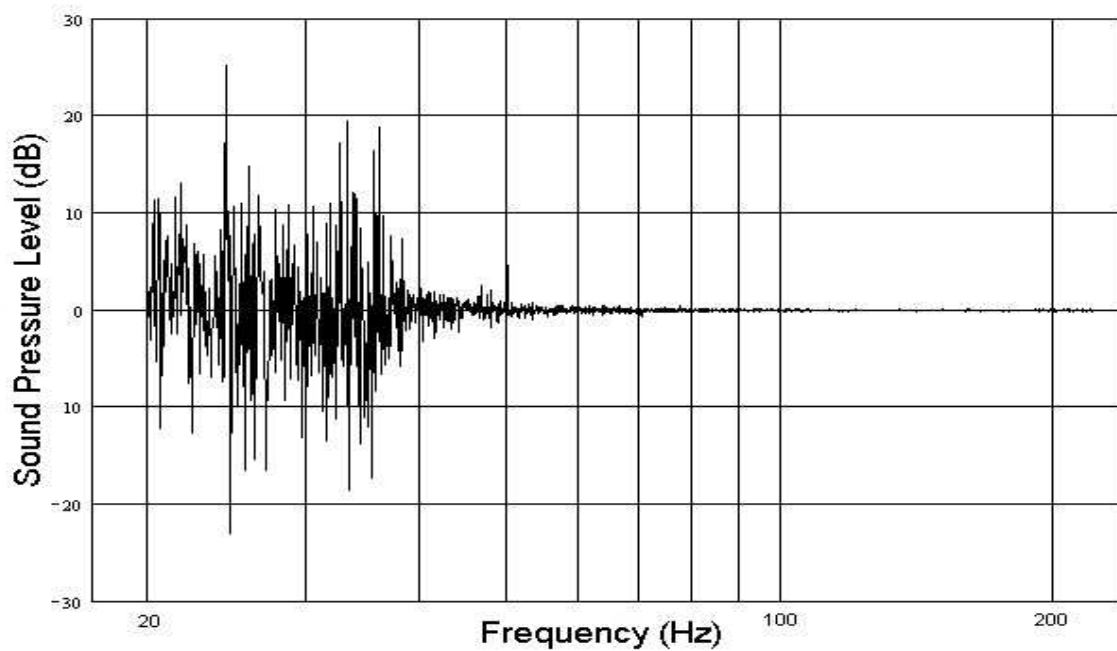


Figure 6.5 - Ratio of magnitudes for two measurements for the same microphone positioned inside the anechoic chamber of the ARU, with the 305 mm loudspeaker as the sound source.

The curve displayed in Fig. 6.6 was obtained with the 457 mm loudspeaker with repeatability within ± 2 dB below 50 Hz, and within ± 0.1 dB above 50 Hz.

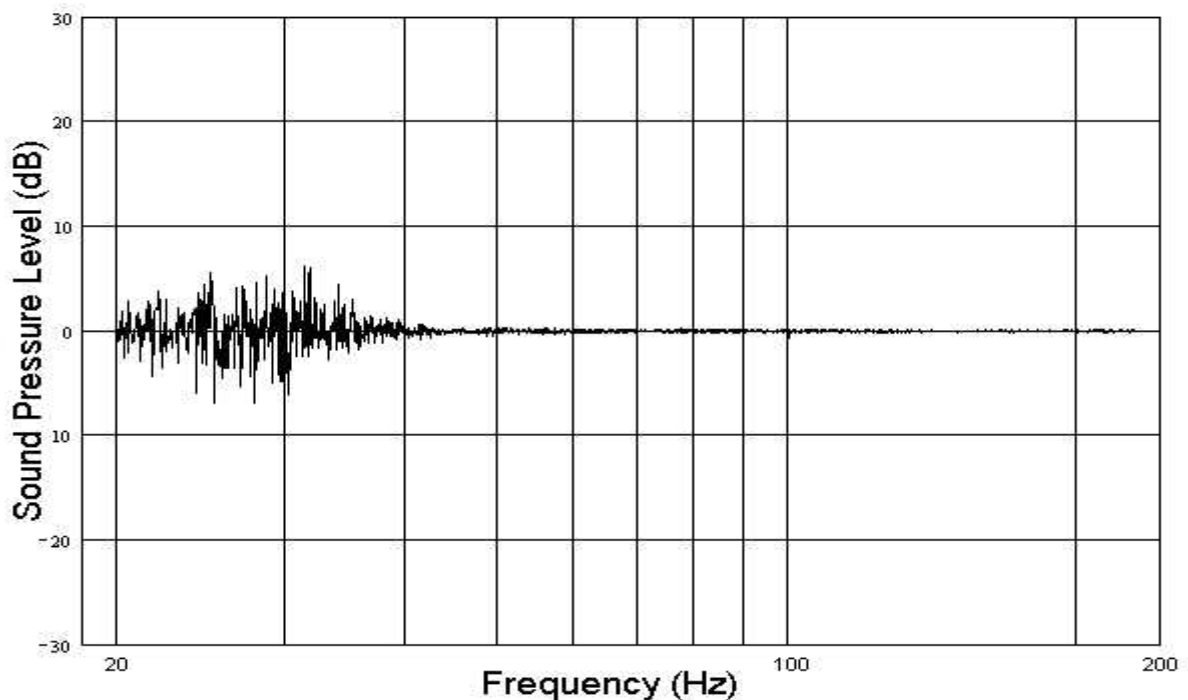


Figure 6.6 - Transfer function indicating the repeatability between two measurements for the same microphone positioned inside the anechoic chamber of the ARU, with the 457 mm loudspeaker as the sound source.

Therefore, a better repeatability, mainly for the frequency range below 50 Hz, is achieved when the 457 mm loudspeaker is used, which is explained by the greater efficiency of the latter in exciting very low frequencies.

It was recognised that a large loudspeaker might be more difficult to represent in a numerical model. This is because, ideally, the sound source is introduced in the numerical model as a point source (see Section 4.5.1). However, it was not physically possible to have in practice a small loudspeaker with the capability to excite very low frequencies. Thus, the 457 mm loudspeaker was selected as the best compromise.

6.3 Finite element model

In chapter 4, the present use of Finite Elements Methods in Acoustics was described. Section 4.5 dealt specifically with the parameters and assumptions used in modelling a rectangular room. Although the preliminary model demonstrated good accuracy when comparing results for room eigenfrequencies with those calculated analytically, it was not a complete model.

The small change in angle at the door position (see section 6.2.2) was initially thought not to be influential. However, comparison of the results provided by the rectangular room model with measurement highlighted discrepancies throughout the frequency range. The curves shown in Fig. 6.7 correspond to the upper microphone results (microphone 1, as shown in Fig. 6.2). The modal characteristics of the enclosure at low frequencies are clearly indicated, as both predicted and measured sound pressure levels display maxima and minima, corresponding to room modes. Although not shown here, similar results were obtained for microphone 2. The first four peaks seen in Fig. 6.7 correspond to modes (1,0,0), (0,0,1), (1,0,1), and (0,1,0), respectively. In the comparison shown in this figure it is possible to see that after the second room mode this numerical model was only able to match a few eigenfrequencies for the shown interval. In the case of the third mode, for example, the discrepancy between predicted and measured mode frequency is approximately 3%.

Thus, a new model of the room was created, taking into account the change in angle at the door position. The new mesh for the improved model is shown in Fig. 6.8. As before, the element size was 0.28 m, and the element type was “HEXA 20”.

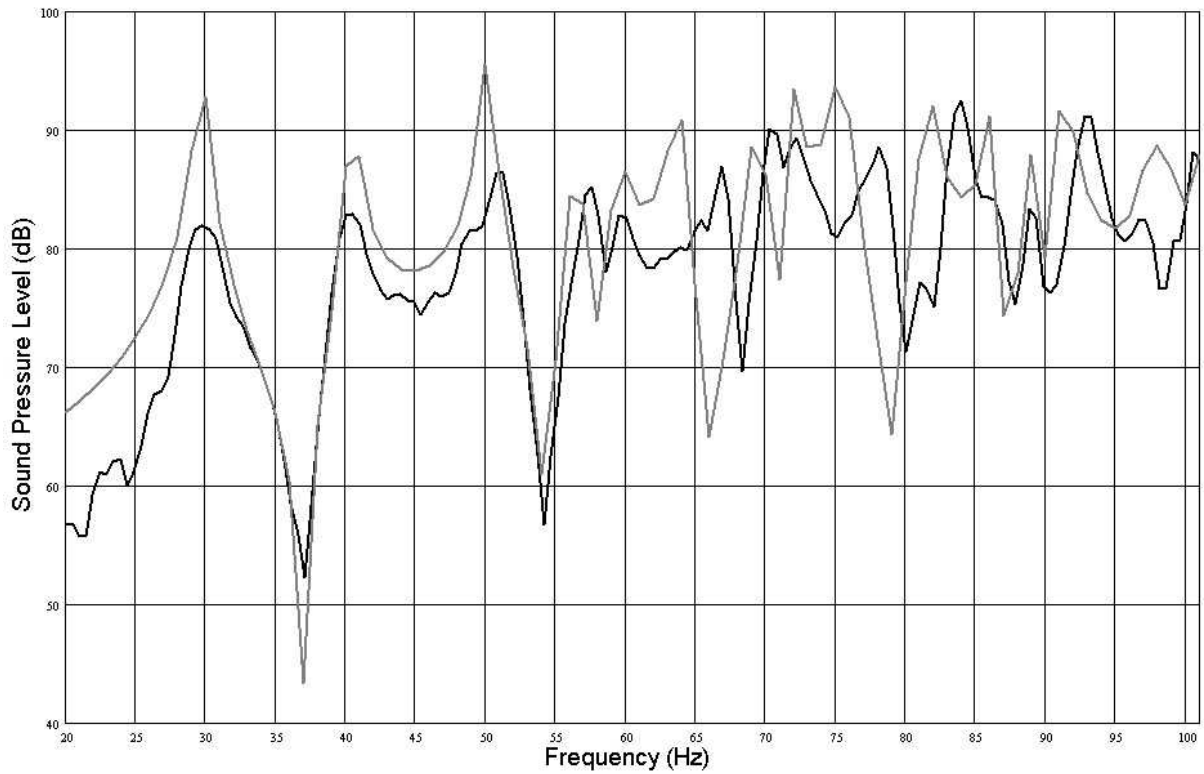


Figure 6.7 - Comparison between (—) measurement and (---) preliminary prediction provided by the rectangular room model.

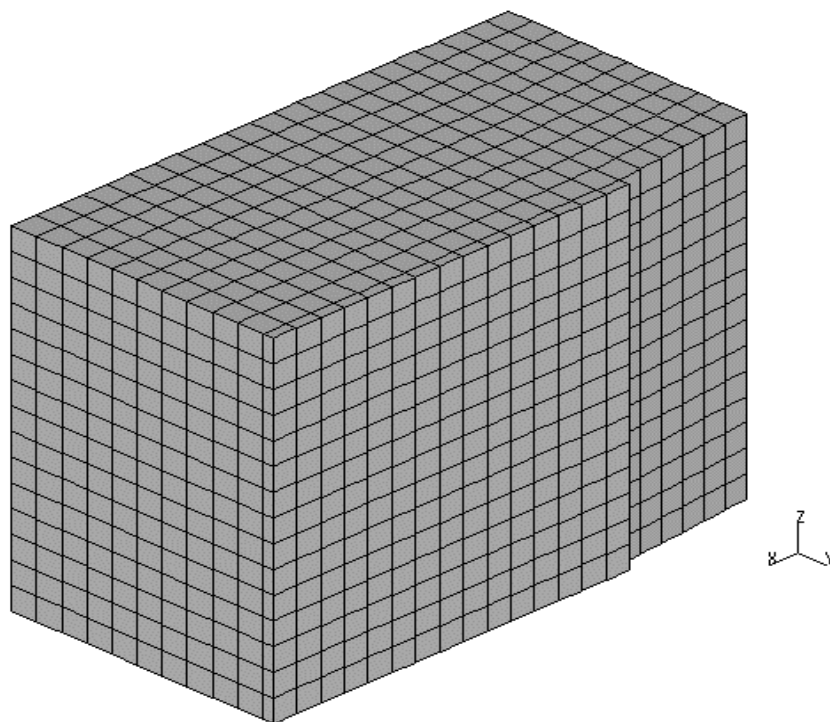


Figure 6.8 - Isometric view of the refined finite element model of the test room.

On comparing the frequency responses provided by the rectangular room model and the improved room model (see Fig. 6.9), it is confirmed that the introduction of the small change in angle at the door position clearly affects the modal distribution, shifting several eigenfrequencies throughout the frequency range of interest.

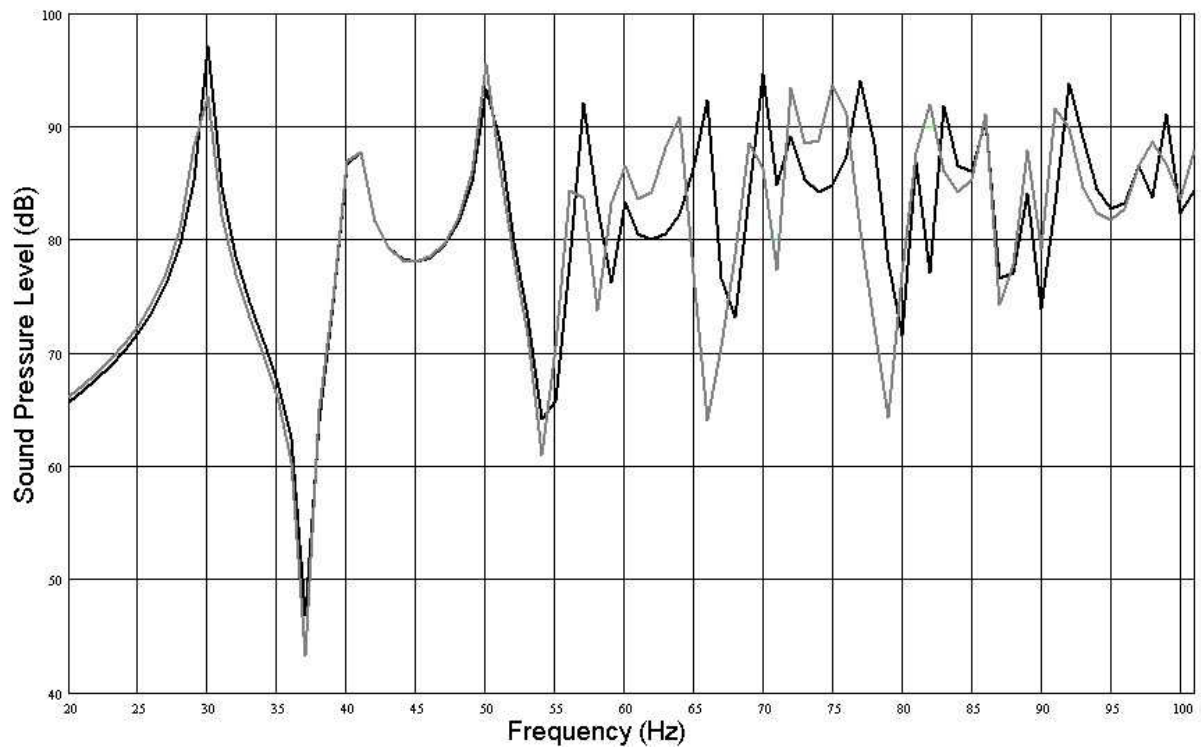


Figure 6.9 - Predicted curves showing the differences between the results of (—) improved room model and (---) rectangular room model.

All the perceivable differences between the curves shown in Fig. 6.9 are exclusively due to geometrical differences between the two numerical models, since all the other parameters were kept the same as those described in section 4.5.

6.4 Results

In the following sections, experimental and numerical results for the empty test room are presented. Comparisons are made and adjustments in the FEM are described which improved the agreement with measurement.

6.4.1 Preliminary comparison

A comparison first was made between measured room frequency response and that obtained from the numerical model, where the room surfaces were assumed non-absorbing (see Fig. 6.10).

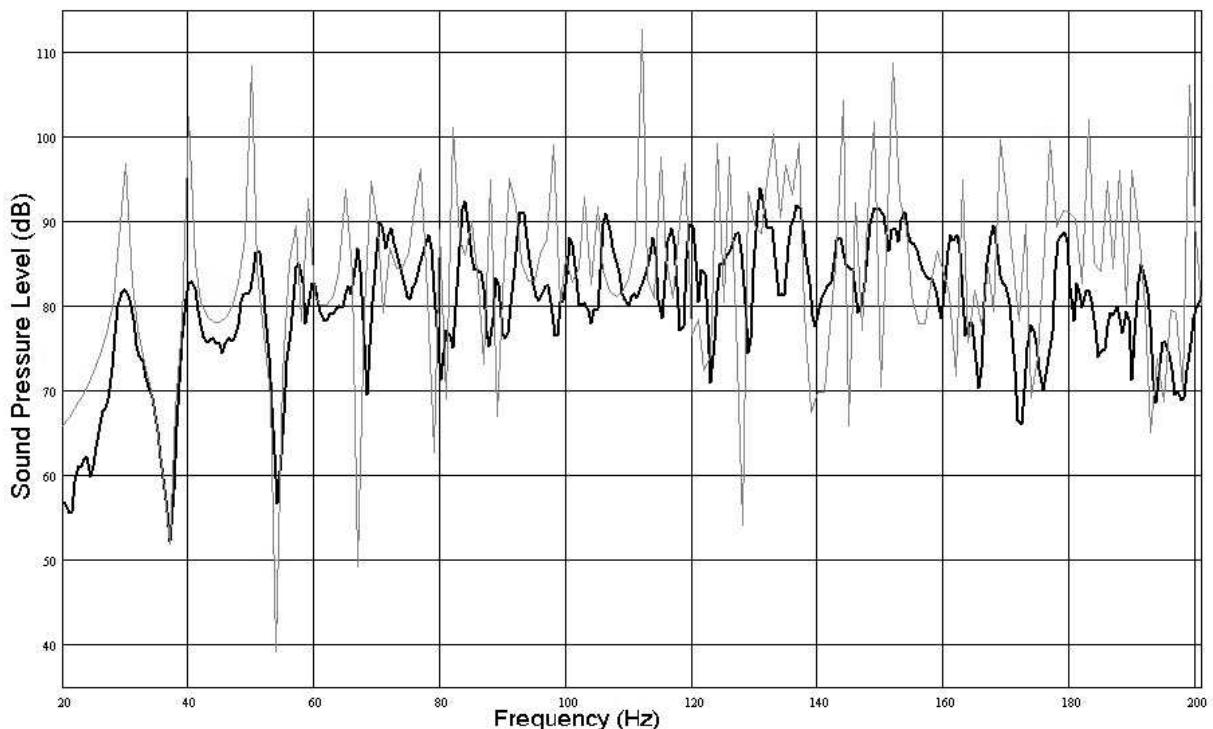


Figure 6.10 - Preliminary comparison between (—) measurement and (---) prediction, for the improved room model with hard boundaries.

Although the predicted curve follows the trends of the experimental curve, in general it overestimates the response. This is mainly due to errors in sound source modelling and assumptions of zero absorption. This was also observed by Maluski (1999), and such errors were further investigated in the present work.

6.4.2 Measurement and prediction of wall vibration

As discussed in chapter 5, even without sound absorptive material inside the room, a possible mechanism of energy loss is introduced by the coupling between the room acoustic modes and the wall vibration modes. The contribution of this mechanism to the total sound absorption inside the room was measured as the vibratory response of one wall of the test room. The measured frequency response was compared to predicted values provided by theory [Leissa (1993)]. This allowed the determination of the most appropriate wall boundary conditions for best fit of predicted and measured eigenmodes.

The wall measured was the back surface (plane $x = 5.78$ m, according to Fig. 6.2), since it was the simplest and most accessible. The internal dimensions were $L_y = 3.04$ m, $L_z = 4.24$ m, and thickness $h = 137$ mm, approximately. The experimental set-up is shown in Fig. 6.11 and the equipment is listed in Table 6.4.

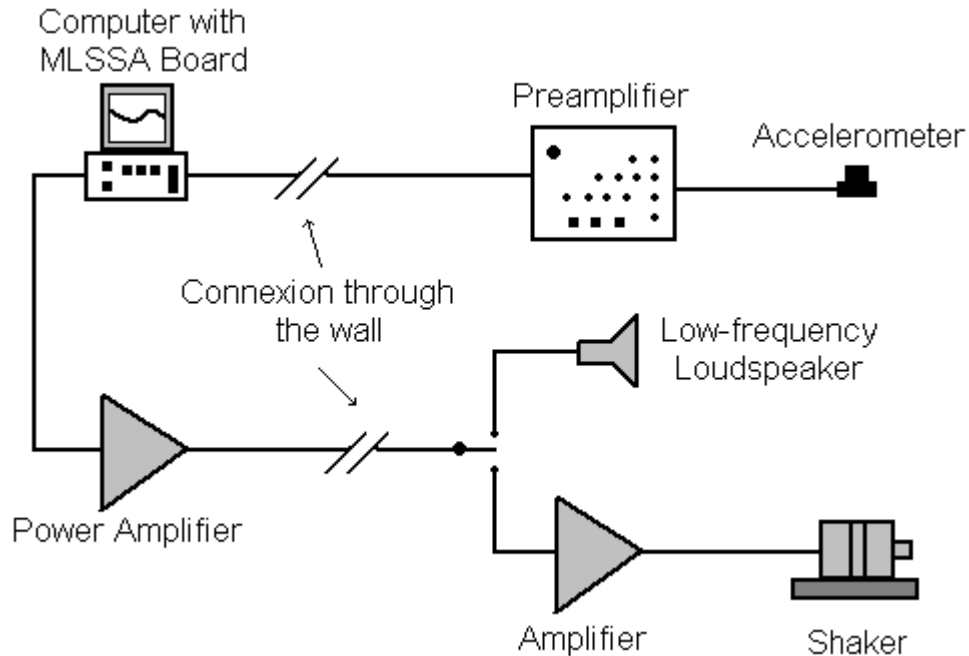


Figure 6.11 - Experimental set-up for the investigation of wall vibration.

Table 6.4 - Equipment used in the experimental set-up shown in Fig. 6.11.

Device	Type
Power Amplifier	Quad 50 E
Loudspeaker	Yamaha SW 118 IV
Amplifier	B&K 2706
Shaker	Ling Dynamic Systems 400 Series
Accelerometer	B&K 4378
Preamplifier	B&K Nexus

The 457 mm loudspeaker was used first as the excitation source. An electrodynamic shaker (Ling Dynamic Systems 400 series) was also used, attached to the wall 0.55 m from the left edge and 0.80 m from the floor, so as not to coincide with any structural node in the frequency range of interest. Measurements were carried out with the accelerometer placed inside and outside the room, in order to investigate

the influence of the sound field on the former, when using the loudspeaker as excitation source. Fig. 6.12 shows two measurements for the accelerometer placed on the external side of the wall, when the latter was excited by the two types of sources. The curves are plotted with measurement of the wall background acceleration level for comparison.

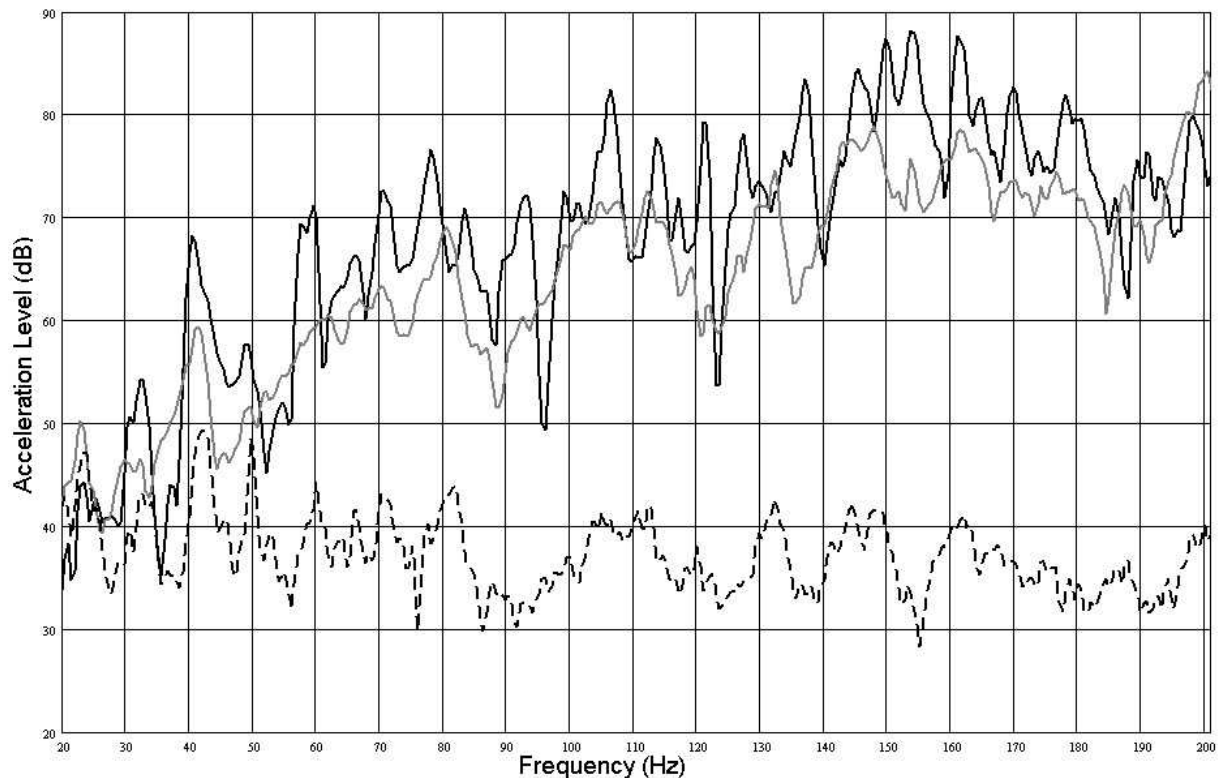



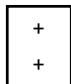
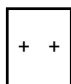
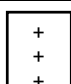
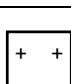
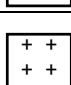
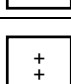
Figure 6.12 - Vibratory response of test room wall. (—) Loudspeaker excitation, (---) shaker excitation, and (-.-) background noise.

It can be concluded that the room walls vibrate when the low-frequency loudspeaker is used as a source inside the room, and that these vibrations contribute to the whole room absorption mechanism mainly at very low frequencies. Evidence of this is contained in the measured room frequency response (see the experimental curve in Fig. 6.7). The first three modes, for example, at approximately 30 Hz, 40 Hz, and 50 Hz, respectively, have a significant loss factor η [Morse and Ingard (1968)], when compared with the first three predicted modes shown in Fig. 6.10, which were obtained considering a room with no absorption. While the first three measured modes have loss factors 9.7%, 4.7%, and 3%, respectively, the corresponding predicted modes for a room with no absorption have loss factors 1.8%, 0.75%, and 0.56%. Thus, since at these low frequencies the air absorption may be completely neglected (see Chapter 5) and the acoustic impedance of the room hard surfaces is

unlikely to produce such an effect, the role played by the wall vibrations in the room absorption mechanism becomes clear.

A second set of measurements was carried out in order to identify the first wall modes. This was done by selecting accelerometer positions likely to be at, or near anti-nodes. Results were then compared with those for positions at corresponding nodes. Consequently, using this technique it was possible to identify the first seven wall modes, which are listed in Table 6.5.

Table 6.5 - Identified wall modes.

Mode Order	Resonance Frequency (Hz)	Modal Numbers	Modal Shape
1 st	24.9	1,1	
2 nd	42.0	2,1	
3 rd	62.5	1,2	
4 th	71.8	3,1	
5 th	80.6	2,2	
6 th	102.5	3,2	
7 th	112.3	4,1	

Using the theory provided by Leissa (1993) the simplest case was considered, which corresponds to simply supported edges (SSSS), as the real boundary conditions were unknown. There were also difficulties due to the imprecision of the values of the wall material properties. The values used are suggested by Gibbs (1974), and listed in Table 6.6.

For the SSSS case, the structural eigenfrequencies are given by:

$$f_{ss} = \frac{\pi}{2} \sqrt{\frac{D}{\rho}} \cdot \left[\left(\frac{m}{L_z} \right)^2 + \left(\frac{n}{L_y} \right)^2 \right], \quad (6.1)$$

where m and n are the structural modal numbers (integers) and D is the flexural rigidity, which in turn is given by

$$D = \frac{E h^3}{12(1 - \nu^2)} \quad (6.2)$$

Table 6.6 - Wall material properties, according to Gibbs (1974).

Property	Value
Young's Modulus	$E = 10^{10} \text{ N/m}^2$
Poisson's Ratio	$\nu = 0.3$
Surface Mass Density	$\rho = 148 \text{ kg/m}^2$

From the wall dimensions and the values listed in Table 6.6, it was possible to calculate all the structural eigenfrequencies below 200 Hz, which is the upper frequency of interest. The values were calculated using the concept of “neutral lines”, i.e., adding half of the thickness value to the wall dimensions L_y and L_z . The eigenfrequencies also were calculated with the FEM program (Sysnoise) for comparison. The wall finite element mesh was constructed with the commercial software Patran, using an element size of 0.28 m, and structural elements “Quad 4”. The element size was chosen in order to match that used in the room model. However, the element type (Quad 4) was a requirement of Sysnoise, in order to model the wall with “Shell” elements, rather than “Plate” elements. The latter allows the use of more precise element types, but restricts the definition of the elements only to the x-y plane.

A relative percentage error was calculated between theoretical and numerical eigenfrequency values, and all the results for the SSSS case are listed in Table 6.7. The same calculations were performed for the case in which all the wall boundaries were assumed to be clamped (CCCC). For this case, Leissa (1993) suggests a table of ratios of wall dimensions, which can be used to calculate the structural eigenfrequencies according to

$$f_{cc} = \frac{r}{2\pi L_y^2 \sqrt{\rho/D}}, \quad (6.3)$$

where r is the given ratio, which in this case corresponds to 0.72. Again, a numerical simulation was performed for the CCCC case, and as for the simply supported case,

theoretical and numerical results are compared in Table 6.8. Although there is agreement between theoretical and predicted results (see Tables 6.7 and 6.8), they have not agreed with measurements (see Fig. 6.13), indicating that the real boundary conditions must lie between the two investigated cases (simply supported and clamped). This was also observed by Maluski (1999).

Table 6.7 - Theoretical eigenfrequencies (TE), numerical eigenfrequencies (NE), and percentage error (E) for the SSSS case.

Mode Order	m,n	TE (Hz)	NE (Hz)	E (%)
1 st	1,1	31.2	31.0	-0.49
2 nd	2,1	63.2	63.1	-0.19
3 rd	1,2	92.7	94.2	1.63
4 th	3,1	116.6	118.4	1.54
5 th	2,2	124.7	124.9	0.12
6 th	3,2	178.1	178.0	-0.04
7 th	4,1	191.3	199.3	4.17

Table 6.8 - Theoretical eigenfrequencies (TE), numerical eigenfrequencies (NE), and percentage error (E) for the CCCC case.

Mode Order	m,n	TE (Hz)	NE (Hz)	E (%)
1 st	1,1	58.3	58.4	0.25
2 nd	2,1	94.9	95.3	0.37
3 rd	1,2	139.1	142.6	2.50
4 th	3,1	155.9	159.3	2.20
5 th	2,2	173.1	174.3	0.71

6.4.3 Adjusted model parameters

In order to obtain the best fit between measurements and predicted results provided by the FE room model, the parameters and inputs of the latter were updated. The first parameter to be adjusted was the wall absorption coefficient that was to be entered in the numerical model in the form of an acoustic admittance – see equation (6.4) and Section 8.3. A parametric study was carried out to determine the value of surface absorption that would give the best agreement with measurements.

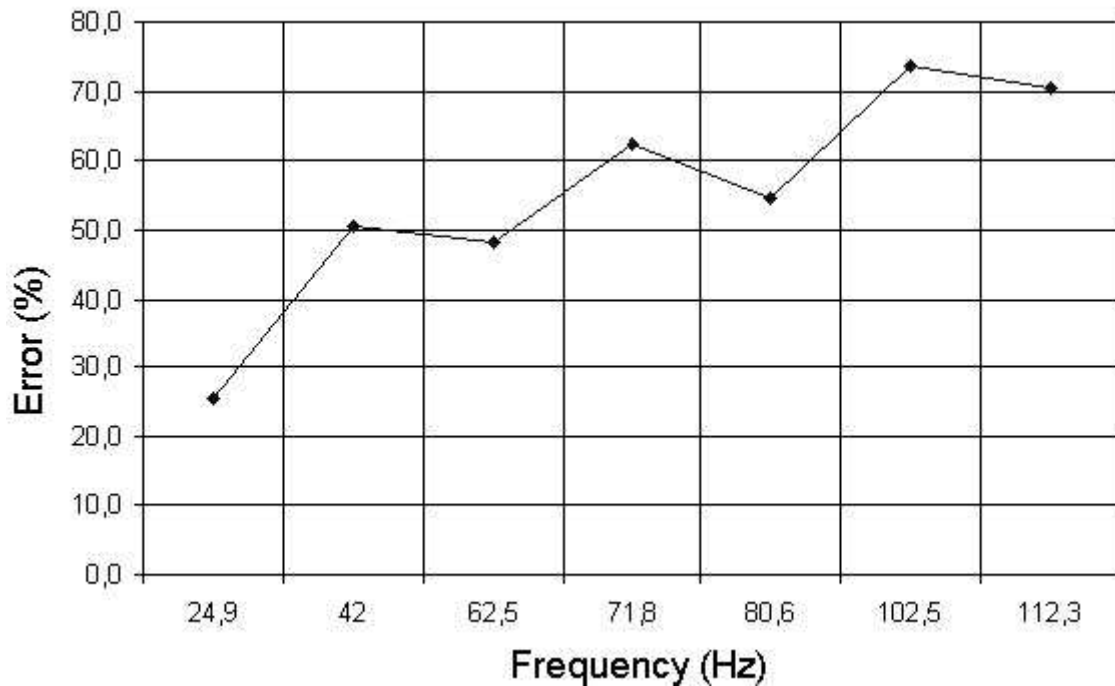


Figure 6.13 - Percentage error between theoretical (SSSS) and measured eigenfrequencies (see Tables 6.7 and 6.5, respectively), as a function of the measured eigenfrequencies.

Three simulations were run, with frequency invariant surface absorption coefficients of 2%, 5%, and 10%, respectively. Fig. 6.14 shows the predicted results for the refined room model, considering hard surfaces and the three different values of absorption. Level differences between predictions for each value of α and measurement are presented in Fig. 6.15 in 1/12th octave bands. The one-twelfth octave bands were calculated with the aid of a computer and plots presented to this resolution were constructed from a logarithmic average of the narrow band results divided by the number of points in each band.

As shown in Fig. 6.15, a surface absorption coefficient of $\alpha_n = 0\%$ (hard wall), overestimates values compared with measurements, and above 40 Hz its corresponding level difference is on average 7 dB \pm 8 dB. A value $\alpha_n = 10\%$ underestimates values compared with measurements and the corresponding level difference is on average -5 dB \pm 3 dB below 110 Hz, and -10 dB \pm 3 dB above this frequency. The corresponding level difference for $\alpha_n = 5\%$ also indicates an underestimation compared with measurements, although to a lesser extent. For this value of absorption coefficient the difference is on average -2 dB \pm 2 dB below 110 Hz, and -6 dB \pm 3 dB above this frequency. The same figure shows that the level difference corresponding to an absorption coefficient of 2% fluctuates around 0 dB

with a variation ± 5 dB, providing the smallest overall discrepancy with measurements.

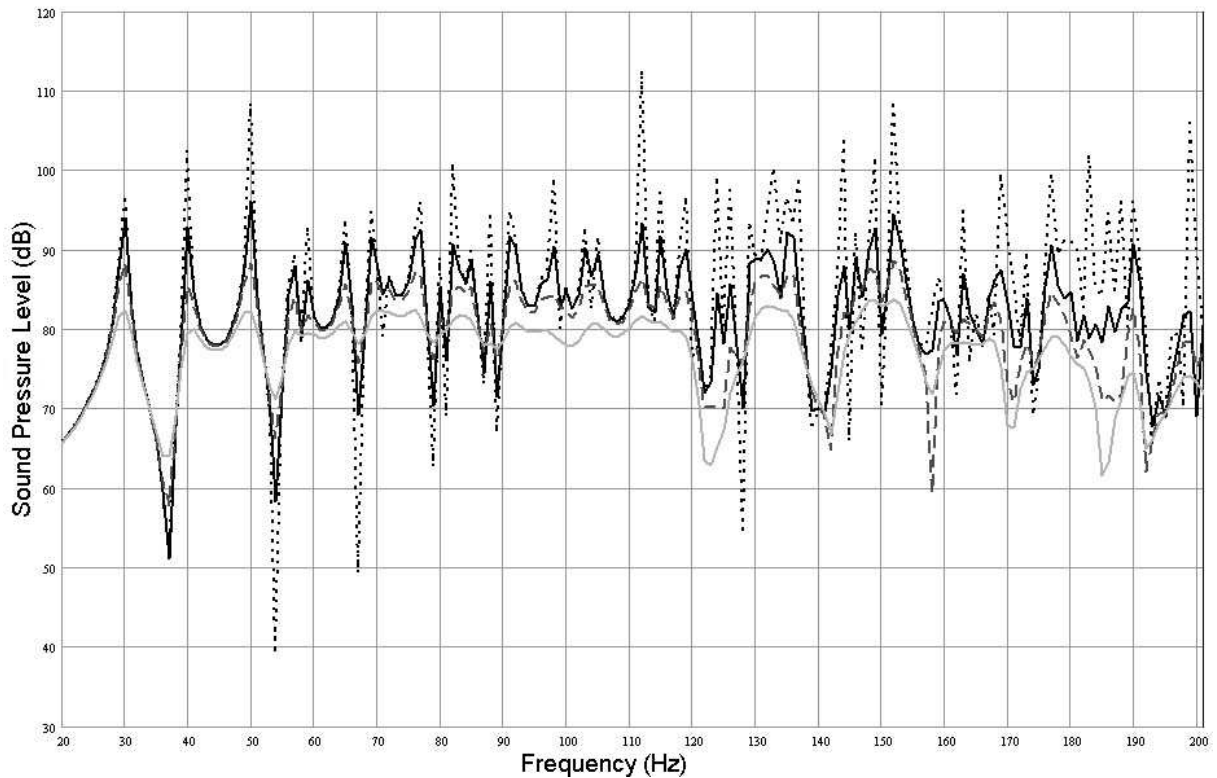


Figure 6.14 - Effect of increasing absorption coefficient on the room frequency response: (· · ·) hard wall, (—) $\alpha = 2\%$, $\alpha = 5\%$ (---), and $\alpha = 10\%$ (-·-·).

Therefore, this value of absorption was selected as the most appropriate to simulate the absorption characteristics of the room surfaces. In obtaining the results plotted in Fig. 6.15, a correction was applied to predicted results in order to include the observed loudspeaker roll-off at frequencies below 100 Hz (see Fig. 6.16 and discussion below).

The developed numerical model considers all room boundaries as locally reacting surfaces, and that a value of absorption enters the model in the form of a normal wall admittance A (assumed to be pure real) which can be calculated by:

$$A = \frac{1}{Z}, \quad (6.4)$$

where Z is the normal wall impedance given by [Gerges (2000)]

$$Z = \frac{1 + \sqrt{1 - \alpha_n}}{1 - \sqrt{1 - \alpha_n}} \rho c_0. \quad (6.5)$$

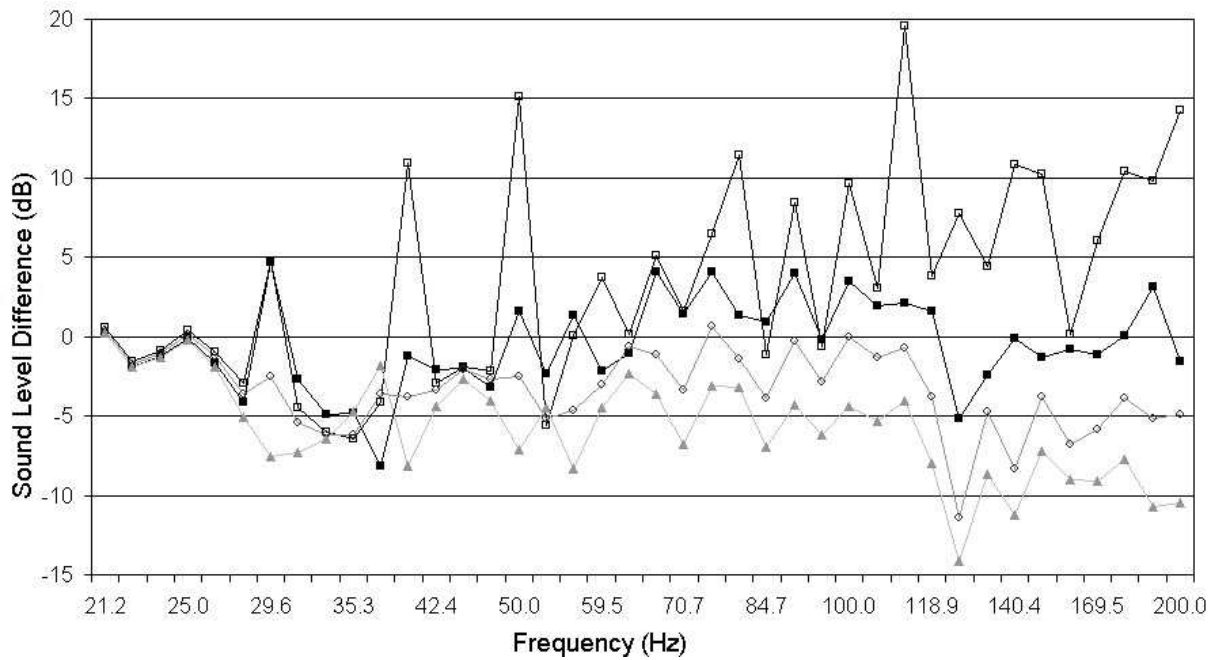


Figure 6.15 - Level differences between measurement and prediction for (—□—) hard wall, (—■—) $\alpha = 2\%$, (—○—) $\alpha = 5\%$, and (—▲—) $\alpha = 10\%$.

The second parameter to be adjusted in the numerical model was the simulated sound source. The loudspeaker frequency response was not flat throughout the frequency range of interest, despite the fact that it is designed to operate at very low frequencies. Thus, the FE model of the actual room was further refined by including a polynomial expansion to fit the loudspeaker roll-off. The acoustic power of the numerical sound source was now expressible as a monotonic function of frequency. The curve representing this polynomial expression, along with a measurement of the empty test room frequency response, is presented in Fig. 6.16.

Also, it was observed that the program Sysnoise utilizes as a default a value of 340 m/s for the velocity of sound in air, c_0 . However, according to Gerges (2000), this parameter is given approximately by

$$c_0 = 331 + 0.6T, \quad (6.6)$$

where T is the temperature in °C. The average room temperature was measured as 20 °C, yielding a value of $c_0 = 343$ m/s, according to equation (6.6). This small difference in sound velocity in air yielded significant shifts in the predicted room modes, since according to equation (3.34), the room eigenfrequencies are directly proportional to c_0 .

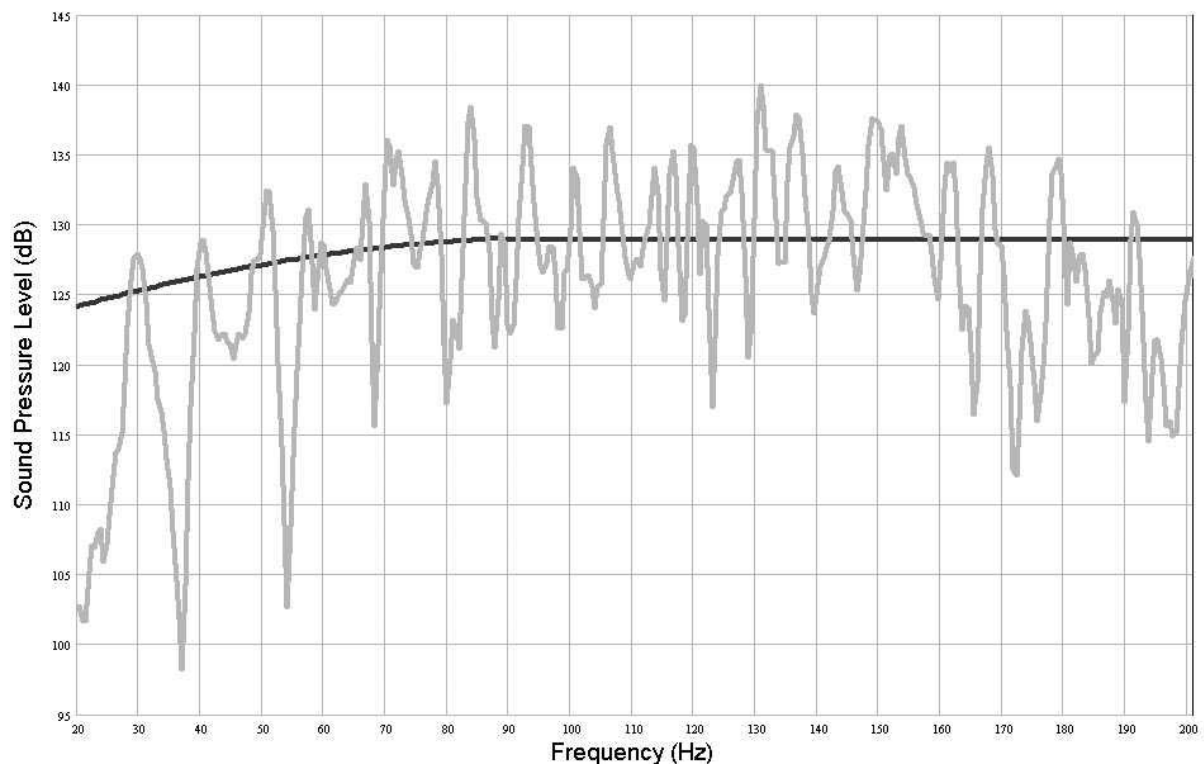


Figure 6.16 - Curve of a polynomial expression simulating the loudspeaker roll-off at lower frequencies.

As a result of these adjustments, it was possible to obtain an improved agreement between measurement and prediction for the empty test room frequency responses, as shown in Fig. 6.17. This is verified in Fig. 6.18, which shows level differences between measurement and prediction for the preliminary numerical model described in Chapter 4 and the new model with adjusted parameters. The results are presented in $1/12^{\text{th}}$ octave bands and comparison shows the reduced overall discrepancy between measurement and prediction achieved with the improved model.

Finally, following the idea introduced in Chapter 4, results are also presented in the form of modal patterns at frequencies 30 Hz, 57.1 Hz, 59.4 Hz and 77.3 Hz (see Figs. 6.19 to 6.22, respectively). For comparison, these figures show the same modes presented in Chapter 4 (rectangular room). Thus it is possible to observe how the small change in the room geometry (see Section 6.2.2) affects both the room eigenfrequencies and eigenmodes.

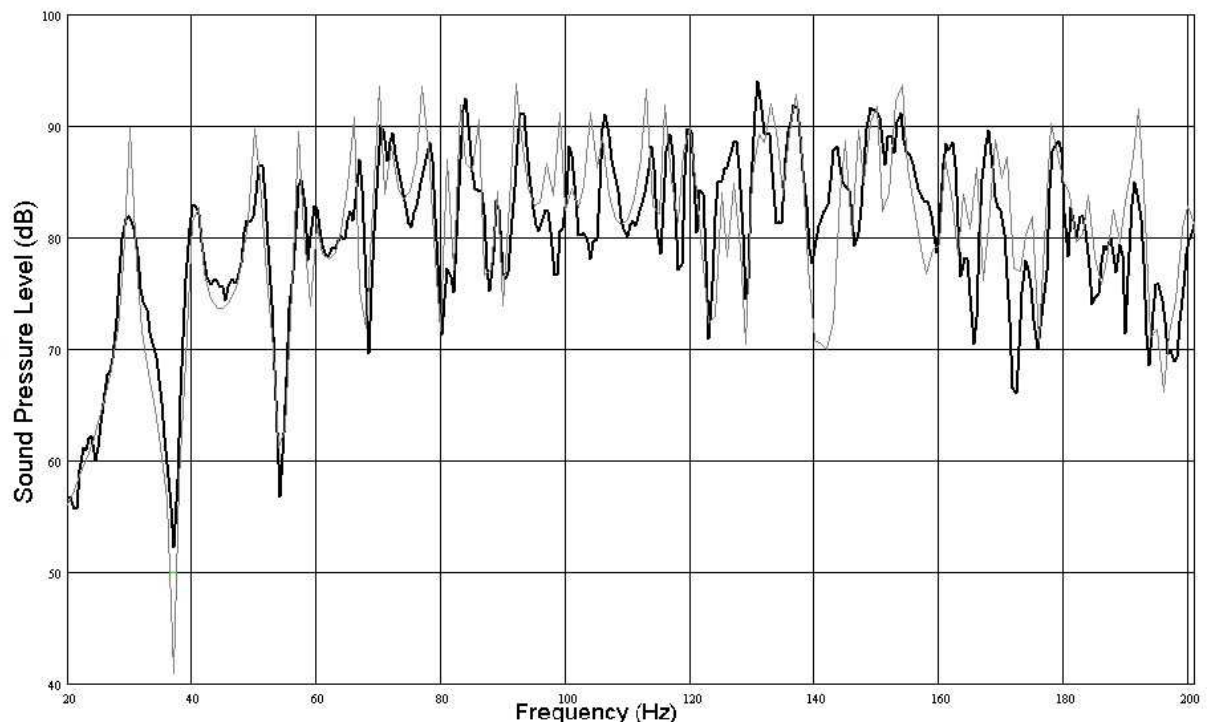


Figure 6.17 - (—) Prediction and (---) measurement, after parameter adjustments.

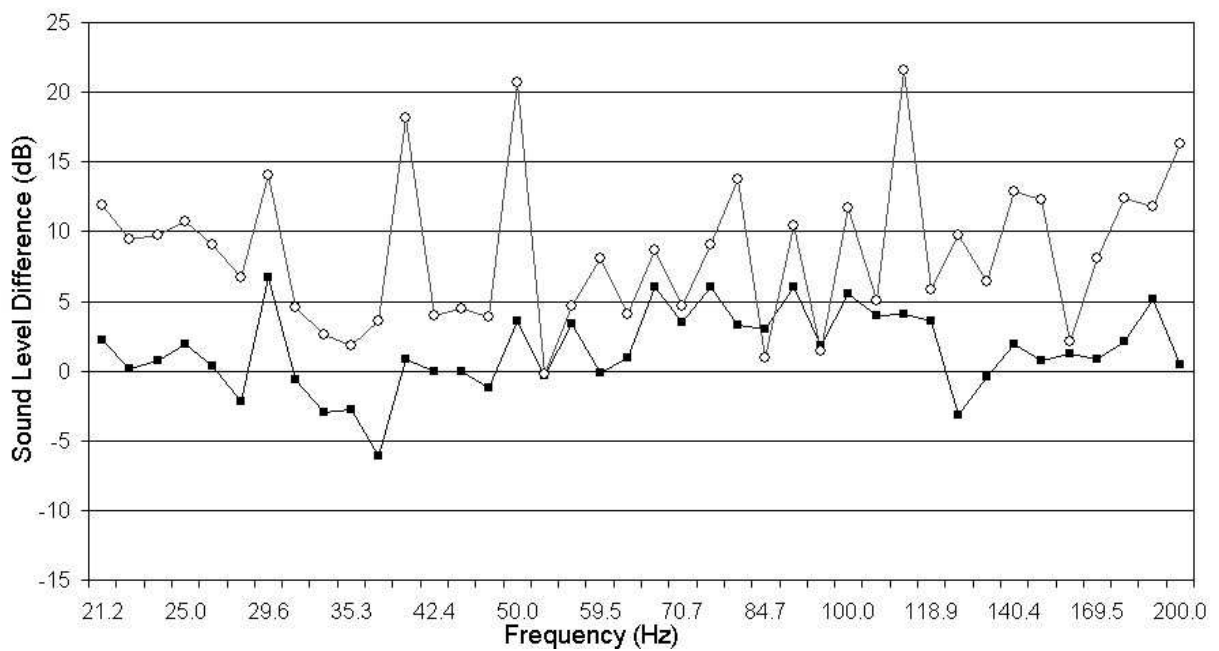


Figure 6.18 - Level differences between measurement and prediction for (—○—) old model (Chapter 4) and (—■—) new model with adjusted parameters.

6.5 Summary

A description has been given of the measurements performed in order to obtain frequency responses for the empty test room, which was to be used as the reference for later measurements with obstacles and absorbers in the room. The adjustments

to the FE model of the empty room have also been described. The process of modelling the empty room has highlighted the need to account for even small irregularities in the room geometry, in order to obtain a good agreement between numerical and experimental results.

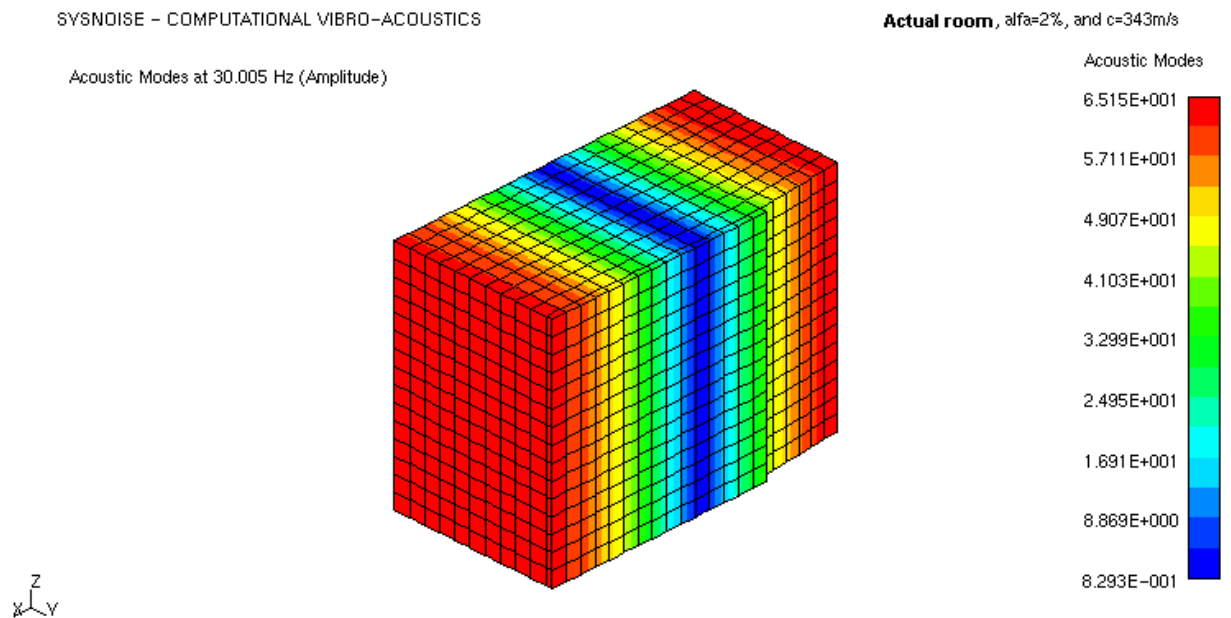


Figure 6.19 - Spatial distribution of pressure amplitude for the first mode (1,0,0).

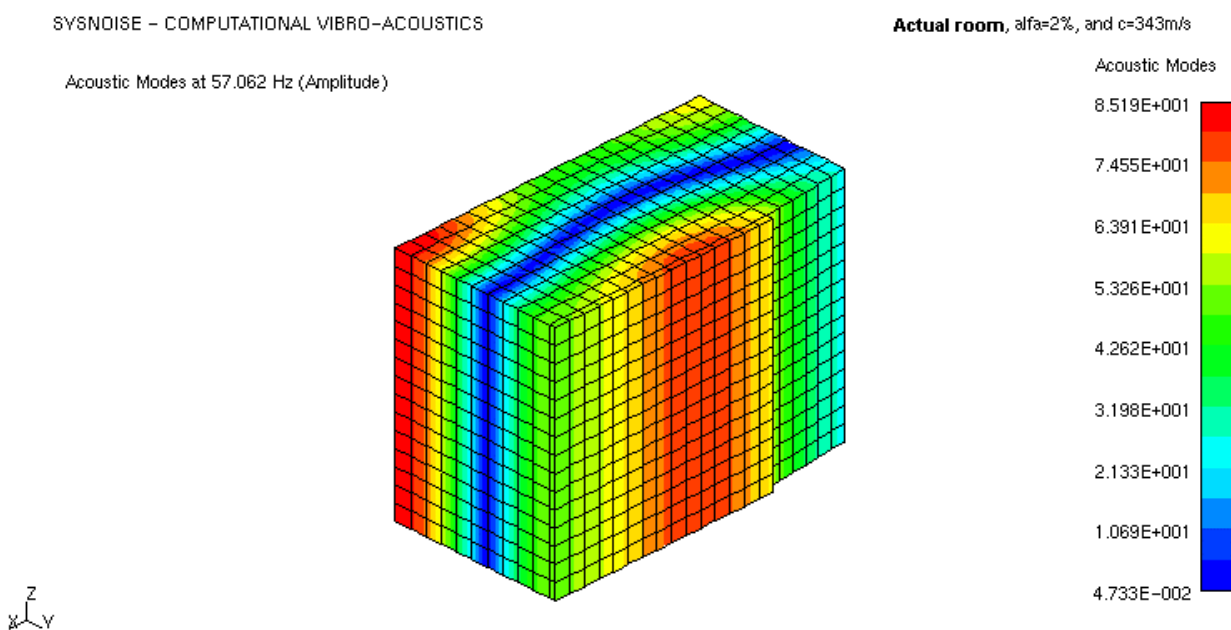
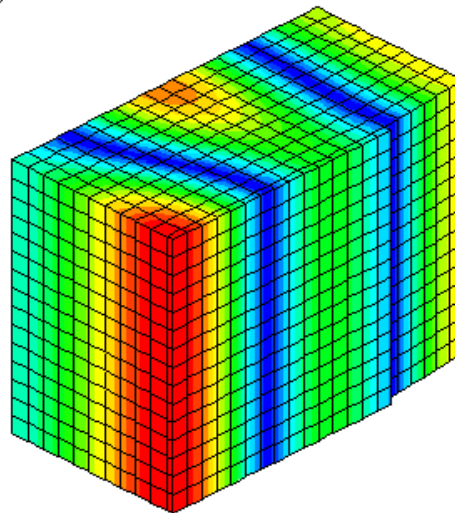


Figure 6.20 - Spatial distribution of pressure amplitude for the fourth mode (0,1,0).

SYSNOISE – COMPUTATIONAL VIBRO-ACOUSTICS

Acoustic Modes at 59.405 Hz (Amplitude)

**Actual room**, $\alpha=2\%$, and $c=343\text{m/s}$

Acoustic Modes

8.769E+001

7.677E+001

6.585E+001

5.493E+001

4.401E+001

3.309E+001

2.216E+001

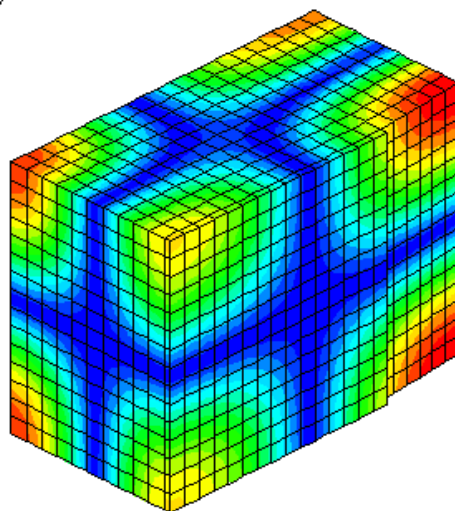
1.124E+001

3.221E-001

Figure 6.21 - Spatial distribution of pressure amplitude for the fifth mode (2,0,0).

SYSNOISE – COMPUTATIONAL VIBRO-ACOUSTICS

Acoustic Modes at 77.333 Hz (Amplitude)

**Actual room**, $\alpha=2\%$, and $c=343\text{m/s}$

Acoustic Modes

1.353E+002

1.183E+002

1.014E+002

8.454E+001

6.763E+001

5.072E+001

3.381E+001

1.691E+001

7.940E-011

Figure 6.22 - Spatial distribution of pressure amplitude for the ninth mode (1,1,1).

Furthermore, measurement of one of the room walls vibrational behaviour clearly showed that these vibrations contribute to the whole room absorption mechanism at very low frequencies. After a parametric survey, a value of absorption coefficient of 2% was found to be the amount of surface absorption that produced the best agreement with measurements. This apparent absorption coefficient of 0.02 included the effect of wall vibration losses in the numerical model, and although this is a

simple damping model, i.e., there is no variation of the absorption coefficient with frequency, the resultant predicted FRFs agreed with measurement within 2 dB \pm 5 dB. Thus, the results presented in Figs. 6.17 and 6.18 show that it was possible to obtain a good fit between measurement and prediction, after simple adjustments mainly of wall impedance and loudspeaker frequency response, justifying the choice of the developed room FE model.

In the following chapters, an investigation of the influence of room contents on the room frequency response is described, where the results of the present chapter serve as a basis for the evaluation of such effects.

6.6 References

- ATKINSON, J. **Measuring with MLSSA**. Stereophile, 13, 118-119, 1990.
- BEAUCHAMP, K., YUEN, C. **Data acquisition for signal analysis**. George Allen & Unwin, Boston, 1980.
- BENDAT, J. S., PIERSOL, A. G. **Random data: analysis and measurement procedures**. 2nd ed., Wiley, New York, 1986.
- BERANEK, L. L. **Acoustical measurements**. Acoustical society of America, Woodbury, NY, 1988.
- BERANEK, L. L., VÉR, I. L. **Noise and vibration control engineering: principles and applications**. John Wiley & Sons, NY, 1992.
- BJOR, O., WINSVOLD, B. **Deterministic excitation signals reduces statistical spread and extraneous noise contamination in sound transmission measurements**. Inter-Noise 94, 1469-1474, Yokohama, 1994.
- CHU, W. T. **Architectural acoustic measurements using periodic pseudorandom sequences and FFT**. Journal of the Acoustical Society of America, 76 (2), 475-478, 1984.
- CHU, W. T. **Room response measurement in a reverberation chamber containing a rotating diffuser**. Journal of the Acoustical Society of America, 77 (3), 1252-1256, 1985.
- EWINS, D. J. **Modal testing, theory and practice**. Wiley, New York, 1984.
- GIBBS, B. M. **The direct and indirect transmission of vibrational energy in building structures**. Ph. D. Thesis, University of Birmingham, Birmingham, 1974.
- GOMES, M. **Obtenção de parâmetros para a avaliação da qualidade acústica de**

- salas através da técnica MLS e acústica de raios.** Master Dissertation, Federal University of Santa Catarina, Florianópolis, 1998.
- LEISSA, A. **Vibration of plates.** Ed. Acoustical Society of America, 1993.
- MALUSKI, S. P. S. **Low frequency sound insulation in dwellings.** Ph.D. Thesis, Sheffield Hallam University, Sheffield, 1999.
- MLSSA. **User Manual.** DRA Laboratories, 1994.
- MOMMERTZ, E., MÜLLER, S. **Measuring impulse responses with digitally preemphasized pseudo random noise derived from maximum length sequences.** Applied Acoustics, 44, 195-214, 1995.
- RIFE, D., VANDERKOOY, J. **Transfer-function measurement with maximum-length sequences.** JAES, 37, 419-444, 1989.
- SAMPAIO, R. **Aplicação da teoria dos números em acústica: técnica de MLS e difusores.** Master Dissertation, Federal University of Rio de Janeiro, Rio de Janeiro, 1998.
- VIVEIROS, E. B. **Evaluation of the acoustical performance of Louvre by impulse response analysis.** Ph.D. Thesis, Federal University of Santa Catarina, Florianópolis, 1999.
- VORLÄNDER, M. **Applications of maximum length sequences in acoustics.** Proceedings of 1st SIBRAMA, Petrópolis, 1996.

CHAPTER 7

ROOM CONTENTS AS OBSTACLES

7.1 Introduction

In chapter 6, measured and predicted frequency response functions (FRFs) were presented for empty rooms with rectangular and slightly non-rectangular shapes. Although most real rooms have (at least approximately) rectangular shapes, invariably they will be filled with various contents. In practice, such contents may be represented by machines in a factory, columns in large enclosures, and (of particular interest here) furniture inside dwellings. The question arises of whether low frequency acoustic characteristics of rooms are substantially altered by the contents. The importance of such an investigation has been highlighted by Maluski (1999) in a study where a finite element model of sound transmission between dwellings has been developed, which demonstrates the importance of the modal characteristics of pressure and vibration fields of rooms and separating wall, respectively. The work also identified important outstanding issues to be addressed, in particular, the need of an appropriate model of sound absorption in small-furnished rooms at low frequencies.

Therefore, the aim of this chapter is to present a preliminary investigation of the effect of room contents on low frequency room responses. Initially, such room contents will be regarded as obstacles, i.e., hard-surfaced objects placed throughout the room volume. In order to quantify the effect of including contents, the results of the empty room, described in chapter 6, will be used as a reference.

7.2 Eigenfrequency shift

According to Wu and Fricke (1991) the acoustic properties of cavities are substantially modified after the introduction of objects, which modify the wave equation or boundary conditions and give rise to volumetric and scattering effects. These effects may even cause changes in the eigenfrequencies of the cavity. In fact, these changes may be exploited to solve problems in acoustic design, non-destructive testing, structural, room, and building acoustics, e.g., in situations where

monitoring of the internal state of a duct or a pipe is important, yet untenable using conventional visual techniques [Antonopoulos-Domis (1980), Wu and Fricke (1990), de Salis and Oldham (2000)]. Using an inverse technique, Wu and Fricke (1990) have developed a method for determination of blockage location and cross-sectional area in ducts, by eigenfrequency shifts. This work was extended, and the Green function method was used to study the eigenfrequency shifts in a two-dimensional rectangular cavity containing arbitrary-shaped small objects. These shifts were then used to obtain the object size and location [Wu and Fricke (1991)]. The investigations were limited to centrally positioned obstacles, due to difficulties in obtaining the required second set of boundary conditions in the 2D cavity. This method was refined by de Salis and Oldham (2000), who developed a rapid technique for reconstructing the internal area function of a duct using eigenvalue shifts, which were measured using Maximum Length Sequence analysis under two sets of boundary conditions. The authors also observed that blockage reconstructions might be successfully achieved excluding the lowest order eigenvalues shifts, establishing that these are not necessarily the most important shifts for the reconstruction process, as initially thought by Wu and Fricke (1991).

In the area of sound transmission in buildings, eigenfrequency shifts may be desired in situations where there is a strong coupling between adjacent rooms, mainly when these rooms are identical, since equal room configurations give poorer sound insulation when compared with cases of unequal rooms [Maluski and Gibbs (1998)].

Akil and Oldham (1995) have demonstrated that machines in factories may be treated as point scatterers at high frequencies, where ray tracing can be employed to predict their effect [Ondet and Barbry (1989), Akil and Oldham (1995)]. The machines are characterised in terms of a scattering cross-section, Q , given by

$$Q = \frac{A}{4\alpha}, \quad (7.1)$$

where A is the measured absorption of the scattering object (total surface area times the material absorption coefficient), and α is an assumed value of absorption coefficient based upon an “intelligent guess”. According to Akil and Oldham (1995), for a typical industrial fitting, a value of 0.1 was assumed appropriate for α . From equation (7.1) it can be seen that the expression for the scattering cross-section of an obstacle with simple shape and uniform surface sound absorption coefficient is

similar to expressions suggested by other researchers [Jovicic (1971), Lindqvist (1982), Kurze (1985), Ondet and Barbry (1989)] namely the scattering cross-section of an object is simply equivalent to its total surface area divided by four.

At low frequencies, the inclusion of furniture in a room may generate additional eigenmodes, mode shifts and selective damping of modes [Melo et al (2001)]. According to Wu and Fricke (1991), the properties of the eigenfrequency shift pattern are uniquely related to the obstruction location, while the amplitudes of such shifts are determined by the blockage size. However, as it was observed during the present work, such effects will depend also on the construction of the obstruction, i.e., how hard or how soft it is.

7.3 Standard unit and experimental set-up

In order to perform a preliminary study of the influence of room contents as obstacles (e.g., furniture) on room frequency responses, a “standard unit” was constructed from lightweight concrete blocks (see Figs. 7.1 and 7.2).



Figure 7.1 - Standard unit constructed of lightweight concrete blocks.

Such a construction, whilst being heavy and reflective, allowed flexibility in changing unit dimensions, and in locating it inside the room. The standard unit was of dimensions $l_x = 1.53$ m, $l_y = 0.88$ m, and $l_z = 0.75$ m and was positioned in three

locations (see Fig. 7.3). The size was chosen in order to approximate a large item of furniture such as a sofa.



Figure 7.2 - Standard unit also showing the detail of its internal construction.

Ideally, the standard unit should have been a solid box, with completely reflective surfaces. However, this ideal condition was not practically achievable, since the lightweight concrete blocks composing the unit were porous, unplastered and presented a sound absorption greater than that of the room surfaces. In order to quantify this effect, the reverberation time was measured, with the standard unit placed in the centre wall position (position b in Fig. 7.3). The results were then compared with the values of reverberation time previously obtained for the empty room (see Table 6.2), and this comparison is presented in Table 7.1.

Table 7.1 - Comparison between values of reverberation time for the empty and furnished rooms, showing the standard unit unwanted sound absorption.

Frequency Band (Hz)	100	125	160	200	250	315	400	500
Empty room rev time (s)	5.78	4.14	4.51	5.82	5.70	5.31	5.36	5.62
Furnished room rev time (s)	2.95	3.07	2.64	3.85	3.51	3.78	3.48	3.79

Using the method provided by ISO R354 (1985) and the values of Table 7.1, the equivalent absorption coefficient of the obstacle surface, α_s may be calculated by [Gerges (2000)]:

$$\alpha_s = \frac{0.161 \cdot V}{S_s} \left(\frac{1}{T_2} - \frac{1}{T_1} \right) + \bar{\alpha}, \quad (7.2)$$

where V is the room volume, S_s is the sample area, T_2 and T_1 are, respectively, the room reverberation times with and without the standard unit, and $\bar{\alpha}$ is the average absorption coefficient of the room walls. The results for α_s are shown in Table 7.2.

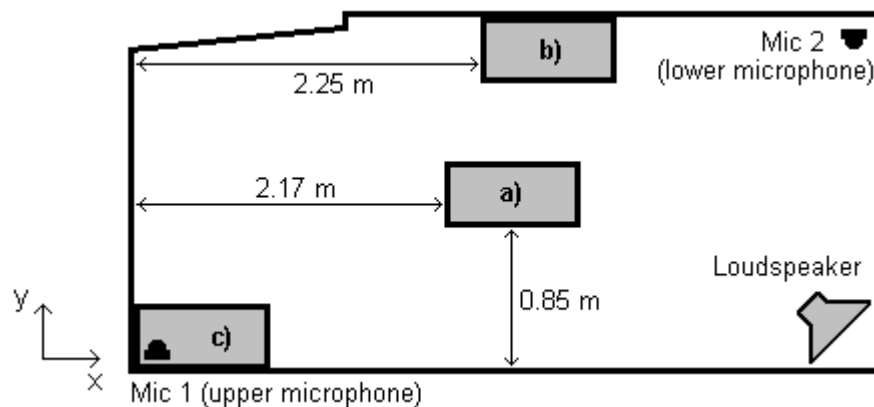


Figure 7.3 - Top view of the standard unit positions within the room. a) Central, b) centre wall, and c) corner position.

The values of absorption are greater than values for smooth dense concrete reported in the literature. For such material the value of absorption coefficient is given as approximately 2% [Kuttruff (1981), Crocker (1997)] and this was exactly the average value obtained for the room walls (experimentally and numerically). The values of Table 7.2, which were obtained based on the reverberation chamber method [ISO R354 (1985)], cannot be considered fully reliable since certain standard requirements were not observed, e.g., room volume and sample area. This problem was circumvented through a series of numerical simulations considering different values of absorption assigned to the standard unit surfaces, as described in Section 7.4.

Table 7.2 - Calculated absorption coefficient for the standard unit surface.

Frequency Band (Hz)	100	125	160	200
Absorption coefficient	0.33	0.18	0.32	0.19

The experimental set-up used to measure room frequency responses in the presence of the standard unit was the same as described in Section 6.2.3 (see Fig. 6.3 and Table 6.3). Again, sound source and receivers were positioned in room corners, in order to excite and measure all room modes. The microphone positions were unaltered to allow comparisons between results for the empty room and room with standard unit. These comparisons served as a basis for the quantification of the effect on room response of contents.

7.4 Numerical model

As described in Section 6.3, a FE model of the empty reference room was successfully developed. The model now was modified in order to include the standard unit. The first difficulty encountered related to the determination of the dimensions of the simulated unit. As the reference room model was adopted as a starting point, the FEM mesh element size was preserved, and therefore obstacles in the new model were required to have dimensions that were a multiple of this mesh size. As the element size in the reference room model was approximately 0.28 m, the standard unit was included with dimensions 1.40 m, 0.84 m, and 0.84 m in the x, y, and z directions, respectively, i.e. the unit was simulated with 5 elements in the x direction, and 3 elements in the y and z directions. These were the closest possible values to the real unit dimensions.

The 45 elements representing the standard unit were selected in the room finite element model, approximately in the same positions as in the real case. For each case, the selected elements were subtracted from the original model, giving rise to three new models representing a room with a hard box either in the floor centre, at the centre of a long wall, or at one corner. Since the values of absorption coefficient obtained for the standard unit (see Section 7.3 and Table 7.2) were not fully reliable, preliminary simulations were performed using different values of surface absorption coefficient (2%, 5%, and 20%) applied to the box surfaces. These initial simulations showed practically identical results, indicating that the absorption characteristics of the standard unit surface material may be neglected in the FE model. Thus, it was decided to adopt the simplest of these configurations, i.e., a constant surface absorption coefficient of 2% was assigned to the box surfaces, completing the model.

7.5 Results

Figs. 7.4, 7.5, and 7.6 show the results for the standard unit positioned at central floor, centre wall and corner positions, respectively. Independent of location, the introduction of the standard unit did not appear to generate any additional acoustic mode in the measured room frequency responses. Counting the number of peaks in the room frequency responses before and after the introduction of the standard unit it is possible to see that there are 16 peaks up to 100 Hz (see Figs. 7.4-a and 7.4-b, for instance). However, the eigenfrequency shifts are clearly observed throughout the frequency range and some of the modes were surprisingly damped (see Figs. 7.4-a, 7.5-a, and 7.6-a for central, centre wall and corner positions, respectively). The mode (1,0,1) at 50 Hz, for example, was shifted approximately 4% downwards for the first two standard unit positions (see Figs. 7.4-a and 7.5-a) and approximately 3% upwards for the corner position (see Fig. 7.6-a), whereas the mode (0,1,0) at 56 Hz suffered a reduction of approximately 10 dB after the introduction of the standard unit, for the centre wall and corner positions (see Figs. 7.5-a and 7.6-a, respectively).

The predicted frequency responses presented similar characteristics (see Figs. 7.4-b, 7.5-b, and 7.6-b), showing eigenfrequency shifts and selective modal damping after the introduction of the standard unit in the numerical model, but apparently no new eigenmodes (the same 16 peaks up to 100 Hz can also be counted in both curves of Fig. 7.4-b).

In order to clearly present the effects of introducing contents on room frequency responses, measured and predicted level differences were obtained as shown in Figs. 7.4-c, 7.5-c, and 7.6-c. In each case, i.e., for each standard unit position, the level differences express the change in the room response after the introduction of the standard unit, with the empty room response as a reference. The experimental level differences shown in Figs. 7.4-c, 7.5-c, and 7.6-c were obtained from the difference of the corresponding experimental curves shown in Figs. 7.4-a, 7.5-a and 7.6-a, and compared with predicted level differences obtained similarly from the difference between the respective predicted results displayed in Figs. 7.4-b, 7.5-b, and 7.6-b. Presenting the results in this manner it was possible to cancel (unwanted) common factors between the room responses with and without the standard unit, e.g., sound source and measuring system characteristics.

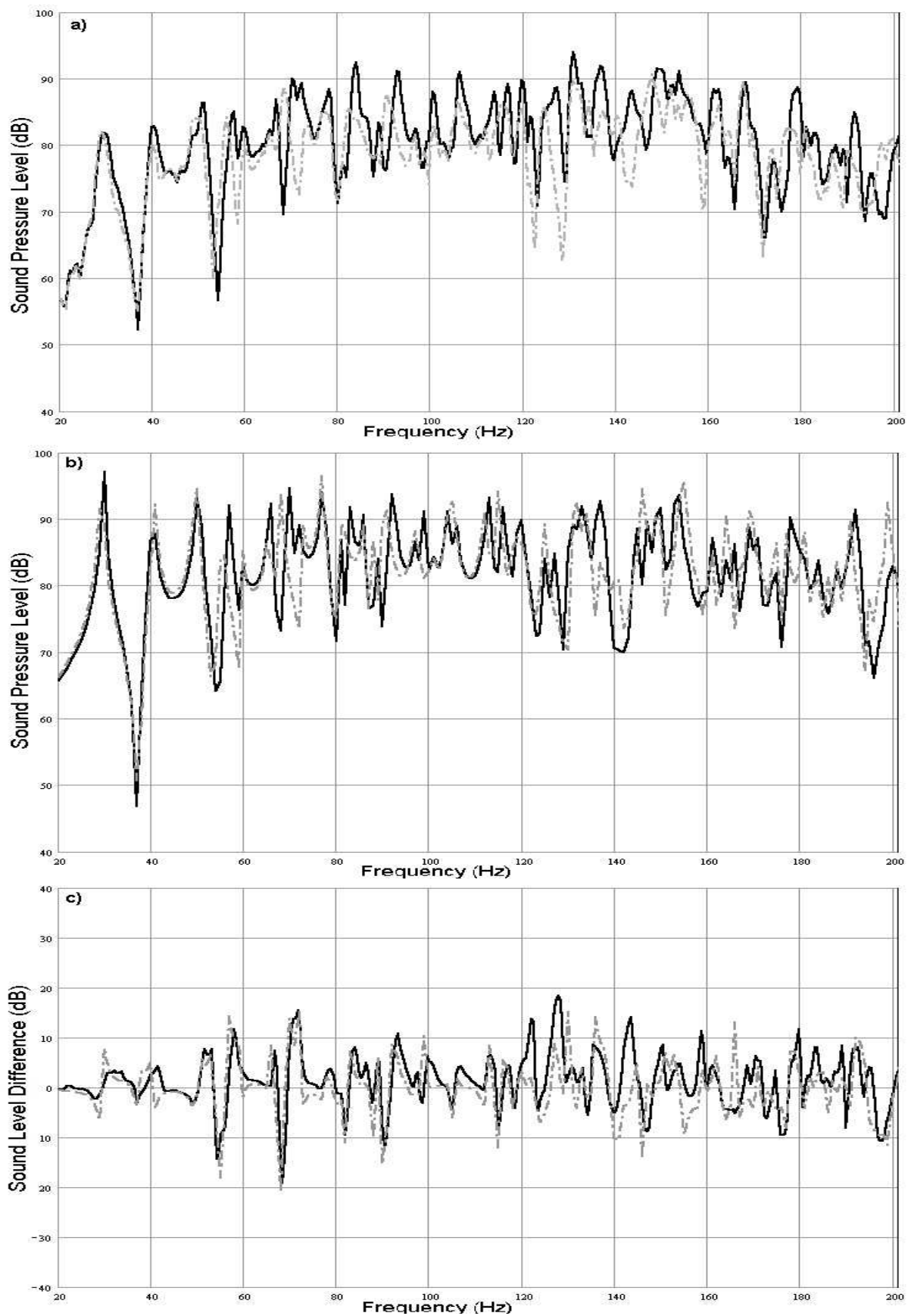


Figure 7.4 - Effect of obstacle on room frequency response. Unit at central position. a) Measurement for (—) empty room and (---) obstructed room. b) Prediction for (—) empty room and (---) obstructed room. c) Level difference (—) between measured values and (---) between predicted values.

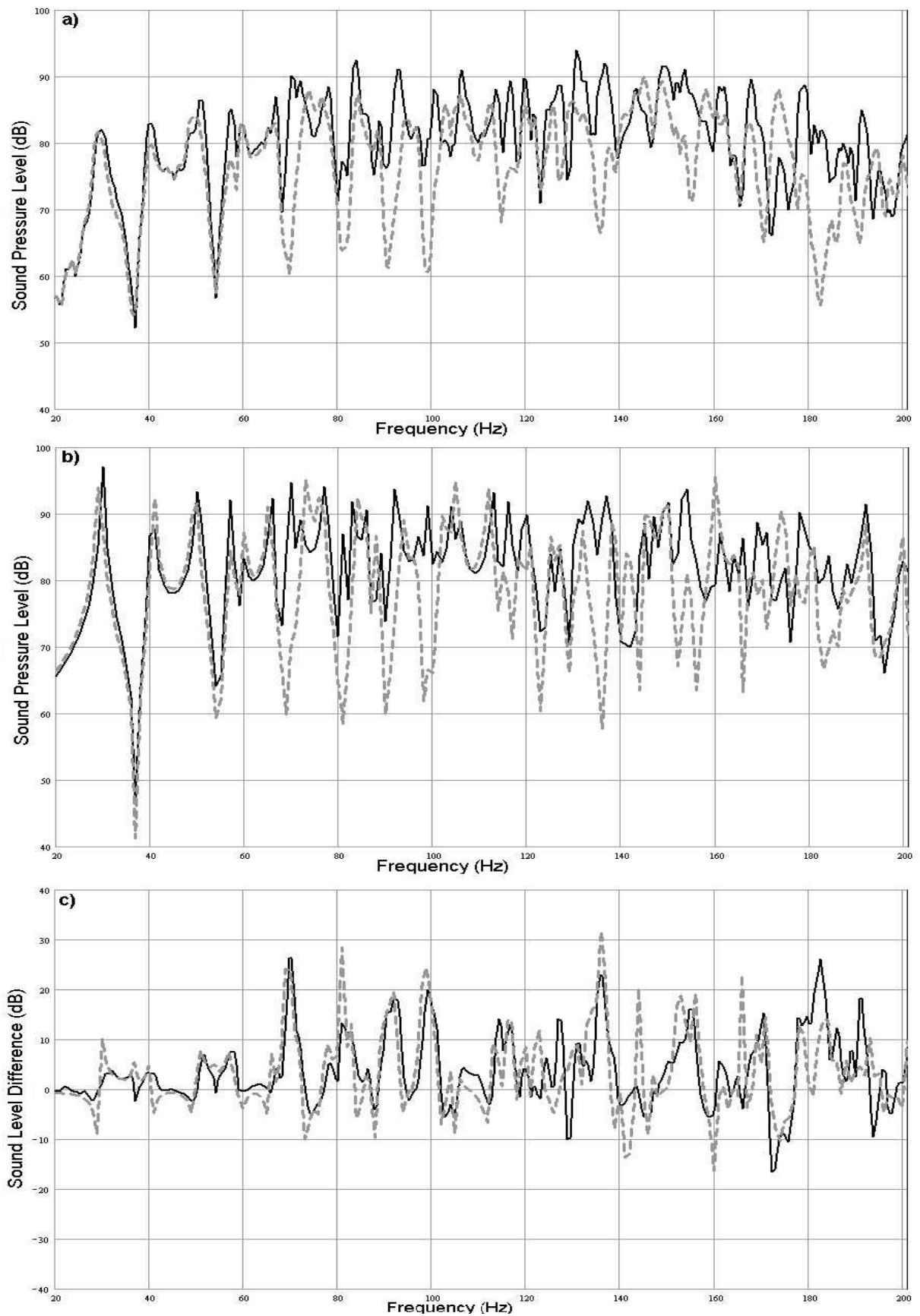


Figure 7.5 - Effect of obstacle on room frequency response. Unit at centre wall position. a) Measurement for (—) empty room and (---) obstructed room. b) Prediction for (—) empty room and (---) obstructed room. c) Level difference (—) between measured values and (---) between predicted values.

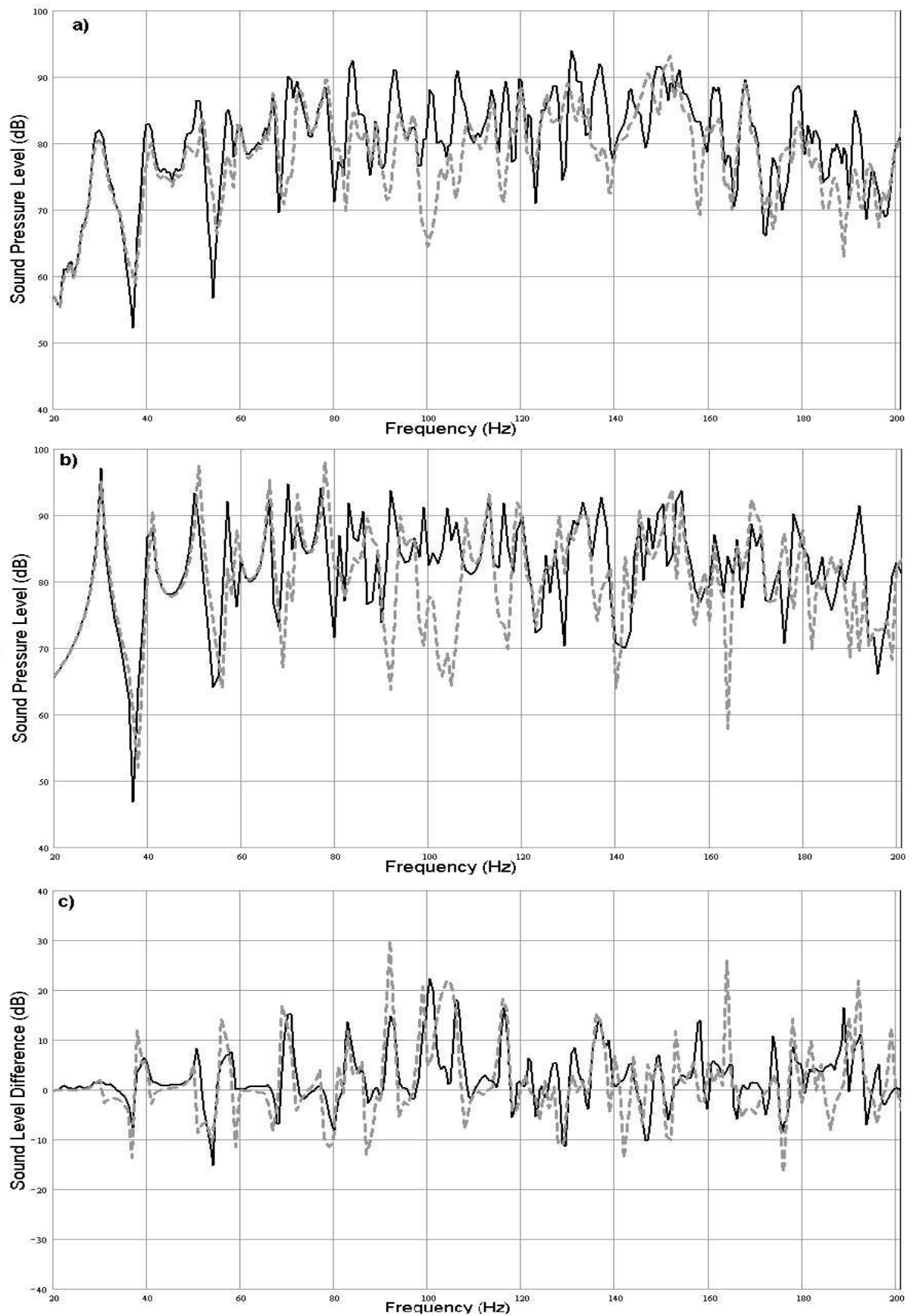


Figure 7.6 - Effect of obstacle on room frequency response. Unit at corner position. a) Measurement for (—) empty room and (---) obstructed room. b) Prediction for (—) empty room and (---) obstructed room. c) Level difference (—) between measured values and (---) between predicted values.

Notice that if the standard unit have not introduced any modification in the room response, then Figs. 7.4-c, 7.5-c, and 7.6-c would simply display a straight line at 0 dB. However, the eigenfrequency shifts, and the (small) additional sound absorption generate the level difference fluctuations observed in Figs. 7.4-c, 7.5-c, and 7.6-c. In fact, both measured and predicted level differences show that when the standard unit is centrally located (Fig. 7.4-c), the level difference fluctuates about 0 dB within a range ± 3 dB for the frequency range below 50 Hz. The mean and range of level differences were simply estimated from visual inspection since it was assumed unnecessary to conduct a statistical analysis of results. Between 50 Hz and 200 Hz the fluctuation about 0 dB is of the order of ± 8 dB (see Fig. 7.7). For this standard unit position the predicted curve presented a fairly good agreement with measurement, mainly up to 120 Hz, as shown in Figs. 7.4-c and 7.7.

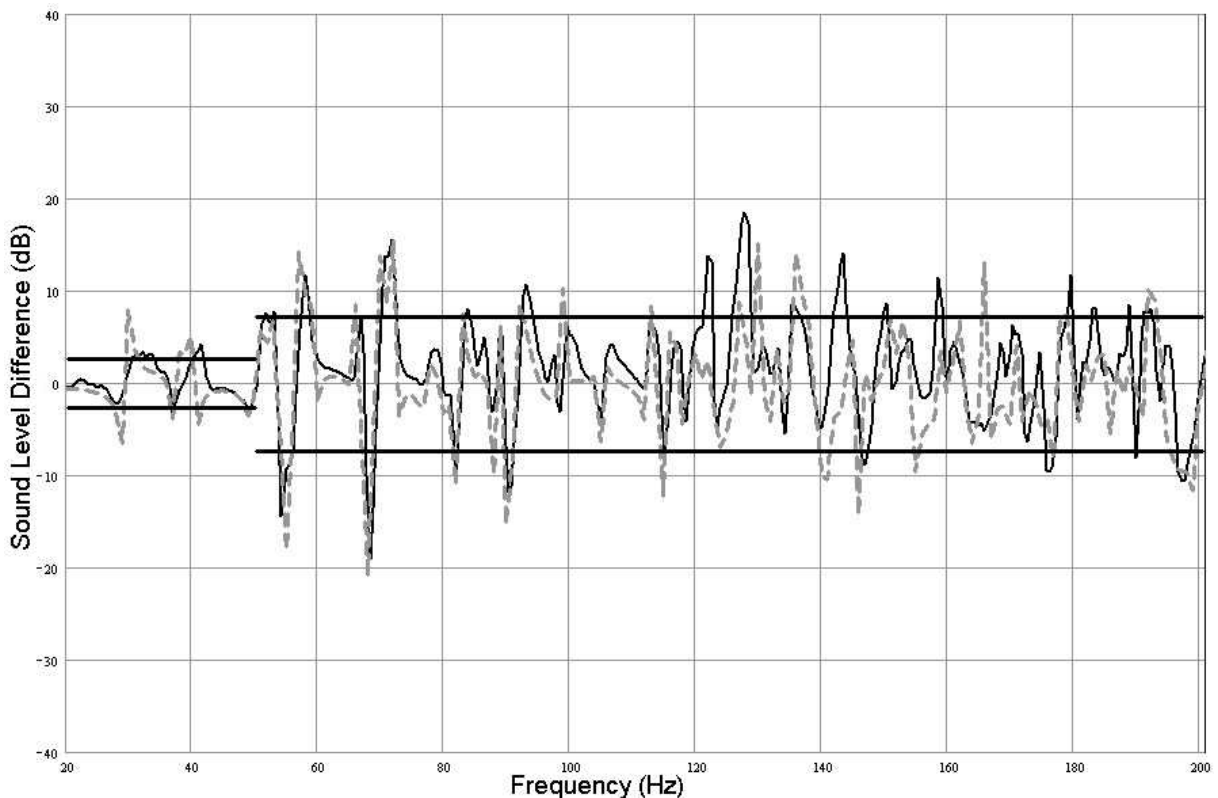


Figure 7.7 - Level difference (—) between measured values and (---) between predicted values. Unit at central position.

For the other two unit locations, the presence of the obstacle within the room has clearly more pronounced effects when compared with the previous case (see Figs. 7.5-c and 7.6-c). Figs. 7.8 and 7.9 show that the change in level difference below 50 Hz is of the order of ± 2 dB and ± 3 dB for the centre wall and corner positions, respectively.

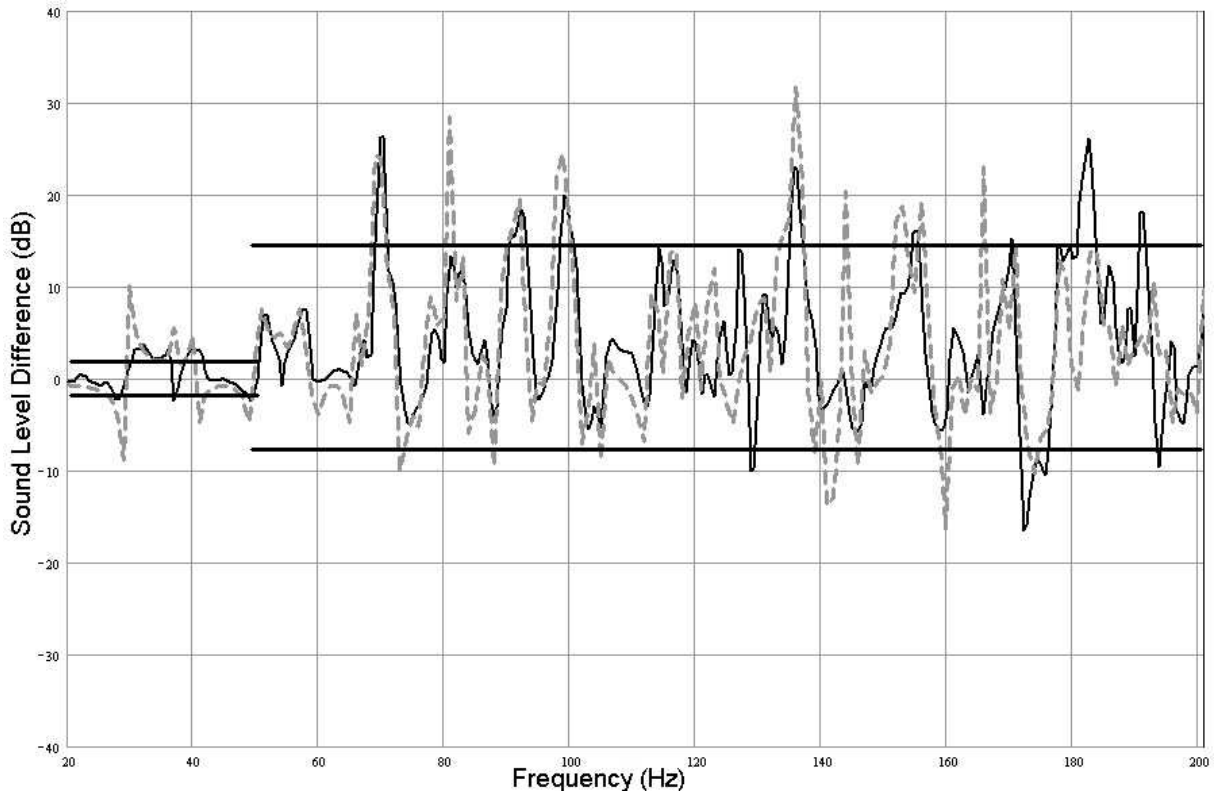


Figure 7.8 - Level difference (—) between measured values and (---) between predicted values. Unit at centre wall position.

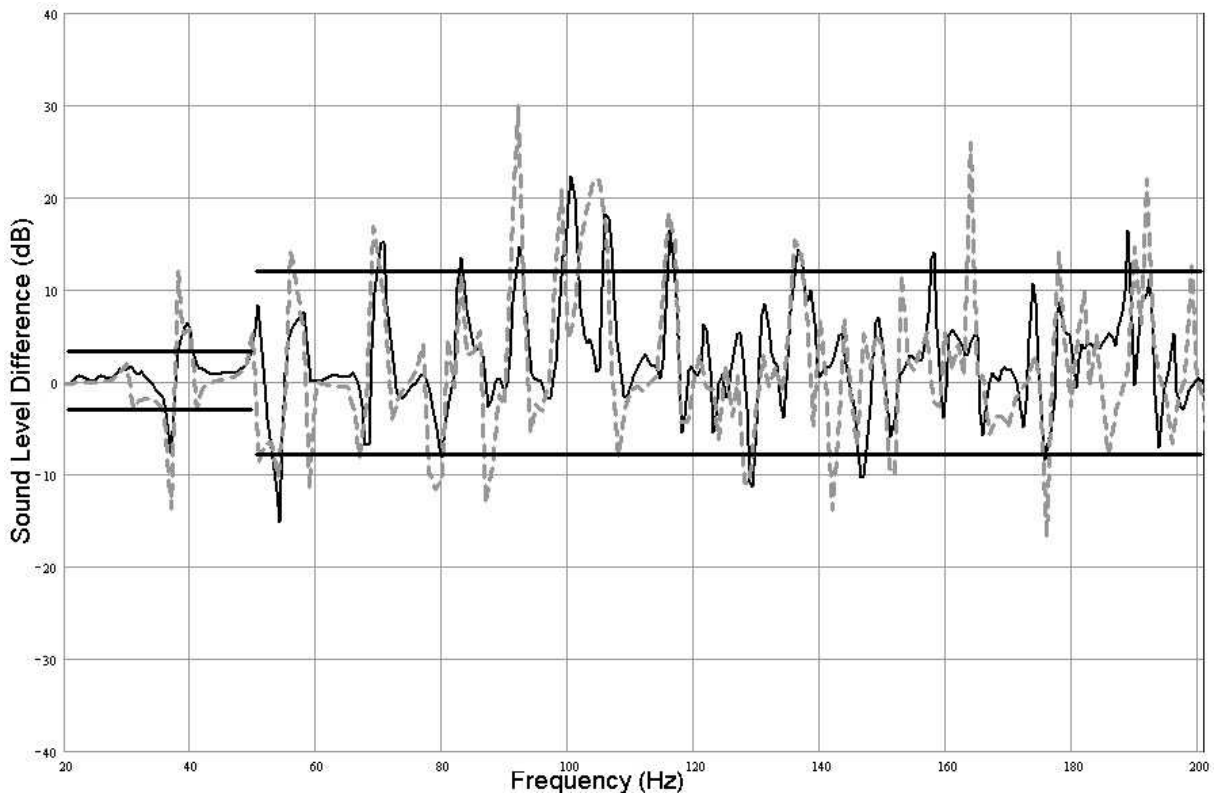


Figure 7.9 - Level difference (—) between measured values and (---) between predicted values. Unit at corner position.

Above 50 Hz, the variation is of the order of +15 dB to -8 dB for centre wall position, and of the order of +12 dB to -8 dB for the corner position, although the most dramatic changes were observed in this last case for individual modes. Predictions are once again in good agreement with experimental results, increasing the confidence in the developed numerical model.

In order to investigate whether the effect of introducing contents on room frequency responses are due mainly to room geometry perturbation or to additional absorption, it was decided to present the results of Figs. 7.4-a, 7.5-a, and 7.6-a in one-third octave bands, as shown in Fig. 7.10 for the same three obstacle positions. In the same way, the compared level differences shown in Figs. 7.7, 7.8, and 7.9 are presented in Fig. 7.11 also in one-third octave bands. Presented in this manner, the eigenfrequency shift effect is practically annulled, and since the compared levels shown in Fig. 7.10 are very similar to each other, regardless of the standard unit position, it is possible to conclude that the additional absorption due to the obstacle presence within the room plays no significant role in modifying the room frequency response, as initially indicated by the preliminary numerical model results of Section 7.4. The presentation of the results in one-third octave bands has additional relevance since standard measurements of sound insulation are to a one-third octave resolution [ISO 140/3 (1995)]. Although the present standards apply to frequencies above 100 Hz, it can be assumed that if future standards are developed for 50 – 100 Hz, then measurements also will be in one-third octave bands. For this frequency interval, the results of Fig. 7.11 show that the measured level difference is on average 1 dB, 2 dB, and 3 dB when the standard unit is located at the central floor, centre wall, and corner positions, respectively.

Finally, results in the form of modal patterns are shown in Figs. 7.13 to 7.15 at the same selected frequencies as in Chapters 4 and 6 (i.e., at 29.3 Hz, 57.4 Hz, 59.6 Hz and 76.5 Hz, respectively) for comparison. The results are presented for the standard unit placed at the centre wall position. When such results are compared with the ones obtained in Chapter 6 for the empty room, then it is possible to observe how the introduction of the standard unit changes the natural frequencies of the room and the associated modal patterns. Notice for example the dislocation of the pressure maxima from the wall centre (Fig. 6.20) to the room lower corner after the introduction of the standard unit in the centre wall position (Fig. 7.13). Furthermore,

as indicated in these figures, an eigenfrequency shift from 57.06 Hz to 57.36 Hz for this room mode can be observed.

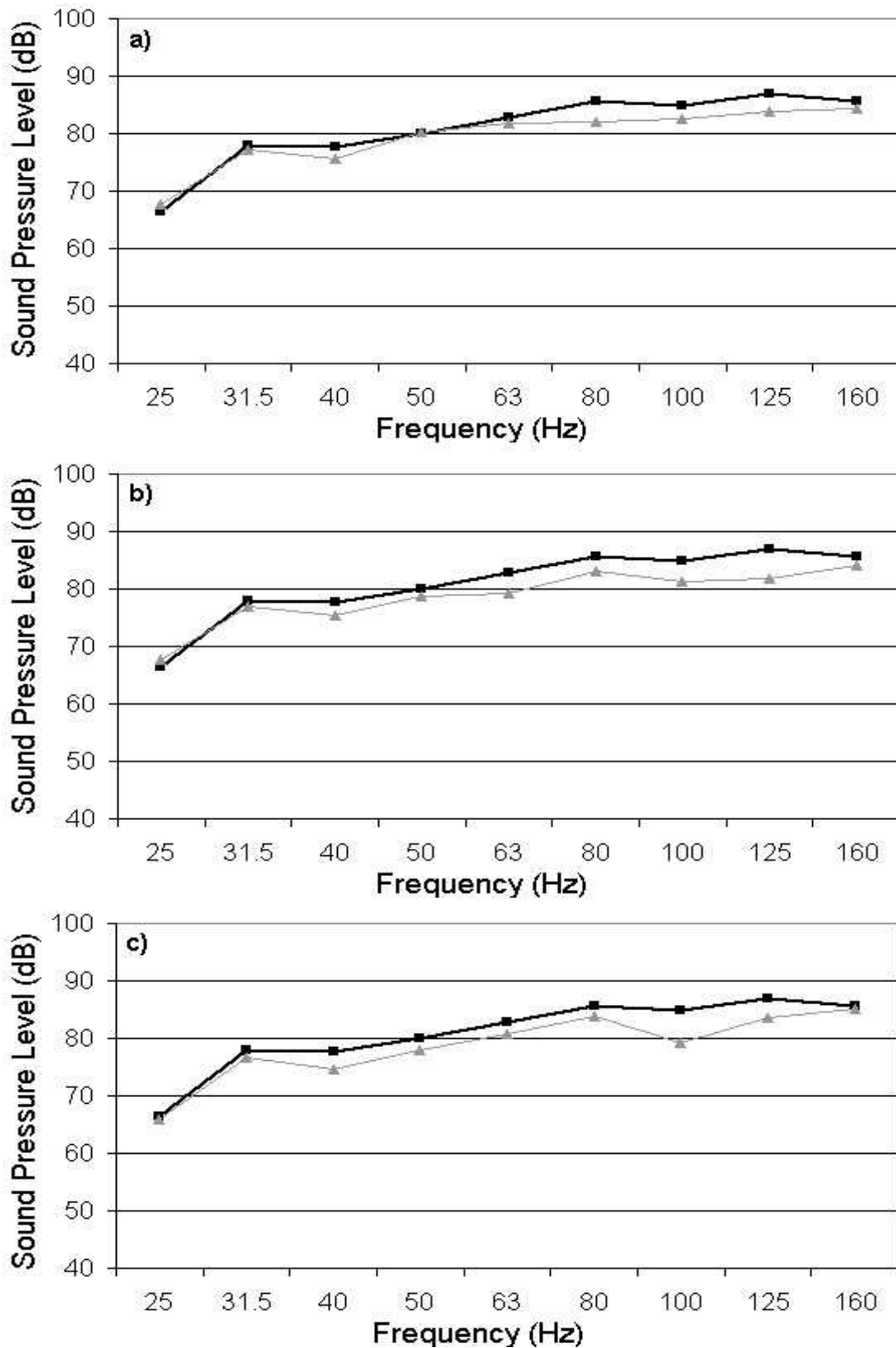


Figure 7.10 - Effect of obstacle on room frequency response. Measurements shown in one-third octave bands. a) Central floor position: (—) empty room and (---) obstructed room. b) Centre wall position: (—) empty room and (---) obstructed room. c) Corner position: (—) empty room and (---) obstructed room.

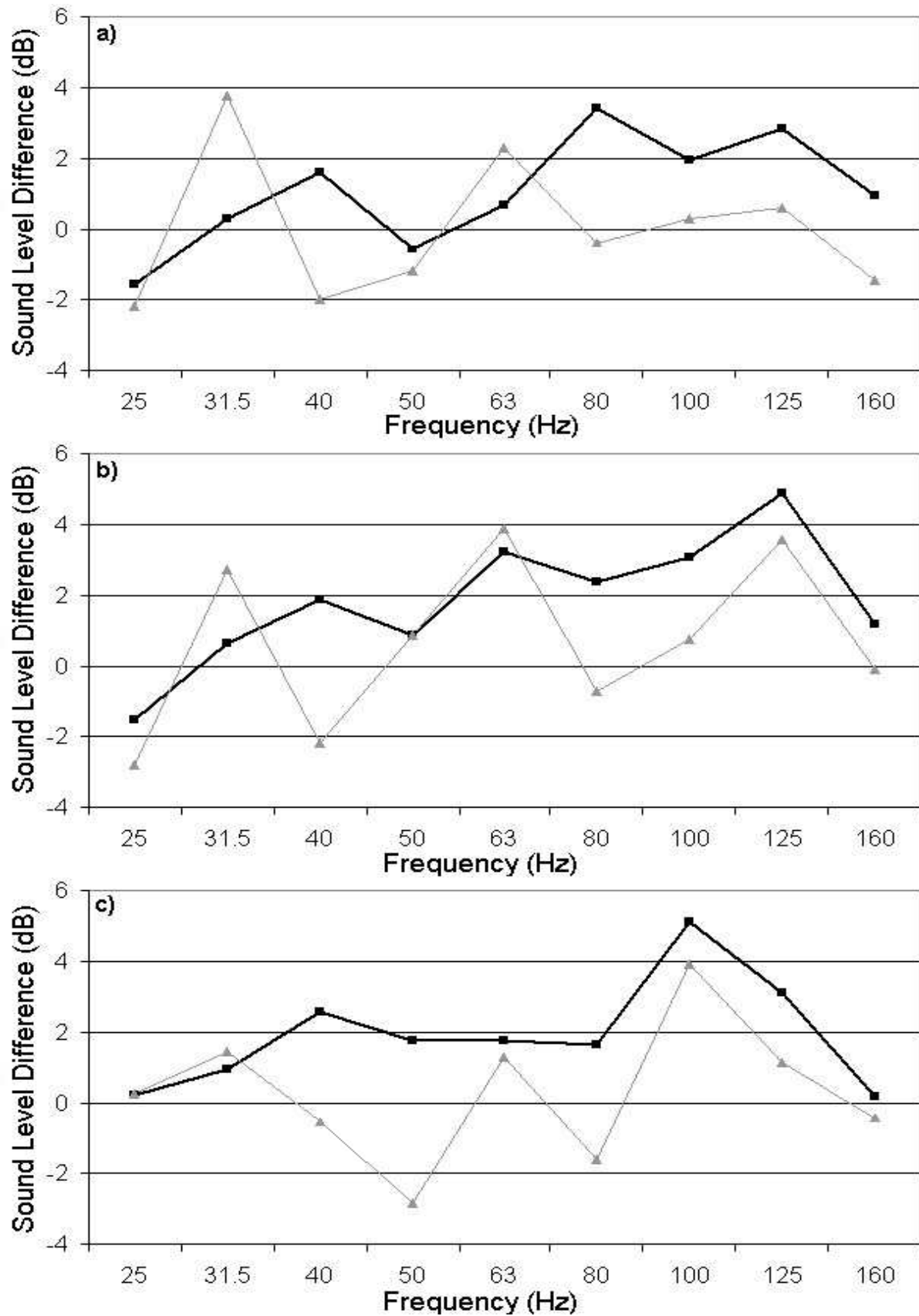


Figure 7.11 - Level difference (—■—) between measured values and (---▲---) between predicted values. Results shown in one-third octave bands. a) Central floor position, b) centre wall position, and c) corner position.

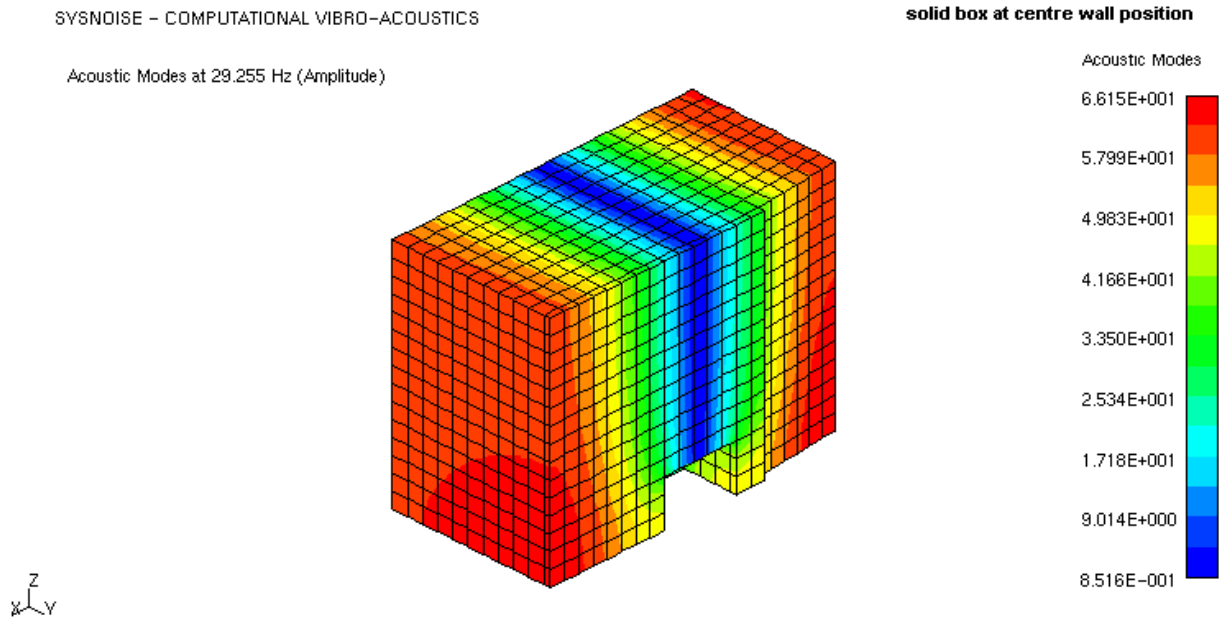


Figure 7.12 - Spatial distribution of pressure amplitude for the first mode (1,0,0).

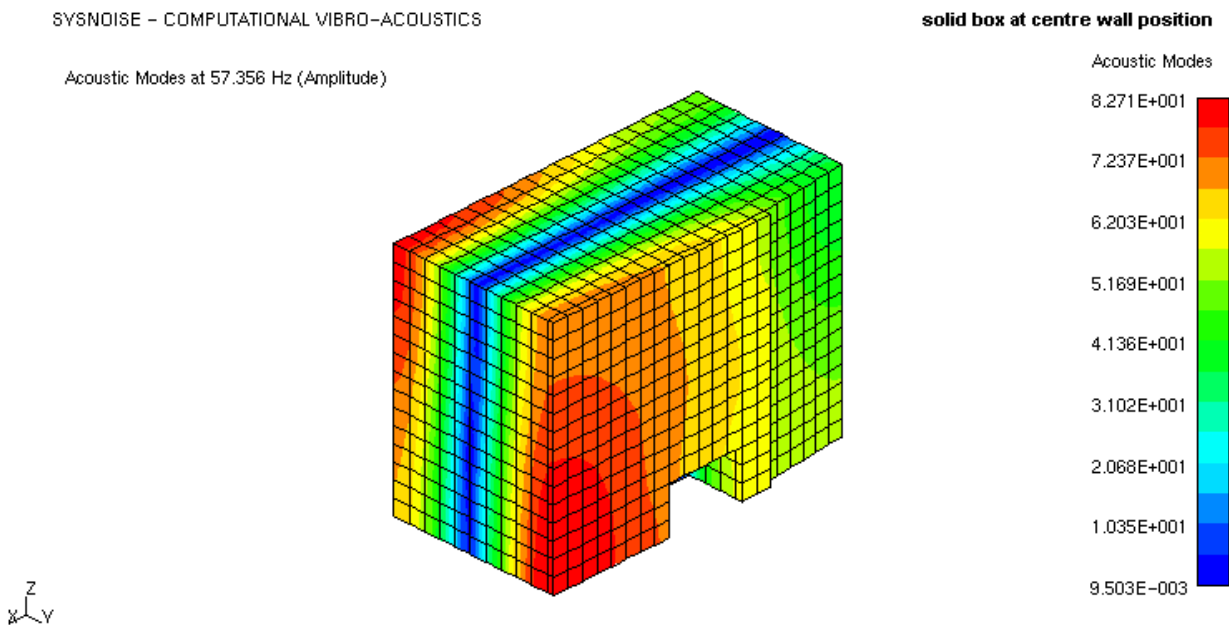


Figure 7.13 - Spatial distribution of pressure amplitude for the fourth mode (0,1,0).

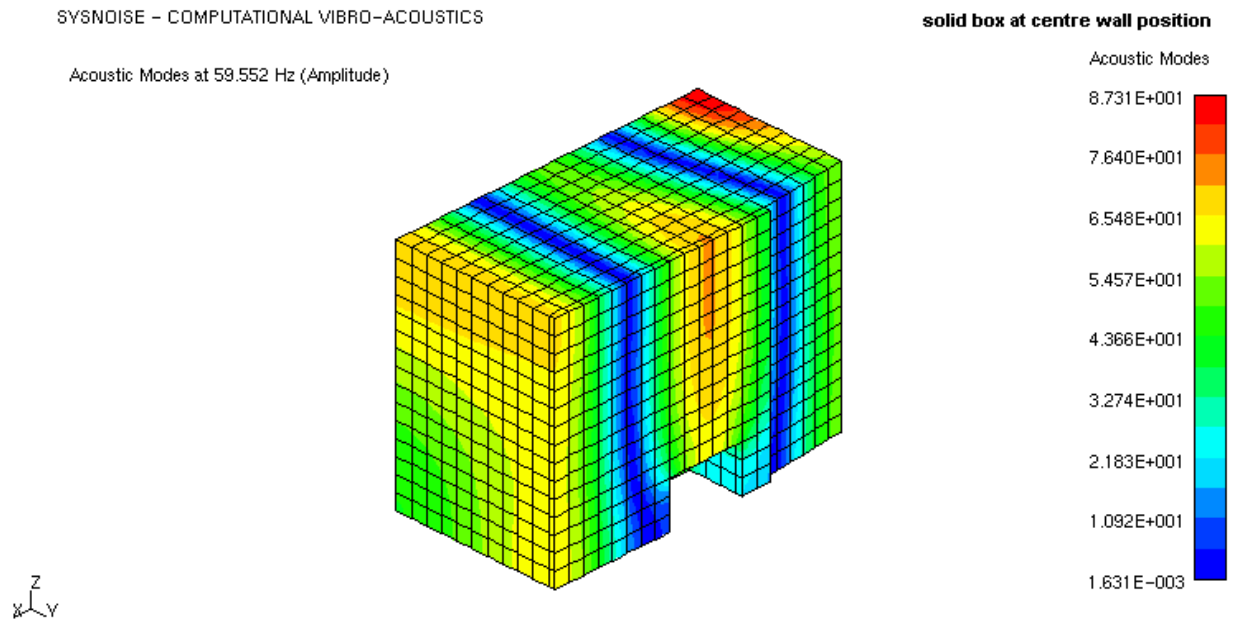


Figure 7.14 - Spatial distribution of pressure amplitude for the fifth mode (2,0,0).

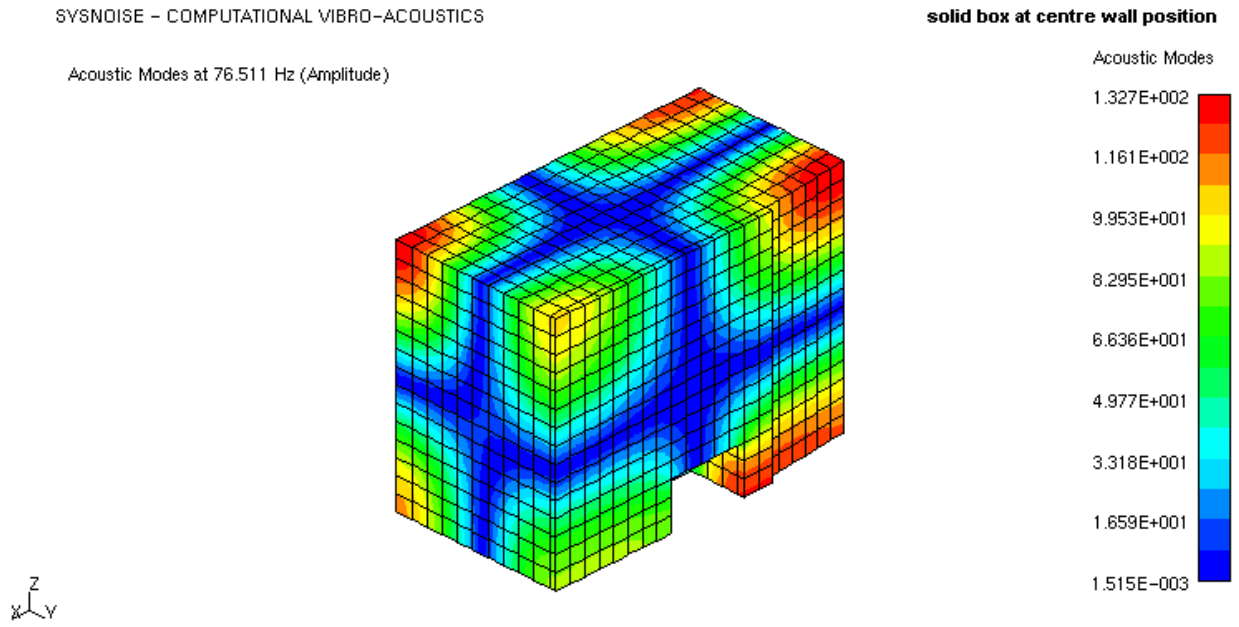


Figure 7.15 - Spatial distribution of pressure amplitude for the ninth mode (1,1,1).

7.6 Summary

In this chapter, a preliminary study of the influence of furniture on low frequency room responses was performed by introducing a “standard unit” at three different positions within the enclosure. The results obtained in Chapter 6 for the empty test room were used as a reference. In each case eigenfrequency shifts and selective modal damping were observed throughout the frequency range of interest, and the numerical results were able to take these effects into account, showing overall good agreement with measurements.

It has been shown that when a large solid item is introduced into the room, on its central floor position, there is little effect on the room frequency response for frequencies below 50 Hz. This is despite the fact that the first three normal room modes occur in this frequency range. However, this might be expected, since the major standard unit dimension is less than one quarter of the sound wavelength at 50 Hz. This situation was observed regardless of the standard unit position and, therefore, it is possible to conclude that the room frequency response is insensitive to location below 50 Hz, considering the present unit dimensions.

Above 50 Hz, the effect of including a solid item within the enclosure is more pronounced. In addition, the influence of location becomes apparent. Obstacles placed along a wall or in room corners will produce a higher change in room responses, if compared with a central location. Furthermore, analysis of the results presented not only in narrow band, but also in one-third octave bands allowed the conclusion that for a solid item within the room, the generated eigenfrequency shifts are the principal reason for the observed changes in the room responses. The obstacle surface absorption characteristics causes little change in the room frequency response (at most 5 dB as observed for the third octave bands 100 Hz and 125 Hz, for the standard unit placed in the centre wall and corner positions, respectively) and need not to be taken into account in the numerical model. However, this may not be the case when there is a layer of highly sound absorptive material covering the standard unit surfaces. This modification may approximate more real furniture and this is explored in Chapter 8.

7.7 References

- AKIL, H. A., OLDHAM, D. J. **Determination of the scattering parameters of fittings in industrial buildings for use in computer based factory noise prediction models: part 1-theoretical background.** Journal of Building Acoustics, 2 (2), 461-481,1995.
- ANTONOPOULOS-DOMIS, M. **Frequency dependence of acoustic resonances on blockage position in a fast reactor subassembly wrapper.** Journal of Sound and Vibration, 72 (4), 443-450, 1980.
- DE SALIS, M. H. F., OLDHAM, D. J. **A rapid technique to determine the internal area function of finite-length ducts using maximum length sequence analysis.** Journal of the Acoustical Society of America, 108 (1), 1-9, 2000.
- GERGES, S. **Ruído: fundamentos e controle.** Federal University of Santa Catarina U.P., Florianópolis, 2000.
- ISO R354. **Measurement of sound absorption in a reverberation room.** 1985.
- ISO 140/3. **Measurement of sound insulation in buildings and of buildings elements - Part 3: Laboratory measurements of airborne sound insulation of buildings elements.** 1995.
- JOVICIC, S. **Prediction of sound level in industrial buildings.** Muller-BBM, 1971.
- KURZE, U. J. **Scattering of sound in industrial spaces.** Journal of Sound and Vibration, 98 (3), 349-364, 1985.
- LINDQVIST, E. A. **Sound attenuation in large factory spaces.** Acustica, 50, 313-328, 1982.
- MALUSKI, S. P. S., GIBBS, B. M. **Variation of sound level difference in dwellings due to room modal characteristics.** Proceeding of Acoustics Performances of Medium-Rise Timber Buildings, 3-4, Dublin, 1998.
- MALUSKI, S. P. S. **Low frequency sound insulation in dwellings.** Ph.D. Thesis, Sheffield Hallam University, Sheffield, 1999.
- MELO, G. S. V., GIBBS, B. M., GERGES, S. N. Y. **A finite element model of sound absorption at low frequencies.** Euronoise-2001, Patras, 2001.
- ONDET, A. M., BARBRY, J. L. **Modelling of sound propagation in fitted**

workshops using ray tracing. Journal of the Acoustical Society of America, 82, 789-802, 1989.

WU, Q., FRICKE, F. **Determination of blocking locations and cross-sectional area in a duct by eigenfrequency shifts.** Journal of the Acoustical Society of America, 87, 67-75, 1990.

WU, Q., FRICKE, F. **Determination of the size of an object and its location in a rectangular cavity by eigenfrequency shifts: first order approximation.** Journal of Sound and Vibration, 144, 131-147, 1991.

CHAPTER 8

ROOM CONTENTS AS ABSORBERS

8.1 Introduction

In the previous chapter, the development of a standard unit allowed a preliminary investigation of the influence of room contents, regarded as hard obstacles, on the acoustic properties of enclosures, at low frequencies. However, hard-surfaced objects do not exclusively compose real furniture inside enclosures. Hence, extending the idea of the previous chapter, it is the intention here to present an investigation of the influence on room frequency responses of the standard unit, when covered by a layer of known sound absorbing material.

8.2 Choice of sound absorption material

The material selected was an open cell porous absorber, consisting of polyurethane flexible foam with a density of approximately 30 kg/m^3 (see Fig. 8.1).



Figure 8.1 - The selected sound absorbing material of thickness 150 mm.

There was no other information available for the used foam, but in a recent work by Balvedi (1998) experimental results for a very similar kind of material yielded the

following values: flow resistance of the order of 45000 rayl/m, tortuosity (structural factor) of the order of 4.0, and porosity approximately 95%. In addition to being an effective sound absorbing material, the selected type of foam was easier to handle than materials such as fibreglass foams.

As discussed in Chapter 5, the sound absorption characteristics of a material is represented by the sound absorption coefficient, α , which may be defined as the ratio between the acoustic energy that is absorbed by the material, and the acoustic energy incident on it. The measurement of the absorption coefficient allows the calculation of a more fundamental material property, the acoustic impedance, Z . Thus, the following section presents the determination of α , and hence Z , for the porous absorber employed.

8.3 Impedance tube measurements

The experimental part of this investigation was performed by means of the impedance tube method (see Section 5.3.3). A standing wave apparatus (Brüel and Kjaer type 4002) was used, driven by a heterodyne analyser (Brüel and Kjaer type 2010). Such a set-up provides scales for direct reading of normal incidence absorption coefficient α_n and distance d between the sample face and the position of the first sound pressure level minimum. A cylindrical sample of diameter 100 mm and thickness 150 mm was cut from a sheet of the foam. The measurement results are presented in Table 8.1.

From the absorption coefficient and distance between sample and measuring point, it is possible to obtain the reflection coefficient, r , and phase angle, Δ , between incident and reflected waves, which are given by [Beranek (1940-a & b), Brüel and Kjaer (1955 & 1979)]

$$\begin{cases} r = \sqrt{1 - \alpha_n} \\ \Delta = \left(\frac{4d}{\lambda} - 1 \right) \pi, \end{cases} \quad (8.1)$$

where λ is the corresponding wavelength at the given frequency. These parameters may be then used in determining the real and imaginary parts of the complex normal acoustic impedance, Z_n , yielding [Brüel and Kjaer (1955 & 1979), Gibbs (1970)]

$$\begin{cases} \operatorname{Re}\{Z_n\} = \frac{1-r^2}{1+r^2-2r\cos\Delta} \cdot \rho_0 c_0 \\ \operatorname{Im}\{Z_n\} = \frac{2r\sin\Delta}{1+r^2-2r\cos\Delta} \cdot \rho_0 c_0 \end{cases} \quad (8.2)$$

The input parameter for the finite element model is the normal acoustic admittance, A_n , which is simply the inverse of Z_n :

$$A_n = \frac{1}{Z_n}. \quad (8.3)$$

Table 8.1 - Impedance tube results.

Frequency (Hz)	Normal absorption coefficient, α_n (%)	Distance between sample and measuring position, d (cm)
90	36	79.6
100	40	71.0
150	58	44.0
200	71	31.4
250	76	24.8
300	85	19.0
350	90	15.7
400	96	21.8
450	95	18.8
500	94	16.7

Table 8.2 lists the values of complex normal impedance and admittance calculated from the values in Table 8.1.

Using the described apparatus, it was not possible to measure absorption coefficients at frequencies below 90 Hz, due to the impedance tube dimensions. In order to obtain α_n corresponding to lower frequencies a linear extrapolation was applied to the experimental results of Table 8.1, assuming a zero value of absorption coefficient at 0 Hz. Such an extrapolation finds support in the literature [Gerges (2000)], and the results are shown in Fig. 8.2. Furthermore, it is interesting to notice that if the real and imaginary parts of admittance A_n , given by equation (8.3), are independently extrapolated to lower frequencies, and an inverse calculation is performed in order to obtain α_n , these calculated extrapolated values agree well with the experimental extrapolated values. Such extrapolation of admittance values and

inverse calculation were performed for frequencies between 21 Hz and 70 Hz, and the results are shown in Fig. 8.3.

Table 8.2 - Complex impedance and admittance results calculated from the values of Table 8.1.

Frequency (Hz)	Re{Z _n } (rayl)	Im{Z _n } (rayl)	Re{A _n } (rayl ⁻¹)	Im{A _n } (rayl ⁻¹)
90	600.38	-1318.17	2.86 * 10 ⁻⁴	6.28 * 10 ⁻⁴
100	611.83	-1218.54	3.29 * 10 ⁻⁴	6.55 * 10 ⁻⁴
150	536.96	-794.13	5.84 * 10 ⁻⁴	8.64 * 10 ⁻⁴
200	515.67	-582.70	8.52 * 10 ⁻⁴	9.62 * 10 ⁻⁴
250	518.82	-511.10	9.78 * 10 ⁻⁴	9.64 * 10 ⁻⁴
300	460.27	-364.41	1.34 * 10 ⁻³	1.06 * 10 ⁻³
350	450.62	-286.10	1.58 * 10 ⁻³	1.00 * 10 ⁻³
400	622.00	13.75	1.61 * 10 ⁻³	-3.55 * 10 ⁻⁵
450	653.66	-12.95	1.53 * 10 ⁻³	3.03 * 10 ⁻⁵
500	682.32	-29.27	1.46 * 10 ⁻³	6.27 * 10 ⁻⁵

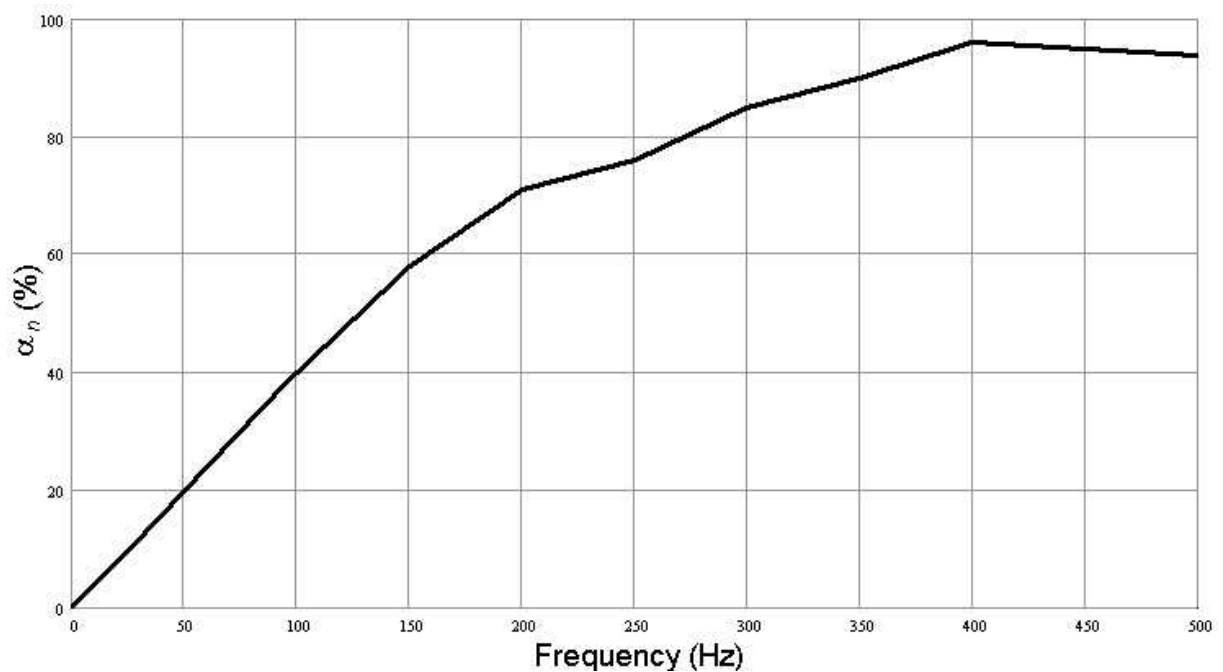


Figure 8.2 - Absorption coefficient for the selected foam extrapolated to low frequencies.

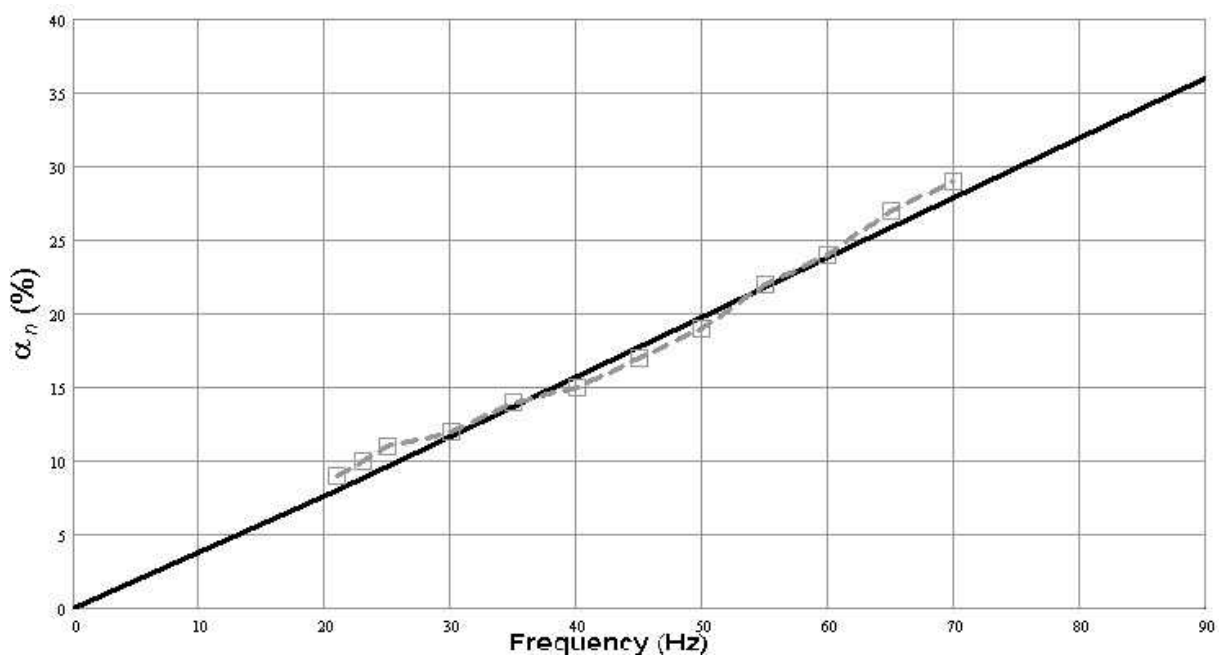


Figure 8.3 - Absorption coefficient for the selected foam extrapolated to low frequencies. (—) Values extrapolated from experimental results, and (---□---) values obtained from admittance results.

The dependence of the absorption coefficient on the sound incidence angle, θ , was analysed for a few discrete frequencies. It was assumed that the material was locally reacting (see Chapter 5). The expression relating absorption and incidence angle is given by [Paris (1928)]

$$\alpha(\theta) = 1 - \left| \frac{\left(\frac{Z}{\rho c_0}\right) \cos \theta - 1}{\left(\frac{Z}{\rho c_0}\right) \cos \theta + 1} \right|^2 \tag{8.4}$$

Fig. 8.4 shows the results for $\alpha(\theta)$ at 90 Hz, 100 Hz, and 150 Hz.

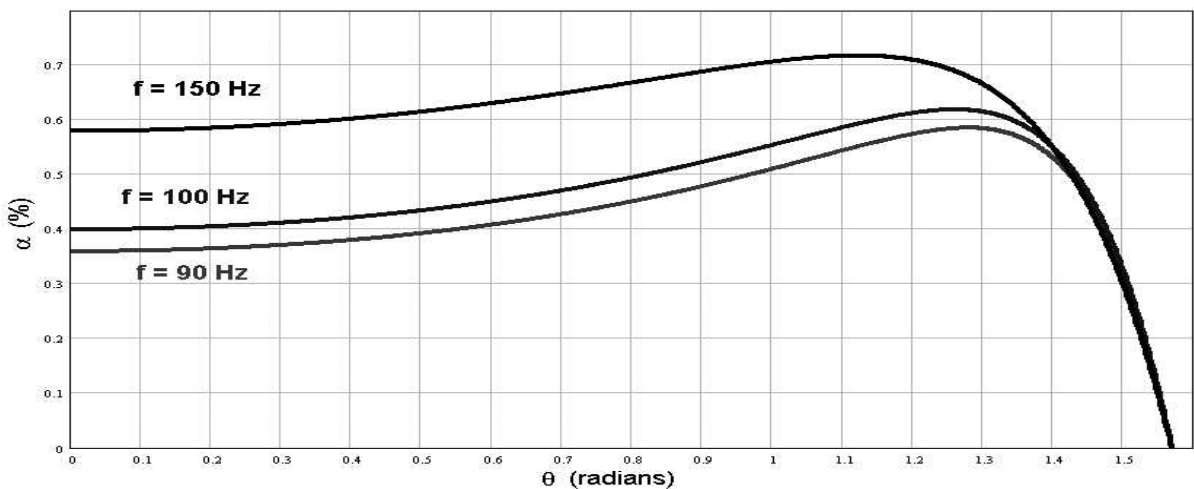


Figure 8.4 - Absorption coefficient, at a few discrete frequencies, as a function of the sound incidence angle.

It can be seen that the lower the frequency, the stronger the dependency of the absorption coefficient on the sound incidence angle. However, this angular dependency could not be incorporated into the numerical model. Most acoustic FE programs, including Sysnoise, convert imposed velocity or impedance boundary conditions to pressure gradient boundary conditions using the linearized frequency-domain equivalent of Euler's equation projected onto the normal direction with respect to the boundary, i.e.,

$$\begin{aligned}\frac{\partial p}{\partial n} &= -i\omega\rho v_n; \text{ for normal velocity boundary conditions} \\ \frac{\partial p}{\partial n} &= -i\omega\rho \frac{p}{Z_n}; \text{ for normal impedance boundary conditions} \\ \frac{\partial p}{\partial n} &= -i\omega\rho p A_n; \text{ for normal admittance boundary conditions.}\end{aligned}\tag{8.5}$$

In principle, it is possible to project the vectorial form of the linearized frequency-domain Euler's equation into any direction to obtain the relation between the impedance or admittance for that incidence angle, and the pressure gradient in the same direction. However, this introduces the pressure gradient in an "arbitrary" direction as an unknown of the acoustic problem. By using the normal direction to the boundary only, the number of unknowns in the problem is greatly simplified [Segaert (2001)]. Nevertheless, it is recognized that this may be one of the reasons for observed discrepancies between predicted and measured frequency responses.

8.4 Absorbing floor area

A preliminary investigation was conducted on the effect of the absorbing material on the room response, by laying large areas of the absorber on the reference room floor. The experimental set-up was the same as described in Section 6.2.3. Room frequency responses were obtained, when the floor had 5.1 m², 8.6 m², and 17.4 m² of the 150 mm foam, corresponding to 29%, 49%, and 99% of its floor area, respectively. The results are shown in Fig. 8.5. In order to quantify the effect of the absorber, the level difference between the room responses for the empty and treated room were obtained, as displayed in Fig. 8.6 for 29% and 49% covered floor, and in Fig. 8.7 for the 99% covered floor. In Fig. 8.6, it is possible to see that up to 70 Hz the change in the empty room frequency response is of the order of 2 dB; above 70

Hz the level difference is on average 6 dB. Similar behaviour is observed for the 49% floor covering despite the extra 20% of absorption.

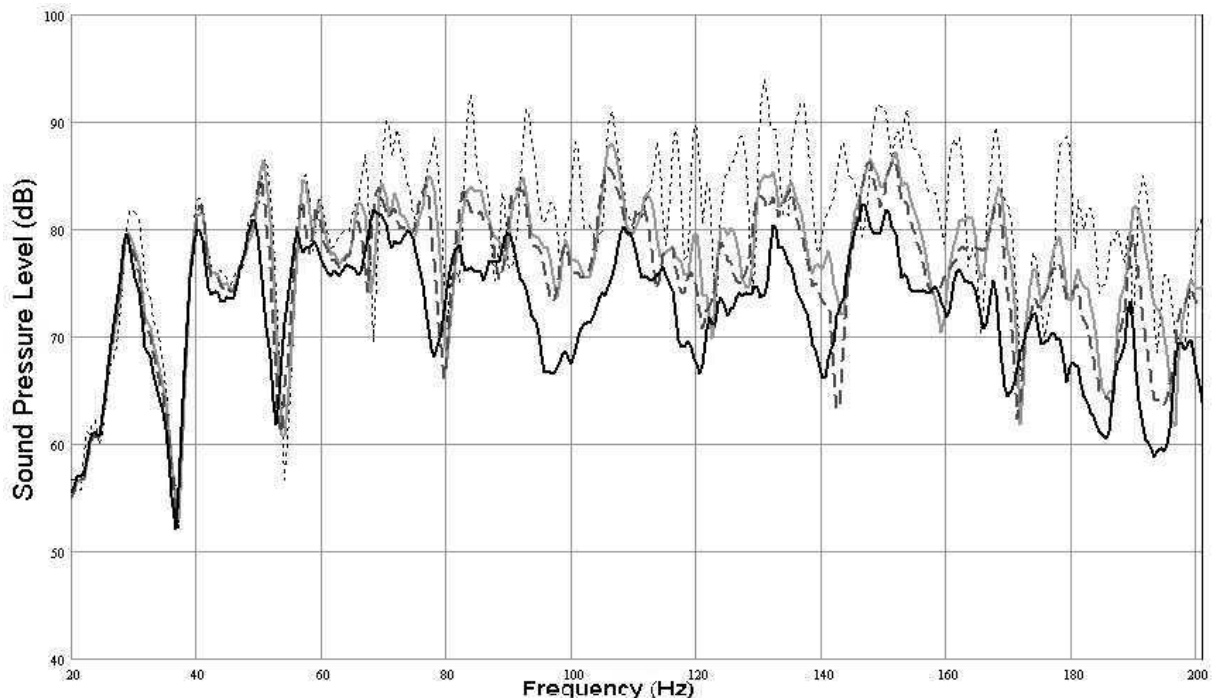


Figure 8.5 - Measurements of room frequency response for (.....) empty room, (—) 29%, (---) 49%, and (—) 99% of the floor area covered with absorption.

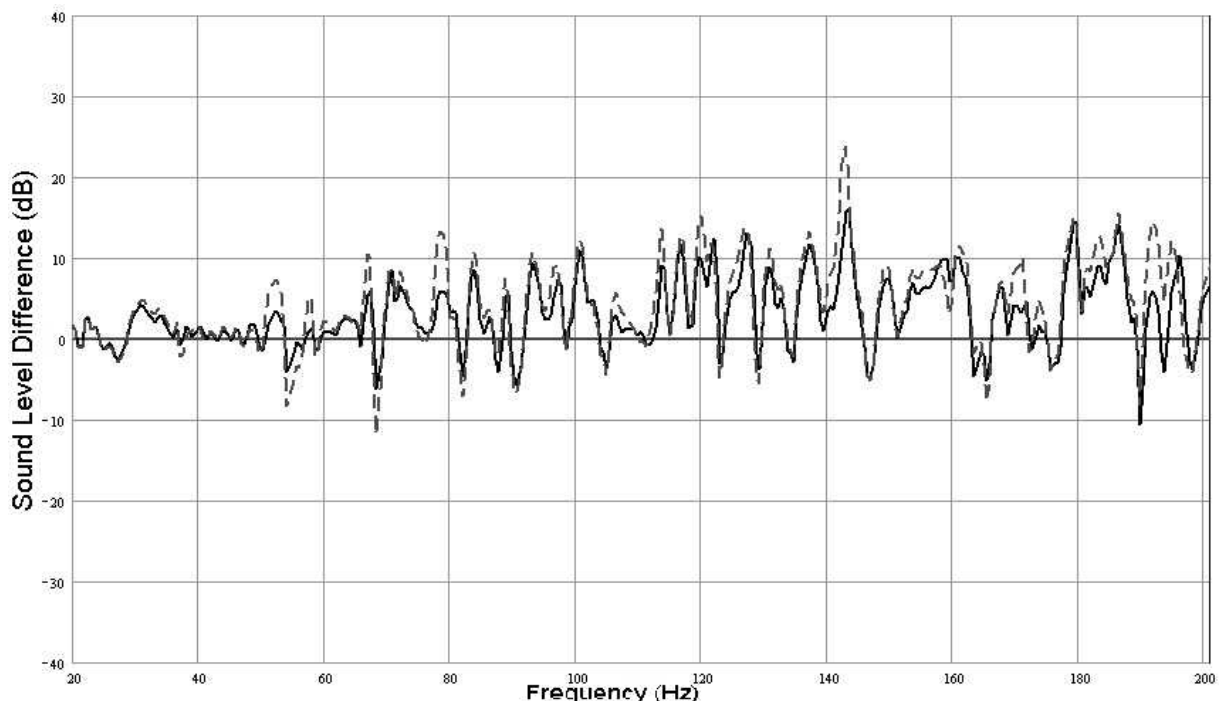


Figure 8.6 - Effect of covering the room floor with absorption material. (—) Level difference between empty and 29% covered floor room responses. (---) Level difference between empty and 49% covered floor room responses.

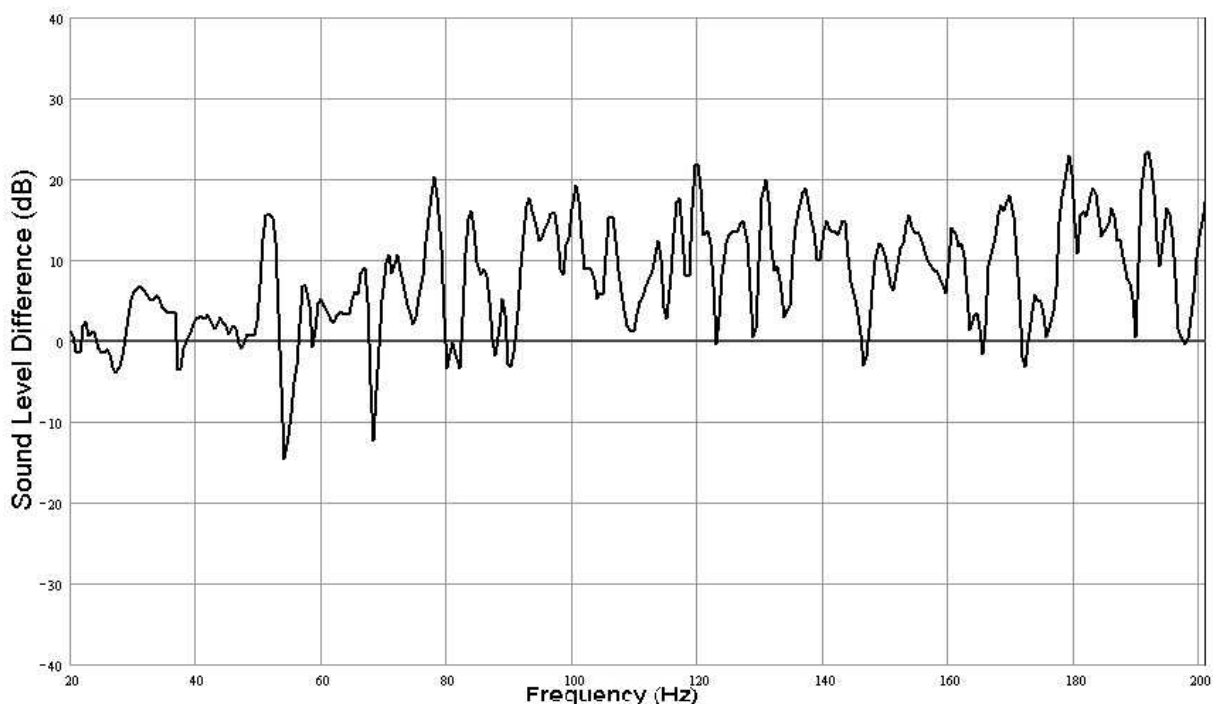


Figure 8.7 - Effect of covering the room floor with absorption material showing the level difference between empty and 99% covered floor room responses.

When 99% of the room floor was covered the room response was clearly modified for all the displayed frequency range, although the effect is greater for frequencies above 50 Hz, as shown in Fig. 8.7. Fig. 8.8 presents the results of the previous figure in one-twelfth octave bands.

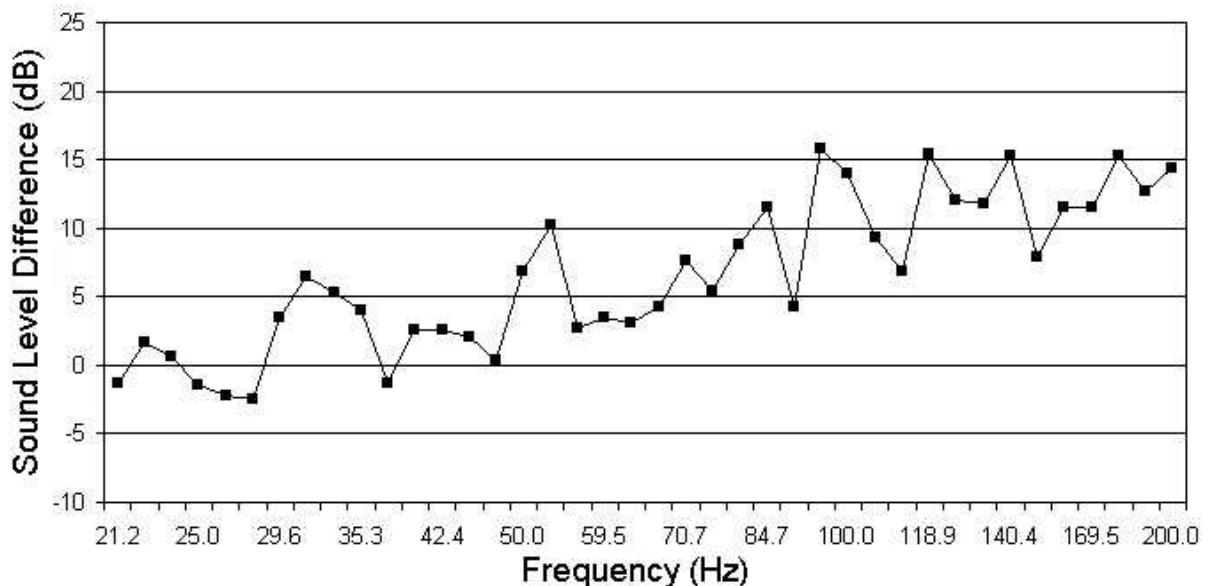


Figure 8.8 - Level difference between empty and 99% covered floor room responses. One-twelfth octave band results.

The change in sound level can be characterised in three frequency regions, each with an average difference and a variation about the average. Up to 45 Hz the

average level difference is of the order of 1 dB with a variation +5 dB to -3 dB. Between 45 Hz and 90 Hz the average level difference is 6 dB with variation +5 dB to -3 dB. Above this frequency the average is 12 dB \pm 4 dB.

The FE model, described in Chapter 6, was modified to simulate the case of 99% floor covering. A predicted room frequency response was obtained after assigning a frequency independent absorption coefficient of 50% to the room floor, and 2% to all the other room surfaces. This result is shown with the corresponding experimental measurements in Fig. 8.9. The predicted curve follows the same trends of the measured curve, despite the fact that only a rough approximation has been made to the absorption of the floor covering.

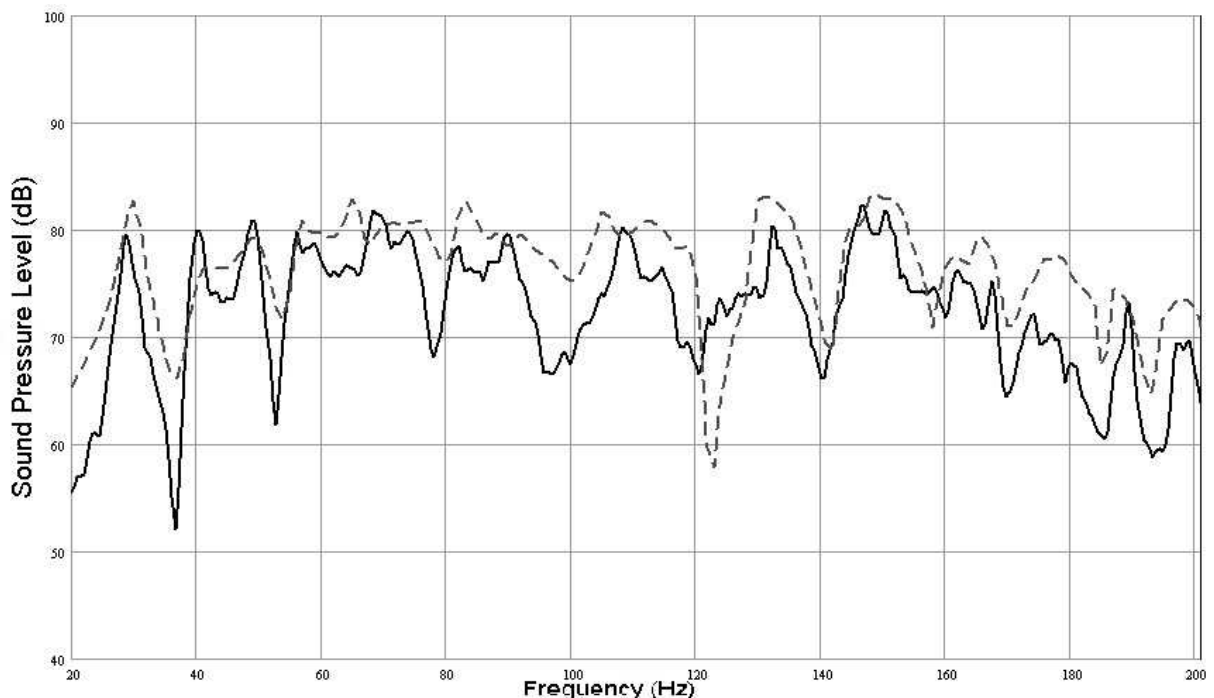


Figure 8.9 - Measured and predicted frequency response of room with floor covered with 150 mm foam of absorption coefficient 50%. (—) Measurement and (---) prediction from first room model.

The preliminary study described provided a level of agreement between measurement and prediction which promised greater agreement if the form of the input absorption data could be refined. This was the basis of the further study of the effect of absorption, both as a floor covering and as surface treatment of room obstructions.

8.5 Covered standard unit

8.5.1 Measurement

In this phase of the investigation of the influence of room contents on acoustic properties of enclosures, the room frequency response was measured with the standard unit covered with a layer of 150 mm of the selected sound absorption material, described in Section 8.2. The covered unit was once again positioned at the same three locations within the room: centre of the floor, centre wall, and corner positions (see Fig. 7.3). The experimental set-up was the same as described in Section 6.2.3.

8.5.2 Prediction

The simulation of the covered standard unit was more complicated than in the previous case of a hard box. The challenge was to correctly simulate the layer of absorption over the unit. As a starting point, frequency independent surface absorption coefficients were assumed, firstly of 20% and secondly of 50% to the box boundaries, in contrast to a value of 2% used for the uncovered box. Fig. 8.10 shows the predicted and measured response for a covered box located in the corner position (see Fig. 7.3). In general, results indicated that the approximate values of absorption gave poor agreement with measurement, indicating the need of a more consistent approach.

The approach was to use the results of normal absorption coefficient measurements presented in Section 8.3. From the low frequency extrapolated absorption coefficient values shown in Fig. 8.2, a set of admittance values was generated for the frequency range from 20 Hz to 200 Hz (see Fig. 8.11). These resultant values of normal acoustic admittances were entered in the finite element model.

8.6 Results

The first result to be shown here is the recalculation of the room response for the case in which the room floor was covered with absorption material, as described in Section 8.4. Previously, a constant absorption coefficient value of 50% was assigned

to the floor, in the numerical model (see Fig. 8.9). The refined model included a frequency dependant normal admittance with values shown in Fig. 8.11 (see Section 8.5.2). The predicted room response is shown with the same experimental curve displayed in Fig. 8.9, and the new result is shown in Fig. 8.12.

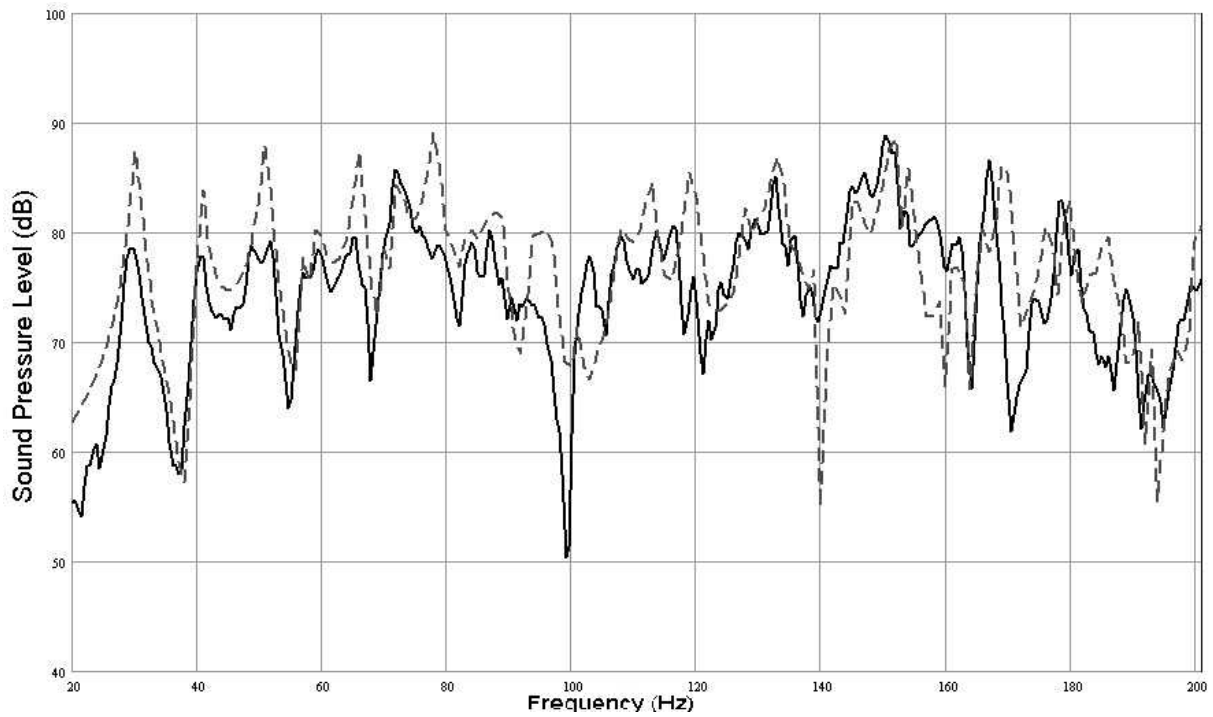


Figure 8.10 - Measured and predicted frequency response of room with standard unit in the corner position and covered with 150 mm absorption material. (—) Measurement and (---) prediction from room model considering a constant value of absorption coefficient of 50% applied to the obstacle boundaries.

Additionally, Fig 8.13 presents level differences between predictions for preliminary and refined model of covered floor, and measurement in $1/12^{\text{th}}$ octave bands. For the preliminary model, considering a value of absorption coefficient of 50% assigned to the room floor (see Fig. 8.9), the average level difference is of the order of $-5 \text{ dB} \pm 3 \text{ dB}$ up to 60 Hz. Above this frequency the level difference is on average $0 \text{ dB} \pm 6 \text{ dB}$. The refined model (see Fig. 8.12) gives a level difference with an average value of 0 dB throughout the entire frequency interval, although with some fluctuations greater than in the previous model. Below 60 Hz there is a variation of $+4$ to -5 dB about the average value, and above this frequency the variation is of the order of $+4$ to -2 dB . The results obtained between measurement and prediction for the refined model validated the use of the developed table of admittance values in simulating the behaviour of the selected absorption material.

The same approach was then adopted for the covered unit cases, described as follows.

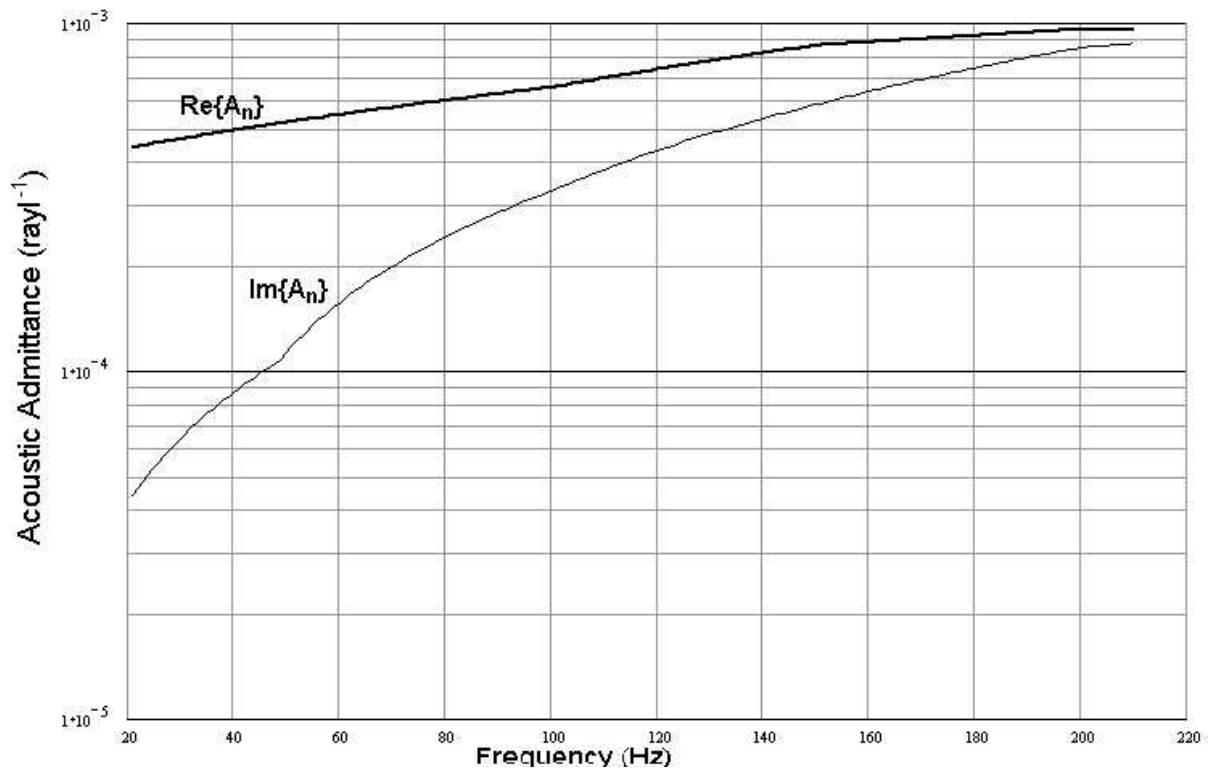


Figure 8.11 - Real and imaginary values of normal acoustic admittance obtained from the extrapolated absorption coefficients of Fig. 8.2.

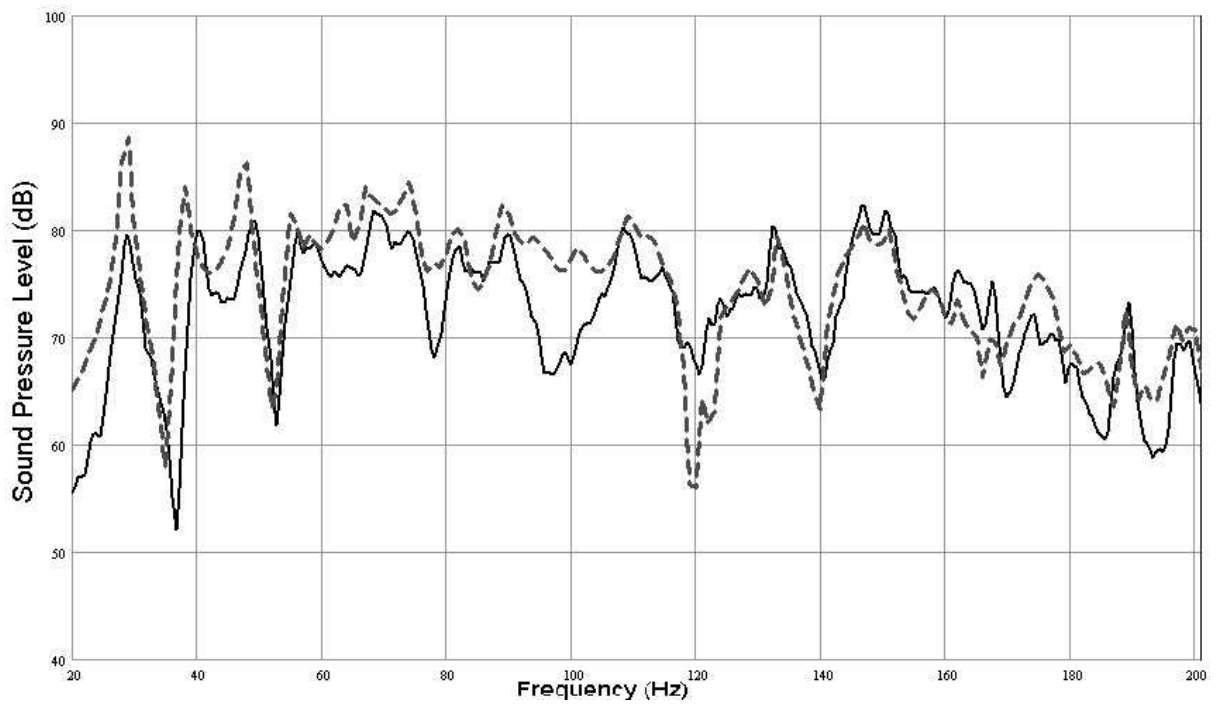


Figure 8.12 - Measured and predicted frequency response of room with floor covered with 150 mm absorption material. (—) Measurement and (---) prediction from refined room model.

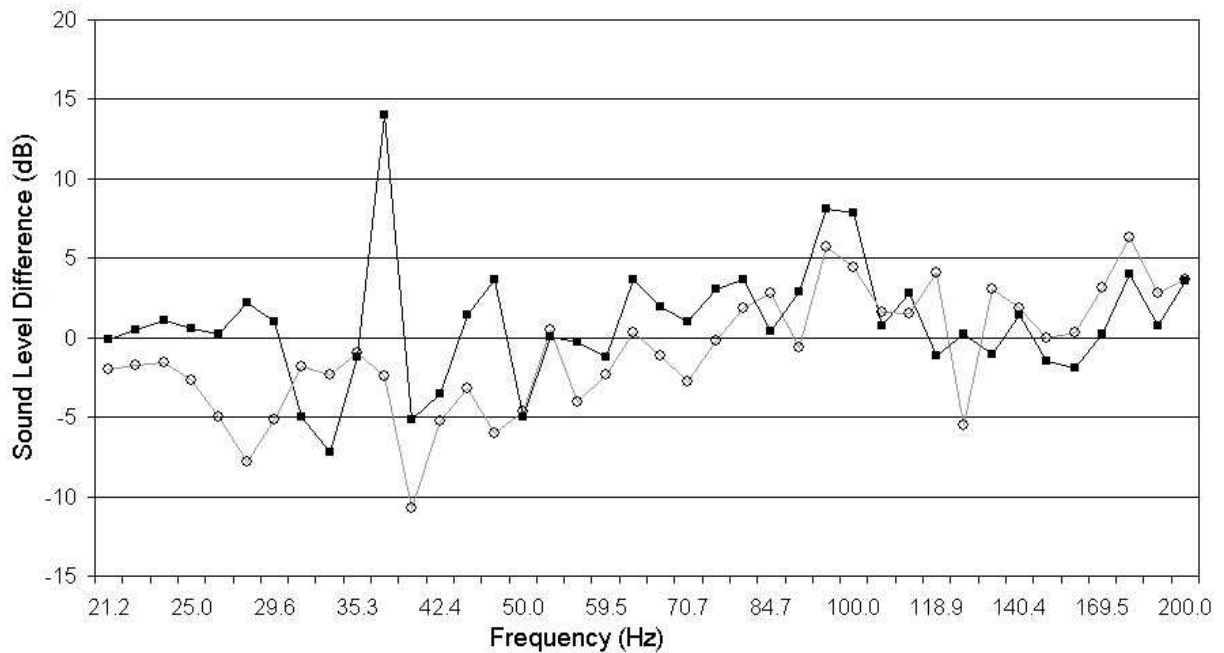


Figure 8.13 - Level differences between measurement and prediction of room with floor covered with 150 mm absorption material. (—○—) Old model of Fig 8.9, and (—■—) refined model of Fig. 8.12.

Fig. 8.14 shows the measurements of FRF for the reference empty room and when the standard unit and the covered unit were positioned in the centre of the room floor.

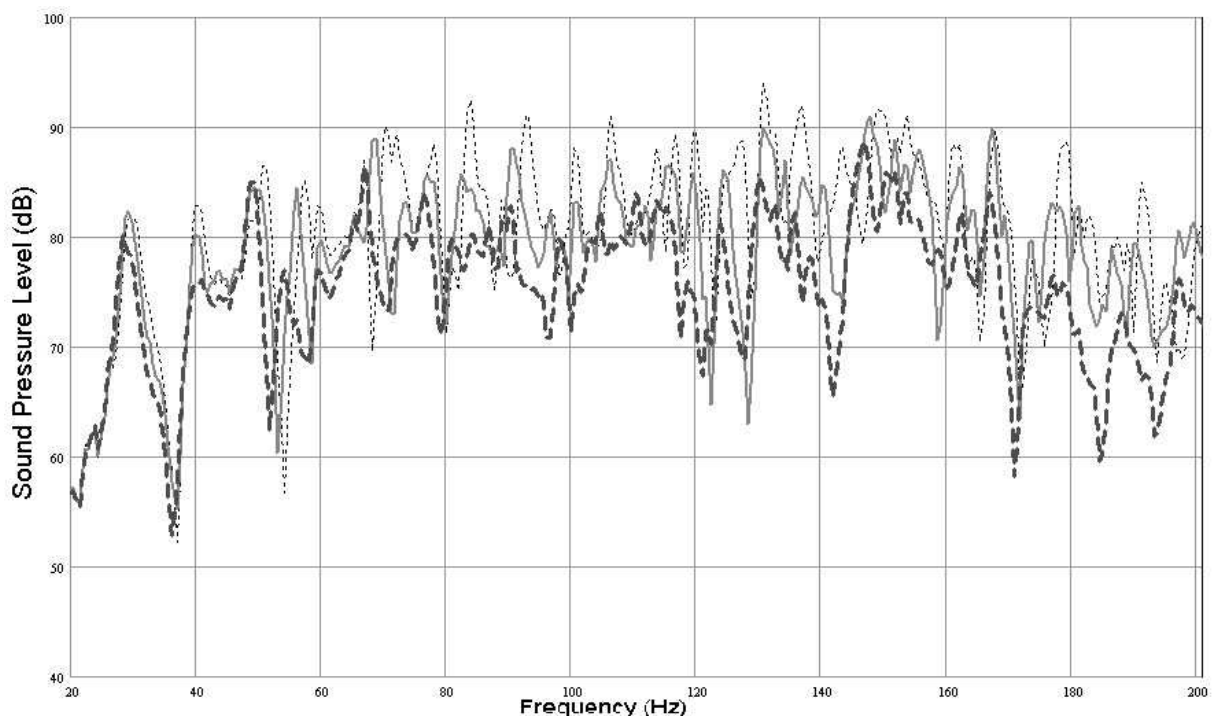


Figure 8.14 - Measurements for (.....) empty room, (—) hard box, and (---) lined box at central floor position.

A visual inspection of this figure reveals that the introduction of a layer of absorption material over the standard unit had a greater effect on the room frequency response, when compared with the previous case of a hard-surfaced box (see Chapter 7). The second room mode at 40 Hz, for example, is reduced 3 dB after the introduction of the solid unit, with an additional 4 dB reduction for the case of the lined unit. Also, while the fourth room mode at approximately 58 Hz was shifted 2.4% downwards in frequency with little level reduction for the solid unit case, in the case of the covered unit the same room mode is shifted 6% downwards and reduced by 8.3 dB.

Fig. 8.15 shows measurement and prediction for the room with the lined standard unit in the central floor position. Also shown here and in future figures containing predicted values, are the eigenfrequencies indicating the first axial modes (A), tangential modes (T) and oblique modes (O).

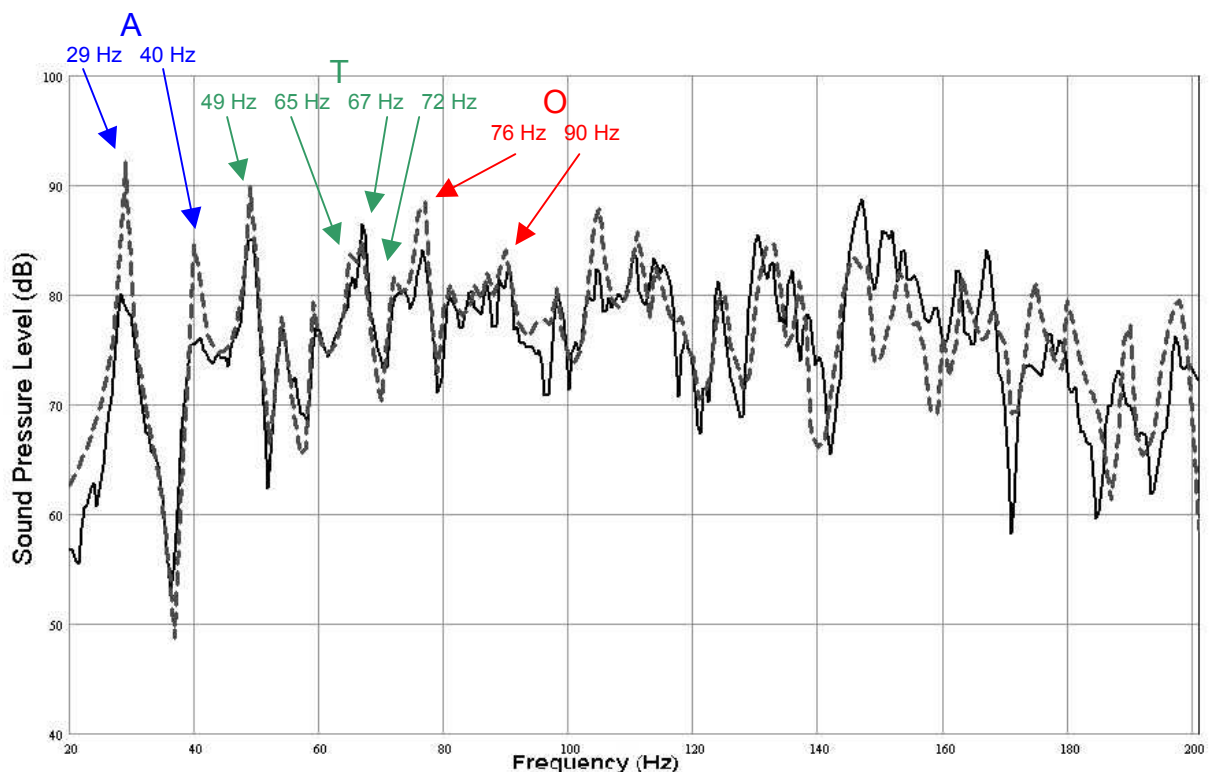


Figure 8.15 - Results for the lined box in the central floor position indicating first axial (A), tangential (T) and oblique (O) modes: comparison between (—) measured and (---) predicted room responses.

However, due to modal superposition, it was not always possible to clearly identify even the first oblique modes in the shown plots. In general, a good agreement between measurement and prediction is indicated. Below 145 Hz the developed finite element model tracks the trend of the experimental room response, despite of all the involved approximations, including extrapolation of the absorption

coefficient values to lower frequencies. Fig. 8.16 shows the predicted and measured level differences in 1/12th octave bands.

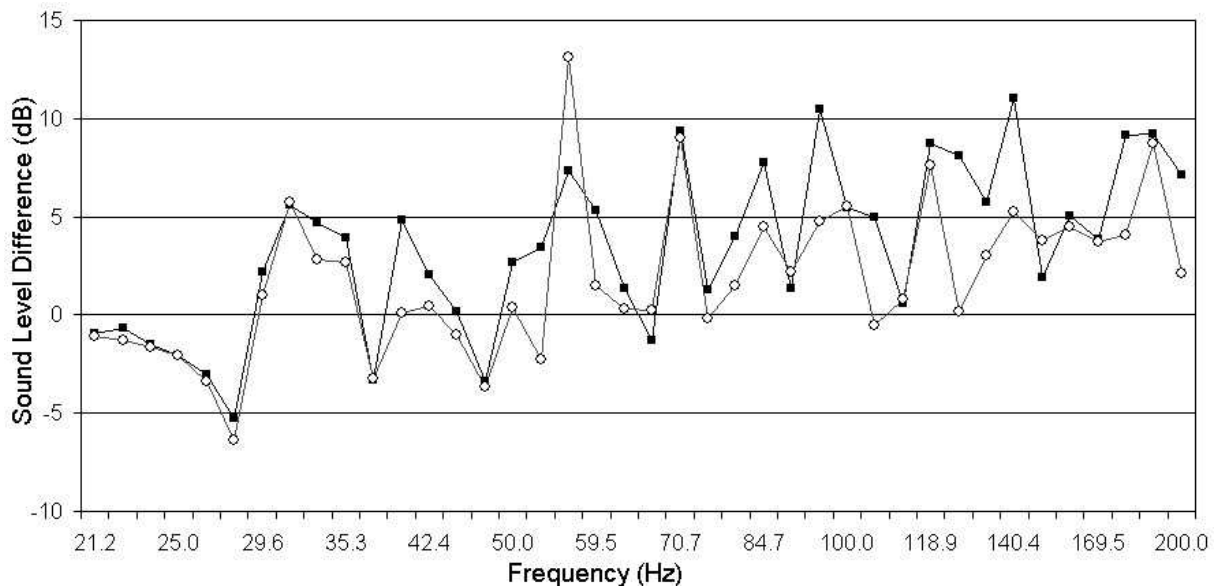


Figure 8.16 - Results for the lined box in the central floor position: comparison between (—■—) measured and (---○---) predicted level differences in 1/12th octave bands.

The results present similarities with those for the uncovered unit (see Chapter 7). When the covered standard unit is centrally located, the level difference has an average value of about 1 dB, but now within a range ± 6 dB for the frequency range below 50 Hz. Between 50 Hz and 200 Hz the experimental level difference is on average 5 dB within a range ± 5 dB. In general, the predicted curves underestimate measurements.

Figs. 8.17 and 8.18, and Figs. 8.19 and 8.20 show the corresponding results for the cases where the covered unit was located centrally along the long wall and at the corner, respectively. For the centre wall position, the general observations described in the last paragraph apply. However, a comparison between Figs. 8.16, 8.18, and 8.20 shows that, although the overall effect of the covered unit on the room properties is greater than in the uncovered box case, here the least influential position was not the central floor position, as it was the case in the previous chapter results. Instead, for the lined box case the corner position was observed to be the least influential. This may be explained by the fact that for the covered unit in the centre of the floor a greater amount of absorption material was present within the room, since no absorption was introduced between the standard unit and the room walls for the other two positions. Thus, since for the corner position the standard unit

is in contact with two room walls, this position received the minimum amount of absorption compared with the other two, leading to a smaller overall effect.

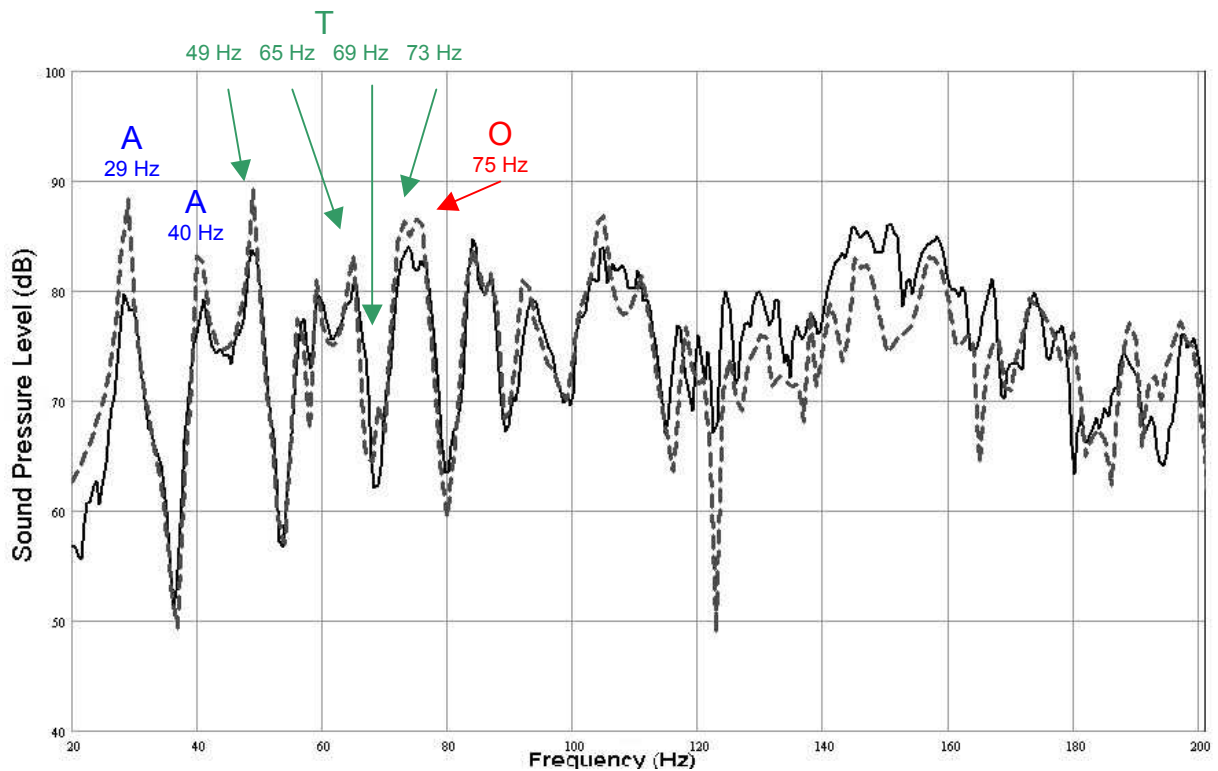


Figure 8.17 - Results for the lined box in the centre wall position indicating first axial (A), tangential (T) and oblique (O) modes: comparison between (—) measured and (---) predicted room responses.

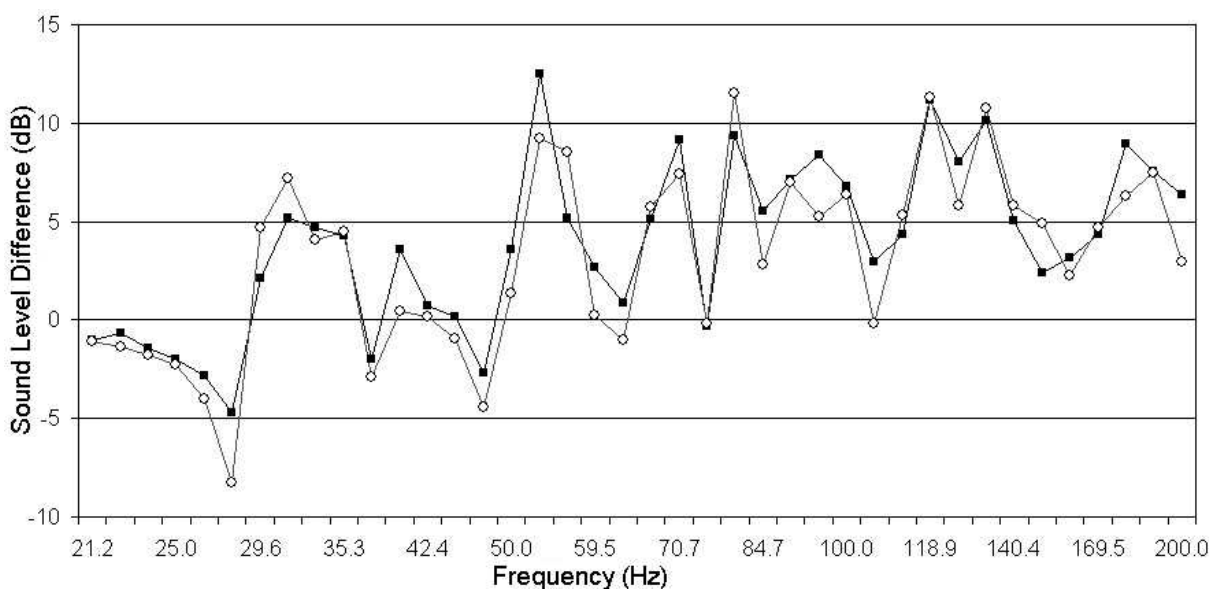


Figure 8.18 - Results for the lined box in the centre wall position: comparison between (—■—) measured and (---○---) predicted level differences in 1/12th octave bands.

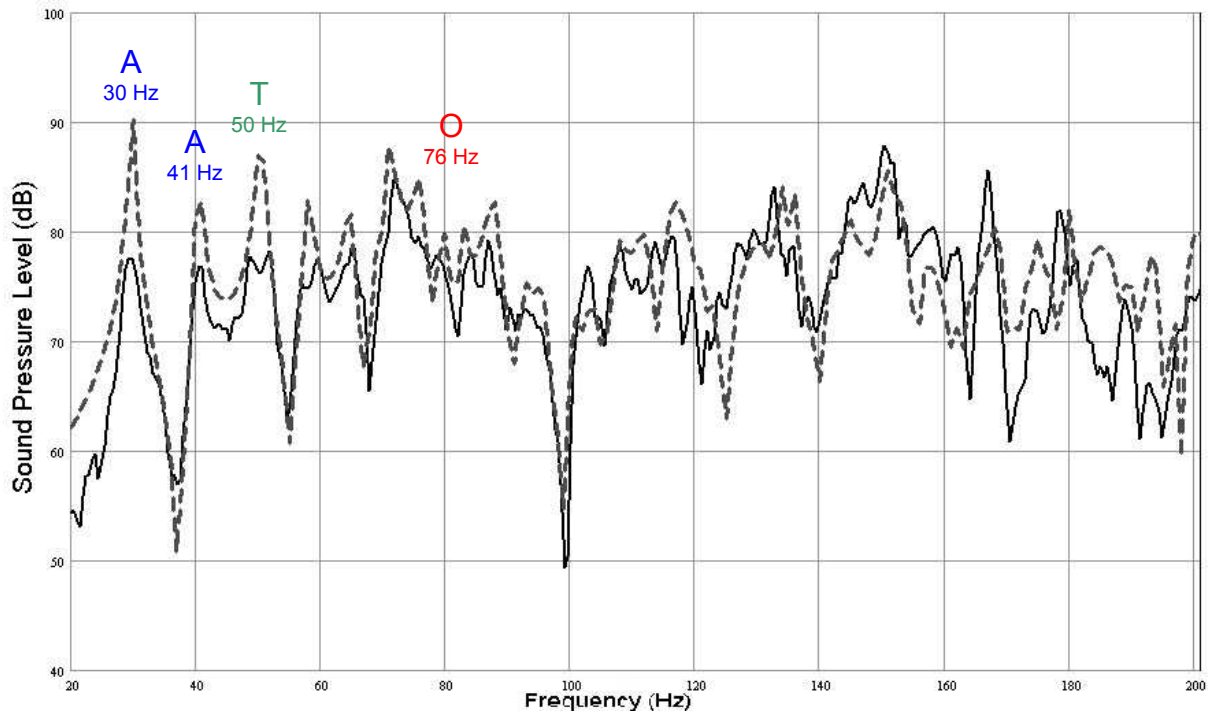


Figure 8.19 - Results for the lined box in the corner position indicating first axial (A), tangential (T) and oblique (O) modes: comparison between (—) measured and (---) predicted room responses.

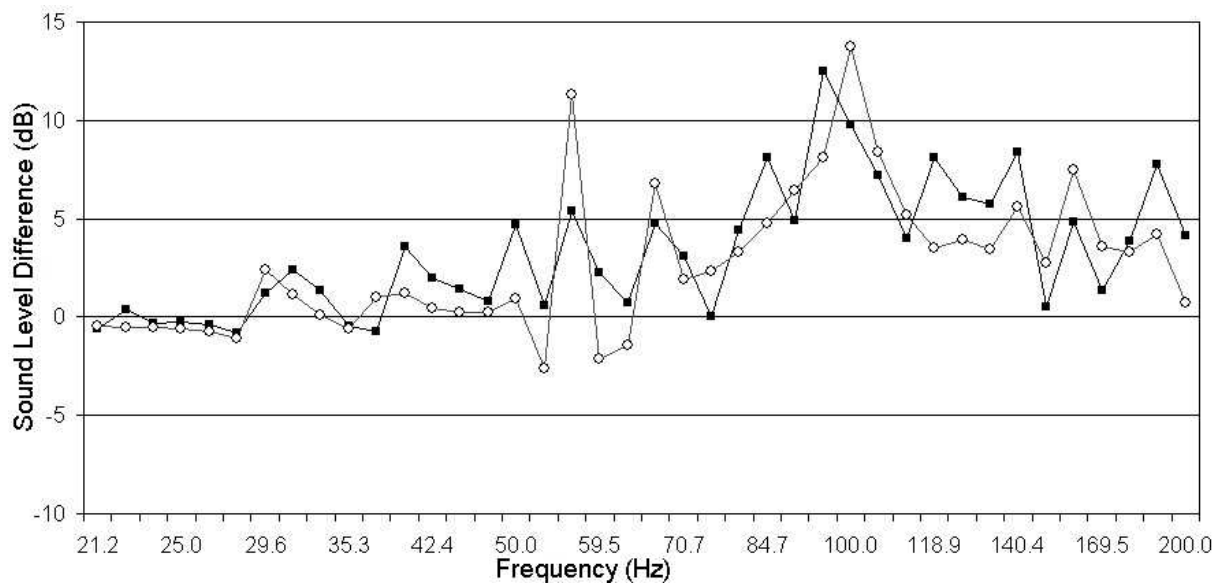


Figure 8.20 - Results for the lined box in the corner position: comparison between (—■—) measured and (—○—) predicted level differences in $1/12^{\text{th}}$ octave bands.

Finally, Fig. 8.21 shows measurements for empty and obstructed rooms in one-third octave bands and Fig. 8.22 shows the resultant level differences between the two conditions. While the results obtained in the previous chapter indicated no absorption effect, Fig. 8.21 shows that the discrepancies are of the order of 5 dB to 10 dB, an effect caused by the absorptive layer covering the standard unit.

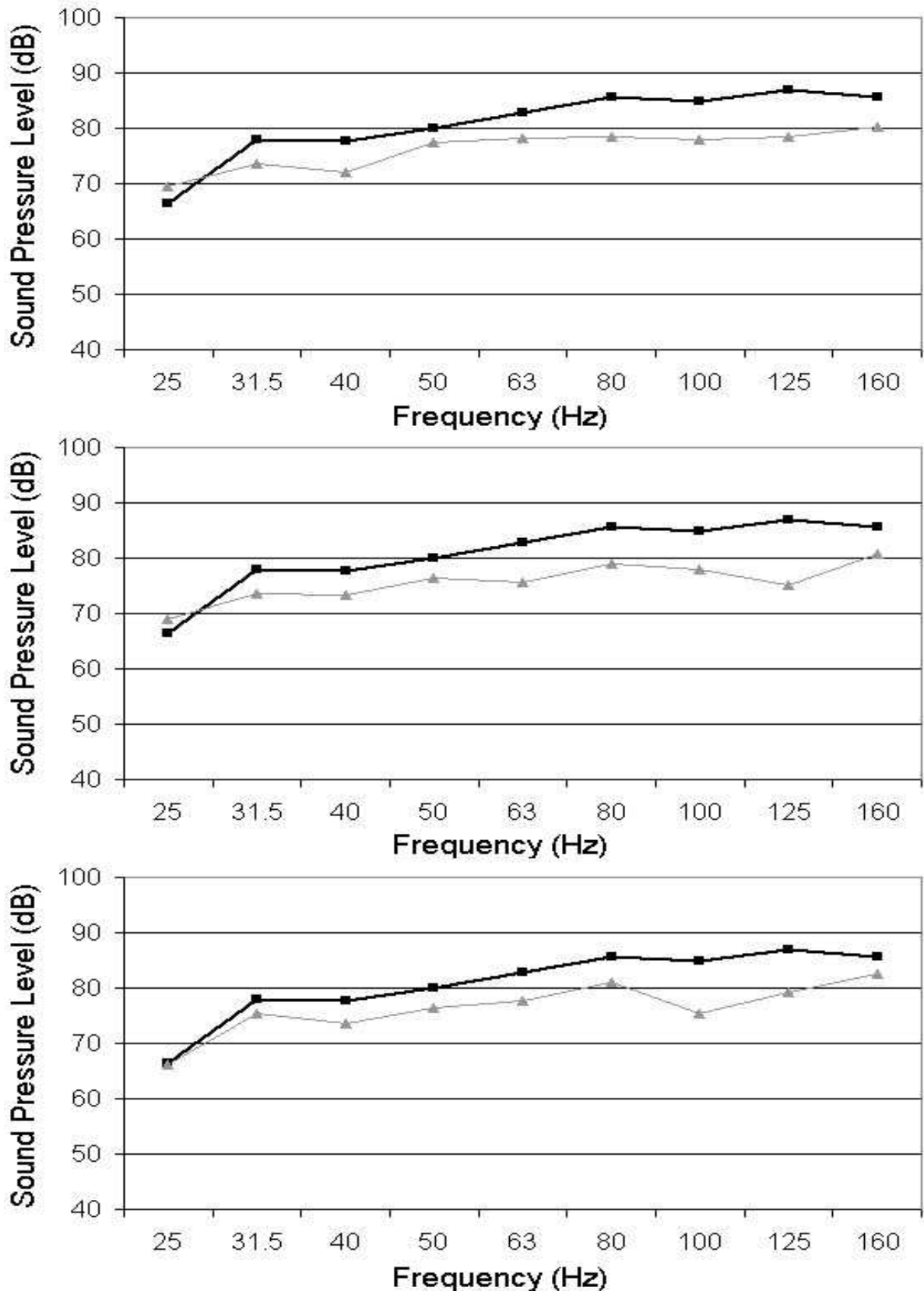


Figure 8.21 - Effect of obstacle on room frequency response. Measurements shown in one-third octave bands. a) Central floor position: (—■—) empty room and (—▲—) obstructed room. b) Centre wall position: (—■—) empty room and (—▲—) obstructed room. c) Corner position: (—■—) empty room and (—▲—) obstructed room.

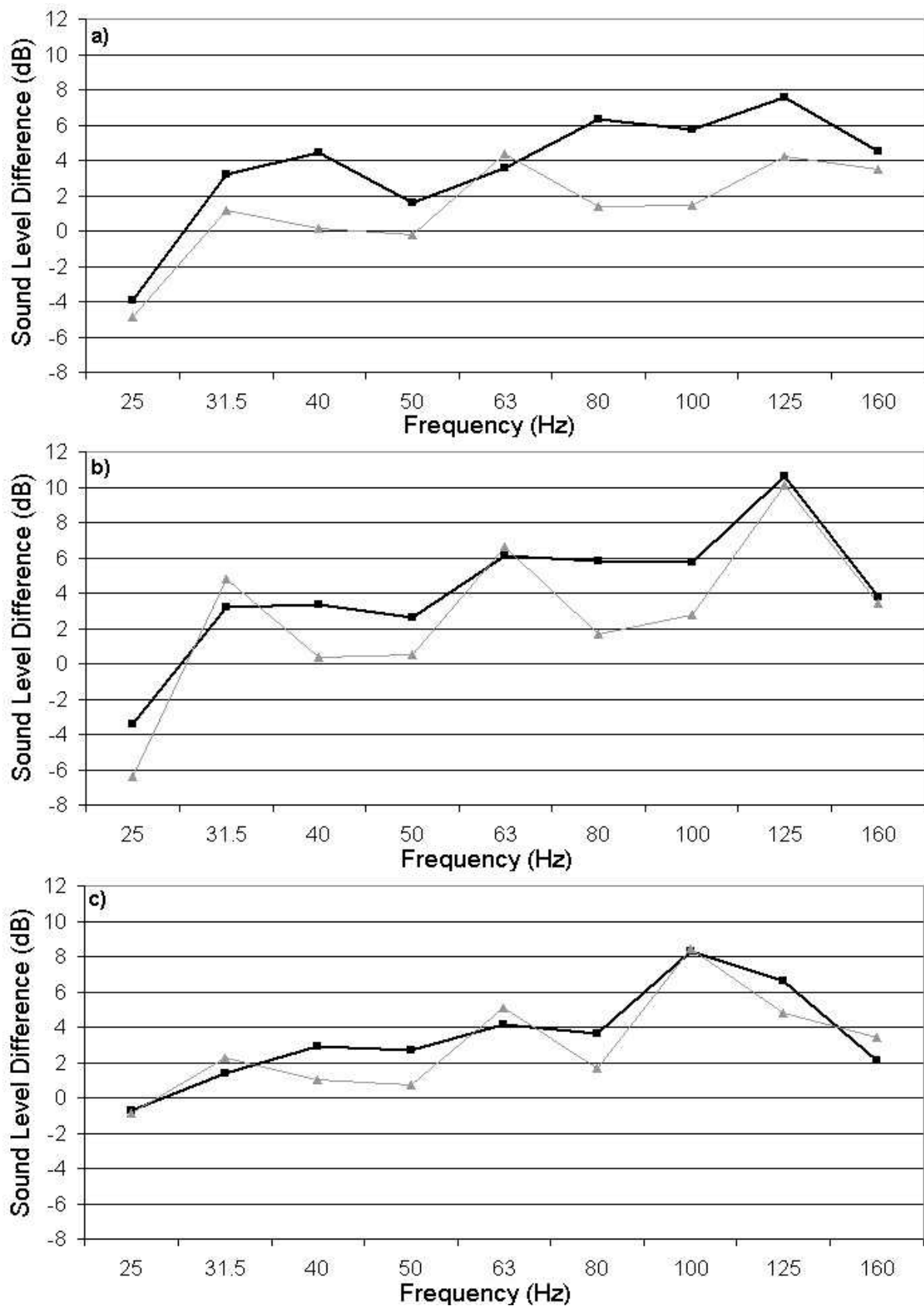


Figure 8.22 - Level difference (—■—) between measured values and (---▲---) between predicted values. Results shown in one-third octave bands. a) Central floor position, b) centre wall position, and c) corner position.

An analysis of Fig. 8.22 reveals that when the covered standard unit is centrally located, the level difference has an average value of about 2 dB, within a range ± 4 dB for the frequency range below 50 Hz. Between 50 Hz and 160 Hz the experimental level difference is on average 5 dB within a range ± 3 dB. For the centre wall case, a similar behaviour is observed below 50 Hz as for the central floor position. However, above 50 Hz the level difference is on average 6 dB, within a range ± 4 dB. Finally, for the corner position the level difference has an average value of about 1 dB, within a range ± 2 dB for the frequency range below 50 Hz. Between 50 Hz and 160 Hz the experimental level difference is on average 5.5 dB within a range ± 2.5 dB.

8.7 Summary

In this chapter, the preliminary FE model described in Chapter 7 has been refined. Measurements and numerical simulations have been repeated for the same standard unit positions, but now considering a layer of a known sound absorption material covering the unit. Preliminary measurements and numerical simulations were conducted with the room floor covered with sound absorbing material, allowing the refinement of the FE model previously developed (see Chapters 6 and 7). An analysis of the results has confirmed the greater effect the lined standard unit has on room responses, when compared with the uncovered box case (Chapter 7). However, although the centre wall position happened to be the most influential one once again, results for the lined box case have replaced the central floor position by the corner position as the least influential one.

In the next chapter the investigation is further developed by considering furniture wholly in terms of absorbing characteristics. This will be done by replacing the lightweight concrete blocks by a unit composed only of the sound absorbing material.

8.8 References

- BALVEDI, A. M. **Medição e simulação acústica de materiais porosos e sistemas multicamadas**. Master Dissertation, Federal University of Santa Catarina, Florianópolis, 1998.
- BERANEK, L. L. **Precision measurement of acoustic impedance**. Journal of the

Acoustical Society of America, 12, 3-13, 1940-a.

BERANEK, L. L. **Acoustic Impedance of Commercial Materials and the Performance of Rectangular Rooms with One Treated Surface.** Journal of the Acoustical Society of America, 12, 14-23, 1940-b.

BRÜEL & KJAER. **Technical review.** N° 1, 1955.

BRÜEL & KJAER. **Standing wave apparatus type 4002.** 1979.

GERGES, S. **Ruído: fundamentos e controle.** Federal University of Santa Catarina U.P., Florianópolis, 2000.

GIBBS, B. M. **The inter-relation between the distribution of absorbent material amongst the room surfaces and the distribution of sound energy and reverberation times within the room.** Master Thesis, University of Sheffield, Sheffield, 1970.

PARIS, E.T. **On the coefficient of sound absorption measured by the reverberation method.** Philosophical Magazine, 5, 489, 1928.

SEGAERT, P. Private communication, 2001.

CHAPTER 9

ROOM CONTENTS AS 'SOFT' ABSORBERS

9.1 Introduction

In chapters 7 and 8, the effect of room contents on the frequency response of a reference enclosure has been presented. The room contents have been represented as solid obstacles (Chapter 7) and as the same solid covered by a layer of sound absorption material (Chapter 8). In this chapter it is presented the results of a further investigation, in which the standard unit was reconstructed using sound absorbing foam only. The absorbing foam was the same material as described in Chapter 8, allowing the construction of a 'soft' unit having approximately the same dimensions as the solid and covered solid. It constitutes the last case to be studied in this work, before the approach to real furniture, which is the subject of the following chapter.

9.2 Effect of absorber thickness

Although the same sound absorption material described in Chapter 8 was used in the experimental part of the present chapter, it differed in that it was of increased thickness, and consequently, with the initial assumption of having greater absorption than previously. Thus, while a layer of 150 mm of the selected foam was used to cover the standard unit (Chapter 8), here the whole unit was composed of the foam, making it impractical for its absorption coefficient to be measured by conventional methods. Preliminary measurements of room frequency response indicate that results for the soft unit were very close to those of the covered unit, presented in Chapter 8. Figs. 9.1, 9.2, and 9.3 show measured frequency response functions for the covered and soft units placed at central floor, centre wall, and corner positions, respectively. Fig. 9.4 shows the same measured results presented as level differences, in one-third octave bands, between the covered unit and soft unit cases. In general, the soft unit is less absorptive in comparison with the covered unit case, but does not differ more than ± 2.5 dB. On first inspection, this may not be surprising. If the soft unit is considered as an absorber of effective thickness 300 mm then

although significantly greater than 150 mm, it is still small compared with the governing wavelength of 6.9 m at 50 Hz.

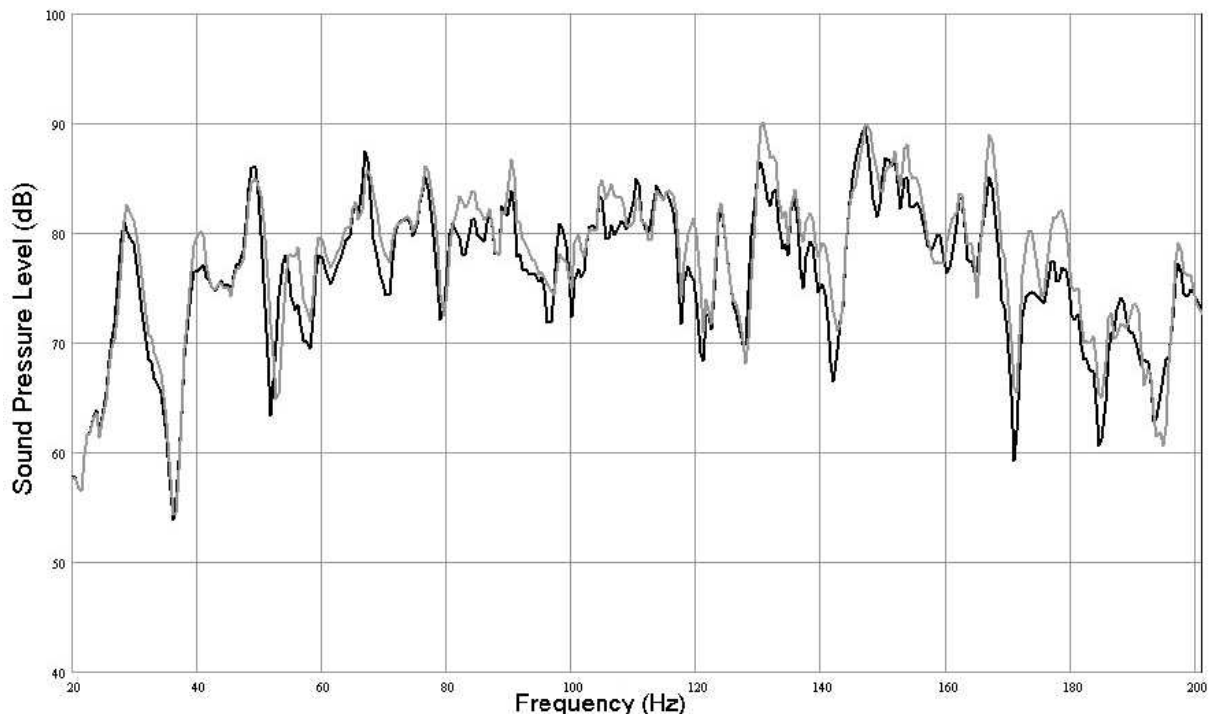


Figure 9.1 - Measured room frequency response for (—) lined box case (Chapter 8) and (---) soft box case. Results for central floor position.

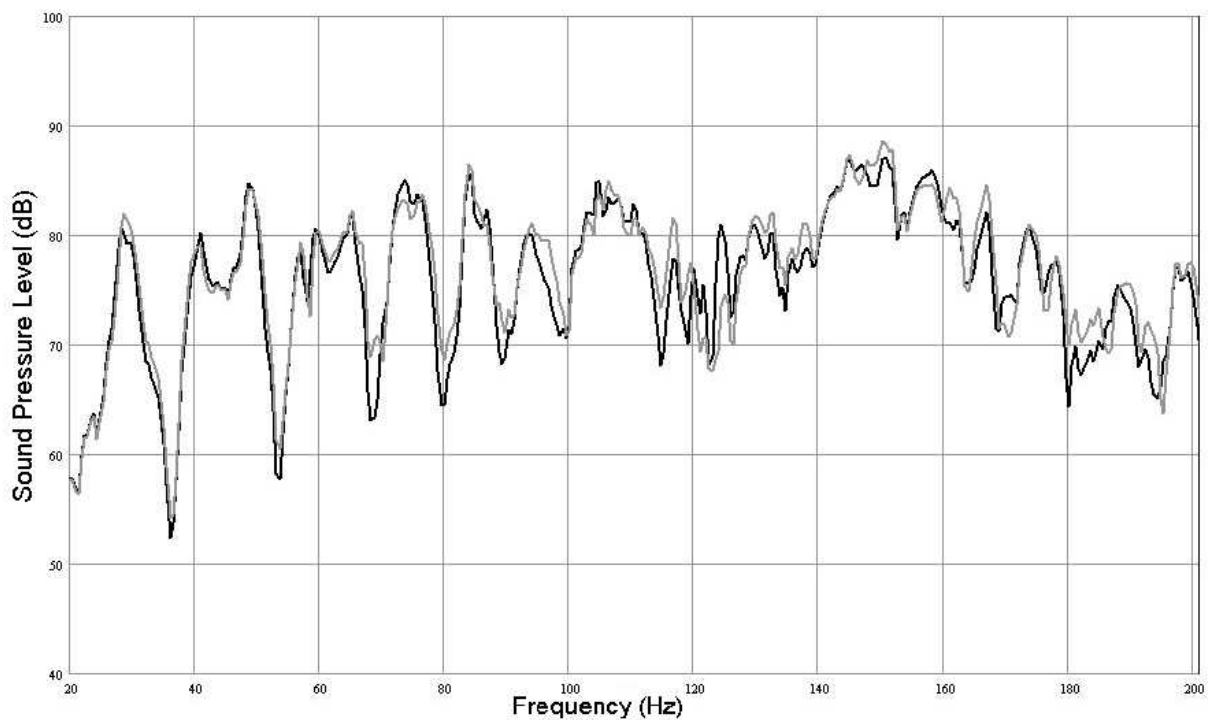


Figure 9.2 - Measured room frequency response for (—) lined box case (Chapter 8) and (---) soft box case. Results for centre wall position.

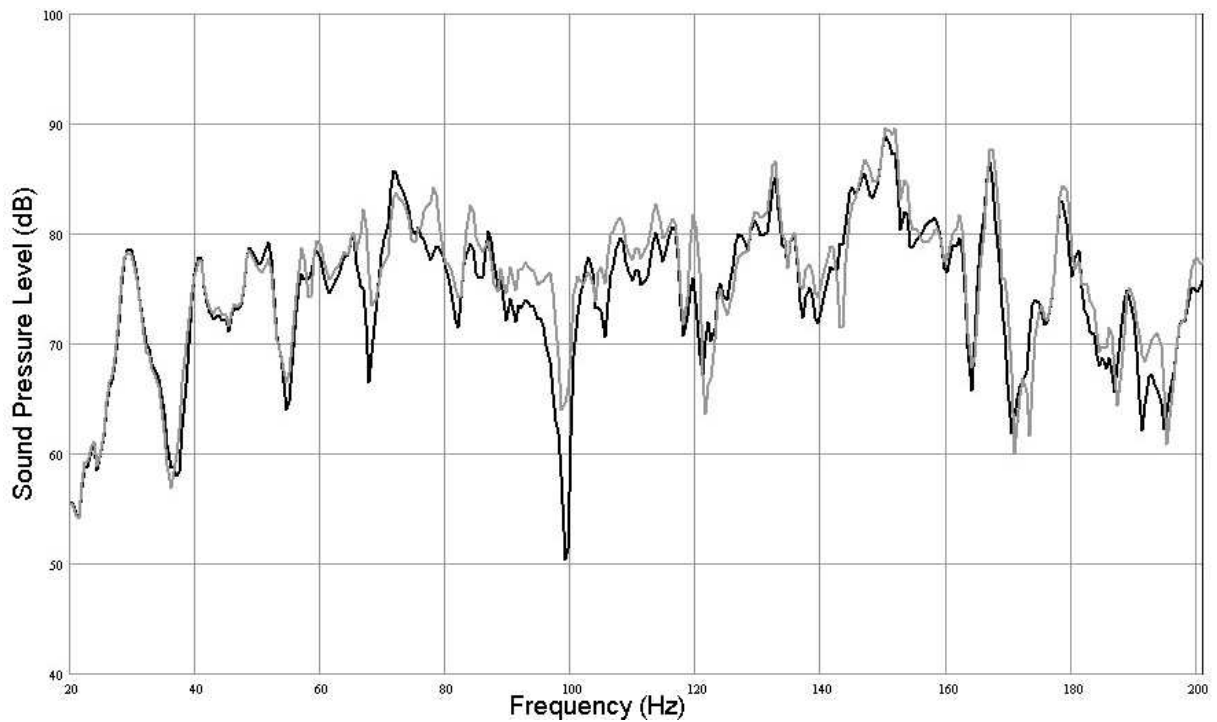


Figure 9.3 - Measured room frequency response for (—) lined box case (Chapter 8) and (---) soft box case. Results for corner position.

However, there are complicating factors. When positioned in a room corner, the foam unit has solid surfaces backing the three exposed front surfaces (whereas the centrally located unit only has the floor surface as rigid backing and a freely suspended unit would have no rigid backing). Therefore, although a corner unit only has three of its six surfaces exposed, they all have rigid backings, which ensure that the sound wave travels through a double thickness of the foam. This exposes a challenge in modelling furniture as absorbers. Should soft furniture be modelled as absorbers only with no internal reflections, or should they be assumed to have a solid core with absorbing covering?

The problem was approached by assuming that the soft unit behaves as if composed of a solid core covered by a layer of absorption. Consequently, different numerical models were created in order to simulate the soft unit case, considering different solid core sizes. The core sizes should (in principle) dictate the effective thickness of the surrounding absorbing foam, as will be further described.

In order to calculate the new admittances as a function of material thickness, measurements of the acoustic impedance Z at thicknesses h and $2h$ must be performed at the same frequency, which give [Zwicker and Kosten (1947), Gibbs (1970), Balvedi (1998), Horoshenkov (2001)]

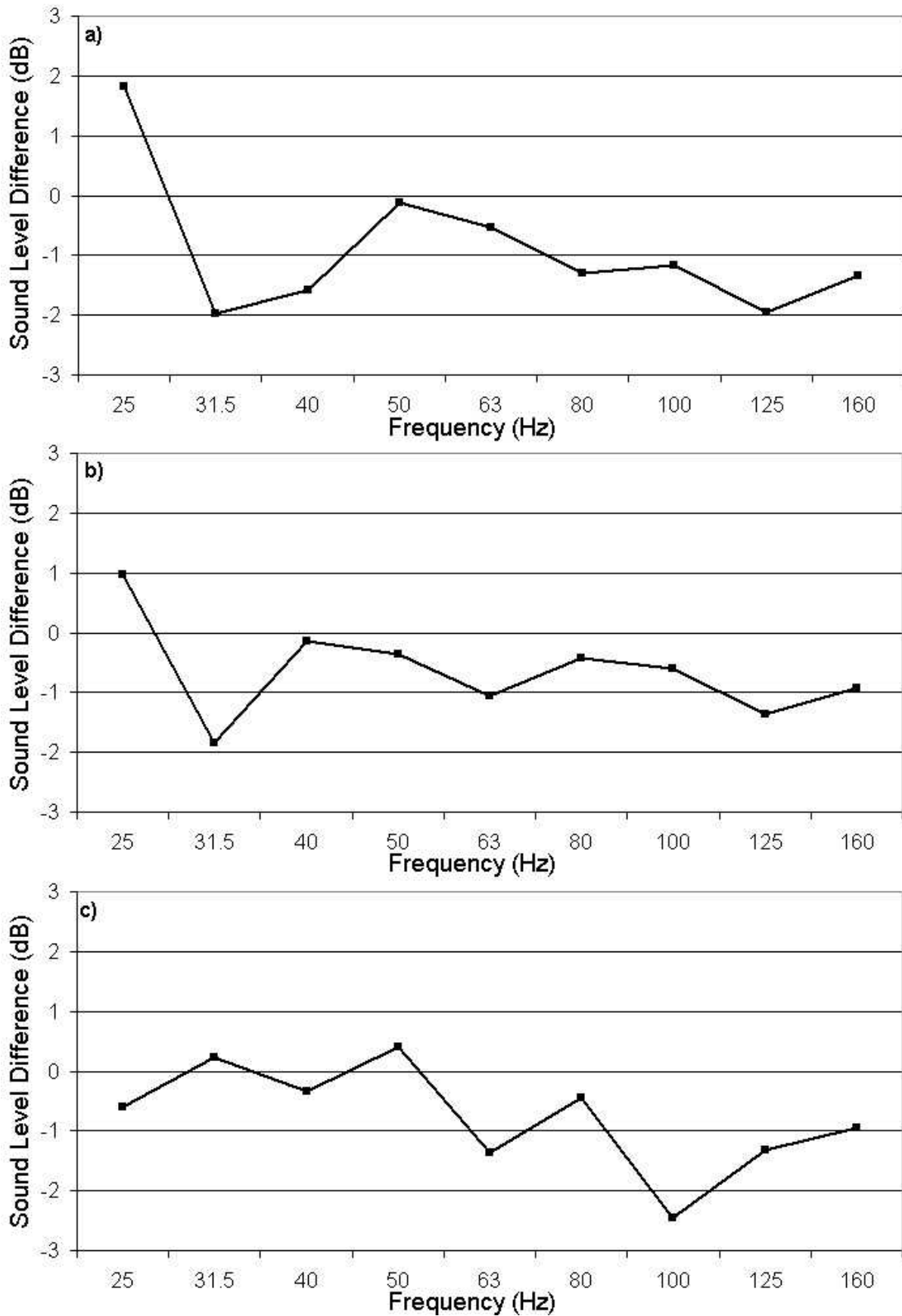


Figure 9.4 - Measured level differences between lined box FRFs (Chapter 8) and soft box FRFs in one-third octave bands. a) Results for central floor position, b) centre wall position, and c) corner position.

$$Z_h = W \coth(\gamma h) \quad (9.1)$$

$$Z_{2h} = W \coth(\gamma 2h), \quad (9.2)$$

where W is the complex characteristic impedance, and γ is the complex propagation constant of the material, as described in Section 5.4.1. Since [Spiegel (1992)]:

$$\tanh(2x) = \frac{2 \tanh(x)}{1 + [\tanh(x)]^2}, \quad (9.3)$$

then:

$$Z_{2h} = W \left[\frac{1 + (\tanh(\gamma h))^2}{2 \tanh(\gamma h)} \right]. \quad (9.4)$$

From equation (9.1):

$$\tanh(\gamma h) = \frac{W}{Z_h} \quad (9.5)$$

Thus, equation (9.4) may be rewritten as:

$$Z_{2h} = \frac{1}{2} \left(Z_h + \frac{W^2}{Z_h} \right). \quad (9.6)$$

From equation (9.6) the characteristic impedance of the material is given by:

$$W = \sqrt{Z_h(2Z_{2h} - Z_h)}, \quad (9.7)$$

and from equation (9.2):

$$\gamma = \frac{1}{2h} \operatorname{atanh} \left(\frac{W}{Z_{2h}} \right). \quad (9.8)$$

Care is needed in the calculation according to equation (9.7) to ensure $\operatorname{Re}\{W\} > 0$ [Horoshenkov (2001)].

Measurements were performed in order to obtain Z for foam thicknesses of 75 mm and 150 mm, for the frequency range 90 Hz to 250 Hz, using the impedance tube method (see Chapters 5 and 8). From equations (9.7), (9.8), and (8.3) admittance values were obtained as a function of thickness and the results are shown in Table 9.1 and Fig. 9.5 for $h = 35$ mm, 75 mm (measurement), 150 mm (measurement), 200 mm, and 300 mm. In general, an increase in thickness is accompanied by an increase in the real part (Fig. 9.5-a) and in the imaginary part

(Fig. 9.5-b) of the admittance. However, above 180 Hz there is a cross-over in the values of the real part for thickness 150 mm and 300 mm. For the imaginary part, cross-overs occur above 140 Hz. This may be explained by the fact that since the absorption coefficient is approaching unity at higher frequencies, then increased thickness would show no increase in absorption (or correspondingly in the real part). For instance, it might even show a slight decrease due to experimental error. However, a clear increase in the real part of admittance is observed at lower frequencies when the absorption coefficient is not near unity (see Fig. 9.5-a).

Table 9.1 - Values of admittance as a function of frequency and material thickness. Grey boxes indicate values obtained from measurements.

Frequency (Hz)	90	100	150	200	250
Re {A} (rayl⁻¹) h = 35 mm	2.654 · 10 ⁻⁵	2.553 · 10 ⁻⁵	4.299 · 10 ⁻⁵	6.341 · 10 ⁻⁵	7.468 · 10 ⁻⁵
Im {A} (rayl⁻¹) h = 35 mm	1.950 · 10 ⁻⁴	2.273 · 10 ⁻⁴	3.405 · 10 ⁻⁴	4.696 · 10 ⁻⁴	5.551 · 10 ⁻⁴
Re {A} (rayl⁻¹) h = 75 mm	7.748 · 10 ⁻⁵	8.801 · 10 ⁻⁵	1.627 · 10 ⁻⁴	2.722 · 10 ⁻⁴	3.571 · 10 ⁻⁴
Im {A} (rayl⁻¹) h = 75 mm	3.790 · 10 ⁻⁴	4.342 · 10 ⁻⁴	6.453 · 10 ⁻⁴	8.713 · 10 ⁻⁴	1.008 · 10 ⁻³
Re {A} (rayl⁻¹) h = 150 mm	2.862 · 10 ⁻⁴	3.291 · 10 ⁻⁴	5.843 · 10 ⁻⁴	8.517 · 10 ⁻⁴	9.782 · 10 ⁻⁴
Im {A} (rayl⁻¹) h = 150 mm	6.283 · 10 ⁻⁴	6.554 · 10 ⁻⁴	8.641 · 10 ⁻⁴	9.624 · 10 ⁻⁴	9.636 · 10 ⁻⁴
Re {A} (rayl⁻¹) h = 200 mm	4.710 · 10 ⁻⁴	4.783 · 10 ⁻⁴	7.392 · 10 ⁻⁴	9.182 · 10 ⁻⁴	9.713 · 10 ⁻⁴
Im {A} (rayl⁻¹) h = 200 mm	6.509 · 10 ⁻⁴	6.348 · 10 ⁻⁴	7.469 · 10 ⁻⁴	7.786 · 10 ⁻⁴	7.859 · 10 ⁻⁴
Re {A} (rayl⁻¹) h = 300 mm	5.685 · 10 ⁻⁴	5.193 · 10 ⁻⁴	7.213 · 10 ⁻⁴	8.557 · 10 ⁻⁴	9.090 · 10 ⁻⁴
Im {A} (rayl⁻¹) h = 300 mm	5.559 · 10 ⁻⁴	5.590 · 10 ⁻⁴	6.540 · 10 ⁻⁴	7.313 · 10 ⁻⁴	7.762 · 10 ⁻⁴

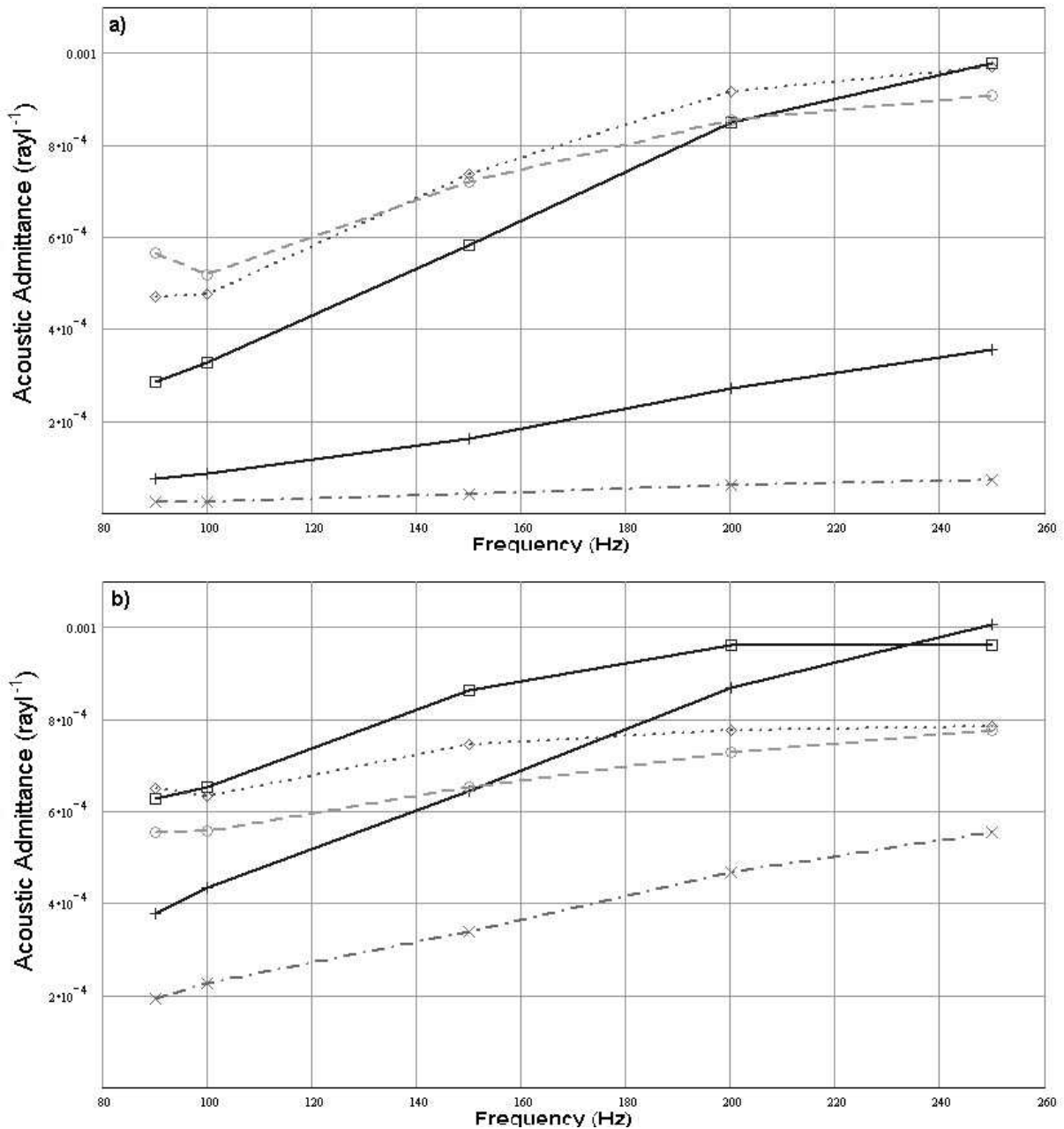


Figure 9.5 - Admittance as a function of frequency and material thickness. (---x---) $h = 35$ mm, (---+---) $h = 75$ mm, (---□---) $h = 150$ mm, (---♦---) $h = 200$ mm, and (---○---) $h = 300$ mm. a) Real values, and b) imaginary values. The solid curves indicate measurements.

In Fig. 9.5-b it is seen that the imaginary part of the admittance increases with thickness up to $h = 150$ mm. Above this thickness, the imaginary part of admittance appears to decrease with increasing thickness. Again, this might be explained in terms of the absorption coefficient. For values of absorption coefficient close to unity the admittance will be predominantly real. The relatively small imaginary part will yield high experimental errors and systematic changes with thickness will be less observable.

Since the thickness of the covering absorbent foam was not less than 150 mm, it was assumed that the same values of admittance, as a function of frequency (as described in Chapter 8), could be applied to the soft box case independently of the different solid core dimensions input to numerical model. The first soft unit model (Soft box 1) included in the numerical room model consisted of a small solid core of dimensions 0.84 m x 0.84 m x 0.56 m. This was the smallest core considered and corresponded with 3 mesh elements in the x and y directions, and 2 elements in the z direction. Two additional cases were still considered with increased core sizes: ‘Soft box-2’ with core dimensions 1.40 m x 0.84 m x 0.84 m (5 elements in the x direction, and 3 elements in the y and z directions), and ‘Soft box-3’ with core dimensions 1.68 m x 1.12 m x 1.12 m, i.e., the soft unit was simulated with 6 elements in the x direction, and 4 elements in the y and z directions.

9.3 Results

Fig. 9.6 shows two predicted room frequency responses corresponding to the cases of Soft box-1 and Soft box-3.

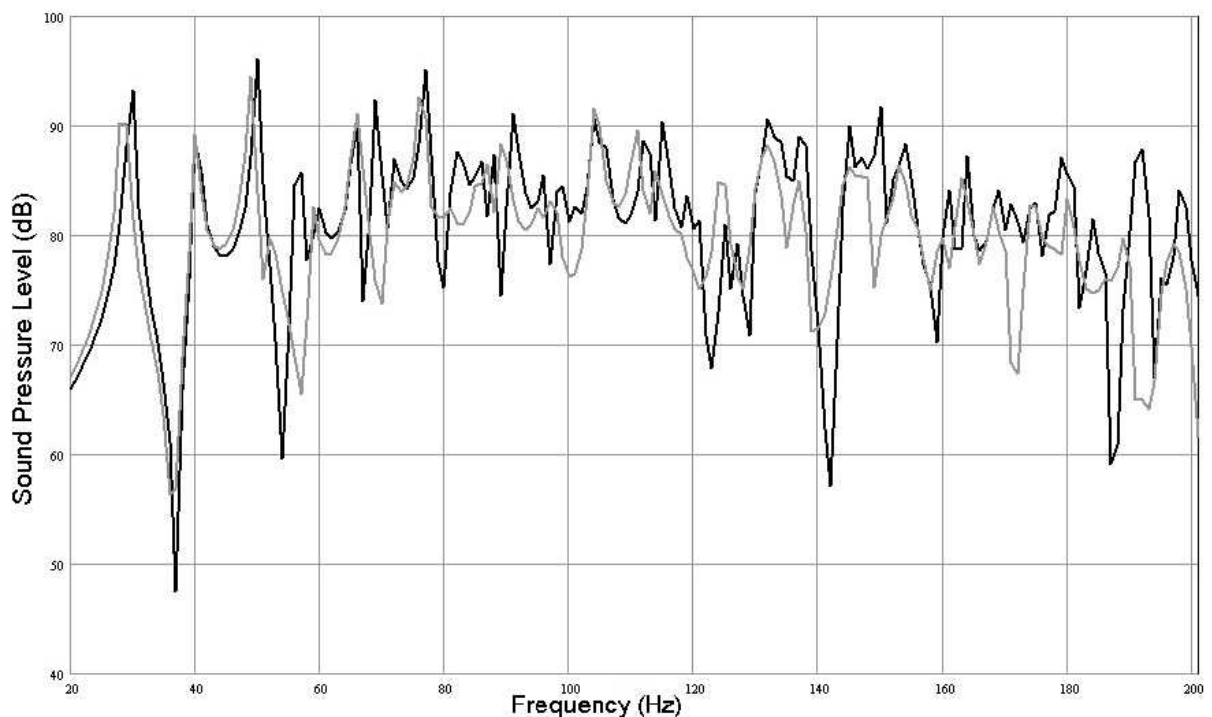


Figure 9.6 - Predicted room responses for (—) smallest solid core case (Soft box-1), and (---) largest solid core case (Soft box-3). Central room floor case.

This figure presents only the two extreme cases for clarity (the models containing the smallest and biggest solid cores). The curves shown are quite different from each other, with the eigenfrequencies much shifted. For example, the fourth room mode shifts from 57 Hz to 52 Hz. In addition there is a greater overall modal damping, possibly due to the increased absorbing surface area. Because of the similarities observed between experimental curves for the soft unit and lined unit cases (see Figs. 9.1 to 9.4), it seems logical to suppose that the numerical model which will provide the best agreement with measurements lies somewhere between the two extreme cases shown in Fig. 9.6. In order to quantify the accuracy provided by each developed model, Fig. 9.7 presents level differences between predictions and measurement in 1/12th octave bands.

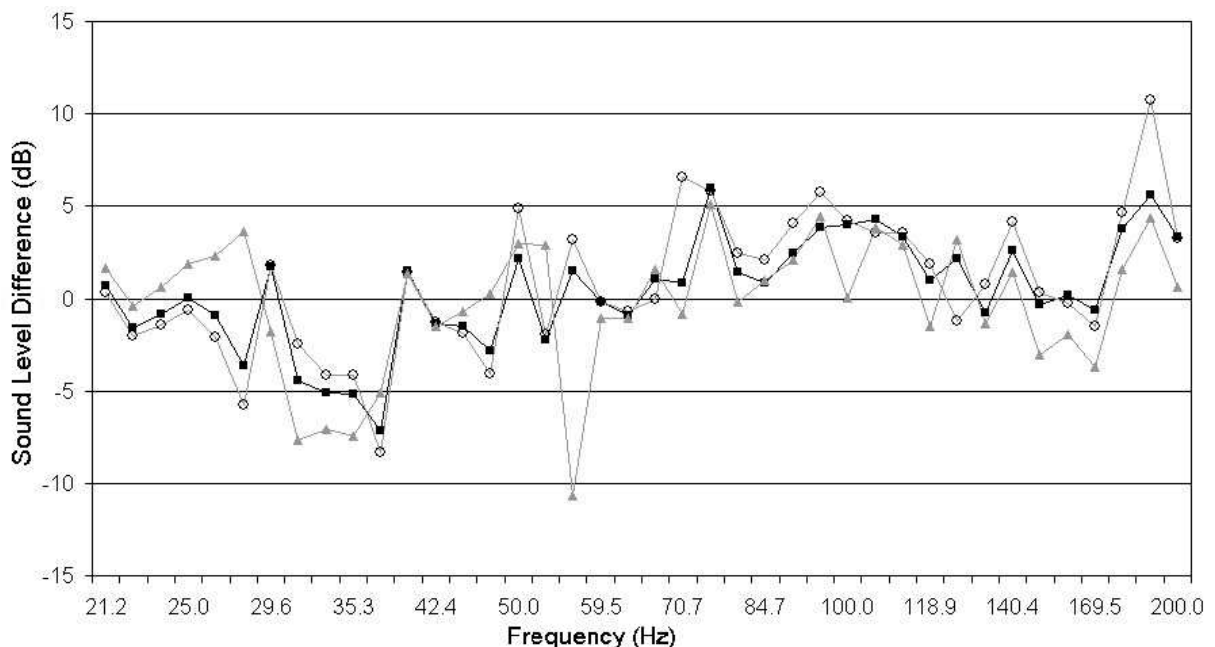


Figure 9.7 - Level differences between measurement and prediction of room with soft unit in the centre of the room floor. (—○—) Soft box-1, (—■—) Soft box-2, and (—▲—) Soft box-3 results.

For the Soft box-1 case, the figure shows a mean level difference of the order of -2.5 dB with a variation +1 dB to -6 dB up to 50 Hz. Similar behaviour is observed for the Soft box-2 case. However, although the same average level also is observed for the Soft box-3 case below 50 Hz, the variation about the mean value is +4 dB to -8 dB. This increased variation is attributed to the larger core size of Soft box-3. Above 50 Hz the level differences are equivalent for the three models, being on average 1 db \pm 3 dB. However, closer inspection reveals that the Soft box-1 (smallest core size) has the greatest discrepancy at high frequencies. The Soft box-2 model (intermediary core size) gives the smallest discrepancies up to 170 Hz, and above this frequency it

is the Soft box 3 model (largest core size) that presents the minimum discrepancy with measurements. This allows the conclusion that as the frequency increases, the effect of core size increases. However, overall, the Soft box-2 model gives the smallest discrepancy between prediction and measurement, and therefore, this model was incorporated into the room model.

Figs. 9.8, 9.9, and 9.10 show narrow band results for the soft unit placed at central floor, centre wall, and corner positions, respectively, considering the Soft box-2 as the prediction model. The agreement obtained between measurement and prediction was as expected, since the experimental results and numerical models for the soft unit were very similar to those for the covered unit (Chapter8), where a close fit between experimental and numerical results was already observed.

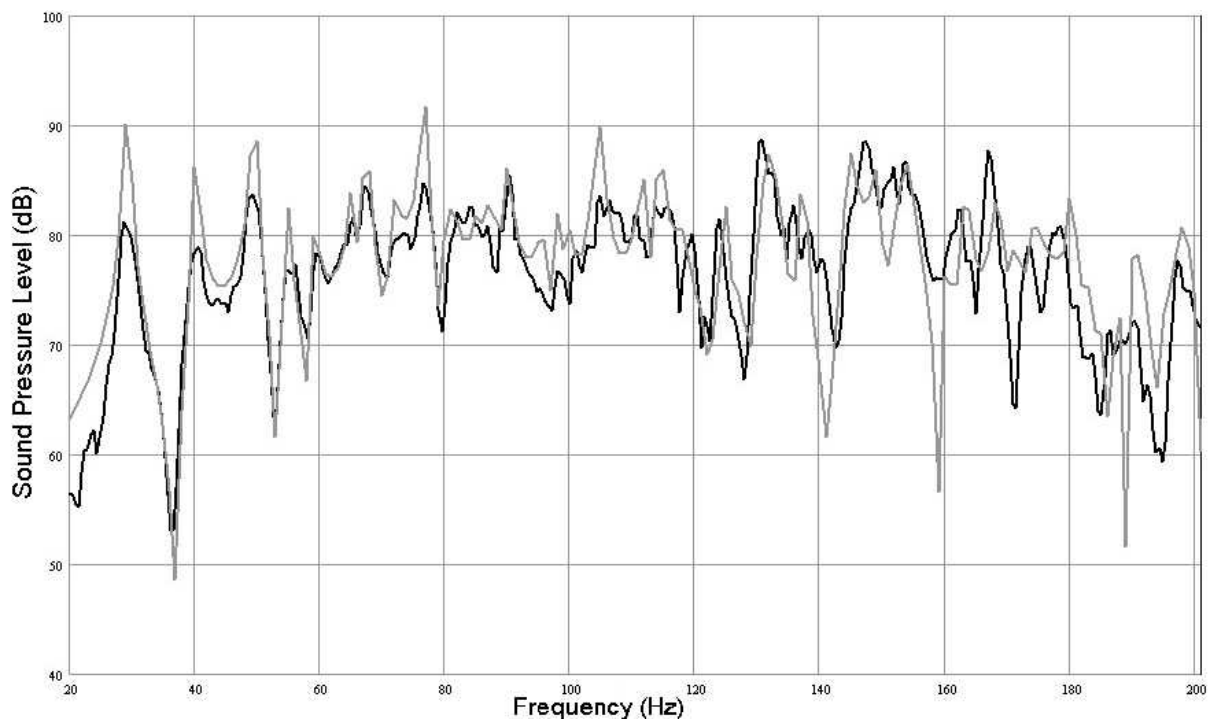


Figure 9.8 - Comparison between (—) measurement for the soft absorber and (---) prediction for the ‘Soft box-2’ model. Central floor position results.

In order to quantify the effect of the soft unit on the room frequency response, measured and predicted level differences were obtained in $1/3^{\text{rd}}$ octave bands (taking the empty room results as a reference) and the results are shown in Fig. 9.11. In this figure, as already indicated for the narrow band results, it is possible to see that the predictions follow the main trends of the experimental results, although the former slightly underestimates the latter. Fig. 9.11-a (centre of room floor position) shows a

mean level difference of the order of $0 \text{ dB} \pm 2 \text{ dB}$, up to 50 Hz. Above this frequency, the difference is on average 3.5 dB with a variation $\pm 1 \text{ dB}$.

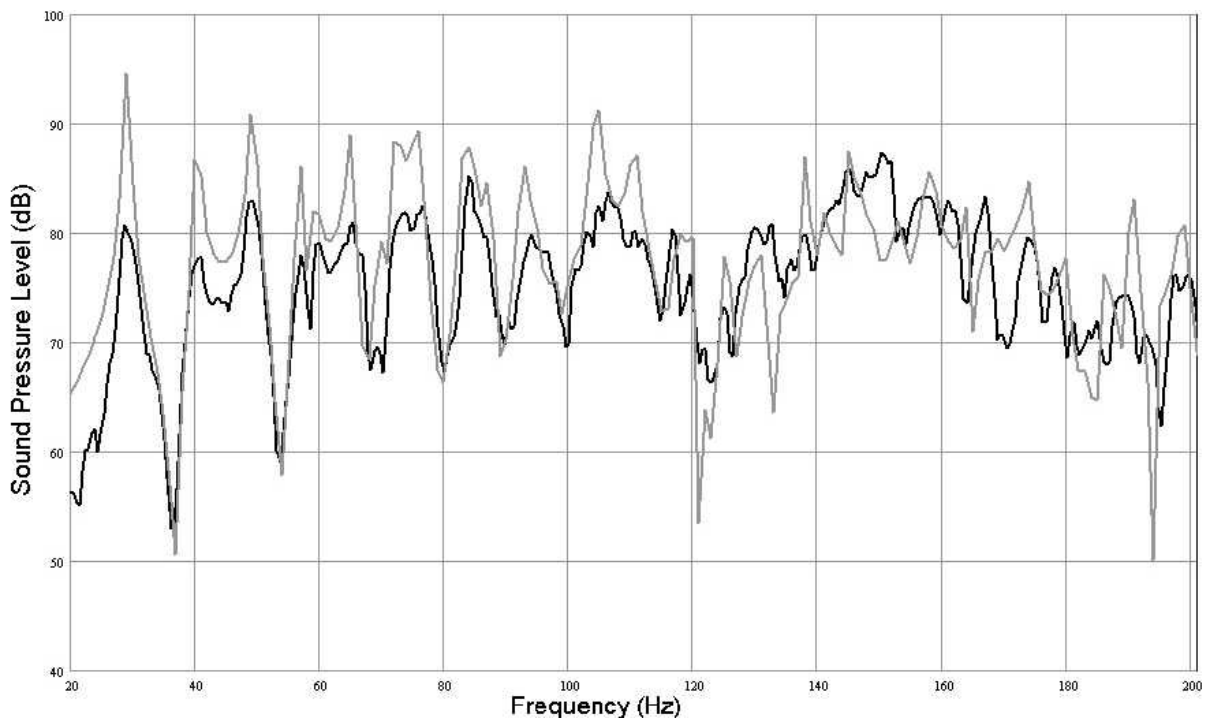


Figure 9.9 - Comparison between (—) measurement for the soft absorber and (---) prediction for the ‘Soft box-2’ model. Centre wall position results.

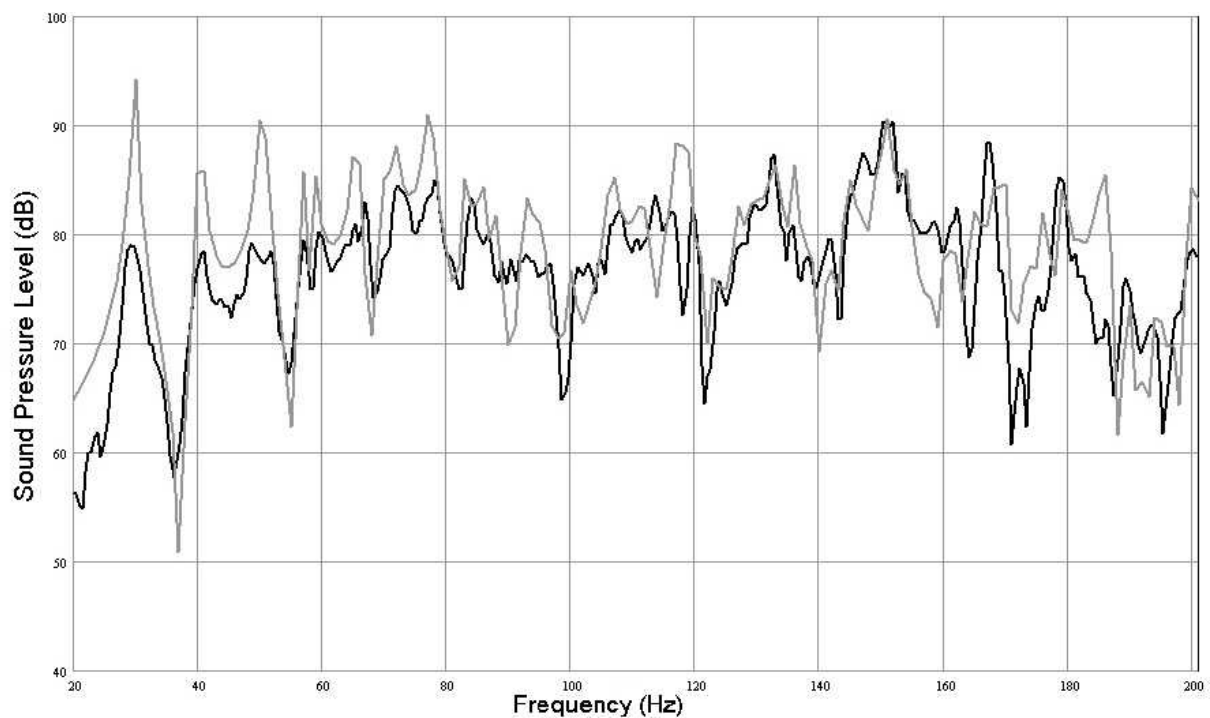


Figure 9.10 - Comparison between (—) measurement for the soft absorber and (---) prediction for the ‘Soft box-2’ model. Corner position results.

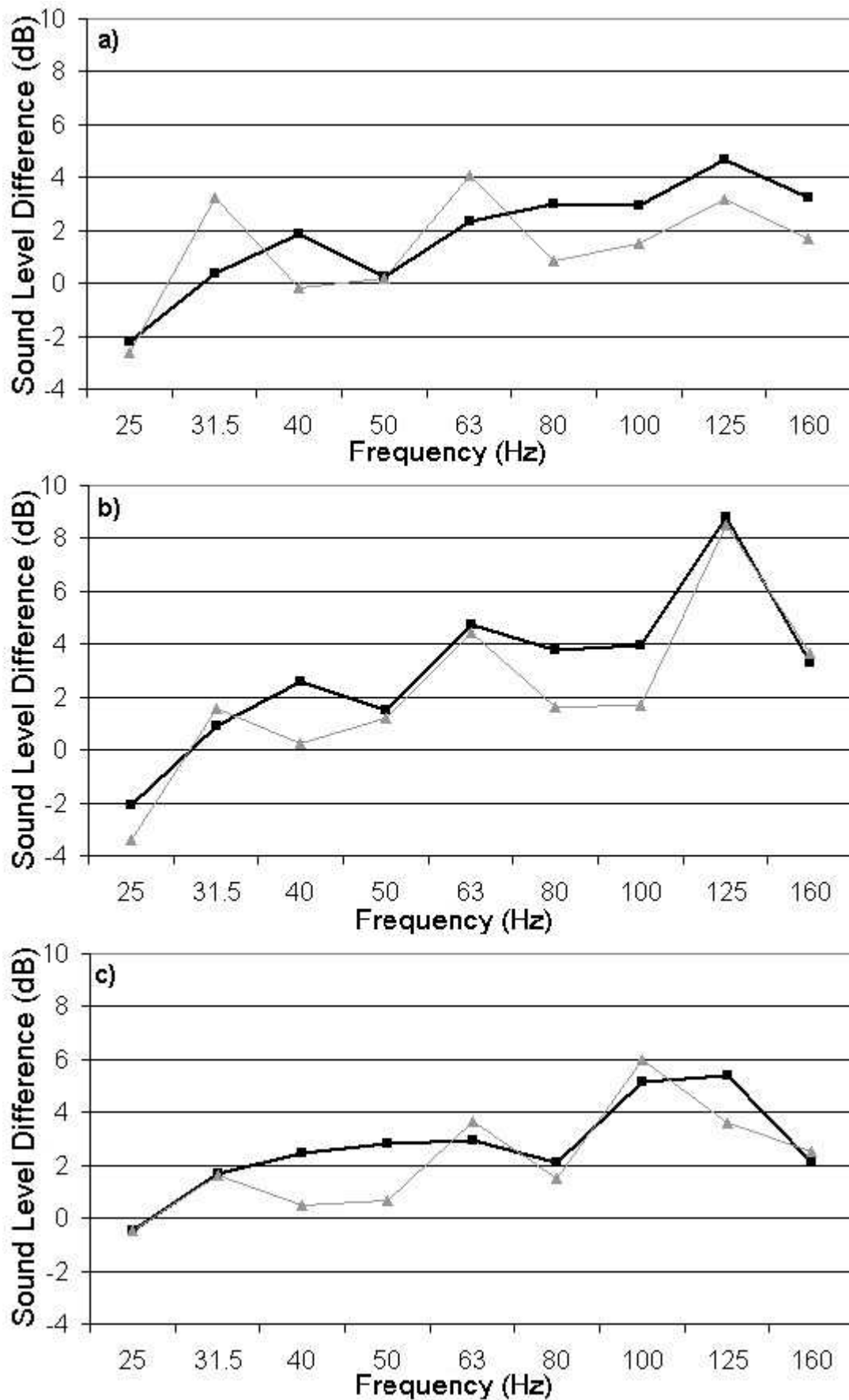


Figure 9.11 - Effect of ‘soft absorber’ shown as level differences in one-third octave bands, taking the empty room results as a reference. Comparison between (—■—) measured level difference and (---●---) predicted level difference. Soft box in a) central floor, b) centre wall, and c) corner position.

In the centre wall position (Fig. 9.11-b), the average level difference is 1 dB with a variation +2.5 dB to -2 dB. Above 50 Hz, the difference is on average 5 dB, with a variation +8 dB to +2 dB. Finally, in the corner position Fig. 9.11-c shows an average level difference of 2 dB with a variation +3 dB to -0.5 dB, but this time up to 80 Hz. Above this frequency the difference is on average 4 dB \pm 2 dB.

Analysis of the results of Fig. 9.11 also reveals that for the soft unit, the centre wall position was again the most influential (see Fig. 9.11-b), particularly in the 125 Hz third-octave band, with both measured and predicted level differences reaching a value of approximately 8.5 dB. While this behaviour was not evident in the covered unit results (see Section 8.6 for a discussion on the possible causes), here, where the standard unit was solely composed of foam, the same amount of absorptive material was always present within the room, making the effect of the standard unit location noticeable.

9.4 Summary

The measured and predicted FRFs for the soft absorber are very similar to those for the covered standard unit presented in Chapter 8. This is despite the fact that a thicker layer of sound absorption material (as in the case of the soft absorber) should provide increased sound absorption. In general, experimental and theoretical results indicated that there is an increase of the absorption coefficient as a function of the material thickness only up to a limiting depth, which seems to be about 150 mm for frequencies below 110 Hz. Above this frequency the material absorption characteristics seem to saturate, no matter how thick it may be. Thus, the approach used in this chapter was to simulate the soft unit also as a solid core with a known set of admittance values assigned to the solid surfaces. The set of admittance values, as a function of frequency, used here was the same one as described in Chapter 8, allowing once again a good agreement between experimental and numerical results.

Similarities between soft and covered unit results indicate that even when the standard unit was entirely constituted of foam, the sound waves were penetrating in this foam only up to a certain depth, depending on the frequency considered. The numerical results have shown an overall good agreement with measurements when the intermediary core size was used, up to 170 Hz. Above this frequency the largest core size provided the minimum discrepancies with measurements, indicating that

the sound was penetrating less in the absorber, as it could be expected at higher frequencies. Consequently, at low frequencies it is believed that real furniture will also, in general, behave as solid objects covered by a layer of absorption, no matter how soft it may be. This is the subject of the next chapter, and the effect of real furniture on room properties is then the final case considered.

9.5 References

BALVEDI, A. M. **Medição e simulação acústica de materiais porosos e sistemas multicamadas**. Master Dissertation, Federal University of Santa Catarina, Florianópolis, 1998.

GIBBS, B. M. **The inter-relation between the distribution of absorbent material amongst the room surfaces and the distribution of sound energy and reverberation times within the room**. Master Thesis, University of Sheffield, Sheffield, 1970.

HOROSHENKOV, K. V. Private communication, 2001.

SPIEGEL, M. R. **Mathematical handbook of formulas and tables**. McGraw-Hill, 1992.

ZWICKER, C., KOSTEN, C. W. **Sound absorbing materials**. Elsevier Publishing Co. Inc., 1947.

CHAPTER 10

ROOM CONTENTS AS REAL FURNITURE

10.1 Introduction

Up to now, the effect on the acoustic properties of an enclosure produced by an idealized element of furniture (the standard unit) has been investigated. Chapters 7, 8, and 9 dealt, respectively, with solid, covered and soft versions of the standard unit. In this chapter, an investigation of the effect on low frequency room response of including real furniture is described. A single element of furniture, a large armchair, also was introduced in the numerical model, using the knowledge developed during the standard unit investigations.

10.2 Armchair

The element of furniture used in this work was a large armchair as shown in Fig. 10.1. It was selected as being representative of traditional furnishing, particularly in British homes. Although not representative of furniture of other countries or of 'contemporary' tastes, it was assumed that its size and constituent materials represented an upper limit in unit absorption and scattering. Lighter and harder furniture would be expected to alter the frequency response of a room to lesser extent. The chair was constructed of a timber frame, with steel spring seat supports. The frame and springs were covered with dense fibrous material, which in turn, was covered with low density fibre padding and cushions. The covering was a thick-woven textile. The overall dimensions were 0.85 m x 0.85 m x 0.85 m.

10.2.1 Measurements

The experimental set-up used to measure room frequency responses in the presence of the armchair, positioned on the three different locations (centre of room floor, centre wall, and corner), was the same as described in Section 6.2.3 (see Fig. 6.3 and Table 6.3). Fig. 10.2-a shows the measured room frequency response in the presence of the armchair (central floor position) and the measured frequency

response of the empty room. In Fig. 10.2-b is shown the level difference between the empty room and the room with chair.



Figure 10.1 - Armchair used in the real furniture investigations.

Visual inspection indicates that the presence of the armchair within the room causes little change in the room frequency response, except at certain frequencies where selective damping of modes can be observed. For example the level difference is 11.5 dB at 127 Hz, 6.4 dB at 178 Hz and 10.7 dB at 195 Hz. The overall difference is on average 0 dB up to 110 Hz with a variation ± 5 dB. Between 110 Hz and 140 Hz the average level difference is of the order of 5 dB with a variation +11 dB to -2 dB. Above 140 Hz the average is again 0 dB with a variation +10 dB to -8 dB. However, no significant eigenfrequency shift was observed. This supports the observations made by Kihlman et al (1994) in an investigation of the influence of furniture in room frequency responses, but where it was stated that with significantly more and heavier furniture, the eigenfrequencies might be affected at low

frequencies. This corroborates the findings of Chapters 7, 8 and 9, in which the investigation for the standard unit revealed eigenfrequency shifts at frequencies as low as 50 Hz.

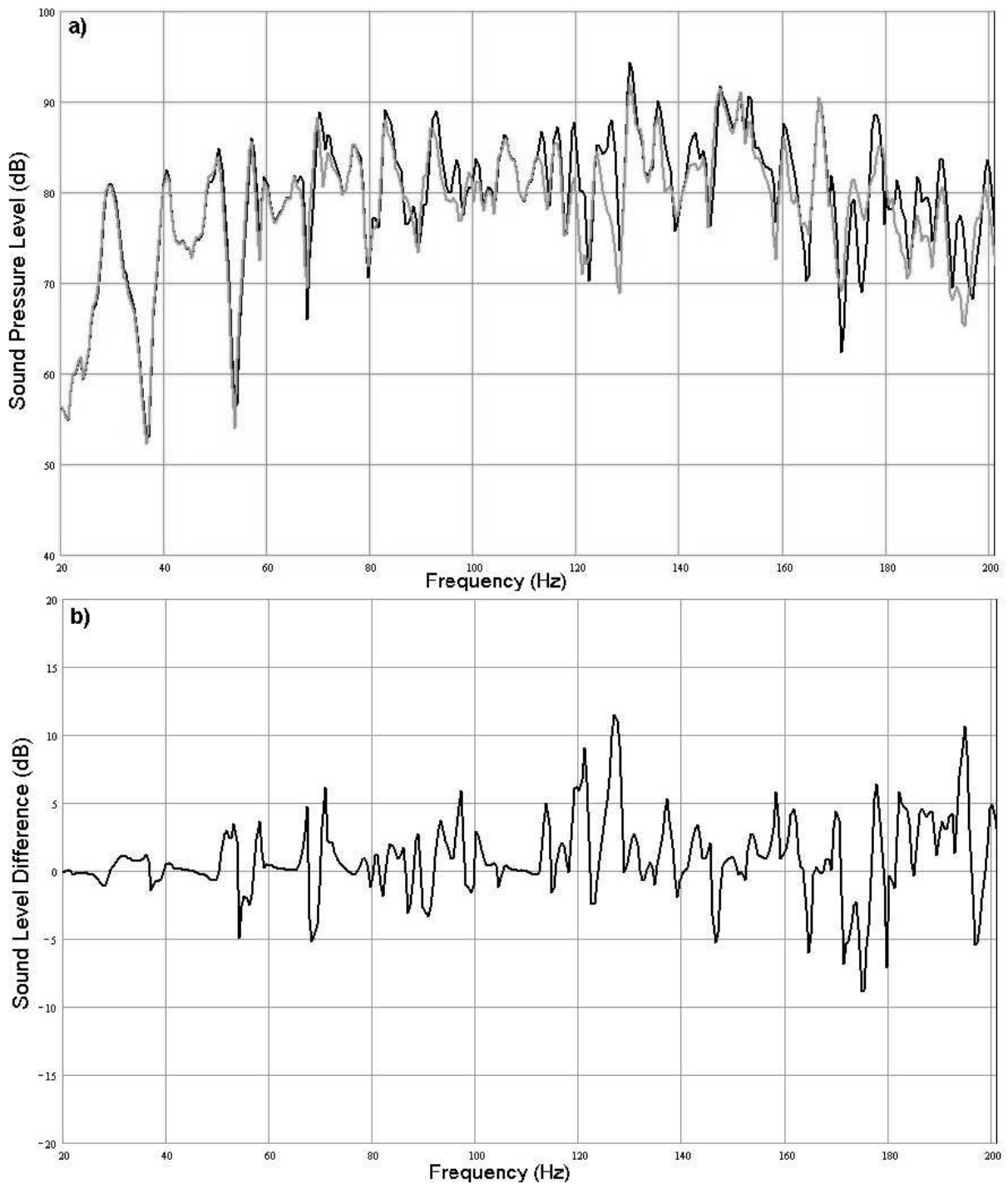


Figure 10.2 - a) Comparison between frequency response measurements for (—) empty room and (---) room with the armchair at central floor position. b) Level difference between the two FRFs.

Figs. 10.3 (a and b) and 10.4 (a and b) show measured frequency response functions for the case of the armchair placed at the centre wall and corner position,

respectively. For these positions it is possible to see that, although no eigenfrequency shift was observed, as in the central floor results (Fig. 10.2), here the absorption is more effective.

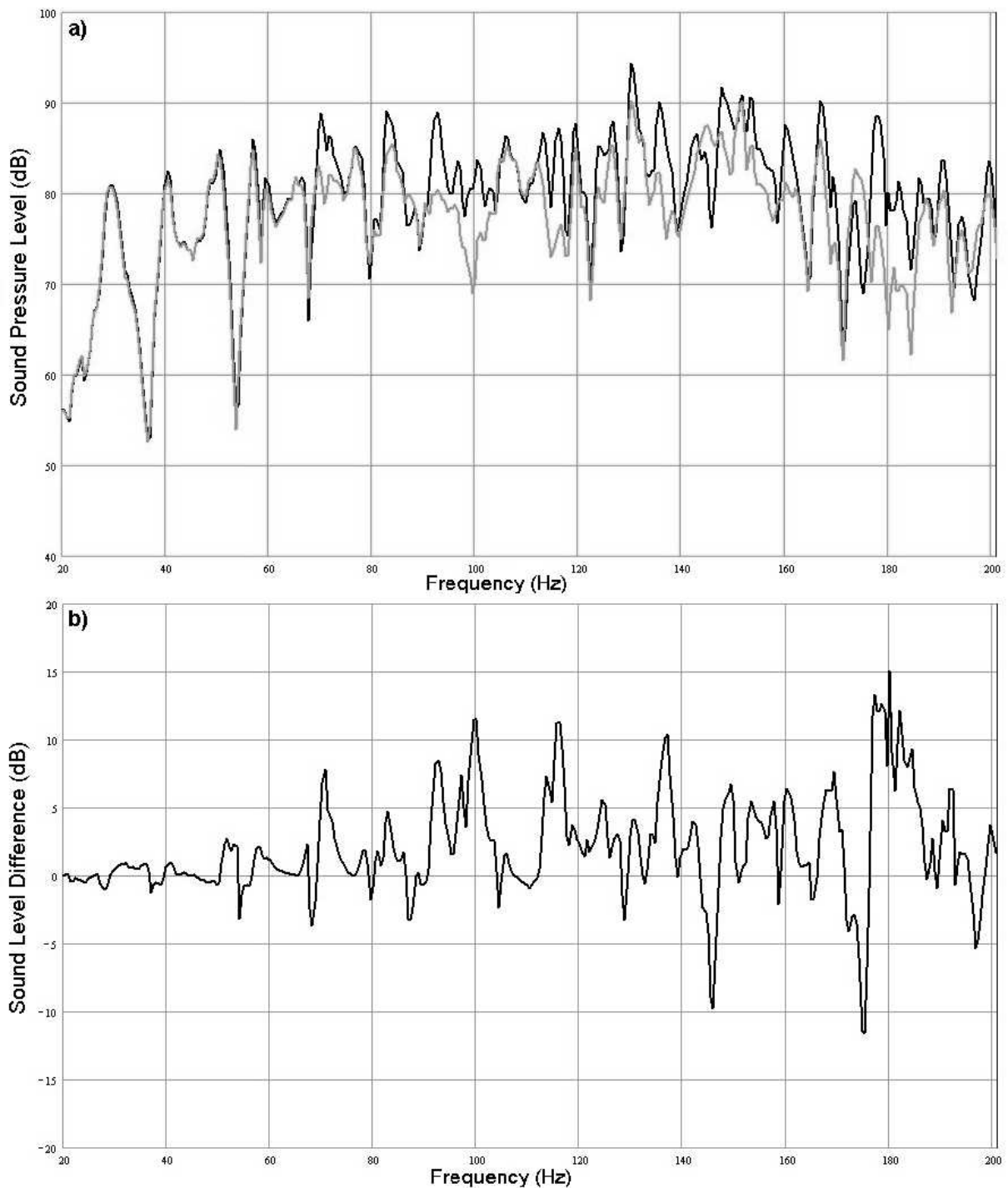


Figure 10.3 - a) Comparison between frequency response measurements for (—) empty room and (—) room with the armchair at centre wall position. b) Level difference between the two FRFs.

As shown in Fig. 10.3-b, for the centre wall case, the average level difference is 0 dB \pm 3 dB up to 68 Hz. Between 68 Hz and 140 Hz the overall difference is on

average 5 dB with a variation +11.5 dB to -3 dB. Above this frequency, the average level difference is of the order of 0 dB, but with a variation +15 dB to -11.5 dB. For the chair in the corner position Fig. 10.4-b shows similar results to those for the centre wall case up to 140 Hz. Above this frequency, however, the average difference is of the order of 5 dB with a variation +15 dB to -9 dB.

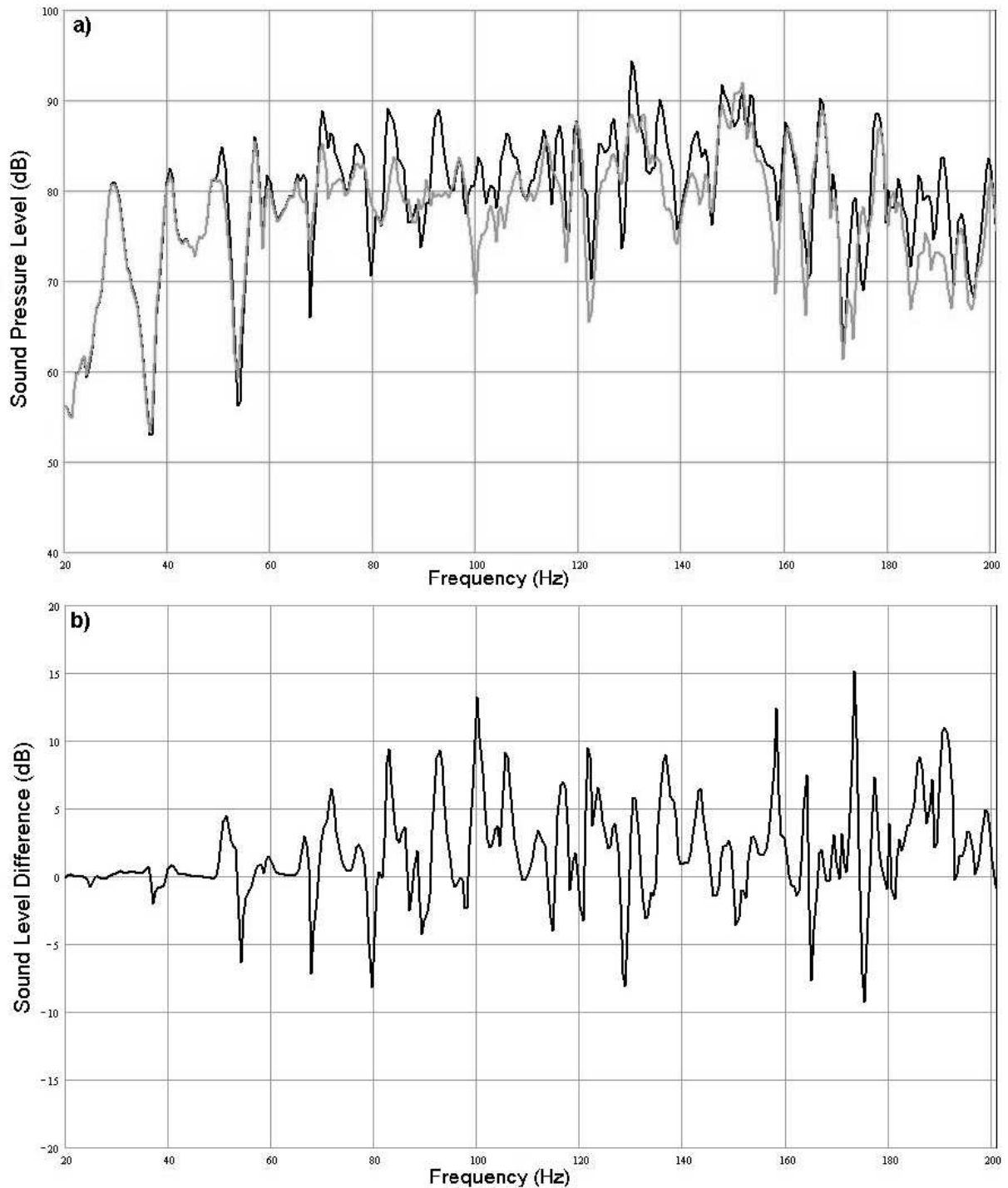


Figure 10.4 - a) Comparison between frequency response measurements for (—) empty room and (---) room with the armchair in the corner position. b) Level difference between the two FRFs.

10.2.2 Numerical model

The procedure for numerically modelling the effect of introducing real furniture was similar to that adopted for the standard unit. Again, it used as a reference the developed FE room model, which had been proven to predict the response of the empty room in detail (see Chapter 6).

The preliminary measurements indicated a small change in response on introducing the chair, particularly below 100 Hz. This has practical significance. If furniture does not have a significant effect in this frequency region then it need not be included as a correction to the measured sound level difference between rooms (see Chapter 1). In this investigation, it also allows a less refined model of absorption than described in chapter 9 for the standard unit.

Two consecutive efforts were made in creating a model of the armchair to be included in the room model. Initially, the investigation aimed to indicate the geometry that should be adopted for the armchair model. Then, a parametric survey was carried out where different admittance values were assigned to the boundaries of the selected chair model, in order to provide the best fit with measured frequency response.

The armchair was first modelled as a cube of volume 0.84 m x 0.84 m x 0.84 m, as it was assumed that for the frequency range of interest (20 Hz to 200 Hz) the sound field would not be (in principle) sensitive to the armchair geometry details. Admittance boundary conditions were prescribed at the box surfaces to take absorption effects into account. As for the case in the previously discussed models for the standard unit (see Chapter 9), sound transmission through the modelled armchair was not included. This contradicts an approach by Estorff and Karstedt (2000) in a study of numerical representation of vehicle seats, where it was assumed that the transmission of sound waves through the seats had a significant effect on the sound pressure distribution in a car [Estorff and Karstedt (2000)]. However, while this may be the case at higher frequencies (that work considered frequencies up to 600 Hz) and for smaller enclosures such as a car cabin, this was not observed during the investigations for the standard unit (see Chapters 7, 8, and 9), and, consequently, the same approach utilised previously was used in the investigation of real furniture.

The first model, 'Chair-1', included a frequency independent absorption coefficient of 2% for the room surfaces. For the box surfaces a constant absorption coefficient of 50% was initially selected as being representative of the armchair absorption characteristics from 20 Hz to 200 Hz. Using the measured and predicted empty room results as a reference (see Chapter 6), the respective measured and predicted level differences were obtained and compared, as shown in Fig. 10.5. The signatures of the predicted and measured level differences are similar, although the numerical model is overestimating the measured values.

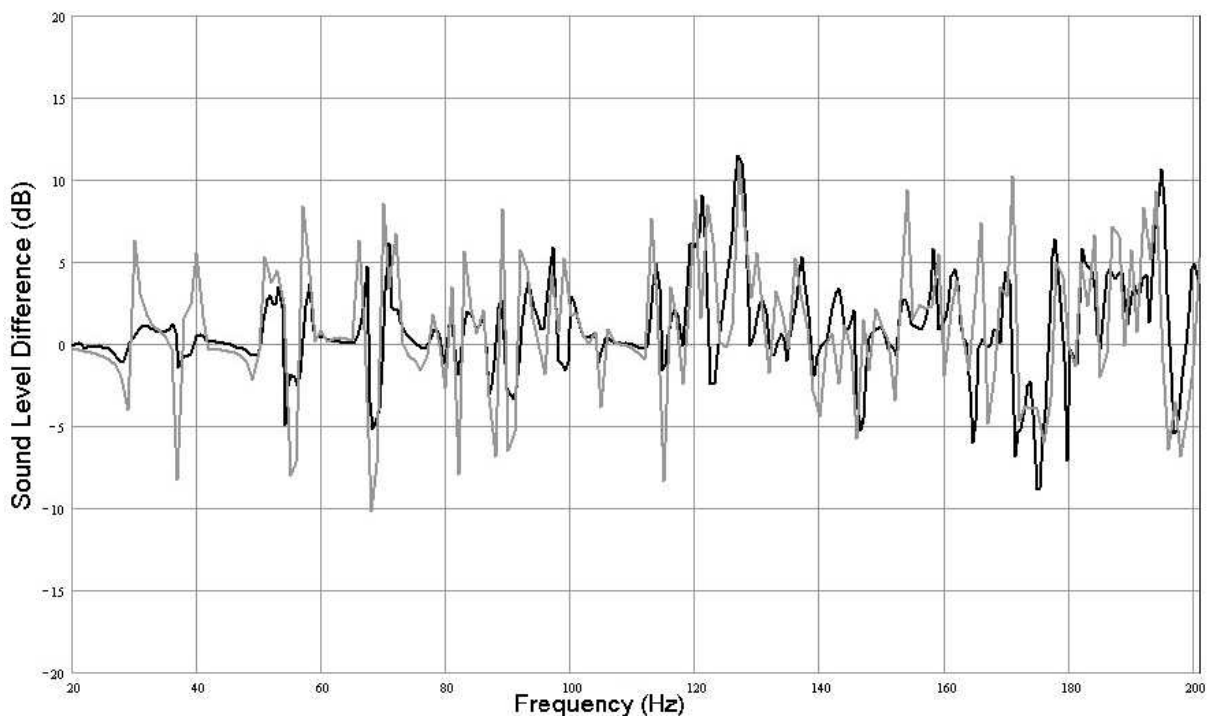


Figure 10.5 - Armchair at central floor position results. Comparison between (—) measured and (---) predicted level differences for the 'Chair-1' model, taking the empty room results as a reference.

A second model of the armchair (Chair-2) included more detail of the geometry and was introduced in the room numerical model, also at the central floor position (see Fig. 10.6). Again, a simple constant absorption coefficient of 2% was applied to the room internal surfaces, while a value of 50% was assigned to the chair surfaces. The results, also expressed as level differences, are shown in Fig. 10.7. Additionally, Fig. 10.8 presents level differences in 1/12th octave bands between predictions for Chair-1 and Chair-2 model, and measurement. The observed average level difference for both plots is of the order of -3 dB with a variation -9.5 dB to 2 dB up to 60 Hz. Above this frequency the level difference is on average 0 dB \pm 5 dB. Although both models presented similar characteristics over the frequency range, the overall agreement between prediction and measurement is slightly improved in the case of

the Chair-2 model, and this model was adopted in predicting the effects of the armchair on the room frequency response.

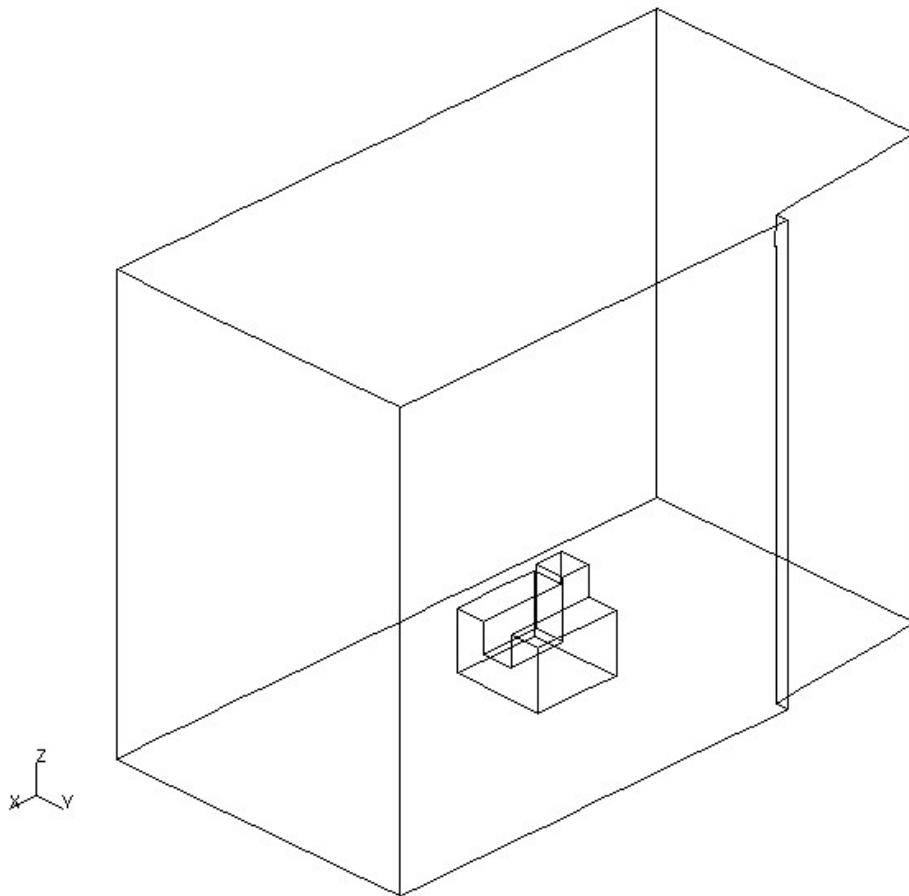


Figure 10.6 - Armchair at central floor position represented by the Chair-2 model.

Having selected the chair model, a parametric survey was performed by prescribing different values of pure real admittance to the chair surfaces in the numerical model, corresponding to frequency invariant absorption coefficients of 30%, 50%, and 70%. The results were obtained for the chair placed at the centre wall position. Fig. 10.9 presents level differences obtained in $1/12^{\text{th}}$ octave bands between measurement and predictions for Chair-2 model with $\alpha = 30\%$, $\alpha = 50\%$ and $\alpha = 70\%$ assigned to the chair boundaries, respectively. The figure shows that, despite a variation in α , the level difference was not significantly altered over the observed frequency range, particularly up to 37 Hz. Above this frequency, the results still presented strong similarities with a variation not larger than 4 dB (at 140 Hz) between the two extreme cases. In general the parametric survey indicates that the chair absorption is playing no significant role in modifying the room frequency response, and the intermediary absorption coefficient of 50% assigned to the chair boundaries was adopted in the investigation of the effect of the armchair on the reference FRF.

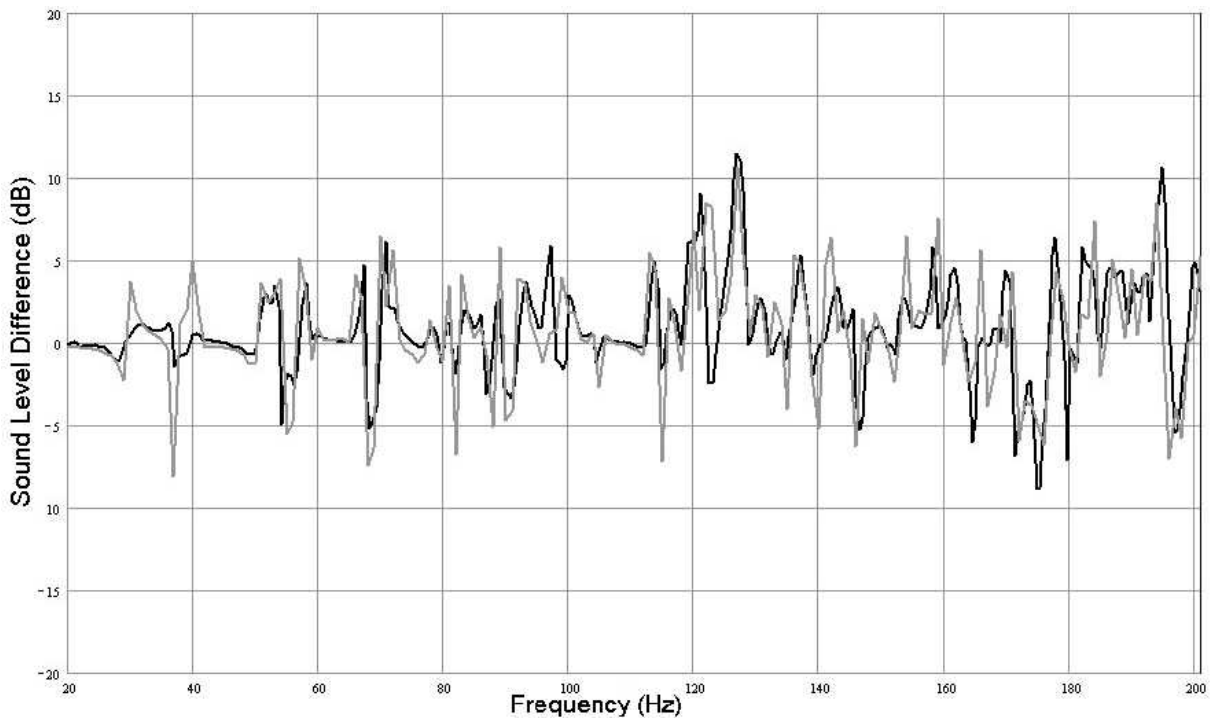


Figure 10.7 - Armchair at central floor position results. Comparison between (—) measured and (---) predicted level differences for the 'Chair-2' model.

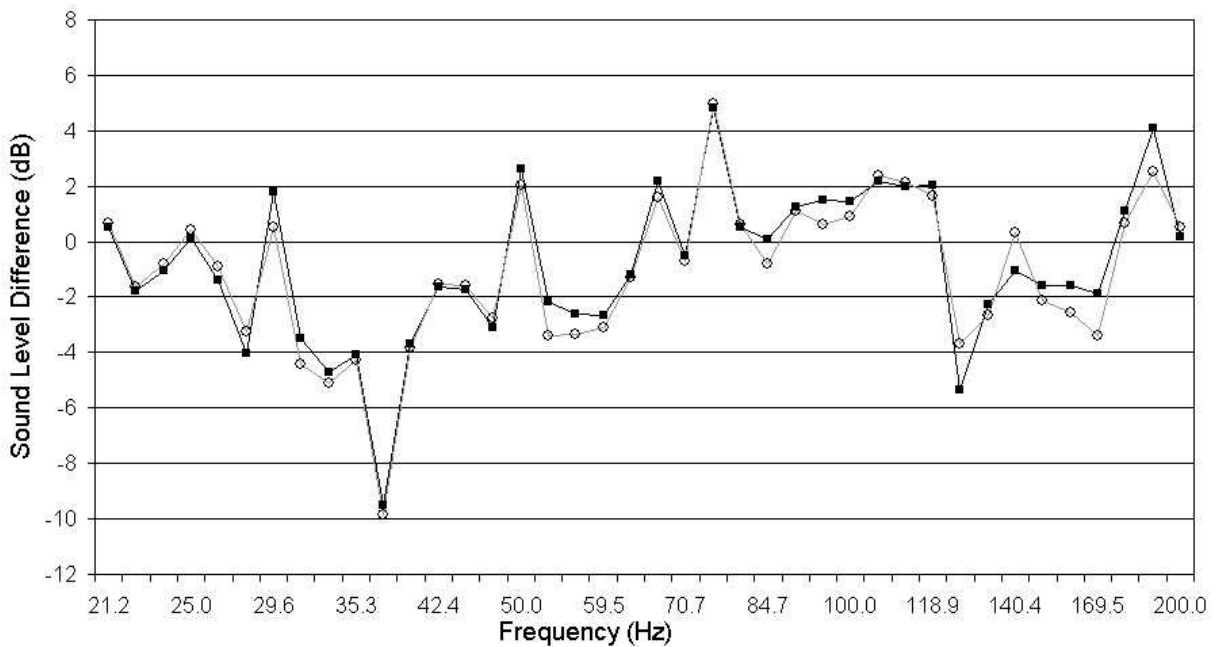


Figure 10.8 - Level differences between measurement and prediction of room with armchair in the centre of the room floor. (—○—) Chair-1 model, and (—■—) Chair-2 model.

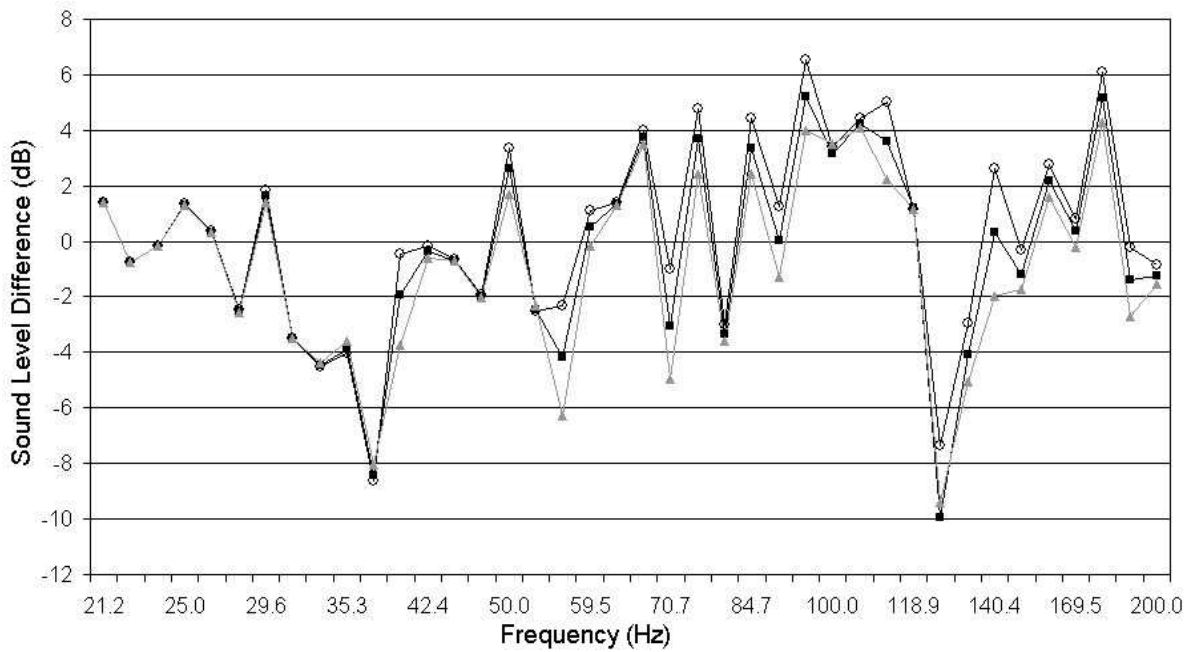


Figure 10.9 - Level differences between measurement and prediction of Chair-2 model at centre wall position. (—○—) $\alpha = 30\%$, (—■—) $\alpha = 50\%$, and (—▲—) $\alpha = 70\%$.

10.3 Results

Figs. 10.10, 10.11, and 10.12 present the level difference (measurement and prediction) in $1/12^{\text{th}}$ octave bands for the armchair placed within the room at central floor, centre wall, and corner positions, respectively.

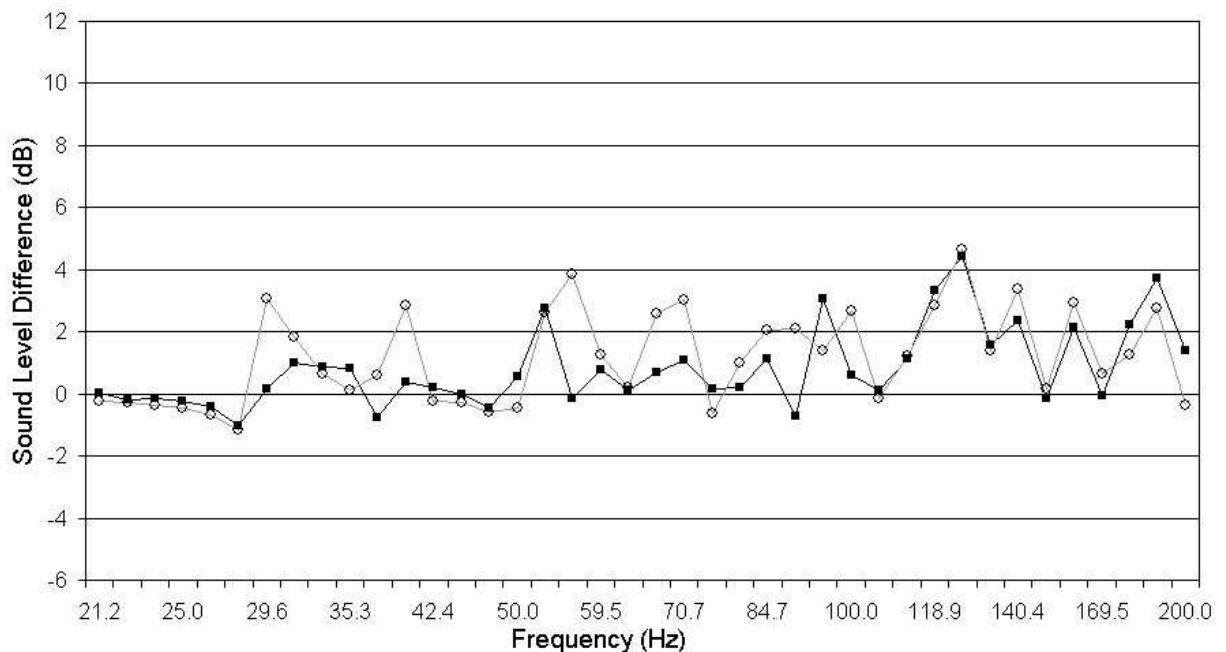


Figure 10.10 - Results for the armchair in the centre of the room floor: comparison between (—■—) measured and (—○—) predicted level differences in $1/12^{\text{th}}$ octave bands.

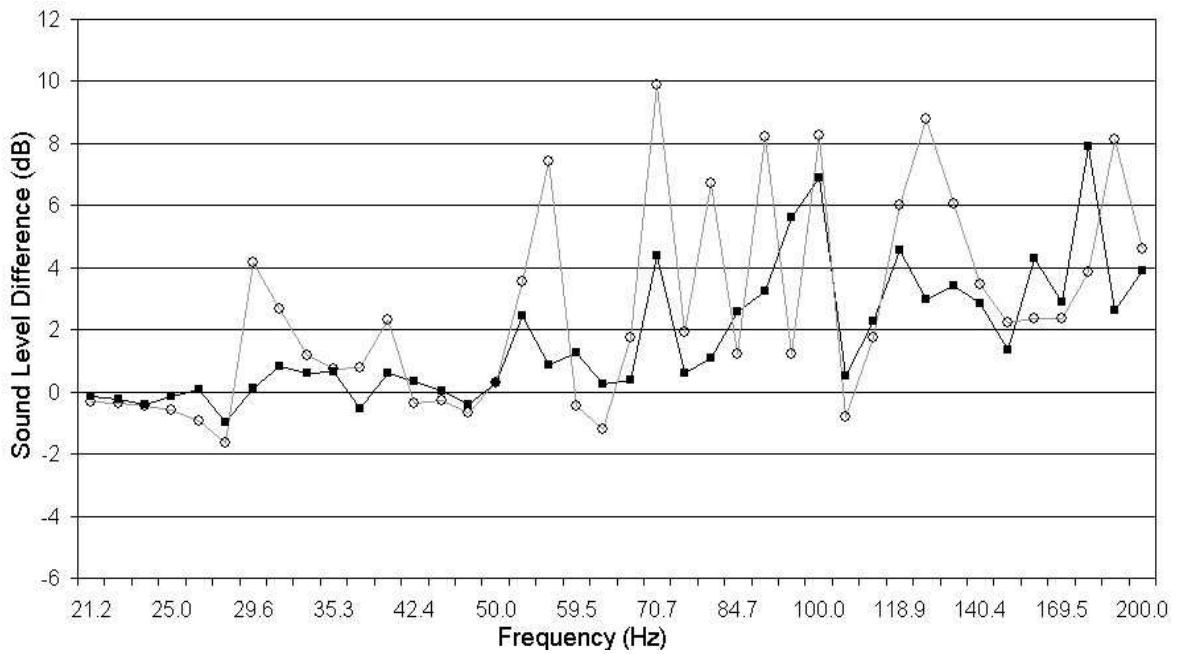


Figure 10.11 - Results for the armchair in the centre wall position: comparison between (—■—) measured and (—○—) predicted level differences in 1/12th octave bands.

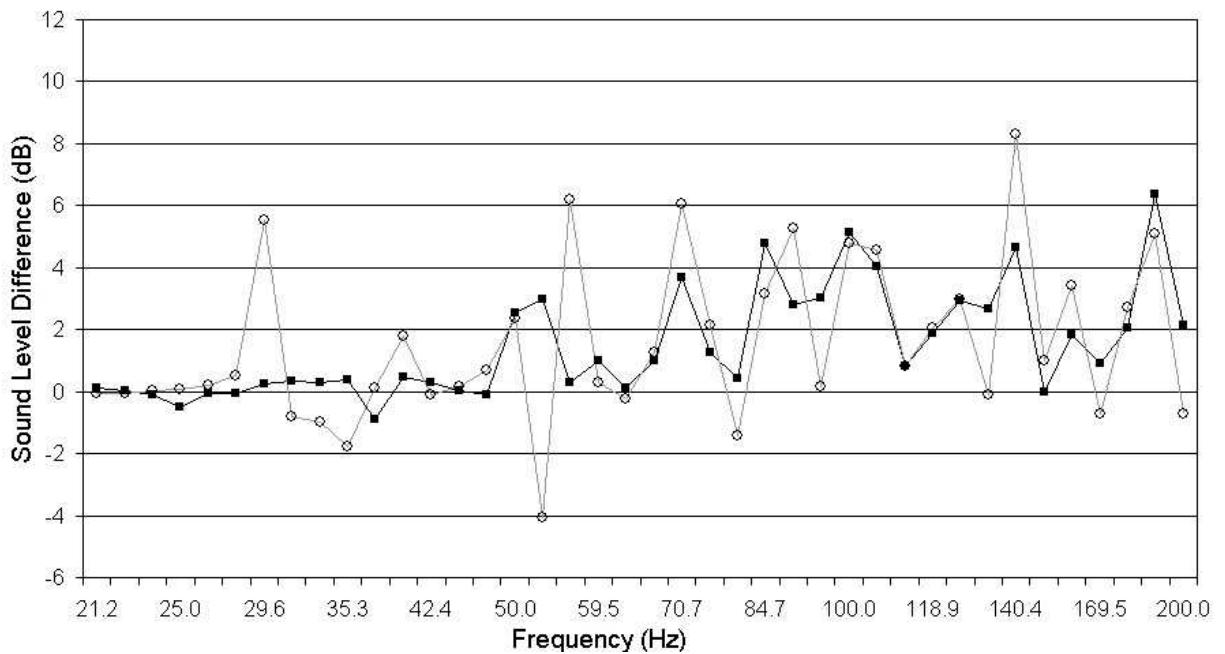


Figure 10.12 - Results for the armchair in the corner position: comparison between (—■—) measured and (—○—) predicted level differences in 1/12th octave bands.

For the armchair at the central floor position (Fig. 10.10) both measured and predicted levels indicate that below 90 Hz the presence of the armchair has no significant effect on the room frequency response (considering the empty room results as a reference). For such interval the average level difference is 0 dB ±1 dB. Above 90 Hz, the measured level difference presents a mean value of approximately 2 dB with a variation 0 dB to +5 dB. The predicted level difference did not present

similar behaviour below 90 Hz, overestimating measurements by 2 dB on average. Above 90 Hz the numerical results matched measurements.

The one-twelfth octave band results for the armchair in the centre wall position (Fig. 10.11) indicate an average level difference of 0 dB \pm 1 dB below 66 Hz. Above this frequency, the measured level difference is on average 3 dB with a variation 0 dB to +8 dB, whereas the predicted level difference is on average 4 dB with a variation -1 dB to +10 dB. The results for the armchair in the corner position (Fig. 10.12) show that the room response is altered above 50 Hz by an average value of 2 dB with a variation 0 dB to +6 dB for the measured level difference. In general, the predicted level difference was observed to match measurements.

Fig. 10.13 shows the effect of the armchair on the reference FRF, this time in one-third octave bands. The measured level differences to this resolution are on average 0 dB up to 63 Hz, 50 Hz, and 40 Hz for the chair placed in the central floor (Fig. 10.13-a), centre wall (Fig. 10.13-b), and corner position (Fig. 10.13-c), respectively. Fig. 10.13-a shows that above 63 Hz the average difference is 1.5 dB with a variation +1 dB to +2 dB when the armchair was centrally located. For the centre wall position, Fig. 10.13-b shows that above 50 Hz the average difference is 2.5 dB with a variation +2 dB to +4 dB. Fig. 10.13-c shows that when the chair was located in a room corner the average difference is of the order of 2 dB with a variation +1 dB to +3.5 dB. Independently of the chair position, the agreement between predicted and measured level differences was observed to improve with increasing frequency, and one possible reason for the observed discrepancies below 80 Hz is the used approach, in which a frequency invariant absorption coefficient of 50% was assigned to the chair boundaries. While such value may be representative of the chair absorption at frequencies above 100 Hz, it is likely to overestimate the absorption process at lower frequencies.

10.4 Summary

In this chapter a description is given of an investigation of the effect of a real element of furniture on room frequency responses. From the previous investigations described in Chapters 7, 8, and 9, it was assumed initially that, at low frequencies, real furniture would in general behave as solid objects covered by a layer of absorption.

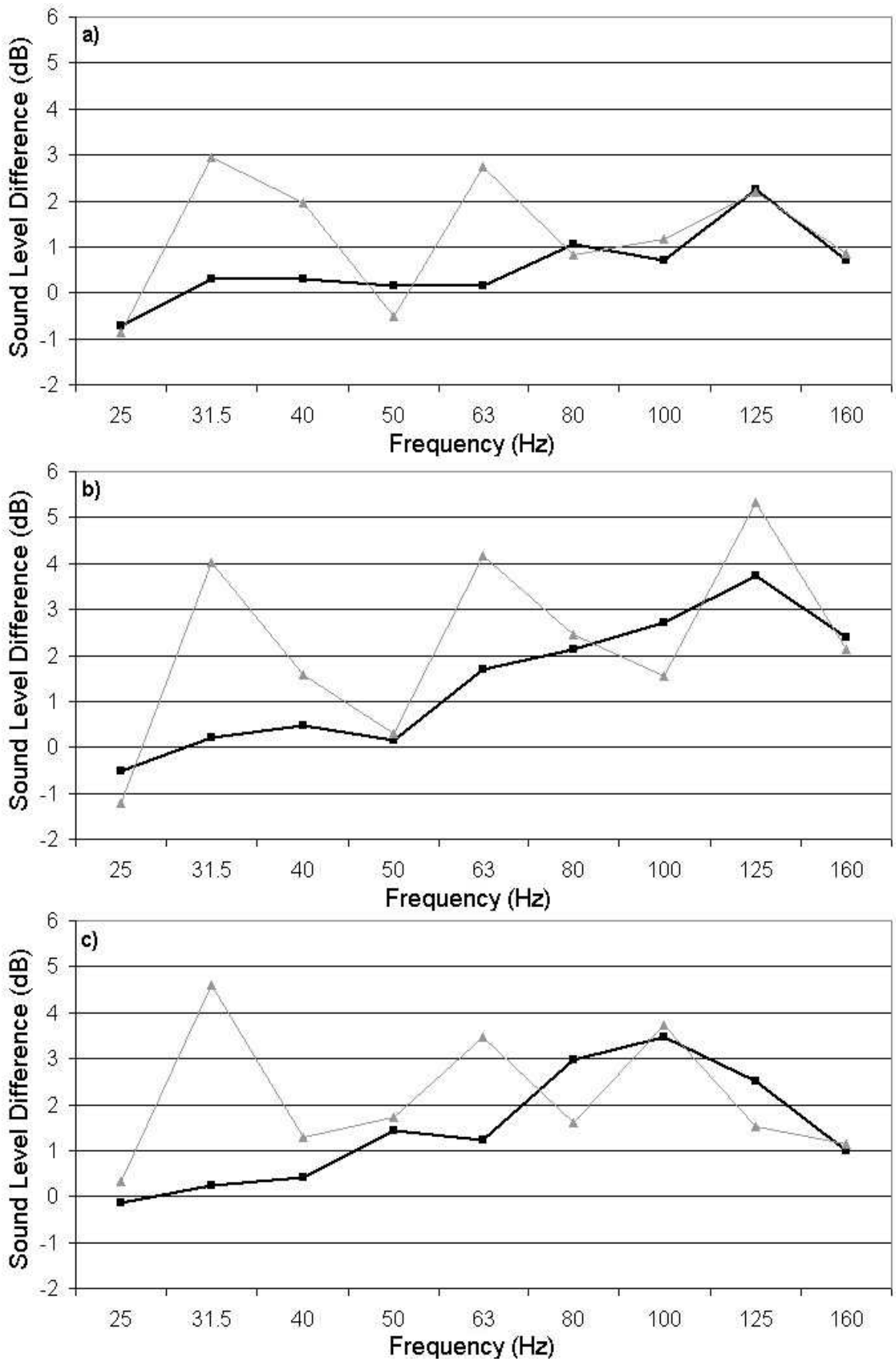


Figure 10.13 - Level difference (—■—) between measured values and (---▲---) between predicted values. Results shown in one-third octave bands. a) Central floor position, b) centre wall position, and c) corner position.

However, experimental results presented in this chapter indicate that the introduction of an armchair at different positions within a reference room does not significantly alter the room frequency response. This was also confirmed by numerical results, where a parametric survey showed that similar FRFs are obtained, even though the boundary absorption characteristics of the modelled chair were increased up to 117% of the initial value. Thus, a detailed modelling of an absorptive element of furniture within an enclosure is not justified. Also, independently of the armchair position, no significant eigenfrequency shift was observed in the results. However, as found for the investigations with the standard unit (see Chapters 7, 8, and 9), the centre wall position was found to be, once again, the most influential, despite the overall small effect.

Because of the small measured effect of the introducing chair, it was not necessary to use the refined model of furniture absorption, described in chapter 9. However, the refined model is available for rooms of large volume and more furniture such as in commercial situations.

10.5 References

ESTORFF, O., KARSTEDT, W. **Representation of seats in numerical models for vehicle acoustics**. Rieter Automotive Systems, 1999.

KIHLMAN, T., KROPP, W., PIETRZYK, A. **Sound insulation at low frequencies**. 1994.

CHAPTER 11

CONCLUDING REMARKS

11.1 Introduction

The general objective of the thesis work was to characterise room absorption at low frequencies. In particular, the sound absorption at room surfaces and that due to room contents such as furniture was to be assessed with respect to their effect on steady-state sound level and therefore on sound level difference between rooms.

The specific objectives of the thesis work were to:

- Develop a model of surface absorption appropriate for a modal description of contained sound fields at low frequencies.
- Develop a model of contents absorption for the same modal description.
- Investigate experimentally, theoretically and numerically the effect of contents such as furniture on the frequency response of small rooms at low frequencies.

A FEM model was developed to describe the relationship between the sound absorption characteristics of the internal surfaces of an enclosure, and its frequency response, for the frequency range from 20 Hz to 200 Hz. The developed numerical models were validated by comparison with experimental results for a small reverberant chamber. In addition, the effect of inserting absorbent furniture was considered. The effect of furniture location was also investigated.

11.2 Conclusions

1. Prior to the investigation, various analytical and numerical approaches were considered. The Finite Element Method was selected as the most appropriate for modelling the frequency response of a room. It is better suited than the Boundary Element Method for the determination of natural frequencies and mode shapes of cavities. It is able to deal with non-

rectangular geometries and uneven distribution of absorption, unlike analytical models.

2. A preliminary FEM model was developed of an empty rectangular test room, which did not involve excessive computer processing time and storage. The computed eigenfrequencies agreed with analytical values within 0.05% in the frequency range of interest (20-200 Hz).
3. It has been demonstrated that in modelling rooms there is a need to account for even small irregularities in the room geometry.
4. Measurement of room wall vibrational behaviour shows that these vibrations contribute to the whole room absorption mechanism at very low frequencies. A parametric survey was conducted where surface admittance was varied to give a best agreement between predicted and measured frequency response. It is shown that a local reaction need only be assumed and an equivalent value of absorption coefficient of 2% gave the best agreement for heavy masonry walls. The resultant predicted FRFs agreed with measurement within 2 dB \pm 5 dB.
5. The influence of furniture on low frequency room response was investigated by first considering a solid standard unit of dimensions $l_x = 1.53$ m, $l_y = 0.88$ m, and $l_z = 0.75$ m. The results obtained for the empty test room were used as a reference. For each location of the standard unit, eigenfrequency shifts and selective modal damping were observed throughout the frequency range of interest. Preliminary simulations were performed using different values of surface absorption coefficient (2%, 5%, and 20%) applied to the box surfaces, and showed practically identical results. Thus, it was decided to employ the simplest of these configurations, and the standard unit was modelled as a change in room geometry with a surface absorption equal to that of the other room surfaces. The agreement between predicted and measured frequency response was within 2 dB with a variation \pm 3 dB up to 160 Hz.
6. It has been shown that when a large solid item is introduced into the room, there is little effect on the room frequency response for frequencies below 50 Hz. This corresponds to a ratio of wavelength to largest obstacle dimension of 4.5. This is despite the fact that the first three normal room modes occur in

this frequency range. This insensitivity was observed regardless of location of the obstacle.

7. Above 50 Hz, the effect of including a solid item within the enclosure is more pronounced. In addition, the influence of location becomes apparent. Obstacles placed along a wall or in room corners will produce a higher change in room response, if compared with a central location. Furthermore, the eigenfrequency shifts are the principal reason for the observed changes in the room responses. The obstacle surface absorption characteristics causes little change in the room frequency response (at most 5 dB at 125 Hz third octave band) and need not to be taken into account.
8. Measurements and numerical simulations were repeated for the standard unit, covered with 150 mm of foam having a known sound absorption coefficient. An analysis of the results has confirmed the greater effect the lined standard unit has on room responses, when compared with the uncovered case. The results confirmed two controlling factors: the ratio of wavelength to absorbent thickness plus obstacle size, and the onset of tangential and oblique room modes. Both are frequency dependant but only the second is room dependant.
9. With respect to the first factor, the results for the covered unit are consistent with those for the solid standard unit in that room obstacles can be assumed 'transparent' to sound if the wavelength:obstacle ratio is greater than 4.5. This was the case for the standard unit below 50 Hz where the average change in FRF is of the order of 2 dB. Similarly, consideration of the results for the 150 mm foam when covering the floor indicate little influence on FRF below 71 Hz. It can be expected therefore that the effect of covering the obstacle with 150 mm foam will have little effect below 50 Hz and this was confirmed experimentally.
10. With respect to the second factor, surface and obstacle absorption might be expected to have an enhanced effect with the onset of tangential and oblique room modes (except for the case when a covered surface is perpendicular to an axial mode). The reference room displayed an onset of tangential modes at approximately 49 Hz, which corresponds to the onset of effectiveness of the obstacle and/or absorber. This has practical implications. Dwelling rooms

typically are of smaller dimensions than the reference room used in this investigation, and the modal density below 100 Hz will be less. In particular, tangential modes will onset at frequencies higher than 80 Hz and obstruction absorption effects may be negligible below 100 Hz. Future standards that are required to measure in the frequency range 50 –100 Hz therefore may be simplified since absorption (measured as reverberation time, for example) need not to be considered.

11. The measured and predicted FRFs for the soft absorber are very similar to those for the covered standard unit. In general, experimental and theoretical results indicated that there is an increase of the absorption coefficient as a function of the material thickness only up to a limiting depth, which seems to be about 150 mm for frequencies below 110 Hz. Above this value the material absorption characteristics seem to saturate, no matter how thick it may be.
12. Numerical results have shown an overall good agreement with measurements when the intermediary core size (1.40 m x 0.84 m x 0.84 m) was used, up to 170 Hz. Above this frequency the largest core size (1.68 m x 1.12 m x 1.12 m) provided the minimum discrepancies with measurements, indicating that the sound was penetrating less in the absorber, as would be expected at higher frequencies.
13. The effect of the soft unit on the reference FRF was at most 8.5 dB at 125 Hz. At frequencies lower than 50 Hz there was no significant effect on the reference room frequency response, and the obstacle may be simply neglected in the room model, without incurring in large errors.
14. Experimental results indicate that the introduction of an armchair at different positions within a reference room does not significantly alter the room frequency response (at most 3.7 dB at 125 Hz). This was also confirmed by numerical results, where a parametric survey showed that practically unaltered FRFs are obtained, even though the absorption characteristics of the modelled chair were increased. Thus, a detailed modelling of an absorptive element of furniture within an enclosure is not justified.
15. Though not shown here, numerical simulations considering obstacles occupying an entire room dimension have shown large effects on room

frequency responses, even at very low frequencies. This will be the case in small enclosures such as a car cabin, airplanes, or even ducts with blockages. This situation may be also representative of enclosures having columns or similar obstacles inside it. In these cases, larger eigenfrequency shifts may be expected when compared to those presented in this work. An example of that was provided by the change in angle at the door position of the investigated room, which proved to be very influential in correctly modelling the latter, despite of being a small perturbation in the room geometry.

11.3 Topics for further research

Based on previous considerations, the present work may be complemented and further developed. The suggested topics for future research are to:

- Model the absorption material as bulk modulus, and not only as superficial impedance value. This would allow the angular sound incidence to be taken into account. However, it would require measurements of material properties, such as flow resistance, and tortuosity.
- Investigate rooms also of lightweight construction, which are representative of modern buildings. Such rooms are likely to have modally reactive boundaries, and should be fully modelled using the theory of boundaries of extended reaction, introduced in Chapter 5.
- Obtain field measurements of sound transmission at low frequencies of ‘typical’ Brazilian dwellings and compare the results with those on the literature, in order to establish general trends.
- Establish criteria and recommendations, regarding sound transmission of Brazilian buildings, for the local authorities.
- Investigate the effect of flanking transmission on the sound transmission between rooms.

APPENDIX

PUBLISHED PAPER

A FINITE ELEMENT MODEL OF SOUND ABSORPTION AT LOW FREQUENCIES

Gustavo da S. V. de Melo^{*}, Barry M. Gibbs^{*}, and Samir N. Y. Gerges[†]

^{*} Acoustics Research Unit (ARU)
School of Architecture & Building Engineering
The University of Liverpool
P.O. BOX 147, L69 3BX Liverpool, England
e-mail: g.melo@liv.ac.uk, web page: <http://www.liv.ac.uk/abe/aru/index.htm>

[†] Acoustics and Vibration Laboratory (LVA)
Mechanical Engineering Department
Federal University of Santa Catarina
Cx.P. 476, Florianópolis-SC, Brazil
e-mail: gerges@mbox1.ufsc.br, web page: <http://www.gva.ufsc.br>

Key words: Finite Elements, Low Frequencies, Room Acoustics, Sound Absorption.

Abstract. *It is recognised that low frequency (below 100Hz) sound transmission into and between dwellings is an increasing contribution to nuisance. This is due to a proliferation of hi-fi systems of high power and enhanced bass response, increased use of domestic mechanical services and devices, and increasing traffic noise break-in. A Finite element (FE) model of the sound transmission between dwellings has been developed which demonstrates the modal characteristics of the pressure and vibration fields of the rooms and separating wall, respectively. The work has highlighted the need for an appropriate model of sound absorption in small furnished rooms at low frequencies. In this paper, a new FE model is used to describe the relationship between the sound absorption characteristics of the internal surfaces of an enclosure, and its frequency response, for the frequency range below 200Hz. In addition, the effect of furniture as solid obstacles is explored, in order to check for eigenmode shifts and selective damping of modes. The effect of furniture location is also investigated.*

1 INTRODUCTION

In the area of sound transmission in buildings, a recent emphasis has been given to the study of the audible frequencies below 100 Hz. This is due to the increase in sources of low frequency noise, e.g., proliferation in hi-fi systems of high power and enhanced bass response, increased use of mechanical services and devices, and increasing traffic noise break-in.

A review of the main low frequency noise sources can be found in the work of Berglund et al.¹ There is a special concern about low frequency noise because of its efficient propagation in air, and because of the reduced ability of structures such as hearing protectors or separating walls to attenuate sound at these frequencies.

Unfortunately, it is at such low frequencies that existing theories of room acoustics and the relationships between sound level difference and sound reduction index are most tenuous. Current standards deal only with the frequency range from 100 Hz to 3150 Hz, and despite the introduction of Annex F in ISO 140/3, for sound insulation measurements at low frequencies,² there is still a poor repeatability between measurement results.³ Diffuse sound field assumptions must be replaced with that which incorporates acoustic and vibration mode distributions.

A study has been undertaken in Liverpool, where a FE model was validated by comparison with scale model measurement.⁴ The associated model of transmission between rooms demonstrates that the modal characteristics of the pressure and vibration fields of the rooms and separating wall, respectively, strongly influence the sound level difference. The work has identified important outstanding issues to be addressed: the need for an appropriate model of sound absorption in small furnished rooms at low frequencies, and the consideration of modally reactive absorption due to the vibration of the walls.

In this paper, a new FE model is used to describe the relationship between the sound absorption characteristics of the internal surfaces of an enclosure, and its frequency response, for the frequency range from 20 Hz to 200 Hz. The numerical model is validated by comparison with experimental results for a small reverberant chamber. In addition, the effect of inserting absorbent furniture is explored. The effect of furniture location is also investigated.

2 FINITE ELEMENT METHOD

Interior acoustic problems, involving boundary conditions, can be effectively simulated through the FE method.^{5,6} A physical model of the initial problem is created and then a model, which will allow the physical problem to be described in terms of mathematical equations. From these equations it is possible to obtain an analytical or numerical solution. However, when transforming the real problem into a mathematical model, a series of approximations is introduced which will produce an associated error. Thus, when constructing the mathematical model one must follow certain criteria (e.g., sufficient discretization of the model and characteristics of the elements used), which will minimise the error in the approximated solution.

3 EMPTY ROOM

3.1 Measurement system

The room investigated was a small reverberant chamber of the Acoustics Research Unit of the University of Liverpool. The room dimensions are $L_x = 5.78$ m, $L_y = 3.04$ m, and $L_z = 4.24$ m. The room was not completely rectangular, having a change in angle at the door position (see Figures 1 and 4).

Measurements were carried out with a loudspeaker and two microphones placed at different corners of the enclosure, in order to excite and measure as many acoustic modes as possible, as shown in Figure 1.

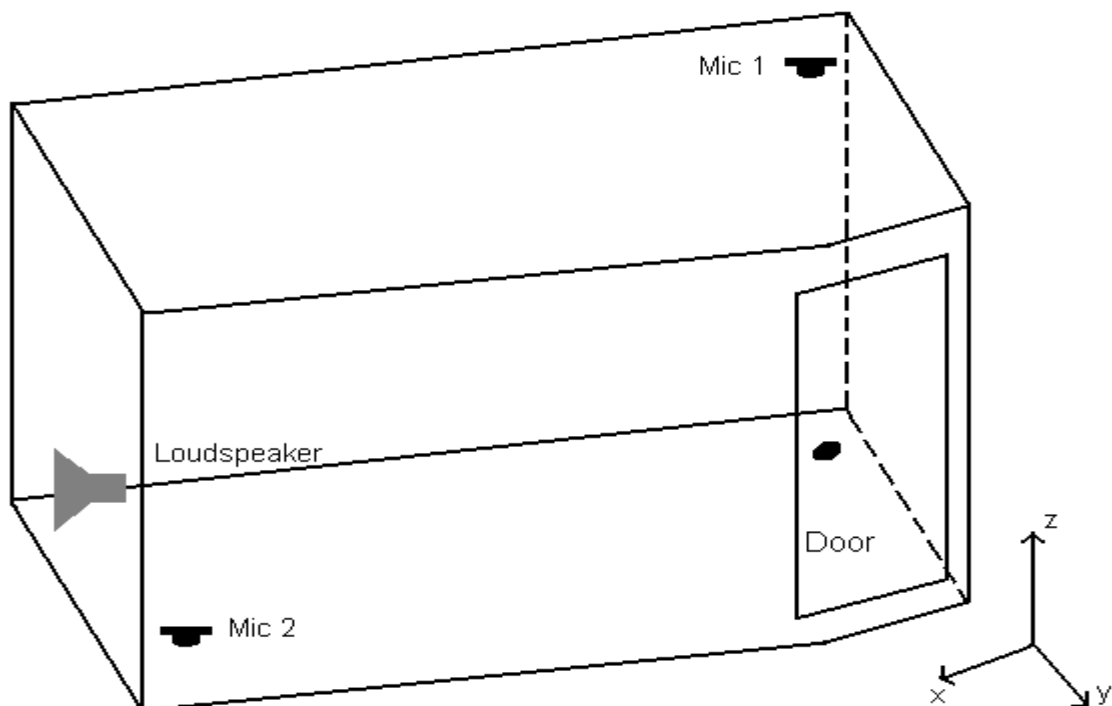


Figure 1: Loudspeaker and microphone positions inside the investigated room

The measured frequency response (sound pressure level versus frequency) was obtained using a Maximum Length Sequence based system (MLSSA) in the Power Spectrum mode.⁷ A schematic of the experimental set-up is shown in Figure 2.

3.2 Discretization of the acoustic field model

The element size to be used in the numerical model is dependent upon the upper frequency of interest, with the assumption that at least six elements would be required to properly represent the pressure field over the governing wavelength. In the present work, the upper frequency of interest is 200 Hz, which gives an element size around 0.28 m. The element type used was HEX20.⁸

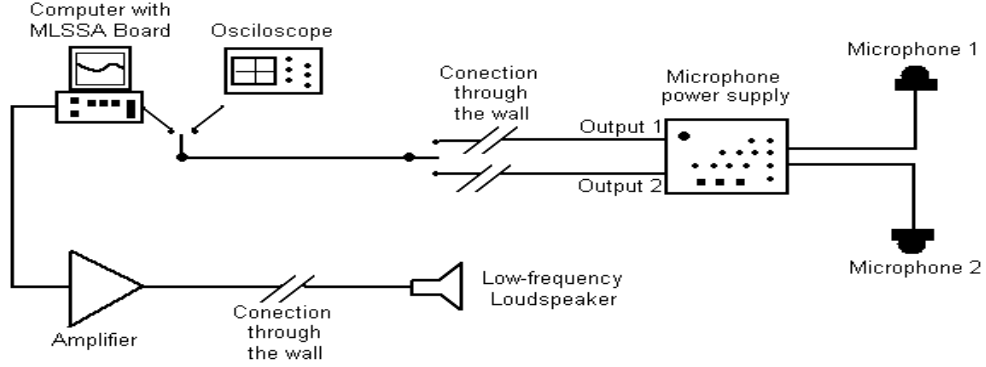


Figure 2: Experimental set-up

In order to verify the accuracy of the model, a second one of a completely rectangular room was created, with the same overall dimensions. It then was possible to compare the numerical and analytical results for the eigenfrequencies of the room.

The analytical eigenfrequencies are given by:

$$f = \frac{c}{2} \cdot \sqrt{\left(\frac{n_x}{L_x}\right)^2 + \left(\frac{n_y}{L_y}\right)^2 + \left(\frac{n_z}{L_z}\right)^2}, \quad (1)$$

where c is the speed of sound in the air, and n_x , n_y and n_z are integers.

To evaluate the error due to the FE discretization, an error E was calculated according to:

$$E = \frac{NE - AE}{AE} \cdot 100, \quad (2)$$

where NE and AE are the numerical eigenfrequency and analytical eigenfrequency, respectively. The results obtained showed that the error was less than 0.05% for all the eigenfrequencies inside the frequency range of interest (see Figure 3).

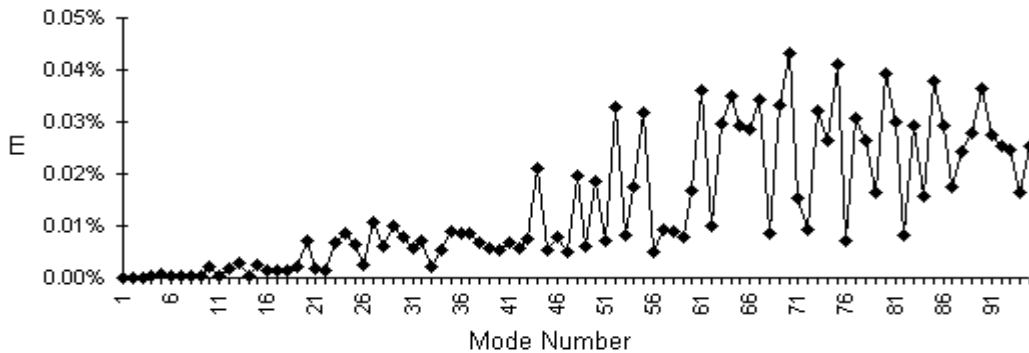


Figure 3: Percentile error between the numerical and analytical eigenfrequencies

The small change in angle at the door position was initially thought not to be influential. However, comparison of the rectangular model with measurement highlighted discrepancies throughout the frequency range. Thus, the room was modelled exactly and its mesh is visualised in Figure 4.

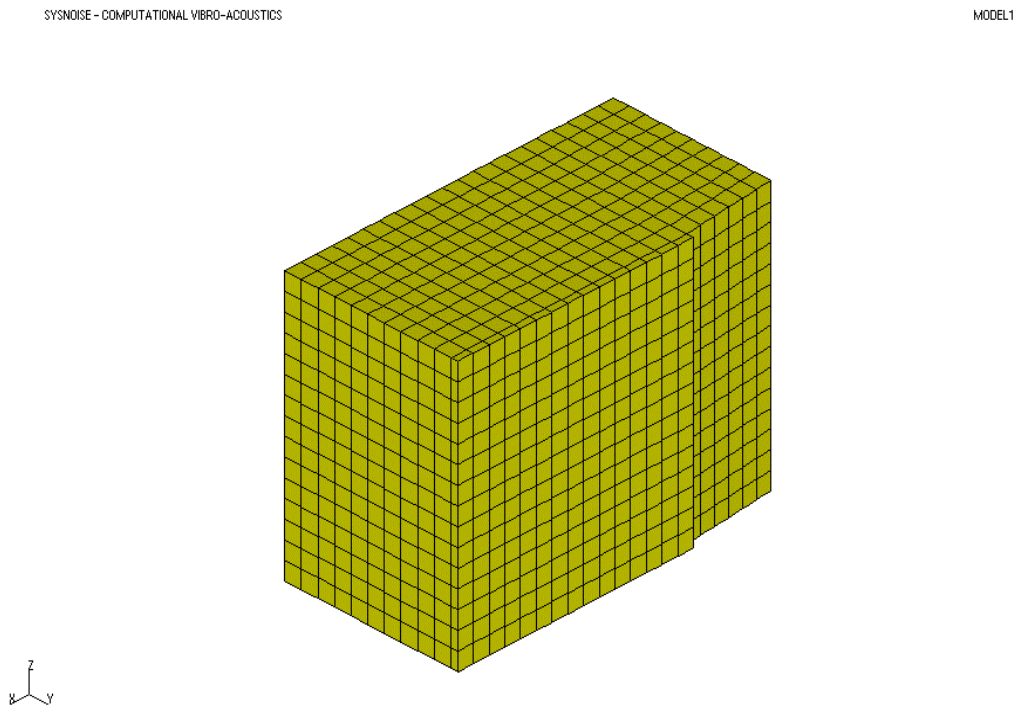


Figure 4: Isometric view of the FE model of the small reverberant chamber

A parametric study was carried out to determine the value of surface absorption that would provide the best fit with measurements. It was found that a surface absorption coefficient of $\alpha = 0.02$, to all frequencies, gave the best overall agreement. The model was refined to account for loudspeaker roll-off at the lower frequencies.

The results in Figure 5 show good agreement between measurement and prediction, and justify the choice of this FE model.

4 FURNISHED ROOM

Furniture in a room acts both as an obstruction and an additional absorption. Akil and Oldham^{9,10} have demonstrated that machines in factories can be treated as point scatters at high frequencies, where ray tracing can be employed.¹¹

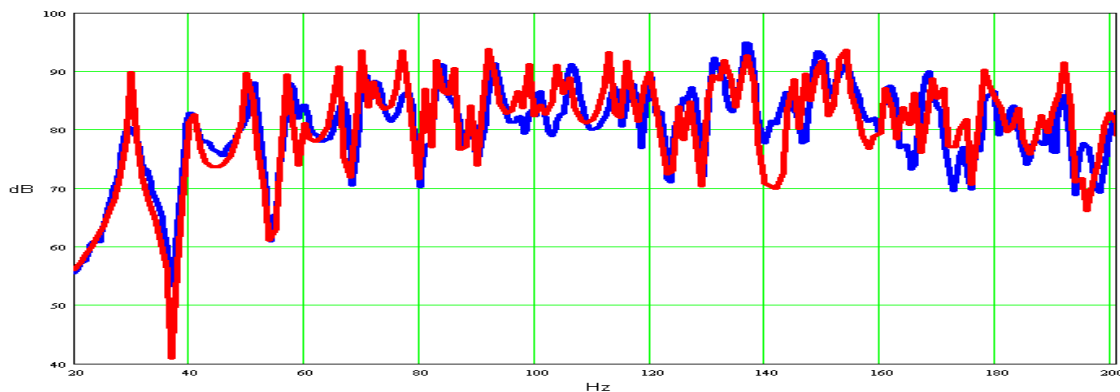


Figure 5: Comparison between measurement (—) and simulation (—) for the empty room

At low frequencies, the inclusion of furniture may generate additional eigenmodes, mode shifts and selective damping of modes. Such effects will depend on the construction of the furniture (how hard or soft), and its location.

In a preliminary study of the influence of furniture on the room response, a “standard unit”, constructed of lightweight concrete blocks, was positioned as shown in Figure 6. The unit was of dimensions $l_x = 1.53$ m, $l_y = 0.88$ m, and $l_z = 0.75$ m.

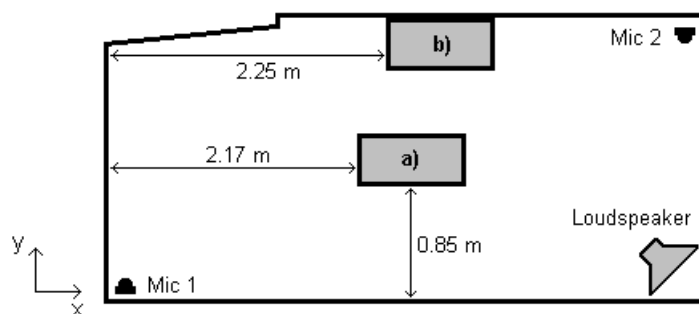


Figure 6: Top view of the standard unit positions within the room. a) Central and b) centre wall position

Measured frequency responses indicated that the unit did not appear to generate additional acoustic modes, but a shift of eigenfrequencies is observed and some of the modes were surprisingly damped (see Figures 7-a and 8-a for the unit placed at central and centre wall positions, respectively).

The predicted frequency responses have also presented similar characteristics (Figures 7-b and 8-b), showing eigenmode shifts and selective modal damping, after the inclusion of the unit in the numerical model.

The measured and predicted changes (expressed as level differences) on the room frequency response, as a result of the introduction of the solid unit, are shown in Figures 7-c and 8-c. Again, predictions are in good agreement with experimental results, showing that the developed numerical model can be used with confidence.

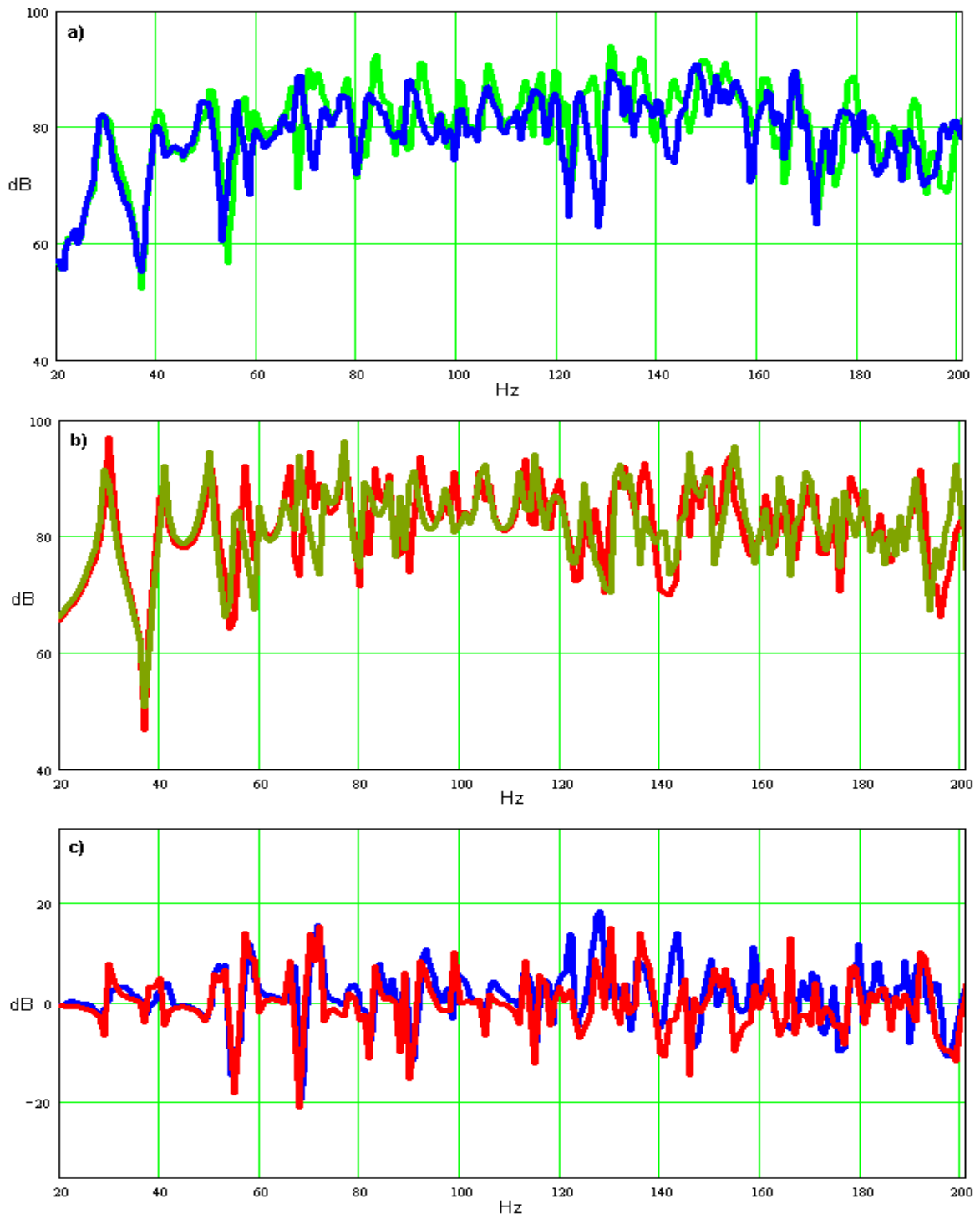


Figure 7: Effect of obstruction on room response. Unit at central position. a) Measurement for () empty room and () obstructed room. b) Prediction for () empty room and () obstructed room. c) Level difference () between measured values and () between predicted values

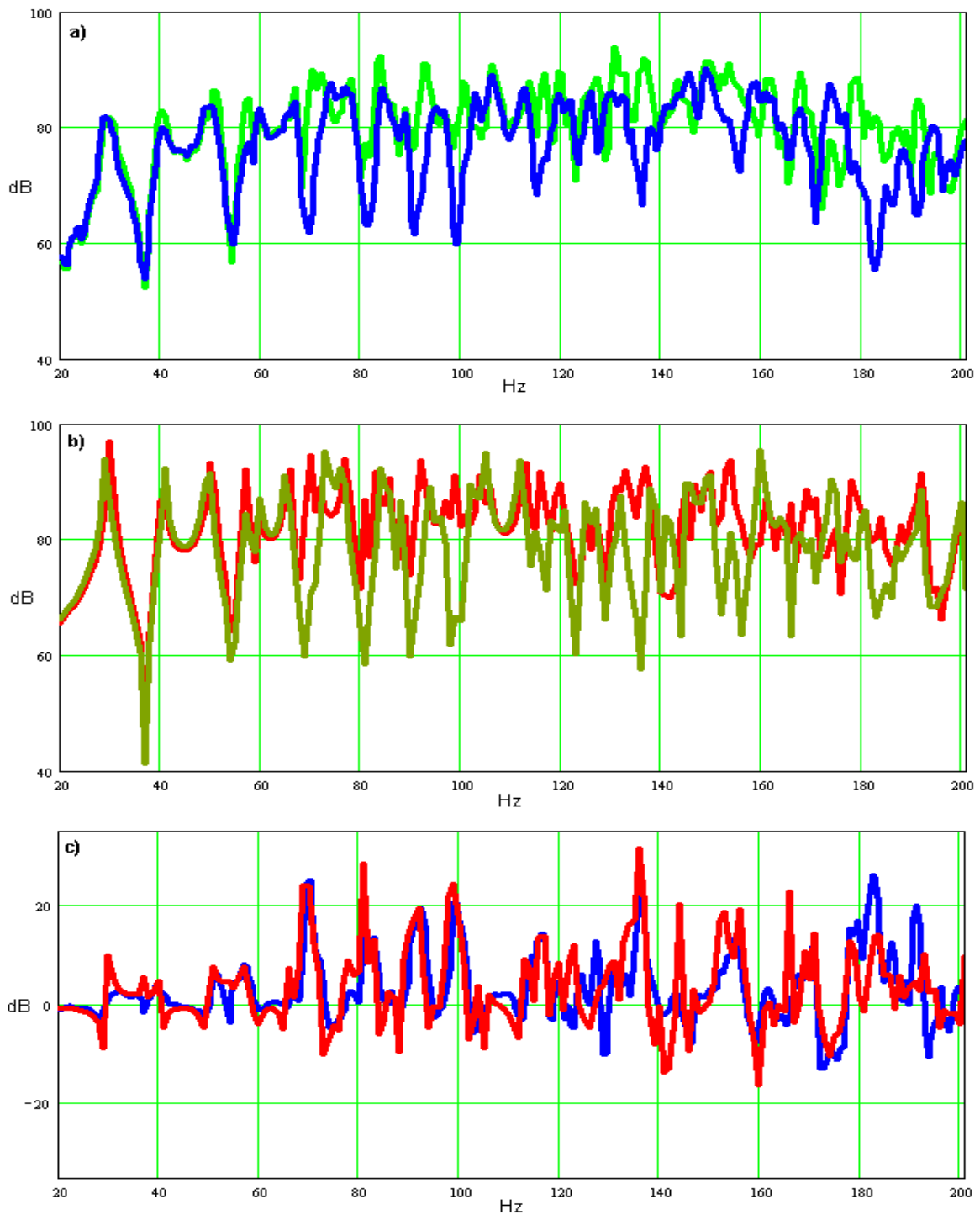


Figure 8: Effect of obstruction on room response. Unit at centre wall position. a) Measurement for () empty room and () obstructed room. b) Prediction for () empty room and () obstructed room. c) Level difference () between measured values and () between predicted values

5 DISCUSSION OF RESULTS

Both measured and predicted level differences show that when the unit was centrally located, the effect of its inclusion is small (Figure 7-c). The change in level difference is of the order of ± 3 dB at frequencies below 50 Hz. Between 50 and 200 Hz the change is of the order of ± 8 dB.

The effect of locating the unit along the wall is more pronounced (Figure 8-c). Again, the change is small below 50 Hz (of the order of ± 2 dB). Above 50 Hz, the variation is of the order of $+ 15$ to $- 8$ dB.

All the numerical results presented in this paper have been obtained considering only locally reactive boundaries. However, at low frequencies there is not only a locally reactive absorption due to the wall material, but also a modally reactive absorption due to the vibration of the walls, when the sound waves impinge on them. This phenomenon will be included into the model in the near future.

6 CONCLUDING REMARKS

A FE model of a small reverberant chamber was developed to investigate the influence of sound absorption on the room frequency response, at low frequencies. The process of modelling the empty room has highlighted the need to account for even small irregularities in the room geometry, in order to obtain a good agreement between prediction and measurement.

A preliminary study of the influence of furniture on the room response was performed by means of the introduction of a “standard unit” at different positions within the enclosure. The numerical results showed good agreement with measurements in both cases.

It has been shown that when a large solid item is introduced into the room centre, it causes little change in the frequency response below 50 Hz. This is despite the fact that the first three normal room modes occur in this frequency range. This might be expected since the major unit dimension is less than one quarter of the sound wavelength at 50 Hz. A similar situation is observed when the unit is located along a wall and, therefore, the room response is insensitive to location below 50 Hz.

Above 50 Hz, the effect of including a solid item is more pronounced. In addition, the influence of location is apparent. Furniture placed along a wall will produce a higher change in room response compared with a central location. A similar behaviour was observed when the solid unit was located in a corner, although results are not presented here.

ACKNOWLEDGEMENT

The authors would like to thank CAPES (linked to the Ministry of Education, Brasilia-Brazil) for the support of this work.

REFERENCES

- [1] Berglund, B., Hassmen, P., Soames Job, R. (1996), "Sources and effects of low-frequency noise", *J. of the Acoustical Society of America*, Vol. 99, N. 5, pp. 2985.
- [2] ISO 140/Part 3 (1995).
- [3] Maluski, S. and Bougdah, H. (1997), "Predicted and measured low frequency response of small rooms", *J. of Building Acoustics*, Vol. 4, N. 2, pp. 73-86.
- [4] Maluski, S. (1999), *Low Frequency Sound Insulation in Dwellings*, Ph.D. Thesis, The University of Liverpool.
- [5] Zienkiewicz, O.C. (1971), *The Finite Element Method in Engineering Science*, McGraw-Hill, London.
- [6] SYSNOISE, Version 5.4 (1999), *User Manual*, LMS.
- [7] MLSSA, Version 9.0 (1994), *Reference Manual*, DRA Laboratories.
- [8] Patran, Version 8.0 (1999), *User Manual*, PDA Engineering.
- [9] Akil, H.A. and Oldham, D.J. (1995), "Determination of the scattering parameters of fittings in industrial buildings for use in computer based factory noise prediction models: Part 1-Theoretical background", *J. of Building Acoustics*, Vol. 2, N. 2, pp. 461-481.
- [10] Akil, H.A. and Oldham, D.J. (1995), "Determination of the scattering parameters of fittings in industrial buildings for use in computer based factory noise prediction models: Part 2-Scale model experiments", *J. of Building Acoustics*, Vol. 2, N. 3, pp. 527-548.
- [11] Ondet, A.M. and Barbry, J.L. (1989), "Modelling of sound propagation in fitted workshops using ray tracing", *J. of the Acoustical Society of America*, Vol. 82, pp. 789-802.